Modelling of Novel Rotating Membrane Bioreactor Processes

A Thesis

By

Franck Anderson Jones

March 2017

Submitted in partial fulfillment of the requirements for the degree of

Doctor of Philosophy

Awarded by

Brunel University

Department of Mechanical, Aerospace and Engineering; Civil Engineering Research, Chemical Process Engineering, Brunel University

ABSTRACT

Previous membrane researches undertaken over the years to develop general dead-end filtration models made use of an approach that combined all three classical fouling mechanisms, namely, pore blocking, pore constriction and cake filtration. More recently researchers have modified and adapted this modelling approach for a cross flow side-stream membrane bioreactor (MBR) system.

Literature also reveals that there have been numerous recent experimental studies conducted on rotating membrane bioreactor (RMBR) systems. Some of these studies have resulted in the creation of RMBR models of the membrane fouling process as well. However, simulation and modelling of the fouling in RMBRs is still a nascent topic to date due to poor understanding and great complexity of the system hydrodynamics involved.

Even when models are developed, they are either too complex to be useful at operational level, or not comprehensive enough to express all possible operational scenarios. In many cases they are simply too difficult to calibrate and thus ending up being more suited as research tools rather than for direct process control. As such, further research is required in this area.

The research reported in this thesis consists of the development and validation of a RMBR system fouling model that incorporates all three classical fouling mechanisms. This thesis work is divided into two main sections. On top of a literature review that thoroughly describes the background theory and general information on MBRs along with their state of the art, the first section of the thesis also explains the specific methodologies used to accomplish all the main tasks carried out in this research work.

The first step of these methodologies involves the setting-up of a rotating MBR system process based upon the FUV-185-A15R Flexidisks membrane module that was developed by Avanti Membrane Technology (USA). This system was used to collect the majority of the data used in this thesis. Since some of these data outputs were compared against non-rotating MBR systems, a similar setting-up process for a bespoke static square MBR system was carried out as well.

Using synthetic wastewater in conjunction with activated sludge, mixed liquor suspended solids in both MBR system bioreactors were increased in levels over time to desired levels (i.e. by periodic excess sludge wasting). Trans-membrane pressure (TMP)-stepping fouling data was then acquired from operations of these membrane ultrafiltration processes. This data was obtained by measuring the flux decline or TMP increase. Following data collection, a dynamic fouling model for this RMBR system was then created in Matlab (using the Genetic Algorithm function).

To do this, hydrodynamic regimes such as air scouring and rotating shear effects along with all the three classical fouling mechanisms were included in the mathematical fouling model that was created from first principles. For the purpose of comparison, a similar fouling model was created without incorporating the rotational effects for the static square MBR system. This included modelling of the hydrodynamics as well. Finally, both these models were validated and calibrated using the data that were collected from both laboratory-based MBR systems.

The second phase of the thesis explores the numerous outputted results produced via model simulations which were then discussed and analysed in great detail. Results from this research indicate that the mathematical models give a decent portrayal and description of the fouling mechanisms occurring within a rotating MBR system. It was found that the rotational mechanisms in terms of fouling prevention accounted for only twelve percent of cake removal with the rest being accomplished through the air scouring mechanism.

However, it was found that although the slowly rotating spindle induced a weak crossflow shear, it was still able to even out cake build up across the membrane surface, thus reducing the likelihood of localised critical flux being exceeded, which would lead to dramatic loss of flux. Furthermore, when compared against the static MBR system, the study concluded that a rotating MBR system could increase the flux throughput by a significant amount.

In conclusion, RMBR systems appear to represent alternative viable solutions when compared against the traditional static MBR systems that currently dominate the industrial and municipal marketplace. In future, RMBR systems may become the systems of first choice once there is a better understanding of the rotational processes, and once research and design into this sector broadens.

Future study areas should thus focus on: whether the forces acting on an activated sludge particle during rotation have a significant effect on the fouling or the shear hydrodynamic regimes; whether activated sludge and benchmark models could be created for rotating MBRs whilst including the shear effects and hydrodynamic regimes; whether model predictive control using these developed RMBR models would enhance efficiency gains within an operational plant; and, whether the real measured soluble microbial products (SMP) concentrations could be used to create an even better SMP predictive model that accurately explains fouling behaviour.

ACKNOWLEDGMENTS

I would like to express countless gratitude to my supervisors Professor Parneet Paul, Head of Civil Engineering, School of Built Environment and Engineering at Leeds Beckett University; Mr Richard Hill, Director of Whitewater Limited Consulting Engineers; and, finally Dr Nuhu Braimah, Lecturer in Construction/Infrastructure Management at Brunel University, whose supports were invaluable to the completion of this arduous endeavour.

My thanks also go to Avanti Membrane Technology (USA) for their technical contribution especially Mr Tzu-Lung Lin, General Manager of Avanti Membrane Technology Inc., who travelled all the way from the USA to Brunel in order to aid me conduct several membrane resistance tests. I would also like to thank the Royal Society (UK) for providing funding to allow this work to proceed.

Much gratitude goes to Mr Gerald Edwardson, Technician (Civil Engineering) – Brunel University, whose help was essential in setting-up the water laboratory and ordering the chemicals for the synthetic wastewater. A word of thanks also goes to Dr Jie Chen – Lecturer – UG projects coordinator, Timetable coordinator – Brunel University, who helped me translate part of the pilot unit's manual from Chinese to English. I would like to give a word of appreciation to Mr Kofi Renner – Brunel University Institute for Environment, Health & Societies, who assisted me in taking the pictures for the activated sludge flocs under the microscope.

I cannot stress this enough, but I would like to dedicate this work to both my parents, Mr and Mrs Jones, whose untold amount of encouragements have helped me stand firm through extremely difficult times.

TABLE OF CONTENTS

LIST OF TABLES

TABLE PAGE

LIST OF FIGURES

FIGURE PAGE

NOMENCLATURE

This thesis's nomenclature includes a glossary of abbreviations made and/or used as well as general jargons; and, provides a list of units, a list of Greek and/or scientific notations and a list of equation symbols used.

Glossary

Activated sludge process, refers to a biological wastewater treatment process that speeds up waste decomposition. Activated sludge is added to wastewater, and the combination is aerated and agitated;

BAP, stands for biomass associated products;

BOD, stands for biological oxygen demand;

BOD_5, refers to biochemical oxygen demand of wastewater during decomposition occurring over a 5-day period;

BPC, stands for biopolymers clusters;

Cake, refers to a gel layer formed on membrane as solids accumulate during fouling;

CAS, stands for conventional activated sludge process(es). Please, refer to activated sludge process;

CFD, refers to computational fluid dynamics;

Cl_2, refers to chemical symbol of chlorine;

Clogging, refers to the accumulation of solids within the membrane channels;

COD, stands for chemical oxygen demand;

DO, stands for dissolved oxygen;

EPA, stands for United States Environmental Protection Agency;

EPS, stands for extracellular polymeric substances;

Floc, refers to fundamentally, clumps of bacteria;

Flux, refers to the amount of permeate produced per unit area of membrane surface per unit time;

Fouling mechanism, refers to a mechanism that is thought of to induce fouling in some form or another;

Fouling, refers to the degradation of membrane filtration performance due to the accumulation of solids (or particles) onto and into the membrane over time;

GA, stands for genetic algorithm, a "tool" that is often used for solving complex optimisation problems;

GE membrane, stands for General Electric membrane (GE Water & Technologies);

HCl, refers to chemical symbol of hydrogen chloride;

HMI, stands for human-machine interface;

IWA, stands for International Water Association;

MBR, stands for membrane bioreactor, a wastewater treatment technology combining membrane separation and activated sludge process. In this thesis, its usage refers to all membrane bioreactor systems (i.e. static submerged, static side-stream, vertical airlift, rotational, etc);

m-code, refers to Matlab programming code;

Membrane autopsy, refers to an operating tool that is used to identify if there is any damage on membrane surface;

Membrane, refers to a porous material where one type of substance can pass more readily than others;

MF, stands for microfiltration, a membrane filtration process;

m-file, refers to Matlab file. It can be run to launch an automated task;

Mixed liquor, refers to activated sludge mixed with raw wastewater;

MLSS, stands for mixed liquor suspended solids;

MLVSS, stands for mixed liquor volatile suspended solids;

MWCO, stands for molecular weight cut-off;

NaOCl, refers to chemical symbol of sodium hypochlorite;

NaOH, refers to chemical symbol of sodium hydroxide;

NESC, stands for National Environmental Services Center;

NF, stands for nanofiltration;

NMR, stands for nuclear magnetic resonance;

OECD, stands for Organisation for Economic Co-operation and Development;

PIV, refers to particle image velocimetry, a flow visualisation technique for velocity vector measurement;

Pore blocking, refers to big particles blocking the membrane pores as it fouls due to their sizes being bigger than those of the membrane pores;

Pore constriction, refers to very small particles constricting the membrane pores from the inside during fouling;

PPE, stands for personal protective equipment;

PVDF, stands for Polyvinylidene (Di)fluoride;

RAS, stands for return activated sludge;

RMBR, refers to rotating membrane bioreactor systems;

RO, refers to reverse osmosis (where osmosis is a process by which solvent molecules tend to go through a semi-permeable membrane from a less concentrated solution into a more concentrated one);

SI, refers to international system (of units);

SMBR, refers to static only membrane bioreactor systems;

SMP, stands for soluble microbial products. They have been the source of many debates but it is generally accepted that they affect fouling in some way;

Synthetic wastewater, refers to artificially created wastewater;

TDS, stands for total dissolved solids;

TEP, stands for transparent exopolymer particles;

Trans-membrane pressure, shortened for **TMP** and defined as pressure difference between two sides of a membrane;

UAP, stands for utilisation associated products;

UF, stands for ultrafiltration;

VRM, stands for vacuum rotating membrane (Huber Technology);

WAS, stands for waste activated sludge;

Wastewater, refers to water that is not clean, one that has been used domestically or in industrial operations;

Wasting; refers to, at its most basic, removing excess micro-organisms from the system;

WWT (*headings only*), refers to wastewater treatment. In its basic form, wastewater treatment is a treatment procedure in which waste or pollutants are remove from wastewater;
WWTP, stands for wastewater treatment plants.

Greek letters

α, in m^2/kg, is the pore blockage parameter;
α', in m^2/kg, is the rate of pore blockage;
α_{in}, in m^3/kg, is the volume of foulants deposited in the pore interior per unit mass of fluid filtered through the membrane;
α_v, unitless (−), is the air scouring coefficient;
β, in kg, is the pore constriction parameter;
$\dot{\gamma}$, in s^{-1}, is the shear rate (e.g. $d\gamma/dt$);
$\dot{\gamma}_l$, in s^{-1}, is the shear rate for laminar flow;
$\dot{\gamma}_m$, in s^{-1}, is the maximum shear rate of the membrane;
$\dot{\gamma}_t$, in s^{-1}, is the shear rate for turbulent flow;
δ', in m^{-1}, is the resistance distribution factor of cake layer;
Δl, in m, is the depth of cake layer;
δ_b, in m, is the boundary layer thickness;
δ_m, in m, is the membrane thickness;
ΔP, in Pa or N/m^2, is the pressure (drop) through the cake layer or sometimes cake's trans-membrane pressure;
$\Delta\Pi$, in bar or Pa, is the osmotic pressure difference;
ε_a, unitless (−), is the air-injection factor;
ε_c, unitless (−), is the cake porosity;
ϵ_{smp}, unitless (−), is the SMP concentration factor;
ζ, in mV, is the zeta potential;
ζ_b, in %, is the blower efficiency;
Θ_c, in m, is the cake's thickness;

λ_a, unitless (−), is the aerator constant;

μ, in Pa.s, kg/m/s or cP, is the viscosity;

μ_w, in Pa.s, is the viscosity of water and is valid for T_w between 0 and 100 °C;

ν, in m^2/s, is the kinematic viscosity;

ρ_b, in kg/m^3, is the bulk cake density;

ρ_f, in kg/m^3, is the density of fluid (e.g. here activated sludge) = ρ_{sludge};

ρ_N, in kg/m^3, is the density of Newtonian fluid;

ρ_{NN}, in kg/m^3, is the density of non-Newtonian fluid;

ρ_{sludge}, in kg/m^3, is the density of activated sludge;

ρ_{water}, in kg/m^3, is the water density;

σ_a, in $m^3.kg$, is a pore constriction related parameter;

σ', unitless (−), is the osmotic reflection coefficient;

τ, unitless (−), is the cake water content;

τ', in Pa, is the shear stress;

τ_0, in N/m^2 or Pa, is the yield stress;

τ_{wm}, in N/m^2, is the mean shear stress at the membrane;

φ, unitless (−), is a constant accounting for total amount of cake layers formed;

ϕ, in kg/m^3, is the volume fraction of foulants (relative to bulk concentration);

Ψ, in kg/m^2, is the amount of fouling;

ω, in rad/s, is the angular velocity.

Symbols (Equations)

A, in m^2, is the remaining membrane area available for permeate;

A_0, in m^2 or ft^2, is the (total) membrane area;

A_b, in m^2, is the blocked membrane area;

A_{free}, in m^2, is the effective membrane area (pore opening) available at any time t;

A_k, unitless (−), is a constant in Jaffrin's shear rate-flux model;

A_u, in m^2, is the unblocked membrane area;

A_{u0}, in m^2, is the initial unblocked membrane area relative to the membrane area;

C, in mg/L, is the particles' concentration;

C'_{MLSS}, in g/L, is the MLSS concentration factor;

C_b, in g/L, is the bulk concentration;

C_d, in kg/m^3, is the solids content in the bulk;

C_G, in mg/L, is the particles' concentration in the gel (or cake) layer;

C_{MLSS}, in g/L, is the bulk MLSS concentration (e.g. here equals C_b);

C_{NaOCl}, in mg/L, is the NaOCl concentration;

C_p, in mg/L, is the particles' concentration in the bulk;

C_{SMP}, in g/L, is the SMP's concentration;

D_B, in m^2/s, is the Brownian diffusion coefficient;

D_{eff}, in m^2/s, is the effective diffusion coefficient;

d_{pi}, in m, is the mean diameter of floc particles forming the cake;

D_S, in m^2/s, is the shear-induced diffusion coefficient;

E, in kJ.mol^{-1}, is the activation energy for viscosity;

F/M, in kg BOD_5/kg ML(V)SS/d, is the food to microbe ratio;

f', unitless (−), is a fraction of foulants contributing to particles deposit growth;

g_o, unitless (−), is the cake removal factor;

HRT (or θ), in h, is the hydraulic retention time;

J, in LMH, gfd, m/d m/h, or m/s, is the flux;

J_0, in m/s, is the initial flux of clean membrane;

J_{air}, in m/s, is the air scouring flux;

J_b, in m/s, is the blocked flux;

J_{LIM}, in m/s, is the limiting flux;

J_{mo}, in m/s, is the initial total flux within membrane;

J_{ss}, in m/s, is the steady state flux;

J_u, in m/s, is the unblocked flux;

k, unitless (−), is the cake compressibility factor;

K_a, in (Pa.s)$^{0.5}$, is the consistency coefficient in Casson equation;

k_{Ab}, unitless (−), is the blocked pores area constant;

k_f, unitless (−), is a constant in Hermia's power law model;

k_i, in s^{-1}, is the first order particle removal coefficient;

K_α, in m^{-1}, is the area distribution density;

k_ω, unitless (−) or rad^{-1}, is the angular velocity factor;

m, in $Pa.s^n$, is the flow consistency index;

Mf, in g, is the dried up mass of cake along with glass jar mass;

Mi, in g, is the glass jar mass plus cake mass weighed together;

Mj, in g, is the glass jar mass;

n, unitless (−), is the flow behaviour index;

N_0, unitless (−), is the number of pores in membrane;

N_b, unitless (−), is the number of blocked pores;

n_f, unitless (−), is an exponent characterising Hermia's power law model:

n_k, unitless (−), is an exponent in Jaffrin's shear rate-flux model;

$N_{\omega r}$, in rpm, is the rotational speed of SpinTek disc motor;

N_ω, in rpm, is the rotating speed of disc motor;

p_b, in Pa, is the blower inlet pressure;

P_{Fe}, in bar or Pa, is the feed or inlet pressure;

P_{fi}, in bar or Pa, is the filtrate or permeate pressure;

$P_{Re,}$ in bar or Pa, is the retentate or outlet pressure;

PT, in bar or Pa, is the pressure at membrane periphery;

Q, in m^3/s, m^3/h, L/h or m^3/d, is the flow rate;

Q_0, in m^3/s, is the initial flow rate;

Q_{air}, in m^3/h, is the air flow rate;

Q_b, in m^3/s, is the flow rate through blocked pores;

Q_g, in m^3/s, is the superficial gas flow rate;

Q_i, in m^3/s or m^3/h, is the influent flow rate;

Q_l, in m^3/s, is the liquid flow rate;

Q_u, in m^3/s, is the flow rate through unblocked pores;

Q_t, in m^3/s, is the total normalised flow rate through the membrane;

Q_w, in m^3/s, is the (permeate) water flow rate;

r, in m, is the radius;

R^2, unitless (−), is the coefficient of determination;

r'_0, in m, is the distance radius from the spinning axis. Thus, $r'_0 = r_o - r_i$;

R', in m/kg, is the unit cake layer thickness per unit mass of fluid filtered;

R'_c, in m^{-2}, is the so-called specific cake resistance;

R_b, in m^{-1}, is the resistance of solids deposit over a region of membrane;

R_{bo}, in m^{-1}, is the initial resistance of solids deposit;

r_d, in m, is the radial distance for $Re_{r,N}$, or $Re_{r,NN}$;

$Re_{r,N}$, unitless (−), is the radial Reynolds number of Newtonian fluid;

$Re_{r,NN}$, unitless (−), is the radial Reynolds number of Non-Newtonian fluid;

R_g, in $J.K^{-1}.mol^{-1}$ or $kJ.K^{-1}.mol^{-1}$, is the universal gas constant;

r_i, in m, is the membrane inner radius;

R_i, in m^{-1}, is the irreversible membrane resistance;

$R_{in,b}$, in m^{-1}, is the membrane resistance and resistance caused by pore constriction;

R_m, in m^{-1}, is the clean membrane resistance;

r_o, in m, is the membrane outer radius;

r_p, in m, is the radius of membrane pore;

R_r, in m^{-1}, is the reversible membrane resistance;

R_{t0}, in m^{-1}, is the initial total membrane resistance;

R_{total}, in m^{-1}, is the total membrane resistance and is often equated to the sum of R_m, R_i and R_{cake} (i.e. cake resistance), with each respectively being in m^{-1};

S_m, in kg or lbs, is the substrate mass;

S_0, in m^{-1}, is the specific surface area;

SAD_m, in $m^3/m^2/h$, is the specific air demand based on membrane area;

SAD_p, in m^3 air/m^3 permeate, is the specific air demand based on permeate volume;

SED, in $kWh.m^{-3}$ permeate, is the specific energy demand (consumption);

SED_r, in $kWh.m^{-3}$ permeate, is the (specific) energy consumption for RMBR;

SRT, in d, is the solids retention time;

t, in h, d, or s, is the (filtration) time;

T_{air}, in K, is the air temperature;

t_b, in s^{-1}, is the time at which a membrane region was first blocked;

t_c, in s^{-1}, is the time constant "tracking" the remaining available membrane area;
TMP, in bar or Pa, is the trans-membrane pressure;
TMP_0, in bar or Pa, is the initial trans-membrane pressure;
T_{room}, in °C, is the room temperature;
TSS, in g/L, is the total suspended solids;
T_w, in °C, is the water temperature;
V, in L, gal or m^3, is the (permeate) volume;
V_b, in m^3, gal, or MG, is the volume of the aeration basin;
V_p, in m^3, is the pore volume;
W_d, in kW, is the sum of power of the rotating disc motor and feed pump (kW);
X_{org}, in kg/m^3 or g/L, is the micro-organism mass per litre;
x_a, in m, is the axial coordinate or distance from axis to membrane surface;
y_b, in m, is the aerator depth.

Units

–, no unit;
°, degree (or arc degree) is used as a unit for angle measurement, usually;
°C, degree Celsius is often the unit used for temperature measurement;
µm, unit micron or micrometre;
bar, unit measurement of pressure such that 1 bar = 10^5 Pa;
cP, centipoise and equals to 10^{-3} Pa.s for water at 20 °C;
d, day;
Da, Daltons;
ft, foot;
g, gram;
g/L, grams per litre;
gal, gallon;
gfd, gallons per square foot per day;
h, hour;

Hz, Hertz;

J, joule is a unit for energy;

K, Kelvin equals to °C + 273.15;

kg, kilogram;

kPa, kilo Pascal (kilo = 10^3);

kW, kilo Watt;

L, litre;

lb, pound;

LMH, litres per square metre per hour;

m, metre;

min, minute;

mg, milligram;

MG, million gallons;

mg/L, milligrams per litre;

mL, millilitre;

mm, milimetre;

mol, Mole is amount of pure substance containing same number of chemical units as there are atoms in exactly 12 grams of carbon-12 (i.e. ^{12}C, $6.02214179 \times 10^{23}$);

MPa, Mega Pascal (where Mega = 10^6);

mV, millivolt;

Pa, usually unit for pressure and is the force applied (N) per unit area (m^2);

pH, numeric scale utilised to identify the acidity or basicity of a solution;

rad, radian is yet another measurement unit of angle;

rpm, revolution per minute measures the frequency of rotation;

s, second is a measurement unit of time;

W, watt.

CHAPTER 1: INTRODUCTION

The introductory chapter of this thesis, first, outlines the rationale for pursuing the topic of study. The next section of the chapter highlights the aim and objectives along with the research questions of the study in detail, the project's background, methodology overview and the novelty and contributions of the research, including the author's personal achievements. The last part of the chapter gives an outline of the thesis structure and a summary of the contents of the remaining chapters to follow-on.

1.1. Rationale for Research

Generally speaking, one of the many reasons of water scarcity and security is that almost all sources of water are fully utilised. Conversely, rainwater harvesting and wastewater reuse via recycling are severely underutilised (Templeton and Butler 2011). Major drawbacks of the latter option, however, are disinfection of product to sufficient level, and other ethical issues.

Indeed, wastewater treatments have been daunting tasks for engineers for decades due to varying influent characteristics and stringent effluent regulations. However, standalone biological wastewater treatment systems such as conventional activated sludge processes (CAS) have been able to circumvent most of these difficulties (Zuthi et al. 2012).

Yet, despite their usefulness soon problems arose: the practice of CAS came at the expense of huge economical costs to achieve the desired effluent water quality especially at medium to large wastewater treatment facilities (Jeppsson 1996, Gernaey et al. 2004).

This is one of the reasons why membrane bioreactors (MBRs) came into the picture and experienced an increase in usage in recent decades. Not only do they allow recycling but they also produce better effluent and permeate quality as well as reduced footprints (Fenu et al. 2010). Nowadays they can also cope with large effluent quantities as well.

Unfortunately, a single persistent issue, namely membrane fouling that is characterised by flux decline or trans-membrane pressure (TMP) increase during MBR filtration operation time, which has been bedevilling this field of research for years, came to light along with the increase usage of MBRs (Judd 2006, Drews 2010). Fouling, which can cause serious clogging issues and permanently damage the membranes if the appropriate precautionary measures are not taken, has been the subject of interesting debates over the years (Ahn et al. 2006, Rosenberger et al. 2006).

Researchers and manufacturers alike have tried to find the best and most effective ways of reducing fouling (thus, also reducing concentration polarisation) in a static membrane bioreactor (SMBR) system, but alas, it seems the hurdle still remains a bit too high to surmount. To help address this issue, rotating membrane bioreactor (RMBR) systems, which seemingly have better performance than conventional SMBRs, were introduced (Bhattacharjee and Bhattacharya 2006).

According to literature, multiple experimental studies have been conducted for said systems (for example, Bouzerar et al. 2003, Frappart et al. 2008) and a few models were created in the process (for example, Engler and Wiesner 2000, Torras et al. 2006, Bentzen et al. 2012, Jørgensen et al. 2014).

In spite of all these efforts, simulation and modelling of the fouling in a RMBR system is still an emerging topic to date due to the poor understanding and great complexity of the system hydrodynamics involved (Yoon 2015). Even when models are created, they are either too complex for a plant operator or not very comprehensive to be useful in the long run.

They are in most cases too difficult to calibrate and are often more suited to be used as research tools rather than for process control. Such inadequacies within this particular field of research have instigated the author of this thesis to purse the topic of study. Because sustainability of energy sources is an increasing issue within this field of research, models are being used to greatly enhance and optimise wastewater treatment plants (WWTPs) processes in order to reduce energy requirements (Lu et al. 2001, Wintgens et al. 2003, Meng et al. 2005, Jiang et al. 2008).

And since these mathematical models can be used to simulate flux decline or TMP increase — thus serve as conduit to increase one's interpretation and understanding of the membrane's fouling mechanisms involved — a focus of this research is to create and validate a comprehensive fouling model that can be applied to RMBR (i.e. laboratory scale, pilot units, and/or WWTPs) designs and controls. Furthermore, by comparing the outputs of a RMBR model to those of a SMBR system, the author aims to examine and discuss the usefulness of RBMRs for municipal and industrial applications or usage.

1.2. Aim and Objectives

Using a RMBR system, the aim of this research work is to study, develop and validate a fouling model that is rich enough to express fouling mechanisms yet practical and accessible by MBR plant operators (including industrial and municipal WWTPs).

The objectives of this thesis are broken down in the following manner:

- Critically investigate and review existing fouling mechanisms and mathematical fouling models for microfiltration (MF) and ultrafiltration (UF) membranes, including the state of the art in their modelling.

- Develop comprehensive fouling models that incorporate three classical fouling mechanisms (i.e. pore blocking, pore constriction and cake filtration) for a RMBR system. These fouling models will additionally integrate the hydrodynamic regimes (i.e. air scouring "flux"), rotational shear and soluble microbial products (SMP) effects. This process will be carried out three folds:

    - Fouling model using constant TMP – The model will be constructed under constant TMP and varying flux. The simulated parameters related to the rotational, shear and hydrodynamics' effects will be used for analysis of the fouling mechanisms.

    - Fouling model using constant flow rate (or flux) – The model will be constructed under constant flow rate or flux and varying TMP using first principle definitions (i.e. Taylor's expansion to truncate filtration area calculations and discuss its implications and accuracy). The simulations' parameters will be used to provide further analysis.

    - A model based on SMP as a function of mixed liquor suspended solids (MLSS) – Relationship between SMP and MLSS will be briefly discussed.

- Critically analyse and investigate fouling behaviours towards establishing differences between a RMBR and SMBR system.
- Provide detailed recommendations as to whether or not the RMBR system could be cheaper, more efficient, and a better alternative to the currently used SMBR based industrial and municipal WWTPs.

1.3. Research Questions

The aim and objectives of this thesis can be summed up through addressing the following questions:

- In a much more practical approach, how can a relatively simple phenomenological membrane fouling model that expresses all the major membrane fouling mechanisms of a real life RMBR plant be developed and validated?

- Using a modelling and comparative study, is it possible to investigate and analyse the fouling behaviour differences between a RMBR and a SMBR system?

- Are RMBR systems viable alternatives to utilise in lieu of the currently available and/or used municipal and industrial WWTPs?

1.4. Project Background

This project was funded by a Royal Society Equipment Grant with the aim of pursuing further relevant research into MBR systems and their developments. Following initial review of relevant literature of the subject matter, it became apparent early on to focus on the modelling and validation of a novel rotating batch-fed aerobic MBR plant in order to address the inadequacies in this particular field of engineering.

The novel system supplied by Avanti Membrane Technology, USA, appears to be a potentially quick and easy approach that might allow a RMBR system to compete directly with traditional aerobic based MBR systems, i.e. hollow fibre, tubular, and flat sheet configurations.

Furthermore, this RMBR system utilises innovative low cost Polyvinylidene (Di)fluoride (PVDF) membranes that could easily be removed in-situ by a push-fit procedure if damaged. More RMBR systems of this type are being produced, globally speaking, such as Huber Technology's commercial versions.

Indeed, the system advocated and tested under this research was a much less energy intensive option that might be suitable for both large scale industrial and municipal situations treating low strength wastewater. However, there are still many uncertainties regarding RMBR systems that are preventing their wide scale adoption, some of which this thesis endeavours to answer.

1.5. Methodology Overview

The methodology followed in undertaking this research is multi-layered. The first layer covers how the novel RPU-185 RMBR system (Avanti Membrane Technology, USA) was set-up and describes its features in details.

A similar setting-up procedure is shown for a bespoke square SMBR system that was created at Brunel University. Using the manufacturer's instructions combined with some research, membrane resistance tests for both MBR types were carried out in order to determine the pristine membrane resistance of each as this would later be used in the fouling models.

The synthetic wastewater, which was produced with carefully mixed dosage of chemicals, was consistently fed to the activated sludge (Thames Water, UK) in order to increase the MLSS concentration to desired levels over time in both MBR system bioreactors (although periodic excess sludge wasting were also performed as needed). The bulk of the TMP-stepping fouling data used during model simulations was obtained from performing membrane UF processes for both systems. This data is obtained by measuring the flux decline or TMP increase.

The next layer of the methodology phase was accomplished by ensuring that a comprehensive fouling model for the RMBR was created in Matlab (using the Genetic Algorithm function). To do this, the hydrodynamic regimes and rotating shear effects along with all three classical fouling mechanisms were included in the mathematical fouling model which in turn was created from first principles.

The three classical fouling mechanisms in question are namely pore blocking, pore constriction and cake filtration. For comparative purposes, a similar fouling model without the rotating effects was created for the square SMBR system along with its hydrodynamic regimes. Lastly, both these models were validated and calibrated using the data that was collected from both laboratory-based MBR systems.

1.6. Novelty and Contribution

If one takes a look at the currently available RMBR models, one will find that most of them are either too detailed or complex on a technical level or extremely difficult to calibrate. In fact, these models are mainly used as research tools rather than for process control and optimisation, thus are not very suitable for plant operators.

At the other end of the spectrum, the models are either too generalised or trivial to be used to conduct any proper analysis pertaining to fouling, and are typically not even related to actual MBR fouling theory.

To address the aforementioned issues and thereby contribute to knowledge, the author of this research has developed a MBR model that matches theory so it is relatively rich enough to express the major fouling mechanisms in a RMBR system.

Furthermore, it is still practical enough to be used by plant operators and relatively easy to calibrate and validate using data sets which are commonly collected by plant operators and laboratory samplers (i.e. this means that mass spectrometry or other complex tests are not needed). This can in turn be used to broaden this field of research which is still in need of more efforts and studies.

1.6.1. Contribution to Knowledge

The novel and knowledge contributive elements of this research can be summarised as follows:

- The successful development of a comprehensive fouling model for a RMBR system that described all three classical fouling mechanisms (i.e. pore blocking, pore constriction and cake filtration). This MBR model, which was constructed under constant TMP conditions, further included the rotating effects and hydrodynamic regimes. The author also:

    - Established another fouling model that was constructed under constant flow rate or flux conditions using first principles.

    - Formulated a model based on SMP as a function of MLSS. The relationship between SMP and MLSS was briefly discussed.

  This novel model developed should help researchers and industry practitioners understand the actual fouling processes occurring, which is very essential for the development of improved RMBR systems in the future.

- Using the software package Matlab, fully calibrated and validated fouling model for the constant TMP/varying flux mode were developed using real data sets from the RMBR pilot unit. The constant flux/varying TMP fouling model was validated the same way as well. The model based on SMP as a function of MLSS and cake thickness was again implemented using Matlab. This should help researchers and industry practitioners understand where RMBRs have improvements over standard SMBR systems.

- A fouling model for a square SMBR system (that included the hydrodynamic regimes) has also been developed by completely switching-off the rotating terms. Initial model validation was performed

using data from Coors (UK), then using data from the bespoke square SMBR made in the laboratory. The fouling model for this system was implemented using Matlab. This direct comparison between systems again will highlight which system performs better, and under which conditions.

- The author was also able to perform a comparative study between the SMBR and RMBR systems by taking cake build-up pictures of both after they had been fouled suspended solids. The impact of this caking on both systems was fully discussed to elucidate which performed better and why.

- Six papers, two of which are impact factor journal papers and four which are conference ones, have been published as a direct consequence of this research work as seen in **sub-section 1.6.2**. This means that this research work has already been peer reviewed internationally.

1.6.2. Publications and Conferences

The published journal papers as a result of this research are listed below:

Paul, P., and **Jones, F.A.**, 2016. Advanced Wastewater Treatment Engineering – Investigating Membrane Fouling in both Rotational and Static Membrane Bioreactor Systems Using Empirical Modelling, *Int. J. Environ. Res. Public Health 13(1)*, 100, doi:10.3390/ijerph13010100 [Impact Factor, 2.035].

Paul, P., and **Jones, F.A.**, 2015. Development of a Comprehensive Fouling Model for a Novel Rotating Membrane Bioreactor System, *Water 7(2)*, 377-397, doi:10.3390/w7020377 [Impact Factor, 1.687].

The written and published conference papers are listed below as:

Jones, F.A., and Paul, P., (2015). Development and Testing of a Fouling Model For a MBR System Using Both Static and Rotating Membranes, Proceedings of the 12th IWA Leading Edge Conference on Water and Wastewater Technologies, Hong Kong, China.

Paul, P., and **Jones, F. A.**, (2015), Investigating membrane fouling in both rotational and static MBR systems using empirical modelling, The 5th Oxford Water and Membranes Research Event - The Water, Food and Energy Nexus, Balliol College, Oxford University, Oxford.

Jones, F.A., and Paul, P., (2014). Calibration and Validation of a Fouling Model for a Rotating Membrane Bioreactor System, Proceedings of the 15th Aachen Membrane

Colloquium, Department of Chemical Engineering, RWTH Aachen University, Germany, p375-386.

Jones, F.A., and Paul, P., (2014). Development of a Comprehensive Fouling Model for a Novel Rotating Membrane Bioreactor System, Proceedings of the International Water Association (IWA) UK 15th National Young Water Professionals Conference, Manchester Metropolitan University, Manchester.

1.7. Organisation of the Thesis

Figure 1.1 gives an overview of this thesis structure and the various chapters it covers and their relationships. The arrows depict the link between chapters (the dashed arrows moreover mean that the comparative study is based upon fouling analysis of both MBRs).

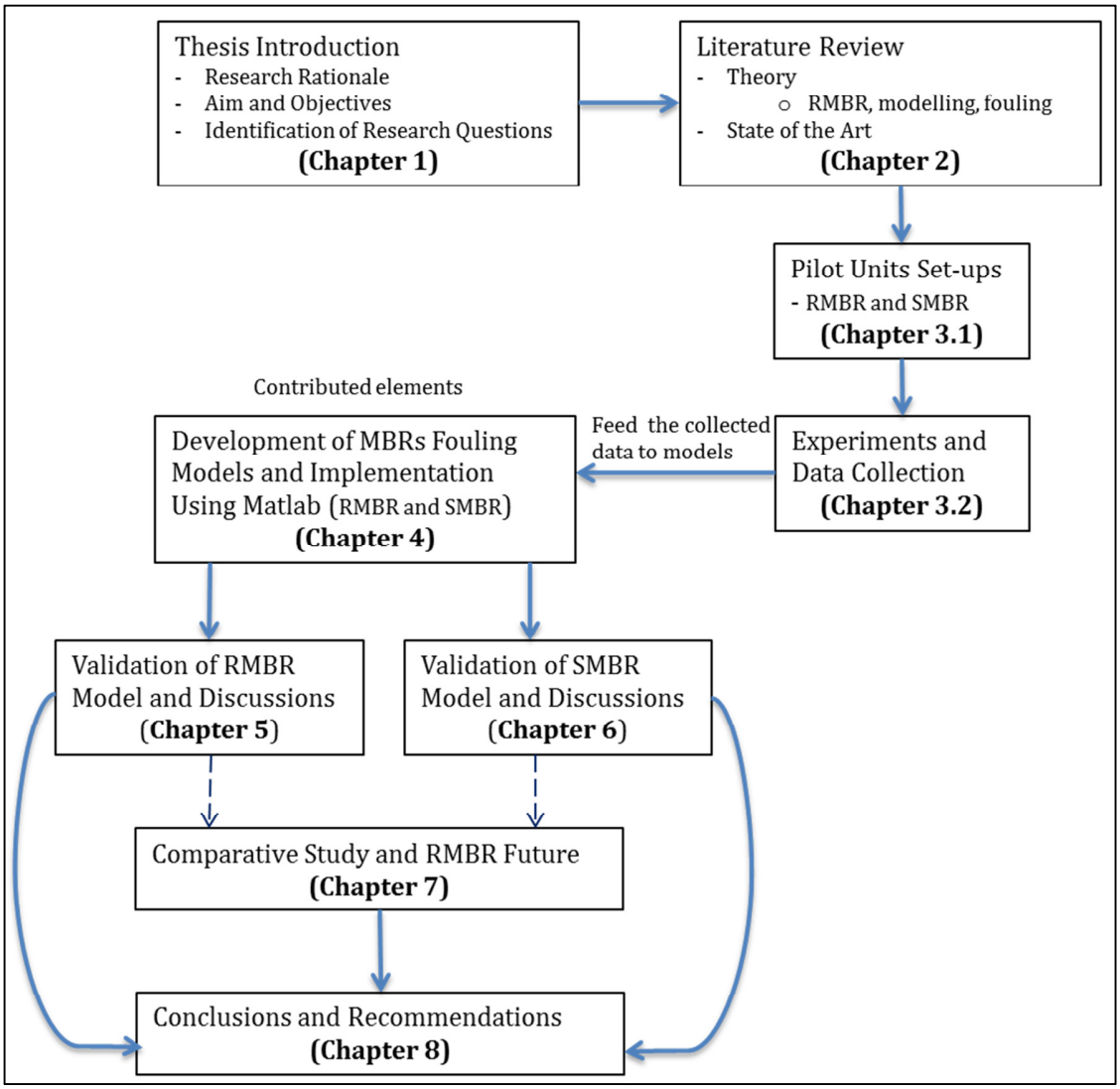

Figure 1.1. Thesis overview and its breakdown by chapter

The chapters of this thesis are briefly arranged as seen below:

Chapter 2 – The literature review, which covers both background theory and state of the art, is an essential part of this thesis. It provides the necessary theories for those unfamiliar with the topics and areas related to this research. As such, familiarisation with wastewater treatment, mathematical modelling and various aspects of fouling are reported here. The state of the art gives the readers and the author a general idea of the latest works that have been conducted in this field of research.

Chapter 3 – In this chapter, the setting-up of both pilot units (i.e. RMBR and square SMBR) are fully described. The experimental methods used for data collection (e.g. chemical oxygen demand and Camlab testing kits, TMP-stepping, clean membrane resistance, food to microbe ratio, MLSS, etc) are explained in full as well.

Chapter 4 – This chapter explores the models' structures of both MBRs (i.e. RMBR and SMBR). Consequently, the detailed overview and derivations of the formulae involved in the creation of the fouling models are demonstrated step by step. The software used and its accuracy in validating the models are also reported.

Chapter 5 – This segment focuses not only on displaying outputted results from simulations of RMBR models but also gives full-on discussions. Graphs obtained from the validation of the fouling model for the RMBR system under constant flux or constant TMP along with the incorporated hydrodynamic regimes and shear effects (including the model based on SMP as function of MLSS) are depicted and analysed. Everything discovered regarding the RMBR in terms of fouling is summarised here.

Chapter 6 – This chapter presents the outputted results from simulations of SMBR fouling model (bar the rotating effects) and discusses them. But prior to validation of the SMBR fouling model, two external data sources are used to verify it. Everything that was found regarding the SMBR in terms of fouling is outlined here.

Chapter 7 – The comparative study between a RMBR and SMBR system, a RMBR's usefulness to the industry in form of discussion and the microscopic view of the activated sludge flocs are highlighted in this chapter.

Chapter 8 – The general conclusions of this thesis, what have been learnt by the author and areas of future studies that could be used to further broaden this specific field of engineering are summarised and detailed in this chapter.

(The time management for this PhD research work, including key tasks, can be found in **APPENDIX A**)

CHAPTER 2: LITERATURE REVIEW

Wastewater (by extension wastewater treatment) is an exceedingly large area that covers multitude of topics. Consequently, understanding its inner workings is a must before attempting to conduct the PhD research work proper. In this chapter, a full literature review that includes the background theory is given in detail. Starting with the theory section, it is divided into three main sub-sections:

i. *Familiarisation with Wastewater Treatment Processes*: This part gives an insight of what to expect from common wastewater treatment methods (i.e. conventional WWTPs and activated sludge processes) and the huge family of MBRs which of course includes RMBRs.

ii. *Modelling*: This sub-section covers the various aspects of modelling in MBRs and what to expect from RMBRs.

iii. *Aspect of Fouling*: Vast and not well understood by the research community, fouling in this sub-section, summarises what is known so far and how they relate to RMBRs.

The state of art section reports relevant researches that have been conducted so far in the field of RMBR and conclusions that can be drawn from them. Finally chapter summary is a small section that gives an overview of this chapter (**note that** every major chapter save the "Introduction" and "Conclusions and Recommendation" will have this small section, so there is no need to reiterate).

2.1. Theory

Theory for wastewater treatment (including its related processes and technologies), which constitutes this thesis' building blocks, involves a sizable set of principles and definitions that one must grasp in order to delve further into the other aspects of this research work. The first step towards achieving that is to familiarise with the basics of wasterwater treatment processes.

2.1.1. Familiarisation with Wastewater Treatment Processes

Wastewater treatment has come a long way not only through the advent of new technologies but also processes as well. There is therefore a long road ahead if one wishes to familiarise with its chief ones. The beginning of familiarisation is the acquisition of basic understanding of knowledge; i.e., that of wastewater treatment.

2.1.1.1. Wastewater Treatment (WWT)

Wastewater, otherwise widely known as sewage, is 99.9% composed of water by mass. The contaminants in wastewater include suspended solids, biodegradable dissolved organic compounds, inorganic solids, nutrients, metals and pathogenic micro-organisms (Metcalf and Eddy 1972, Hammer 1975, Templeton and Butler 2011).

Naturally, the fundamental purpose of wastewater treatment is to remove the waste or pollutants from wastewater and household sewage, both as effluents, domestic, commercial and institutional by using engineering means to better safeguard the environment in a manner commensurate with economic, public health, social, and political affairs (Metcalf and Eddy 1972, EPA 2004).

Wastewater treatment processes or methods are commonly categorised as physical operations (i.e. physical forces are used to remove pollutants), biological processes (i.e. removal of pollutants by biological activities) and chemical processes (i.e. contaminants are removed by addition of chemicals or chemical reactions). These categorised processes are employed throughout the widely accepted four levels of wastewater treatment that are namely preliminary treatment, primary treatment, secondary treatment and tertiary or advanced treatment (Metcalf and Eddy 1972, EPA 2004).

Preliminary treatment is the first stage of wastewater treatment. This step aims to remove or to reduce the coarse solids in wastewater that may otherwise affect the normal operation of the treatment system (Parr et al. 2002, EPA 2004). After preliminary treatment, wastewater treatment is moved on to the next stage, the so-

called primary treatment. The main purpose of primary wastewater treatment is to remove the portion of the pollutants that will settle or float.

Physical operations such as sedimentation and fine screening are employed at this stage. The next stage of wastewater treatment after primary treatment is secondary treatment. Secondary treatment, at times known as biological treatment, comprises a wide range of attached-growth and suspended-growth biological systems, which are mainly designed to remove organic matter and suspended solids (Metcalf and Eddy 1972).

Being the final stage of wastewater treatment, tertiary or advanced treatment has but one purpose: to further improve the effluent quality before it is discharged to the receiving environment (e.g. ocean, lake, river, irrigation, ground). If the so-called effluent polishing (i.e. disinfection) process is employed, it is always the final process (Parr et al. 2002). Other steps include sand filtration, nutrient removal, disinfection (e.g. chlorination, ultraviolet or UV, ozone or O_3), nitrogen removal and phosphorous removal (Kothandaraman and Evans 1972, Hammer 1975, EPA 1976, Baker et al. 2002, Chaudhary et al. 2003).

2.1.1.2. Activated Sludge Process

By definition, activated sludge is a mass of micro-organisms (e.g. sludge particles) produced in wastewater by the growth of organisms in aeration tanks. This mass of micro-organisms is usually different from primary sludge in that the sludge particles contain many living organisms (e.g. bacteria, fungi, and protozoa, etc.) that can feed on the incoming wastewater (Beychok 1967, NESC 2003, Henze et al. 2008).

The activated sludge process was first discovered in 1913 in England by Arden and Lockett (Beychok 1967). But they first used the term activated sludge in 1914, when they published their findings (Arden and Lockett 1914). Although its usefulness was recognised, it was not until the late 1930s that this biological treatment process became widespread in the rest of the world (Benidickson 2011). Since then, the use of activated sludge processes has for the most part, solved the growing issue of wastewater treatments (Henze et al. 2008).

As Figure 2.1 shows, running a conventional activated sludge process (CAS) entails four organised components that are listed below (NESC 2003, Henze et al. 2008):

- An aeration tank where the biological reactions transpire.
- An aeration source that provides air, oxygen and mixing.
- A clarifier (tank or basin) where the solids settle, and are separated from treated wastewater.

- A means of collecting the solids either to return them to the aeration tank, a procedure known as return activated sludge (RAS), or to remove them from the process. This latter procedure is known as waste activated sludge (WAS).

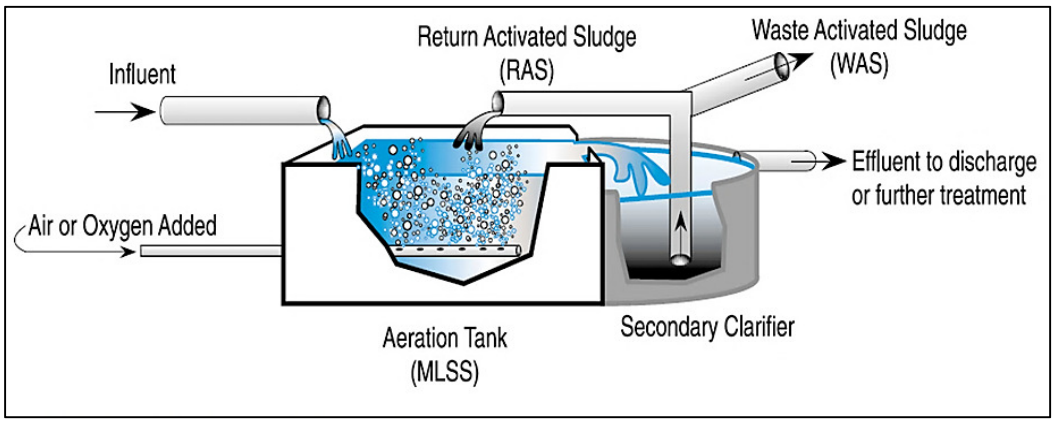

Figure 2.1. Schematic of a CAS (NESC 2003)

During an activated sludge process (Figure 2.1), air or oxygen is added to a mixture of screened wastewater combined with organisms to develop a biological floc (composed mainly of bacteria, fungi, protozoa and a range of other filter feeding species) that reduces the organic content of the wastewater (Sustarsic 2009). This combination of wastewater and biological mass is generally known as mixed liquor.

With adequate food (i.e. the biochemical oxygen demand of wastewater during decomposition occurring over a 5-day period or BOD_5) and oxygen, the aerobic bacteria multiply rapidly (von Sperling 2007). By the time the waste reaches the end of the tank (usually between four to eight hours), the bacteria have used most of the organic matter to produce new cells (NESC 2003).

The organisms settle at the bottom of the clarifier tank, separating from the clearer water. A portion of the bacteria is removed as it settles, and the partially cleaned water (known as supernatant) flows on for further treatment as required. The resulting settled solids, described as activated sludge, are returned to the head of the aeration system to reseed the new wastewater entering the tank (Sustarsic 2009).

This portion of the floc is commonly referred to as RAS. The excess sludge known as WAS, is removed from the treatment process to keep the ratio of biomass to food supplied in the wastewater in balance, and is further treated by digestion, either under anaerobic or aerobic conditions prior to disposal (Henze et al. 2008, Sustarsic 2009).

Aeration is not only an important part of an activated sludge system but also key to running other wastewater treatment processes as well. As broad definition, aeration is the process of bringing water and air into close contact in order to remove

dissolved gases, such as carbon dioxide, and to oxidise dissolved metals such as iron (Henze et al. 2008, Stenstrom and Rosso 2010). Aeration can also be used to remove volatile organic chemicals in water.

In activated sludge processes, aeration provides the dissolved oxygen (DO) and mixing of the activated sludge and wastewater in the aeration basin. The micro-organisms require DO in the system in order to carry out their metabolic processes, and to stabilise the organics (i.e. carbonaceous biochemical oxygen demand or CBOD) in the wastewater (EPA 1989, Henze et al. 2008).

Thus, there must be sufficient DO level not only for the free swimming and small clusters of microbes, but also for those microbes that are in the centre of larger flocs (Lindberg and Carlsson 1996). Most wastewater treatment processes hold DO levels between 2 to 3 mg/L. With anything above 3 mg/L, electrical power is usually wasted (Holenda et al. 2008). Table 2.1 shows typical DO levels used in wastewater treatment processes.

Table 2.1. DO levels commonly used in wastewater treatment processes (Wilén and Balmér 1999, Henze et al. 2008)

	Bulking potential	**Normal process**	**Nitrification process**
DO levels (mg/L)	Less than 1 mg/L	1 to 2 mg/L	2 to 3 mg/L

Activated sludge process is the suspended growth process that is commonly used in industrial and municipal wastewater treatment plants (WWTPs). This comes as no surprise for it offers many benefits (NESC 2003, Henze et al. 2008):

- It can yield high chemical oxygen demand (COD), biological oxygen demand (BOD) and nutrients removal rates when designed and operated according to local requirements. Indeed, this suspended growth process is capable of removing over 90% of suspended solids.

- This process has flexibility; thus, numerous modifications can be tailored to meet specific requirements (e.g. nitrogen removal or nitrification).

- Activated sludge process is the best documented and most commonly used form of secondary wastewater treatment.

- It can produce high quality effluents if the right capital costs are covered.

Despite its benefits, the activated sludge process has several drawbacks (Jeppsson 1996, NESC 2003, Gernaey et al. 2004):

- Its cleaning procedure can be very difficult (e.g. high biomass concentrations are kept in aeration tanks, making them irritating to remove).

- This process typically requires tertiary treatment. Thus, most WWTPs need at least three huge tanks (which temperature changes often affect greatly).

- There are issues of getting well settled sludge with this treatment process.

- With activated sludge process, huge economical costs are generally required to achieve the desired effluent water quality particularly at medium to large wastewater treatment facilities.

For further reading and information on activated sludge processes, please refer to:

- **Viessman Jr et al. 2008**: *Good material for knowing about factors affecting the settling of sludge.*

- **Ward 1996, Lin et al. 2009b, Zhang et al. 2009, Makowska et al. 2013**: *These materials should provide the reader with further insight on nitrification and denitrification processes.*

2.1.1.3. Membrane Bioreactors (MBRs)

As described by Stephenson et al. (2000), a membrane is commonly thought of as a material through which one type of substance can pass more readily than others, thus presenting the basis of a separation process. Figure 2.2 describes the biological treatment technology for the biological degradation of soluble organic impurities, namely MBR.

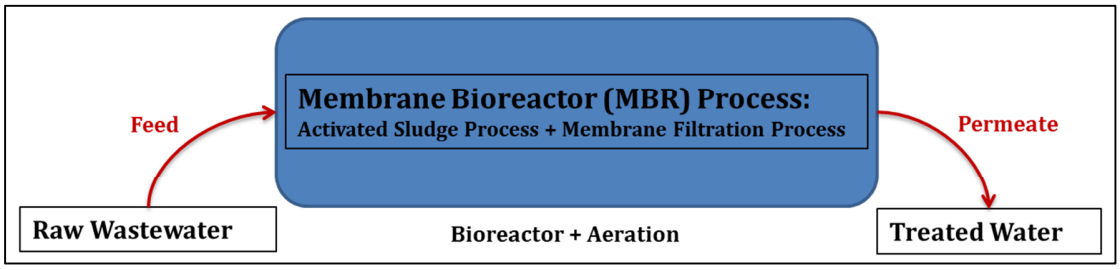

Figure 2.2. Simplistic yet typical MBR diagram

MBR is a treatment process involving the combination of membrane filtration (e.g. processes such as MF or UF) with a suspended growth bioreactor, typically activated sludge processes (Cicek et al. 1998). The membrane component uses low pressure MF or UF membranes, and for the majority eliminates the need for clarification and tertiary filtration.

The elevated biomass concentration in the MBR process allows for effective removal of both soluble and particulate biodegradable materials at higher loading rates. Thus, increased sludge retention times ensure complete nitrification even in extremely cold weather (Fenu et al. 2010).

Since development of the coupled activated sludge-membrane sewage treatment system by Dorr-Oliver in the late sixties (Smith Jr et al. 1969), and the introduction of their anaerobic MBR system in the early eighties (Sutton et al. 1983), MBRs have emerged as an alternative bioreactor configuration in cases where space and water resources are limited.

Initially, very low membrane flux and permeability, limited membrane life, high membrane costs, high capital and operational costs as well as inadequate knowledge on membrane application in wastewater treatment were predominant factors hindering broad application of the MBR technology. But, with the emergence of less expensive and more effective membrane modules and the implementation of ever tightening water discharge standards, MBR systems regained interest (Li et al. 2008). Over the years, MBR systems have had a wide variety of applications.

Some successful past applications involved solid-liquid separation (Yamamoto et al. 1989), water recycling in buildings (Kimura 1991), landfill leachate treatment (Manem and Sanderson 1996), municipal wastewater treatment for small communities (Buisson et al. 1998) and industrial wastewater treatment (Berube and Hall 2001).

Additionally, industrial applications have ranged from the removal of nitrogen to food processing wastewaters to the use of MBR technology to deal with organics in wastewaters originating from production of pharmaceuticals and/or manufacturing of polymeric membrane materials (Cicek 2003, Li et al. 2008). MBRs are beyond question innovative wastewater treatment technologies, and their widespread use in industry is understandable since they boast many benefits (Stephenson et al. 2000, Judd 2006, Hai and Yamamoto 2011):

- Slower growing organisms, such as nitrifying bacteria and those capable of degrading complex organics, can be readily maintained in MBRs.

- The small footprint of MBRs and the high quality effluent they produce make them particularly useful for water reuse applications.

- MBRs can be operated at higher mixed liquor suspended solids (MLSS) levels compared to conventional settlement separation systems, thus reducing the reactor volume to achieve the same loading rate.

- High mixed liquor concentration in the bioreactor allows wastewater to be treated efficiently at extended solids retention times (SRTs), thus minimising biomass yield.

- They have a rapid initial process start-up due to retention of all microbial seed material.

- MBR systems can be readily configured to achieve biological nitrogen and phosphorus removal if required.

- MBRs can function unattended except for occasional routine performance checks and maintenance of mechanical components.

Although MBRs are renowned technologies, using them has several disadvantages (Cicek 2003, Basile 2015):

- High operation and maintenance costs can make MBRs expensive (e.g. costly ceramic membrane units).

- When using MBRs, concentration polarisation and other membrane fouling problems can lead to frequent membrane cleaning (e.g. requires clean water and chemicals). This halts filtration operations.

- Since MBRs retain all suspended solids and most soluble organic matter, the activated sludge may exhibit poor filterability and settleability properties.

- When MBRs are operated at high SRTs, inorganic compounds accumulating in the bioreactor can reach concentrations that can be extremely harmful to the microbial population or membrane structure.

2.1.1.3.1. Membrane Systems, Membrane Separation Processes and MBR Operation Modes

Membrane systems are primarily divided into two groups: dead-end filtration and crossflow filtration systems (Li et al. 2008). Each of these filtration systems can be identified based on the feed stream's flow direction as shown on Figure 2.3.

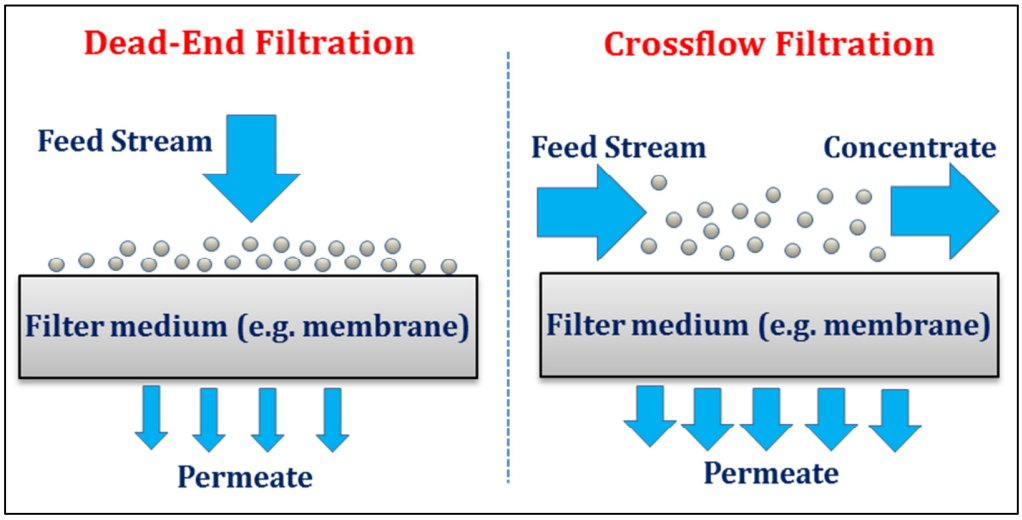

Figure 2.3. Dead-End and Crossflow filtration

During dead-end filtration (Figure 2.3 left), the feed stream applied to the membrane passes through it, obtaining permeate. Since there is no concentrate stream, all the particles that can be filtered by the membrane settle on its surface (Bertera et al. 1984). Raw feed water is sometimes used to flush the accumulated material from the membrane surface. Dead-end filtration is particularly effective when the feed water carries low levels of foulants. Many surface water filtrations, pre-treatment for seawater Reverse Osmosis (RO), and tertiary filtrations generally employ such filtration systems (Li et al. 2008).

Conversely, in crossflow filtration systems (Figure 2.3 right) feed stream is pumped with a crossflow tangential to the membrane, obtaining permeate streams and a concentrate (Koros et al. 1996). This filtration type is particularly effective when the feed stream carries high levels of foulants such as suspended solids and macro-molecules. As crossflow filtration systems tend to produce higher, more stable permeate rates compared to dead-end filtration systems, they are widely employed today (Li et al. 2008). They are therefore applied for the main membrane separation processes.

Membrane separation processes are typically classified into four categories based on the membrane pore size and the molecular weight cut-off (MWCO) of solutes said membrane can reject (Judd 2006, Gupta et al. 2008). These membrane separation processes are namely UF, MF, nanofiltration (NF) and RO. Table 2.2 summarises these membrane separation processes based on membrane pore size and MWCO of rejected solutes or particles by membrane (Judd 2006, Gupta et al. 2008).

Table 2.2. Classified membrane separation processes

Separation process	**Pore size (µm)[j]**	**MWCO (Da)[jj]**	**Type of particles removed**
UF	0.01 – 0.1	10^3 – 5 × 10^5	Cells, bacteria, macromolecules, proteins, viruses
MF	> 0.1	> 5 × 10^5	Oil emulsions, bacteria, particles, yeast, colloidal haze
NF	0.001 – 0.01	< 10^3	viruses, divalent ions, endotoxins, organic compounds
RO	< 0.001	< 100	Ions, salts, small organic molecules

[j], micrometre (micron) = µm; [jj], Da = Daltons

MBRs usually have two modes of operation: constant trans-membrane pressure (TMP) and constant flux. During constant TMP operation, deposition and fouling cause a decline in flux. The flux decline is initially rapid, but eventually becomes more gradual (Gupta et al. 2008). When constant flux operation is employed, the effect of deposition and fouling increases with TMP, which is initially gradual, but accelerates prior to cleaning (Judd 2006).

An additional semi-constant TMP mode is often employed. The modified constant pressure mode keeps the initial TMP just enough to obtain the target flux. If flux declines, TMP is raised slightly to obtain the target flux. This mode closely mimics the constant flux mode (Gupta et al. 2008).

2.1.1.3.2. Membrane Material and Membrane Module Shape

Available on the market, membranes used for filtration operations are typically made of organic (e.g. polymerics such as polyethylene, polyethersulfone, polyolefin), or inorganic (e.g. ceramic, metallic such as stainless steel) materials (Visvanathan et al. 2000, Basile et al. 2015).

Amongst inorganic materials, ceramics have seemingly been the focus of attention for quite some time now. The process of many industrial applications requires reliability, robustness and stability; and, the usage of ceramics guarantees just that. Unsurprisingly, ceramic membrane technology is frequently used as an adequate alternative selection for treating high strength industrial waters of low flow rates (Tolkou et al. 2014).

Organic membranes are most frequently applied in (waste)water treatment because of their cheaper manufacturing costs compared to ceramic membranes (which are roughly ten times more expensive than organic membranes). Amongst organic materials, Polyvinylidene (Di)fluoride (PVDF)s especially, are more widely utilised due to their thermal and chemical stability and low associated costs (Ji et al. 2015).

A summarised comparison between PVDFs and ceramics is presented in Table 2.3 (Kawai 1969, Janocha 1999, Stephenson et al. 2000, Zhu et al. 2009, Tolkou et al. 2014, Ji et al. 2015).

Table 2.3. Membrane material comparison: PVDF against ceramic

Comparative factor	**PVDF[z] (polymeric)** Chemical formula: $(C_2H_2F_2)_{ni}$	**Ceramic**
Maintenance	Easy to clean and replace	May require special chemicals or cleaning methods
Economics (Associated costs)	Cheap manufacturing costs means overall membrane cost is cheaper than ceramics (*~ one tenth of ceramic price*)	Expensive raw materials means overall membrane cost is high (*though often compensated for by a long service life*)
Performance	High permeate flux	High permeate flux (*sometimes higher than PVDF*)
	Low fouling	Low fouling (*in some cases, the presence of small particles have caused rapid fouling*)
	Robust (*good durability*)	Robust (*high durability*)
	Chemical stability (*high*)	Chemical stability (*high*)
	Thermal stability	Thermal stability
	High flexibility; Lightweight	Low flexibility; High weight
	Specifics: High dissipation factor; poor resistance to fuming acids	**Specifics**: Brittle nature (*high sensitivity to mechanical shock*)
MBR systems	crossflow	dead-end, crossflow
Membrane module shape	Flat sheet	Flat sheet (*dead-end*), tubular
MBR pore size	Mostly UF, MF but sometimes NF is used	UF, MF, NF

[z], C = Carbon, H = Hydrogen, F = Fluorine; $_{ni}$ = constant based on C-F and C-H bonds

MBRs are typically made of two primary parts; the biological unit responsible for the biodegradation of the waste compounds and the membrane unit (or module) responsible for the physical separation of the treated water from mixed liquor (Judd 2006). It is commonly accepted that membrane units come in three different shapes. These are namely hollow fibre, tubular and flat sheet membrane modules (Judd 2011). Figure 2.4a, b and c shows the three membrane module shapes used in MBR applications.

Hollow fibre membranes (Figure 2.4a) utilise numerous long porous strands that are packed inside a body. Each strand is narrow in diameter and quite flexible. They

usually are available only in the very low nominal MWCO ranges (Li et al. 2008). Tubular modules (Figure 2.4b) have tube like structures with porous walls, and are generally used to process demanding feed streams such as those with very high dissolved solids (e.g. oil, grease or fat) and suspended solids (Judd 2011).

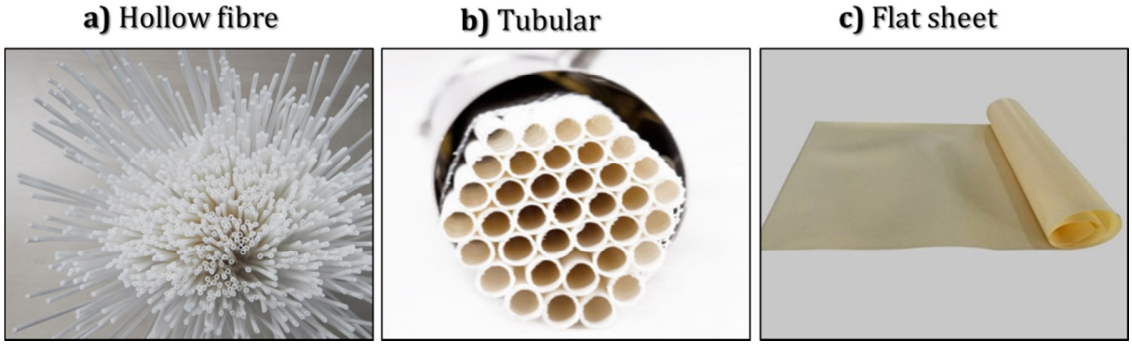

Figure 2.4. Typical flat sheet, hollow fibre and tubular membranes module (Source: a- Renovo Water, b- Xylem Flow Control, c- TECH INC)

Flat sheet membranes (Figure 2.4c) are quite versatile as they can handle the four main membrane separation processes (i.e. MF, UF, NF and RO). These membranes are known to produce high flux rates with reasonable capital costs (Li et al. 2008). They can further be divided into two groups: plate and frame and spiral wound.

Plate and frame modules are used for small to medium scale applications that deal with high membrane fouling potential (i.e. wastewater to be treated contains a high amount of fouling agents and/or has high viscosity). Oppositely, spiral wound modules are applied for applications that deal with low membrane fouling potential (Yoon 2015). Table 2.4 gives an overview of the main type of membrane modules that are used for MBR filtration operations.

Table 2.4. Membrane modules utilised in MBRs (Summarised from Judd 2006, Li et al. 2008, Yoon 2015)

Membrane module shape	**Module structure or operating method**	**Driving force**	**Membrane pore size**
Flat Sheet	Plate and frame	Pressure	MF, UF
	Submerged membranes	Vacuum	MF, UF, NF
	Spiral wound	Pressure	UF, NF, RO
Hollow Fibre	Contained in pressure vessels	Pressure	MF, UF, RO
	Submerged module without pressure vessels	Vacuum	MF, UF
Tubular	Pressure filtration	Pressure	MF, UF
	Vacuum filtration with bubbling	Vacuum	MF, UF

Like membrane modules, MBRs associated with them employ varied configurations. The main two MBR configurations will be highlighted in **sub-section 2.1.1.3.3**.

2.1.1.3.3. MBR Configurations: Side-Stream and Submerged

Traditional MBR configurations fundamentally consist of side-stream MBRs and submerged MBRs. In a side-stream MBR (sometimes referred to as external MBR), the membrane module is located outside the bioreactor (Basile 2015). The mixed liquor (e.g. biomass) is pumped through the membrane module and back to the bioreactor. The driving force here is the pressure created by high crossflow velocity along the membrane surface (Urbain et al. 1998, Cicek 2003).

While no longer mainstream, this MBR has had its fair share of past applications. An example of past application involved phenol degradation (Léonard et al. 1998). Phenol degradation rates of up to 120 $kg.m^{-3}.d^{-1}$ were achieved with this MBR configuration whilst allowing for improved control via independent adjustment of SRTs and no toxic effects of high phenol concentration were observed.

In a submerged (sometimes called immersed, internal or integrated) MBR, the membrane module is installed in either the main bioreactor or in a separate tank (Rosenberger et al. 2006). The aeration mode generates crossflow that scours the membrane surface and provides oxygen to the biomass (Radjenovic et al. 2008). Since the membrane module is directly placed into the process tank (resulting in a

less energy intensive system), it is essential to create a slight vacuum inside it for filtration (Yamamoto et al. 1989). This is measured as TMP.

Submerged MBRs are popular amongst researchers, and industrial and municipal WWTPs. This is because, they require less energy for filtration than side-stream MBRs, produce high quality effluent, have reduced footprint and low capital costs (Le-Clech et al. 2005). Some past applications for this MBR configuration included usage of inorganic coagulants to control membrane fouling (Wu et al. 2006), and aquaculture effluent reuse (Pulefou et al. 2008).

Table 2.5 below gives an overview comparison between side-stream and submerged MBRs (Côté et al. 1998, Jefferson et al. 2000, Lesjean et al. 2004, Judd 2006, Gupta et al. 2008, Li et al. 2008, Judd 2011, Hai and Yamamoto 2011, Yoon 2015)

Table 2.5. Summary comparison between side-stream MBRs and submerged MBRs

Comparative factor	**Side-stream MBRs**	**Submerged MBRs**
Market	Predominant before the 90s but now only hold a small market share	Mainstream and hold most of market share
Economics (Associated costs)	All around expensive (*high building costs for crossflow system; excessive energy costs needed for liquid circulation*)	Reasonably economical: (*consume less energy*; *hollow fibres seem cheaper than plate and frames)*
Energy consumption	~ 2 to 10 $kWh.m^{-3}$	~ 0.3 to 2 $kWh.m^{-3}$
Maintenance	Easy maintenance due to the accessibility of the externally installed membrane unit	Have online backwash (*often*) for quick membrane cleaning when fouled; but, hands-on chemical wash/cleaning can be a chore
Performance	Irregular flux rates (*often*); but, can produce provided high fluxes with right set-up	Capable of producing high fluxes (*usually*)
	Average, unstable filtration performance; constantly needs high crossflow velocity	Usually good, stable filtration performance
	Very susceptible to fouling	Air scouring is designed to reduce fouling; prone to clogging with hollow fibre membranes
	high biomass concentration	high biomass concentration
	A membrane operating life of seven years or more	A membrane operating life of five years may be possible
	Specifics: operators exposure to hazardous mixed liquor is limited	**Specifics**: operating conditions are very feasible; recycle pump is not needed
Membrane module shape	Tubular (*horizontal or vertical position*), flat sheet	Plate and frame (*flat sheet*), hollow fibre, tubular
Space or Footprint Requirements	Larger footprint; needs large space for set-up	Reduced footprint; less space needed for set-up results in compact system

For further reading and information on another MBR configuration, vertical airlift MBR (which unfortunately did not quite "take off"), please refer to:

- **Imasaka et al. 1989, Xu et al. 2002, Futselaar et al. 2007, Yoon 2015**: *Good reading materials for providing insight on the ins and outs of airlift MBRs*

2.1.1.3.4. Air Scouring and Intermittent Aeration in MBRs

Broadly speaking, aeration applied to MBRs serves two main purposes: the first is to provide oxygen transfer to the biomass and the second is to produce shear stress on the membrane surface to control fouling (Le-Clech et al. 2006, Li et al. 2008, Radjenovic et al. 2008, Böhm et al. 2012).

Hence, air scouring though a key technical challenge, is important in MBRs (especially submerged MBR). Air flow rate must be uniform across the nozzles so that the membranes above them are evenly scoured, or else, a localised membrane fouling occurs where the air scouring is not sufficient (Judd 2006, Yoon 2015). The areas affected by the fouling expand since the flux in unaffected zones must increase to compensate for the loss in fouled area.

As fouling rates are exponentially proportional to the flux, membrane fouling can spread very quickly across the membrane's cassettes. Thus, maintaining a uniform aeration underneath the membrane module is crucial for yielding stable membrane filtration (Judd 2006). But in order to reduce costs, air scouring must be managed. Periodic increase and decrease of air scouring flow rate is effective in reducing overall air scouring demand. This is a basic principle of intermittent aeration.

The overall aeration demand rate can be reduced with the intermittent aeration without increasing membrane fouling rate (Judd 2006). A perfect example of the implications of intermittent aeration can be seen through the study conducted by Guibert et al. (2002). They used hollow fibre immersed membrane modules to filter (i.e. UF) bentonite suspension. Their results showed that an intermittent aeration with 10 s – 10 s cycle produces less fouling rate (for fluxes up to about 52 LMH), a method which is often used by GE membranes (Yoon 2015).

By performing aeration for 50% of the total operating time, around 30% of net aeration saving can be achieved whilst not affecting membrane performance (Yoon 2015). According to Buer and Cumin (2010), this cycle time can be modified to 10 s – 30 s (10 s aeration and 30 s pause) to save even more air scouring under favourable conditions.

2.1.1.4. Rotating MBRs

RMBRs come in many forms, some of which are bespoke systems where a rotating disc operates near a stationary circular membrane or, regular systems where the membrane module rotates on a single shaft driven by a motor. In the latter case, the membrane module is typically made of circular-shaped membranes that are stacked together (Jaffrin 2008, Schuler 2009, Avanti Membrane Technology 2013). An example of this is shown on Figure 2.5.

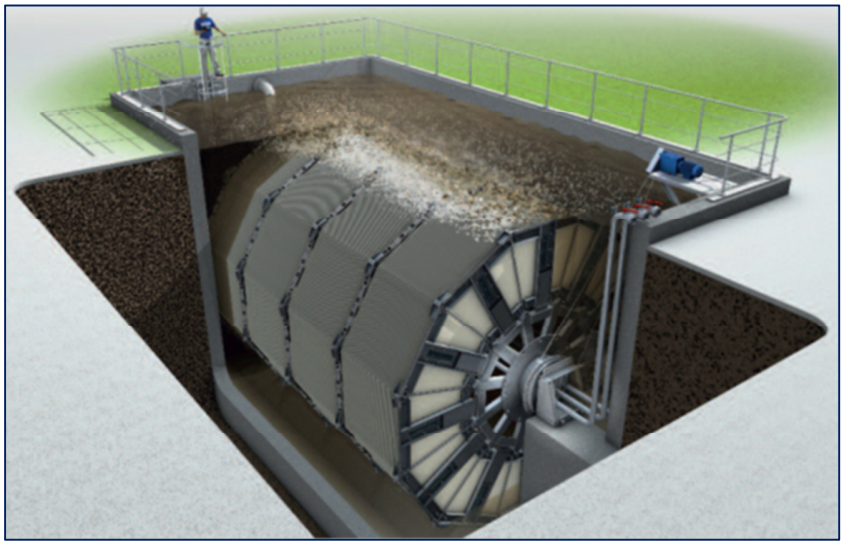

Figure 2.5. Huber's vacuum rotating membrane (VRM), a RMBR (Source: Huber Technology)

Generally speaking, investigating the impact of shear in MBRs is complicated by the complexity of shear generated in multi-phase systems. However, with (bespoke) RMBRs, the shear can be controlled by varying the rotational speed or the radial distance of membrane discs areas open for filtration (Aubert et al. 1993, Engler and Wiesner 2000, Jaffrin 2008, Jørgensen et al. 2014).

In RMBR systems, by applying a slight overpressure of 0.2 to 1.5 bar, the filtrate passes through the separation layer on the membrane disc outside in, and is drawn off via or along the shaft. The particle layer on the membrane surface is controlled by means of the centrifugal force field created (Serra et al. 1999). This enables the laminar particle layer adhering on the filter disc and thereby rotating together with the discs to flow off.

Thus, the particle layer is continuously renewed (Serra et al. 1999, Jaffrin et al. 2004). Simply put, the rotation of the membrane discs produces a shear at the membrane surface which scours the deposited materials from the membrane, thereby maintaining low resistance to flow through the membrane (Jaffrin et al. 2004, Sarkar and Bhattacharjee 2008).

RMBRs have been shown to produce high, very stable permeate fluxes in the MF, UF, NF or RO range (Bhattacharjee and Bhattacharya 2006). The reason is simple: RMBR systems generate high shear rates (e.g. up to 2×10^5 s^{-1}; sometimes much more) that are orders of magnitude greater than conventional UF MBR systems (Jaffrin 2008, Liu et al. 2012).

This in turn prevents cake formation (fouling by extension) and concentration polarisation in UF and NF (Ding et al. 2002, Jaffrin et al. 2004). It is worth mentioning that the effect of shear on RMBRs was confirmed by Aubert et al. (1993). They showed that on a rotating membrane disc, the back transport increases with shear stress on the membrane or cake surface due to shear induced erosion, which leads to a lower flux decline (Jørgensen et al. 2014).

RMBRs have also demonstrated that cleaning their membrane module via chemical backwash or bath once or twice a year is sufficient for all operations (Schuler 2009). Moreover, they have been shown to have relatively uniform TMPs (Bouzerar et al. 2003, Sarkar et al. 2011).

The main advantages of RMBRs seemingly stem from the so-called dynamic crossflow filtration which has significant effects on filtration performance when compared with conventional crossflow filtration (Kroner and Nissinen 1988, Bentzen et al. 2012). Figure 2.6 presents a visual representation of the clear difference between the two filtration types.

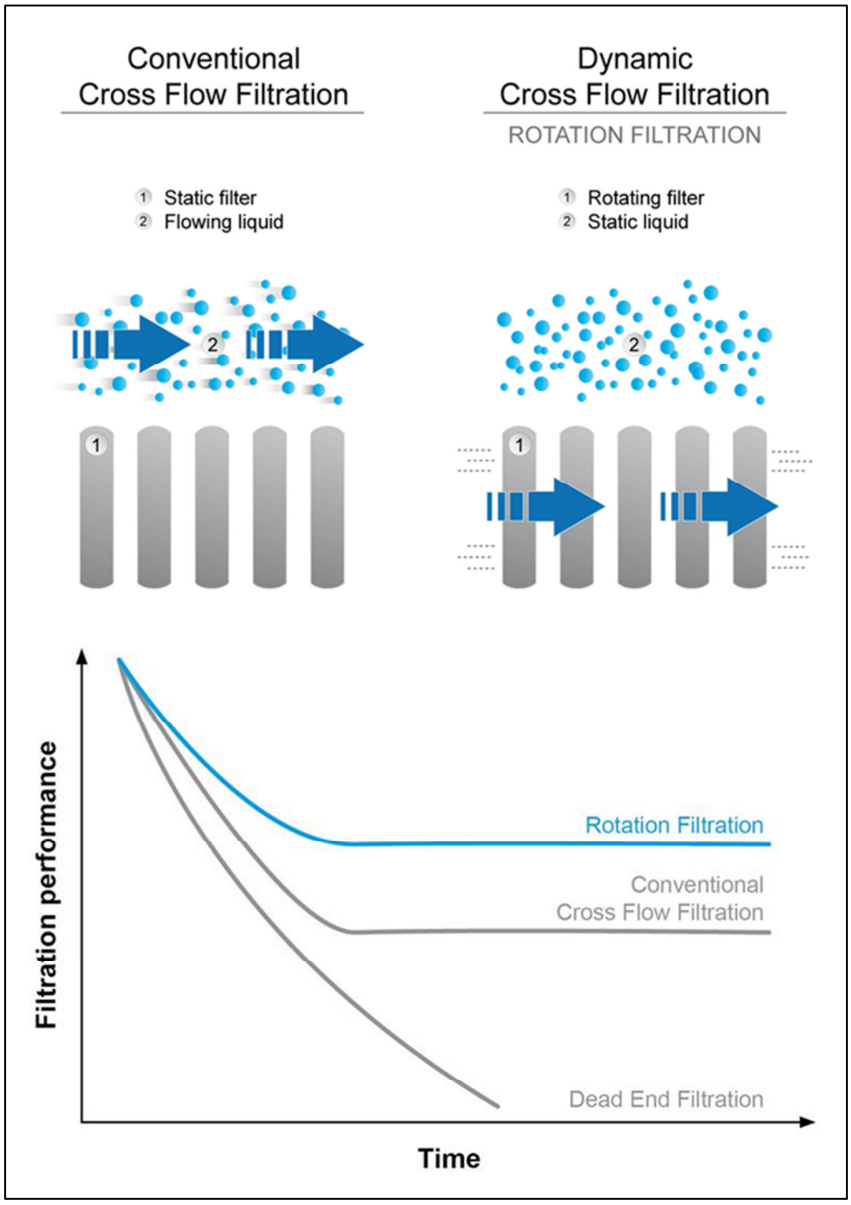

Figure 2.6. Dynamic crossflow vs conventional crossflow. The graph at the bottom indicates that RMBRs produce higher, more stable filtration performance when compared with conventional crossflow and dead-end systems (Source: kerafol.com, KERAFOL Keramische Folien GmbH)

Conventional crossflow (Figure 2.6 top left) systems require applying to the feed a pressure higher than that of permeate, together with a tangential fluid speed high enough to diminish solute accumulation on the membrane which might cause fouling (Li et al. 2008). But, a high tangential speed induces a high pressure drop along the membrane. This reduces the TMP in the downstream part of the membrane module and decreases the average permeate flux.

Conversely, in dynamic crossflow filtration (Figure 2.6 top right), the shear effects at the membrane are created by a moving part such as a disc or a rotor (Jaffrin et al. 2004, Jaffrin 2008) rotating near fixed membranes or by membranes rotating around a shaft (Kroner and Nissinen 1988, Jaffrin 2008). Because of this, RMBRs tend to boast larger filtration capacities when compared with conventional crossflow and dead-end filtration systems.

Using RMBRs has several disadvantages that include their high system complexity, high cost of manufacture and limited membrane area. In addition, the centrifugal force produced within the membrane discs creates a back pressure that may reduce their efficiency (Jaffrin et al. 2004, Sarkar and Bhattacharjee 2008). Due to their usefulness (as their benefits outweigh their setbacks), the applications of RMBRs have increased a fair amount over the years.

Past applications including research studies involved microbial suspensions (Kroner and Nissinen 1988), colloidal suspension of activated carbon (Aubert et al. 1993), oil wastes (Reed et al. 1997, Ebrahimi et al. 2013), water (Serra et al. 1999), skimmed milk (Ding et al. 2002, Jaffrin et al. 2004, Frappart et al. 2008, Luo et al. 2010, Meyer et al. 2015), polysaccharides produced by fermentation (Brou et al. 2003), mineral suspension (Bouzerar et al. 2003, Ding et al. 2006, He et al. 2007, Tu and Ding 2010), yeast suspension (Jaffrin et al. 2004, Liu et al. 2012), black liquor (Bhattacharjee and Bhattacharya 2006), synthetic sewage (Wu et al. 2008), wastewater reclamation (Zuo et al. 2010), dairy wastewater (Luo et al 2010), bovine serum albumin or BSA (Sarkar et al. 2011, Dutta et al. 2012), kaolin (Liu et al. 2012), chicory juice (Luo et al. 2013), sludge (Bentzen et al. 2012, Jørgensen et al. 2014), sugar beet juice (Zhu et al. 2016) and aqueous suspensions (Ji et al. 2016).

Configuration wise, many RMBR studies tend to favour flat sheet membranes (Reed et al. 1997, Serra and Wiesner 2000, Sarkar et al. 2011, Jiang et al. 2013). This is not surprising as flat sheet membranes are easy to maintain and quite versatile as they can handle the four main membrane separation processes (Li et al. 2008). Other configurations that have been employed include a rotating helical membrane (Liu et al. 2012) and a combination of crossflow filtration and centrifugal separation in a rotating tubular membrane (Ji et al. 2016).

In terms of materials used for RMBRs, membrane materials preferred have mainly been PVDFs (Engler and Wiesner 2000, Zuo et al. 2010, Luo et al. 2013) and ceramics (He et al. 2007, Bentzen et al. 2012, Ji et al. 2016). This is because PVDFs and ceramics yield high fluxes, although the latter often produce higher flux rates than the former. However, the low cost and fouling rate of, and the ease to cleaning PVDFs (Avanti Membrane Technology 2013, Ji et al. 2015), means that the more expensive ceramics (Tolkou et al. 2014) might eventually fall out of favour. In addition to the aforementioned two, other materials such as polyethersulfone and cellulose triacetate have been utilised as well (Bhattacharjee and Bhattacharya 2006, Dutta et al. 2012).

The energy a RMBR consumes depends on the membrane disc technology and size. The energy consumed per m^3 permeate (SED_r) by a single membrane disc can be determined with Equation 2.0 (Luo et al. 2010, Zsirai et al. 2016):

$$\begin{cases} SED_r = W_d/Q \\ W_d = 0.141.\, e^{0.000756.N_\omega} \end{cases} \quad (2.0)$$

Where,
N_ω, in rpm (revolution per minute), is the rotating speed of disc motor;
Q, in m^3/h, is the (permeate) flow rate; and,
W_d, in kW, is the sum of power of the rotating disc motor and feed pump (kW).

The values of SED_r found in research studies seem to range from 0.1 to 2 $kWh.m^{-3}$ (Espina et al. 2008, Tu and Ding 2010, Ratkovich and Bentzen 2013, Zsirai et al. 2016). When compared to conventional MBRs whose energy consumption ranges from 0.3 to 10 $kWh.m^{-3}$ (Côté et al. 1998), it is quite clear that RMBRs consume less energy. This assertion is in-line with researches done by Serra et al. (1999) and Jaffrin (2008). They concluded that a RMBR appears to consume low energy levels.

2.1.1.5. Synthetic Wastewater

Synthetic wastewater, also known as synthetic sewage (or waste), is an artificial wastewater that is made through chemical synthesis or a combination thereof (e.g. often combined with real wastewater components), to emulate natural wastewater or sewage, serve as influent feed source, or be used as a combination of both natural sewage and influent feed source (OECD 1992).

Various researchers have used synthetic wastewater in their studies in lieu of raw wastewater and for good reasons. For one, those who cannot access raw sewage can easily and readily make one in the lab. Secondly, because these waste solutions are prepared to meet certain demands, researchers can expect consistent data output. Thirdly, the handling of fabricated wastewater is much safer than the handling of raw wastewater (e.g. danger of possible bacterial infection with raw wastewater).

However, there are few issues that arise from using synthetic wastewater. Since many of them are so study specific, they are usually not reusable for another research. Moreover, there is cost related concern. Raw wastewater can be obtained for free (depending on the situation) whereas with artificial wastewater, special and specific ingredients need to be bought (e.g. chemicals) to meet requirements.

This makes synthetic wastewater pricy by comparison. Despite these setbacks, they have had a variety of applications over the years. Fruitful past applications (e.g. researches) are summarised in Table 2.6 in terms of synthetic wasterwater created.

Table 2.6. Synthetic wastewaters used in various research studies

References	Synthetic wastewater created	Application involved
Nopens et al. (2001)	Syntho was a mixture of synthetic wastewater and a minor fraction of pre-settled real domestic wastewater; the synthetic influent comprised of chemical compounds, food ingredients and trace metals	stability analysis
Ahn et al. (2006)	Glucose and ammonia as carbon and nitrogen sources with fixed COD	EPS and SMP formation degradation
Leitea et al. (2008)	Glucose-based substrate that was sometimes mixed with sodium bicarbonate	production of hydrogen and organic acids
Baghapour et al. (2011)	Sucrose-based synthetic wastewater that was prepared using beet sugar molasses (sucrose) as the main substrate and tap water	reduction of excess sludge production
Torres et al. (2013)	Saccharose and meat extract along with other chemical supplements	removal of organic matter and toxicity
Hou et al. (2014)	Glucose as carbon source, nutrients, trace metals and buffering compounds	stirring strategies on the sludge granulation
Lee and Gagnon (2015)	Salt and organic stock solution with the intent of emulating produced water from oil and gas production	design of electrocoagulation system

A conclusion that can be drawn from these research studies is that there is not a magical formula for creating a synthetic wastewater that will work for all MBRs and their associated filtered feeds (e.g. activated sludge). This is because one of the main factors affecting its creation is study requirements.

2.1.2. Modelling

Models are useful for making hypothetical predictions about a system as well as deducing the behavioural patterns of said system. In order to construct a successful model, the modeller must, to a considerable degree, understand the system's mechanics. To that end, technicalities related to the modelling of MBRs must be known.

2.1.2.1. Modelling of MBRs

Modelling and design of MBRs involve a number of parameters to take into account. However, the main ones normally used for modelling are: flux, TMP, food to microbe ratio (F/M), SRT, hydraulic retention time (HRT), MLSS and specific air and specific energy demand. Amongst them, flux has often been reported as the main parameter that controls or indicates the membrane performance and productivity (Chang et al. 2002, Braak et al. 2011).

By definition, flux, J, is the volume of permeate produced per unit area of membrane surface per unit time. Its SI unit is m/s though others are often used as well (i.e. litres/m^2/hour or LMH, gallons/square foot/day or gfd, m/d). The formula for this simplified version of flux can be calculated using Equation 2.1 shown in Table 2.7 below. The permeate flux typically declines with time and when this happens, the flux can be calculated using the resistance in series model (Jefferson et al. 2000, Chang et al. 2002).

The formula used for this model is in line with many other equations used in heat/mass transfer, electric current flow, etc, where flux is proportional to driving force (i.e. TMP) and inversely proportional to the resistances (Gupta et al. 2008). This is shown in Equation 2.2.

In systems where osmosis is present, it is possible to calculate the flux with the so-called osmotic pressure, which is defined as the pressure that needs to be applied to a solution to prevent the inward flow of water across a semi-permeable membrane (Gupta et al. 2008). Osmotic pressure is sometimes defined as the minimum pressure needed to nullify osmosis.

The reduction in TMP due to the effect of osmotic pressure is proportional to the decline in flux (Kedem and Katchalsky 1958). The formula for this flux is denoted by Equation 2.3. Flux in a membrane can also be limited by the phenomenon known as concentration polarisation. The flux can in this case be calculated by balancing the convective particle transport towards the membrane and diffusive particle back transport as shown in Equation 2.4 (Bian et al. 2000, Yoon 2015). Table 2.7 sums up the different flux model formulations.

Table 2.7. The various flux equations used in MBR models

Flux model	Equation	Reference
Simple (basic definition)	$J = \frac{Q}{A_0} = \frac{V}{A_0.t}$ (2.1)	Judd 2006
Resistance in series model	$J = \frac{TMP}{\mu.(R_{total})}$ (2.2)	Jefferson et al. 2000, Chang et al. 2002
Osmotic pressure	$J = \frac{TMP - \sigma'.\Delta\Pi}{\mu.(R_{total})}$ (2.3)	Gupta et al. 2008
Concentration polarisation	$J.C = -D_{eff}\frac{dC}{dx_a}$ (2.4) – $J_{SS} = -\frac{D_{eff}}{\delta_b}.\ln\left(\frac{C_p}{C_G}\right)$ (2.5)	Yoon 2015

Where,
A_0, in m^2 or ft^2, is the (total) membrane area;
C, in mg/L, is the particles' concentration;
C_p, in mg/L, is the particles' concentration in the bulk;
C_G, in mg/L, is the particles' concentration in the gel (or cake) layer;
D_{eff}, in m^2/s, is the effective diffusion coefficient. It conceptually includes the effects from thermodynamic diffusion, shear induced diffusion, and all other hydrodynamic forces that moves particles away from membrane surface;
J_{ss}, in m/s, is the steady state flux. This flux can be obtained by integrating Equation 2.4 using steady state boundary conditions, i.e., at $x_a = 0$, $C = C_G$ and at $x_a = \delta_b$, $C = C_p$;

Q, in m^3/s, L/h or m^3/d, is the (permeate) flow rate;
R_{total}, in m^{-1}, is the total membrane resistance. Its value is often equated to the sum of clean membrane, irreversible fouling and cake resistance; with each respectively denoted by R_m, R_i and R_{cake}, and each in m^{-1};
t, in hours (h), days (d) or seconds (s), is the (filtration) time;
V, in litres (L), gallons (gal) or m^3, is the (permeate) volume;
x_a, in m, is the axial coordinate or distance from axis to membrane surface;
δ_b, in m, is the boundary layer thickness (m);
$\Delta\Pi$, in bar or Pa, is the osmotic pressure difference;
μ, in Pa.s, kg/m/s or centipoise (cP), is the (fluid) viscosity;
σ', unitless (−), is the osmotic reflection coefficient.

In MBRs, TMP (bar or Pa), is defined as the average applied pressure from the feed to the filtrate side of the membrane or simply the pressure difference between two sides of a membrane. This indicates that TMP is merely the hydrostatic pressure

gradient across a membrane. TMP is denoted by Equation 2.6 as follows (Ho and Zydney 2002):

$$\text{TMP (bar)} = \left(\frac{P_{Fe} + P_{Re}}{2}\right) - P_{fi} \quad (2.6)$$

Where,
P_{fi}, in bar or Pa, is the filtrate or permeate pressure;
P_{Fe}, in bar or Pa, is the feed or inlet pressure; and,
$P_{Re,}$ in bar or Pa, is the retentate or outlet pressure.

SRT (in days, d) is the average time a unit of cell mass stays in the activated sludge system, and is based on the suspended solids. This is sometimes called sludge age. However, there is a minute difference between the two. That is to say, sludge age is based on what is in the aerator while SRT is based on what is leaving the activated sludge process, including the solids in the clarifiers (Baxter and Woodman 2009). SRT is an important design factor that provides a theoretical indication of how long the micro-organisms remain in the aeration tank.

Thus, sludge wasting should be carried out periodically to maintain the proper SRT (Sustarsic 2009). While early MBRs were operated at SRTs as high as 100 days with MLSS levels up to 30 g/L, the recent trend is to apply lower SRTs (i.e. 10 to 20 days). This results in more manageable MLSS levels (Judd 2006, Sustarsic 2009). Because of these newly set operating conditions, the oxygen transfer in and the pumping costs of MBRs have somewhat decreased and the overall system maintenance has been simplified. SRT can be calculated using Equation 2.7 below (Baxter and Woodman 2009):

$$\text{SRT (Days)} = \frac{\text{(pounds/day) of suspended solids in the system}}{\text{(pounds/day) of suspended solids wasted from system}} \quad (2.7)$$

HRT (hours, h) is the average time that a water molecule spends in the aeration tank. Changes in HRT of an activated sludge process can affect its biological activity (i.e. nitrification if performed). It is given by Equation 2.8 (Metcalf and Eddy 1991):

$$\text{HRT (hours)} = \frac{\text{Volume of the aeration basin } (V_b)}{\text{Influent flow rate } (Q_i)} \quad (2.8)$$

During activated sludge process, mixed liquor is defined as a blend of wastewater (that is raw, synthetic or settled) and activated sludge within the aeration basin. MLSS is the concentration of suspended solids in said mixed liquor (Basile et al. 2015). It is generally measured in milligrams per litre (mg/L) but sometimes grams per litre (g/L). The MLSS level can also be expressed in pounds (lbs). This is given by Equation 2.9 (Baxter and Woodman 2009):

$$\text{MLSS (lbs)} = \text{MLSS } \left(\frac{\text{mg}}{\text{L}}\right) \times \text{volume of aeration basin (MG)} \times 8.34 \quad (2.9)$$

Where, unit MG stands for million gallons.

Though MLSS is considered a critical operational parameter for aerobic MBRs (i.e. presence of air is required), its influence on fouling has not been consistent (Judd 2011). It does however, have a direct impact on viscosity (Judd 2006, Basile et al. 2015). Occasionally the MLSS is determined alongside the mixed liquor volatile suspended solids (MLVSS). MLVSS is typically defined as the micro-biological suspension within the aeration tank in an activate sludge process (Metcalf and Eddy 2003).

In other words, it is the portion of the MLSS that is actually eating the incoming food. The volatile solids concentration in a sample of mixed liquor will mainly consist of micro-organisms and organic matter (Bitton 1997). MLVSS shares the same units as MLSS. As a rule of thumb, the MLVSS/MLSS ratio generally ranges between 0.65 and 0.90 for an activated sludge process (Bitton 1997, Metcalf and Eddy 2003, von Sperling 2007). For MBR systems, this ratio seems to be around 0.75, sometimes much less (Judd 2006).

F/M is the ratio of the amount of food (BOD_5 or COD), expressed as kg (or lbs) of COD (or BOD) applied per day, to the amount of micro-organisms, expressed as the solids inventory in kg (or lbs) of volatile suspended matter (Doble and Kumar 2005). Because the F/M is a process control number that helps one determine the proper number of micro-organisms within a system, it is important to maintain it to ensure optimum plant operation (Metcalf and Eddy 2003).

A high F/M means there is a greater quantity of food relative to the quantity of micro-organisms available to consume that food but the bacteria will not form a good floc (Metcalf and Eddy 1991). Thus, operating one's system at a high F/M will typically result in poorly settled sludge. On the other hand, a low F/M means that there is a limited amount of food.

Only when the food supply is limited do bacteria begin to develop thicker slime layers and clump together to form flocs that settle well. The units of F/M are (mass of food)/(mass of microbes × time), or kg BOD_5/kg ML(V)SS/d. The F/M, expressed in kg BOD_5/kg MLSS/d, can be calculated using Equation 2.10 as follows (Metcalf and Eddy 1991, Doble and Kumar 2005):

$$\frac{F}{M} = \frac{BOD_5\left(kg/m^3\right) \times \text{influent flow rate } \left(m^3/d\right)}{\text{Solids } (kg/m^3) \times \text{Volume of aeration basin } (m^3)} \Leftrightarrow \frac{F}{M} = \frac{S_m.Q_i}{X_{org}.V_b} = \frac{S_m}{HRT.X_{org}} \quad (2.10)$$

Where,
S_m, in kg or lbs, is the substrate mass or COD or BOD_5 (i.e. food); and,

X_{org}, in kg/m^3 or g/L, is the micro-organism mass (kg or lbs) per litre or the MLSS level in the aeration basin.

Specific air demand based on membrane area or SAD_m (m^3/m^2/h) is defined as air scouring flow rate per membrane area and generally ranges from 0.18 to 0.60 (m^3 air/m^2 membrane area/h). SAD_m values that are close to 0.18 are obtained only with intermittent aeration (Côté et al. 2004). Its mathematical formula is given by Equation 2.11 as follows (Li et al. 2008, Judd 2011):

$$SAD_m = \frac{Q_{air}}{A_0} \tag{2.11}$$

Where,
Q_{air}, in m^3/h, is the air flow rate.

Specific air demand based on permeate volume or SAD_p (m^3 air/m^3 permeate) is defined as air scouring volume per permeate volume. SAD_p values often range from 7 to 24 or higher, and those close to 7 can only be obtained at favourable biological conditions with intermittent aeration (Judd 2011, Yoon 2015). SAD_p is particularly useful for industry as it is an indication of the cost performance of the membrane. It can be determined with Equation 2.12 (Judd 2011, Braak et al. 2011).

$$SAD_p = \frac{Q_{air}}{J.A_0} \tag{2.12}$$

Specific energy demand or SED (kWh.m^{-3} permeate) is defined as the energy spent per unit permeate volume and is therefore a direct indicator of the MBR's energetic and cost performance. It is proportional to SAD_p. Given an aerator system at a fixed depth in a tank, SED can be calculated with Equation 2.13 as shown below (Braak et al. 2011):

$$SED = \left(\frac{p_b.T_{air}.\lambda_a}{2.73\times10^5.\zeta_b.(\lambda_a-1)} . \left[\left(\frac{10^4 y_b + p_b}{p_b} \right)^{1-\left(\frac{1}{\lambda_a}\right)} - 1 \right] \right) . SAD_p \tag{2.13}$$

Where,
p_b, in Pa, is the blower inlet pressure;
T_{air}, in K (Kelvin) = °C + 273.15, is the air temperature;
y_b, in m, is the aerator depth;
ζ_b, in %, is the blower efficiency;
λ_a, unitless (−), is the aerator constant (~1.4).

The above formulae might be useful for modelling and designing MBRs; however, it is good practice to have reference values in order to run a MBR plant successfully. Table 2.8 provides further units for the F/M, which are inter-convertible using the

ratios of COD/BOD and MLVSS/MLSS. Generally, MBRs run at much lower F/M than CAS so as to mitigate membrane fouling and maintain high oxygen transfer efficiency (or sufficient aeration rate).

For instance, the preferred F/M range for MBRs is approximately one fourth to a half of that of CAS. For example, municipal MBRs typically run at F/M between 0.05 and 0.15 g BOD/g MVLSS/d whereas CAS operate at F/M ranging from 0.2 to 0.3 g BOD/g MVLSS/d (Brepols 2010). Table 2.8 depicts the preferred values for operation and design of MBRs and CAS. These values have been summarised from Cicek et al. (1999), Metcalf and Eddy (2003), Judd (2006), Brepols (2010), Hai and Yamamoto (2011) and Yoon (2015).

Table 2.8. Normally preferred values for design and operation of MBRs and CAS

Operation or design parameter	**Unit**	**MBR**[ii]	**CAS**
F/M	g BOD/g MLSS/d	0.04 - 0.12	0.16 - 0.24
	g COD/g MLSS/d	0.08 - 0.24	0.32 - 0.48
	g BOD/g MLVSS/d	0.05 - 0.15	0.2 - 0.3
	g COD/g MLVSS/d	0.1 - 0.3	0.4 - 0.6
MLSS	g/L	8.0 – 12.0	2.0 – 4.0
MLVSS	g/L	6.0 – 10.0	1.7 - 3.4
Flux	LMH	5.0 – 300	N/A[i]
SRT	d	10 – 30	5.0 – 10
HRT (Θ)	h	5.0 – 12	4.0 – 8.0
MLSS	g/L	8.0 – 15	2.0 – 4.0
DO level	mg/L	1.0 – 2.0	1.0 – 2.0
Sludge production	kg.(kg BOD)$^{-1}$	0.0 – 3.0	0.6

[i], N/A = Not Applicable; [ii], Applicable to MBRs in general

2.1.2.2. Modelling of Rotating MBRs

RMBRs involve the use of rotation to create shearing effects that must be accounted for in models on top of standard MBR equations. As described by Bentzen et al. (2012), viscosity is a property that influences the hydraulic regime and transport phenomena of fluids. It is defined as the ratio between shear stress and shear rate. The viscosity of Newtonian liquids such as water exhibits a linear shear stress and shear rate relationship. This relationship formula between both is thus given by Equation 2.14 (Bentzen et al. 2012):

$$\mu = \frac{\tau'}{\dot{\gamma}} \qquad (2.14)$$

Where,
$\dot{\gamma}$, in s^{-1}, is the shear rate (e.g. $d\gamma/dt$); and,

τ', in Pa, is the shear stress.

However, some particulate suspensions such as activated sludge are referred to as non-Newtonian fluids (Rosenberger et al. 2002). A non-Newtonian fluid is broadly defined as one for which the relationship seen in Equation 2.14 is not a constant. In other words, when the shear rate is varied, the shear stress does not vary in the same proportion (or even necessarily in the same direction). The viscosities of such fluids will therefore change as the shear rates are varied.

Activated sludge typically exhibit pseudoplastic behaviour (Rosenberger et al. 2002, Laera et al. 2007). This kind of fluid tends to depict decreasing viscosity with increasing shear rate and their flow behaviour type is sometimes known as shear-thinning (Yang et al. 2009). In attempt to characterise non-Newtonian behaviour, viscosity has been modified many times. The widely used models are Bingham (Equation 2.15), Casson (Equation 2.16), Power Law (Equation 2.17) and Herschel Bulkley (Equation 2.18). They are summarised in Table 2.9.

Table 2.9. Shear and viscosity equations typically used for modelling

Shear calculation model	**Equation**	**Reference**
Bingham	$\tau' = \tau_0 + \mu.\dot{\gamma}$ (2.15)	Yang et al. 2009
Casson	$\tau' = ({\tau_0}^{0.5} + K_a.\dot{\gamma}^{0.5})^2$ (2.16)	Seyssiecq et al. 2003
Ostwald (or power law)	$\tau' = m.\dot{\gamma}^n$ (2.17)	Bentzen et al. 2012
Herschel Bulkley	$\tau' = \tau_0 + m.\dot{\gamma}^n$ (2.18)	Steffe 1996

Where,
K_a, in $(Pa.s)^{0.5}$, is the consistency coefficient in Casson equation;
m, in $Pa.s^n$, is the flow consistency index;
n, unitless (−), is the flow behaviour index;
τ_0, in N/m^2 or Pa, is the yield stress.

Equation 2.17 is valid for shear-thinning, when $0 < n < 1$ (Steffe 1996). For an activated sludge in MBR, Rosenberger et al. (2002), proposed empirical models for m and n as function of the total suspended solids, TSS (g/L), as presented in the equation 2.19 below (Bentzen et al. 2012):

$$\begin{cases} m = 0.001.\, e^{2.TSS^{0.41}} \\ n = 1 - 0.23.\, TSS^{0.37} \end{cases} \quad (2.19)$$

Jaffrin (2008) did an extensive review of shear-enhanced membrane filtrations such as RMBRs. In his review, he denoted two formulae for the shear rate respectively for laminar and turbulent flow which are shown in Equation 2.20.

$$\begin{cases} \dot{\gamma}_l = 1.81.(k_\omega.\omega)^{1.5}.r.\nu^{-0.5} \\ \dot{\gamma}_t = 0.057.(k_\omega.\omega)^{1.8}.r^{1.6}.\nu^{-0.8} \end{cases} \quad (2.20)$$

Where,
r, in m, is the radius;
k_ω, unitless (−) or rad^{-1}, is the angular velocity factor;
$\dot{\gamma}_l$, in s^{-1}, is the shear rate for laminar flow;
$\dot{\gamma}_t$, in s^{-1}, is the shear rate for turbulent flow;
ν, in m^2/s, is the (fluid) kinematic viscosity;
ω, in rad/s, is the angular velocity.

The implications of viscosity lead to the phenomenon known as laminar flow. It is defined as the movement of one layer of fluid past another with no transfer of matter from one to the other; and, viscosity is the friction between these layers (Jaffrin 2008). In addition, there is a certain maximum speed at which one layer of fluid can move with relation to another, beyond which an actual transfer of mass occurs. This is known as turbulence (Andersson et al. 2001).

Flow regimes for Newtonian and non-Newtonian fluids that are either laminar or turbulent are determined by the Reynolds number (Re), and in the case of RMBRs, the so-called radial Reynolds number (Re_r). Also, this value depends on the radial distance, r_d (m), from a set spinning axis (acting as a reference line), and angular velocity. Their formulae are represented by Equation 2.21 as follows (Murkes and Carlsson 1988, Andersson et al. 2001):

$$\begin{cases} Re_{r,N} = \frac{k_\omega.\omega.r_d^2}{\nu};\ \nu = \frac{\mu}{\rho_N} \\ Re_{r,NN} = \frac{\rho_{NN}.(\omega.r_d)^{2-n}.r_d^n}{m} \end{cases} \quad (2.21)$$

Where,
$Re_{r,N}$, unitless (−), is the radial Reynolds number of Newtonian fluid;
$Re_{r,NN}$, unitless (−), is the radial Reynolds number of Non-Newtonian fluid;
ρ_N, in kg/m^3, is the density of Newtonian fluid;
ρ_{NN}, in kg/m^3, is the density of non-Newtonian fluid.

It is worth noting that the flow regime is considered laminar when $Re_{r,N}$ or $Re_{r,NN} \leq 2 \times 10^5$; and consequently, is turbulent when $Re_{r,N}$ or $Re_{r,NN} > 2 \times 10^5$ (Bentzen et al. 2012).

2.1.2.3. Model Calibration

Model calibration is generally understood as the estimation of model parameters to fit a certain set of data obtained from the full-scale WWTP under study (Gernaey et al. 2004). If model calibration is used for educational purposes or comparison of design alternatives for non-existing municipal WWTPs or other situations where qualitative comparisons are sufficient, default parameter values can be applied (Petersen 2000).

There are three model calibration approaches that can be utilised: the mathematical optimisation approach which relies purely on mathematical optimisation, the process engineering approach which is based on understanding of the process and the model structure and the BIOMATH calibration model (Petersen 2000, Vanrolleghem et al. 2003). In many cases, the result of model calibration is not a unique set of parameters but a parameter set that results in acceptable predictions of the effluent concentration, sludge production, and also the internal concentration dynamics (if data are available) for the WWTP under study (Vanrolleghem et al. 2003).

A major problem encountered in calibration of WWTP models is indeed the lack of identifiability of the model parameters. It therefore becomes important to obtain informative data that allow constraining the model parameters within realistic boundaries (Gernaey et al. 2004). The calibration of models has always not been well documented; however, Petersen et al. (2002) surmise that in order to conduct a proper model calibration, the following data and variables are needed:

i. *Design data*: Includes reactor volume, pump flows and aeration capacities.

ii. *Operational data*: Flow rates, as averages or dynamic trajectories, of influent, effluent, recycle and waste flows. Additional parameters include pH, aeration and temperatures.

iii. *Characterisation for the hydraulic model*: e.g. the results of tracer tests.

iv. *Characterisation for the settler model*: e.g. zone settling velocities at different MLSS concentrations.

v. *Characterisation for the biological model*: Sludge composition (e.g. VSS or COD), reaction kinetics (e.g. growth and decay rates), reaction stoichiometry (e.g. yields), etc.

In numerous WWTP model studies, the process engineering calibration approach is combined with the mathematical approach, by applying the sensitivity analysis (van Veldhuizen et al. 1999, Meijer et al. 2001, Petersen et al. 2002).

2.1.2.4. Modelling Simulation Software

Being able to create mathematical models is one thing, but implementing them is another entirely separate issue. In truth, knowing how to make a model is just as important as knowing how to implement it in order to obtain adequate results. This is where software programs come into play. Researchers have used a range of software packages to simulate their models over the years. The most commonly used simulation programs for wastewater treatment modelling are Biowin, GPS-X, Simba and Matlab & Simulink (Copp 2002, Judd 2011).

As described by Copp (2002), BioWin is a dedicated process simulator that makes use of linked process units to simulate biological wastewater treatment systems to predict potential effects of operational changes such as placing unit processes in and out of service or to evaluate the relative effectiveness of different facility upgrades. It was developed by EnviroSim as a Microsoft Windows™ application and appears to have a decent user base.

In fact, Latimer et al. (2008) have recommended the use of BioWin for the biological process design of large WWPTs that utilise MBRs. However, the underlining activated sludge models (Henze et al. 1987) of BioWin are not explicitly defined (Copp 2002), which could be disorientated for the user.

More user friendly than Biowin, GPS-X is described as a modular, multipurpose and advanced modelling environment for the simulation of wastewater treatment systems (Olsson and Newell 1999). It was designed by Hydromantis, and is supplied with a large number of models covering almost all system processes units found in wastewater treatment, including anaerobic reactors, nutrient removal, and several units for sludge operation.

It features a somewhat easy interface and comprehensive suite of wastewater models. GPS-X appears to be the best choice in wastewater process simulation for many as demonstrated by researches conducted by Nasr et al. (2011), Abdel-Kader (2013) and Zeng et al. (2013). However, it should be noted that the software's licensing fee per year is rather expensive.

Designed by ifak, SIMBA is a simulation environment based on Matlab & Simulink for the modelling of wastewater treatment systems (Olsson and Newell 1999). SIMBA extends Matlab & Simulink using block libraries for biological and chemical treatment processes (e.g. activated sludge, biofilm processes, chemical precipitation and sedimentation using different models, sewer systems).

SIMBA facilitates the definition of new user-defined conversion models using a formalised matrix format (FOX – Formal Open matriX format) which is based on the matrix format propagated by the published activated sludge models (Copp 2002).

Speaking of matrices, Matlab can manipulate them in various forms. MATLAB (MATrix LABoratory), as explained by Copp (2002) is a high performance language for technical simulation, and integrates visualisation and programming in a common environment. It is an interactive system that includes a large library of predefined mathematical functions. Matlab also provides the user with the possibility to extend this library with new functions.

The code for such functions are based on mathematical notation and can often be formulated in a fraction of the time it would take to write similar programs in a scalar language, such as C or Fortran (Olsson and Newell 1999). In short, for a moderate level (or an experienced) user, it is possible to simulate wastewater treatment processes (provided these models are appropriately implemented) with it as one would with any other wastewater treatment modelling software package.

As add-on software program, Matlab integrates Simulink for modelling, simulating and analysing any type of dynamic system (Copp 2002). Simulink provides a graphical user interface for building models as block diagrams and manipulating these blocks dynamically. It can also handle linear, non-linear, continuous-time, discrete time, multi-variable and multi-rate systems.

Additionally, the proficiencies of Simulink may be further extended by the use of S-functions which can be written in the Matlab language, C or Fortran, using a pre-defined syntax, and allow users to add their own algorithms to Simulink models (Jeppsson 1996). Despite its flexibility, Matlab has one major disadvantage; and that is its performance time. Every single line of an m-file is read and executed one after another, making it slow when compared to compiling languages such as C or Fortran (Jeppsson 1996).

2.1.3. Aspects of Fouling

Fouling is a complex mechanism that inevitably affects the filtration performance of MBRs over time. Hence, knowing and understanding its various aspects is not only important for better management of MBRs but also in modelling its overall effect in said MBRs.

2.1.3.1. Membrane Fouling

Figure 2.7 shows a typical membrane that has been fully fouled over time.

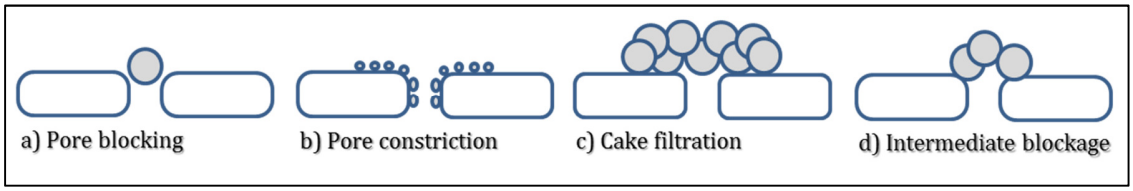

Figure 2.7. A typically fouled membrane

Over time, the filtration performance of a MBR unavoidably degrades. This is due to the deposition of soluble and particulate materials onto and into the membrane, which is attributed to the interactions between activated sludge components and the membrane (Judd 2006). This major drawback (and process limitation) remains one of the most challenging issues facing further MBR development (Chang et al. 2002, Fenu et al. 2010, Hai and Yamamoto 2011, Yoon 2015).

Fouling of membrane is a very complex phenomenon with diverse interlinkages among its causes. It is therefore very difficult to localise and define it clearly as well as to establish any kind of generic behaviour pertaining to it in MBRs (Pinnekamp and Friedrich 2006, Hai and Yamamoto 2011).

Membrane fouling leads to a significant increase in hydraulic resistance, manifested as permeate flux decline or TMP increase when the process is operated under constant TMP or constant flux conditions respectively. In systems where flux is maintained by increasing TMP, the energy required to achieve filtration increases. Alternatively frequent membrane cleaning is therefore required, increasing significantly the operating costs as a result of cleaning agents (Fenu et al. 2010).

Sometimes, a biofilm (or slime) can form onto the membrane's surface or inside it due to the growth or accumulation of micro-organisms (Pinnekamp and Friedrich 2006, Judd 2006, Zuthi et al. 2012). This is widely known as biofouling (or biological fouling). The organisms accumulate on the surface of the membrane using mostly extracellular polymeric substances or EPS (e.g. proteins, polysaccharides, lipids, nucleic acids).

This process can occur under either aerobic (i.e. requires the presence of oxygen) or anaerobic (i.e. absence of oxygen) conditions (Judd 2006). Understandably, the biofilm structure is quite complex. In general, biofouling causes a reduction in the membrane's permeability (and performance).

It is commonly accepted that there are two types of membrane fouling: reversible fouling and irreversible fouling (Ahn et al. 2006, Judd 2006, Zuthi et al. 2012). As mentioned before, fouling arises when materials either form a layer on the surface of the membrane or plug its pores. This leads to flux decline. Since the cake layer formed is for the most part readily removable from the membrane, if an appropriate physical cleaning protocol is employed, this is often categorised as reversible fouling (Chang et al. 2002, Zuthi et al. 2012).

Contrary to that, internal fouling caused by the adsorption of dissolved matter into the membrane pores and pore blocking, is considered irreversible and is generally only removed by chemical cleaning (Judd 2006). However, restriction of membrane fouling to reversible or irreversible may not always be appropriate. For example, Chang et al. (2002) commented that gel layer formation over a membrane surface is most often irreversible although it is notionally reversible since it forms a cake layer.

Some types of membrane fouling by pore blocking and adsorption may be partially reversible depending on the strength of adhesion and the vigour of the physical wash. Although the origin of fouling has yet to be truly defined, it is commonly believed by researchers that fouling is affected or caused by the following (Chang et.al 2002, Fenu et al. 2010, Zuthi et al. 2012, Basile et al. 2015):

i. *Membrane*: e.g. configuration, material, hydrophobicity, porosity and pore size, etc. As shown by Shimizu et al. (1990), membrane pore size can affect fouling. Moreover, larger pore size does not always lead to greater flux due to internal fouling (Chang et.al 2002, Judd 2006).

ii. *Biomass*: i.e. MLSS, EPS, soluble microbial products (SMP), floc structure, dissolved matter and floc size. High levels of MLSS mean faster formation of cake layer on the membrane surface. It should be noted that high levels of EPS or SMP will increase biofouling on the membrane. Furthermore, smaller particles combined with EPS can form a denser cake layer that will be harder to get rid of off the membrane surface.

iii. *Operating conditions*: e.g. configuration, aeration, HRT/SRT, TMP, etc. Flux is a main issue here. High flux rates mean faster formation of cake layer on the membrane surface. In addition, TMP rises more quickly when the unit is operated above the so-called critical flux. Membranes in general tend to operate better at sub-critical flux rates, but fouling is inevitable in long term operations.

While membrane fouling is still a challenging aspect within the field of MBR, there is another phenomenon that has a similar impact or effect on membranes. It is known as clogging (sometimes called sludging). By definition, clogging is the accumulation of particles (or solids) within the membrane channels (Judd 2006, Judd 2011, Gkotsis et al. 2014). Because the solids (or materials) are physically lodged between the surfaces of the membrane, typical chemical cleaning of fouled membranes does not necessarily work.

It has to be physically washed via jet cleaning or similar washing methods. As with fouling, clogging can also cause large decreases in membrane permeability. If the clogging is severe, it can generally be countered by removal of the membrane module from the bioreactor and cleaning its parts individually with a low pressure hose of some kind. However, there are risks of compromising the integrity of the membrane's fibres (Gkotsis et al. 2014).

2.1.3.1.1. Fouling Mechanisms

Flux decline rates are dependent upon fouling mechanisms the fouled membrane is subjected to. For the UF (or MF) of colloidal species under constant TMP, Hermia (1982) proposed four traditional fouling mechanisms. These classical fouling mechanisms are described through Equation 2.22 with a power law formula as follows:

$$\frac{d^2t}{dV^2} = k_f.\left(\frac{dt}{dV}\right)^{n_f} \Leftrightarrow \frac{d^2t}{dV^2} = k_f.(J.A_0)^{-n_f} \qquad (2.22)$$

Where,
k_f, unitless (−), is a constant in the power law model; and,
n_f, unitless (−), is an exponent characterising the model.

In the above model, for some constant k_f, when exponent n_f = 2, the fouling mechanism occurring is considered to be of pore blocking nature (Figure 2.7a). Additionally, when n_f = 0, 1 and 1.5, fouling mechanisms occurring are respectively considered to be cake filtration (Figure 2.7c), intermediate blockage (Figure 2.7d) and pore constriction (Figure 2.7b). Needless to say, during the course of the filtration process, n_f changes with time.

Ultimately whenever this happens, the relative importance of each fouling mechanism at a specific point during the filtration process becomes unquantifiable (Hermia 1982, Duclos-Orsello et al. 2006). In fouling models dealing with fouling mechanisms, composite fouling (i.e. more than one foulant or fouling mechanism working simultaneously) is a common occurrence (Gupta et al. 2008).

Consequently, depending on the composition of the fluid being filtered and the interactions between the membrane and bulk liquid, one fouling process may dominate over the others or conversely all fouling mechanisms may occur simultaneously during the filtration time (Duclos-Orsello et al. 2006).

In many cases, this appears to be the best way to determine the fouling mechanisms occurring within a MBR system. For instance, Ho and Zydney (2000) stated that one classical fouling mechanism may not be enough to accurately describe the fouling process over an entire filtration course.

During fouling there is an accumulation of particles, solutes, and colloidal species inside the membrane pores and on its surface. This leads to an obstruction of the membrane's pores by particles larger than said membrane's pores (Duclos-Orsello et al. 2006). This is referred to as pore blocking and is represented on Figure 2.7a.

In the pore blocking model, which is described by Equation 2.23 (Duclos-Orsello et al. 2006), the flux is shut-off by particle accumulations depositing on the membrane surface, and filtrate can only pass through the unblocked pore area.

As such, the rate of pore blockage is assumed to be proportional to the flow rate through unblocked pores, Q_u (m^3/s), and bulk concentration, C_b (g/L). The pore blockage parameter, α (m^2/kg), represents the membrane area blocked per unit mass of particles accumulation. As membrane fouls, Q_u decreases exponentially with time.

$$\frac{dA_u}{dt} = -\alpha . Q_u . C_b \qquad (2.23)$$

Where,
A_u, in m^2, is the unblocked membrane area. This is the membrane area which the particles have not blocked yet.

The intermediate pore blockage fouling mechanism shown on Figure 2.7d is similar to the complete pore blockage model and accounts for the possibility that particles can land on top of other deposited particles. In this case, the rate of pore blockage is assumed to be proportional to the ratio of the unblocked membrane area over the total membrane area. This is denoted by Equation 2.24 (Duclos-Orsello et al. 2006, Paul 2013):

$$\frac{dA_u}{dt} = -\alpha' . Q_u . C_b . \frac{A_u}{A_0} \qquad (2.24)$$

Where,
α', in m^2/kg, is the rate of pore blockage.

After the membrane has been fouled, a likely outcome is that the diameter of the membrane's open pores might be reduced. This is known as pore constriction and is portrayed on Figure 2.7b. This model denoted by Equation 2.25 (Duclos-Orsello et al. 2006), accounts for fouling that occurs in the internal structure of the membrane. With the pore constriction model, membranes are assumed to have straight through cylindrical pores. The rate of change of pore volume is assumed to be proportional to Q_u and C_b.

$$\frac{dV_p}{dt} = -\alpha_{in}.\, Q_u.\, C_b \qquad (2.25)$$

Where,
V_p, in m^3, is the pore volume. A scalar value for this volume equals $N_0.\, \pi.\, r_p^2.\, \delta_m$, with N_0 (−) being number of pores in membrane, δ_m (in m) being membrane thickness, r_p (in m) being radius of membrane pore;
α_{in}, in m^3/kg, is the volume of foulants deposited in the pore interior per unit mass of fluid filtered through the membrane.

Lastly, often there will be a deposition of layers of particles (i.e. build-up of solids) onto the blocked membrane's surface. This is the so-called cake filtration which is seen on Figure 2.7c. The cake filtration model, which is denoted by Equation 2.26 (Yuan et al. 2002), assumes that a uniform cake layer forms over the entire membrane surface. This fouling layer is permeable to fluid flow with resistance, R_b (m^{-1}). The rate of change in R_b is related to $J_b.f'.C_b$ (Yuan et al. 2002, Duclos-Orsello et al. 2006).

$$\frac{dR_b}{dt} = f'.\, R'.\, J_b.\, C_b \qquad (2.26)$$

Where,
J_b, in m/s, blocked flux
f', unitless (−), is a fraction of foulants contributing to particles deposit growth; and,
R', in m/kg, is the unit cake layer thickness per unit mass of fluid filtered.

There is also another aspect of caking that must be understood, namely the so-called cake layer compaction. The cake (or gel) layer that forms as a result of fouling onto a membrane's surface acts as a filtration barrier. It increases TMP at constant flux mode or decrease flux at constant TMP mode. This layer of gel not only grows thicker over time because of the solutes carried by the convective flow towards the membrane but it also becomes more compact, causing a moderate increase in filtration resistance (Yoon 2015).

Understanding the mechanism of cake layer compaction is crucial to understanding the cause of performance loss in MF or UF. The pressure drop, ΔP (Pa or N/m^2),

through the cake layer can be calculated with the Carmen-Kozeny formula denoted by Equation 2.27 (Yoon 2015):

$$\Delta P = \frac{5.\mu.S_0^2.(1-\varepsilon_c)^2.J}{\varepsilon_c^3}.\Delta l \quad (2.27)$$

Where,

Δl, in m, is the cake layer's depth.

According to Equation 2.27, ΔP increases as specific surface area, S_0 (m^{-1}), increases and cake porosity, ε_c (−), decrease under a constant flux. S_0 is also known as surface area per volume that increases when particle size decreases. By definition, ΔP through the cake layer equals to the force squeezing the unit area of cake layer, which is expressed as N/m^2.

Thus, the higher ΔP is, the stronger the squeezing force to the cake layer becomes (Tarabaraa et al. 2004, Li et al. 2012, Yoon 2015). As water flows through the cake layer, it becomes exposed to the force that squeezes it. According to Tiller (1953), cake layer compaction can be highlighted in three phases as shown below:

- The pressure drop in a cake layer is a dynamic phenomenon that occurs only when water moves through the cake layer. The effective squeezing force to the cake layer is proportional to the pressure drop in the cake layer, if all other conditions remain constant.

- TMP does not directly affect the cake layer compaction and instead flux rate is directly correlated with the force squeezing cake layer.

- Cumulative solids compression effect exists toward the bottom of cake layer since the squeezing force in one sub-layer transfers to the next sub-layer.

2.1.3.1.2. Mitigation Methods

Since fouling is a phenomenon that tends to lead to increase in energy consumption, high chemical consumption and short membrane life expectancy, it must therefore be managed in order to sustain operation of MBR systems; hence, why mitigation measures are required (Judd 2006). Mitigations come in many different forms.

For instance, coarse bubble aeration or air sparging is used to scour the surface of the membranes to control biofouling (Li et al. 2008). As the bubbles generated by aeration are essential for suppressing build-up of cake layer due to fouling, most submerged MBRs employ configurations that allow membrane surfaces to come into contact with air bubbles, which then induce moderate shear stresses (Ueda et al. 1997, Bouhabila et al. 1998, Günder and Krauth 1998).

A less utilised mitigation process is gas sparging. Defined as injection of gas (usually air) to induce a two-phase flow or introduce large air bubbles, gas sparging has proven to be an effective and yet simple technique for enhancing MF and UF processes (Chang and Judd 2002). This can help maintain a stable permeate flux over longer time periods. The two-phase flow pattern depends on the air-injection factor, ε_a (−). Its formula is represented by Equation 2.28 (Chang and Judd 2002) as:

$$\varepsilon_a = \frac{Q_g}{(Q_g + Q_l)} \tag{2.28}$$

Where,
Q_g, in m^3/s, is the superficial gas flow rate; and,
Q_l, in m^3/s, is the liquid flow rate.

The flow pattern is categorised according to the value of ε_a (Cabassud et al. 2001, Chang and Judd 2002) as follows:

i. *Bubble flow*: $\varepsilon_a < 0.2$, air bubbles are dispersed in the liquid phase.

ii. *Slug flow*: $0.2 < \varepsilon_a < 0.9$, flow comprises alternate slugs of gas and liquid.

iii. *Annular flow*: $\varepsilon_a > 0.9$, continuous gaseous phase occupies the centre of the pipe.

Some studies have shown that slug flow is the most efficient regime for significant enhancement of flux (Mercier et al. 1997, Chang and Judd 2002). The usage of gas bubbling (i.e. gas-liquid, two-phase flow) to enhance the performance of various membrane filtration processes has been extensively employed and reviewed by Cui et al. (2003). Nevertheless, in MBR systems, many fundamentals of multi-phase flow are still unknown and difficult to observe experimentally.

Consequently, the rates of aeration that are applied to MBRs are judged according to previous experiences and manufacturers recommendations (Drews 2010). In RMBR systems, for the most part, rotation of membrane discs produces a scouring effect (i.e. increases in shear stress prevent particles adhering to the membrane surface) that helps reduce fouling (Jaffrin et al. 2004, Bentzen et al. 2012).

Even with the aforementioned built-in membrane fouling preventions or MBR enhancement features, further anti-fouling methods may still be needed to lessen huge membrane fouling harms caused via membrane filtration processes, which will inevitably happen. Membrane anti-fouling stratagems come in the dozens and for the most part appear to be fairly effective. They are described as follows (Judd 2006, Li et al. 2008, Gupta et al. 2008, Hai and Yamamoto 2011):

i. *Intermittent permeation (or relaxation)*: The filtration is stopped at regular time interval for couple of minutes before being resumed. Particles deposited on to the membrane's surface tend to diffuse back to the bioreactor; this phenomenon being increased by the continuous aeration applied during this resting period. Relaxation allows filtration to be maintained for longer period of time before the chemical cleaning of the membrane is performed.

ii. *Backwashing (backflushing)*: In traditional backwashing, permeate water is pumped back to the membrane, and flow through the pores to the feed channel, dislodging internal and external foulants. Marcucci et al. (2001), cleaned UF membranes by backwashing for 90 seconds at every 20 minutes under a 0.4 bar TMP. Backwashing can also be performed with air. In this method, pressurised air in the permeate side of the membrane builds up and releases a significant pressure within a very short period of time.

Air typically does not go through the membrane. If it did, the air would dry the membrane and a rewet step would be necessary by pressurising the feed side of the membrane. Moreover, backwash can be enhanced with chemicals. That is to say, a low concentration of chemical cleaning agent can be added during the backwashing period. Backwashing increases the operating costs since energy is required to achieve a pressure suitable for permeate flow reversion.

iii. *Back pulsing:* Frequency impulses (normally 0.1 to 2 Hz) can be applied over the membrane for very short periods, resulting in efficient removal of fouling (or dirt) layer. This method is most commonly used for ceramic membranes. The problem with this technique is that it requires high pressure resistant membranes.

iv. *Chemical cleaning*: Unfortunately, relaxation and backwashing effectiveness will ultimately decrease with operation time as more irreversible fouling accumulates on the membrane surface. Therefore, chemical cleaning may also be required. This anti-fouling method involves the use of chemical cleaning agents such as sodium hypochlorite (NaOCl), citric acid, or alkaline compounds. The membrane can thus be chemically cleaned with a slightly diluted solution of nitric acid at room temperature.

Cicek et al. (1998) reported that a ceramic membrane required weekly cleaning for about two hours using 5.25% NaOCl heated to 60 – 80 °C along with concentrated nitric acid. Conversely, Bouhabila et al. (2001) showed that in case of less permeability, membrane can be soaked in chloride water (e.g. 2000 mg/L Cl_2/L) for 24 hours. In a different study, Zuo et al. (2010) chemically flushed their rotating PVDF membrane module with water, NaOH and HCl. They recovered 90% of their original operation flux.

v. *Mechanical cleaning*: This strategy involves washing (or cleaning) the fouled membrane mostly without reliance on chemical cleaning agents. Some past examples involved the use of plastic particles (Rosenberger et al. 2011) and moving beads (Shim et al. 2015).

2.1.3.2. Membrane Fouling in MBRs

Membrane fouling in MBRs tends to display varied and often peculiar behavioural patterns, one of which is the sudden TMP rise or the so called TMP jump.

2.1.3.2.1. TMP jump and Critical Flux

Braak et al. (2011) described the membrane fouling behaviour of a MBR operated under constant flux operation mode in three stages as follows:

i. *A fast but short rise in TMP*: Conditioning fouling. Strong interactions, among which adsorption, between the membrane surface and colloids including EPS, cause initial fouling and pore blockage.

ii. *A long period during which TMP augments slightly*: Slow, steady fouling. The particles settle on the membrane surface and form the cake layer. The duration of the second step, or sustainability time, depends on the permeate flux (Guglielmi et al. 2007).

iii. *A very strong rise of TMP*: TMP jump. During the previous step, permeability is not much affected but fouling is not uniform. Some areas suffer stronger fouling because of flux heterogeneities along the membranes. This is a self-accelerating phenomenon, which leads to exponential fouling. TMP jump could also be induced by a sudden change in the biofilm developed in the membrane (Hwang et al. 2008).

Over the years, many theories have attempted to explain the sudden TMP rise. The best known theories (or models) that researchers have come up with are detailed below as follows (Judd 2006, Li et al. 2008, Yoon 2015):

i. *Area loss (Inhomogeneous fouling) model*: The area loss model attempts to explain the observed TMP profiles in nominally sub-critical filtration of upflow anaerobic sludge. The TMP jump appears to coincide with a measured loss of local permeability at different positions along the membrane, due to slow fouling by EPS. This model also argues that the flux redistribution (to maintain the constant average flux) results in regions of sub-critical flux and consequently in rapid fouling and TMP rise.

ii. *Pore loss model*: This model is based on the same concept as the area loss model. But, while the area loss model considers macroscopic redistribution of flux, the pore loss model focuses on microscopic scale. In MBR systems, it is expected that both mechanisms occur simultaneously.

iii. *Percolation model*: The macromolecules passing the cake layer can deposit inside it and reduce cake porosity. Once cake porosity reaches a threshold level, permeability of the cake reduces sharply and TMP must rise to keep a constant flux.

iv. *Osmotic pressure model*: In RO, once ions pass cake layer and are rejected by the membrane, back diffusion to the bulk is restricted due to the hindrance of cake layer. Consequently, ions tend to accumulate near membrane surface. Likewise, the cake layer formed by EPS and SMP on MF or UF membranes can restrict the back diffusion of charged molecules in the cake layer.

v. *Quorum induced biofouling*: Micro-organisms communicate with each other using small molecules called quorum and change metabolic activity or state as a whole group depending on environment.

   There are various types of quorums, but N-Acyl homoserine lactone has been identified as a main quorum related to cake layer compaction (i.e. cake layer being exposed to a squeezing force). There is no firm consensus on this theory yet, but it is interesting to note that the AHL content in the cake layer of hollow fibre membranes is strongly correlated to the TMP.

The TMP jump has also been explained by poor oxygen transfer existing within the fouling layer (Judd 2011, Gkotsis et al. 2014). As a result of transfer limitation, micro-organisms present within the biofilm layer can die, thus releasing extra levels of SMP. Experimental data have shown an increase in SMP concentration at the bottom of the fouling layer when the level of DO declines (Judd 2011).

In addition to TMP jump, there are various flux types that are related to membrane fouling in MBRs. These include: critical flux, sustainable flux, limiting flux, threshold flux and critical flux for irreversibility. Figure 2.8 depicts the various flux types that are linked to membrane fouling in MBRs and briefly summarises them.

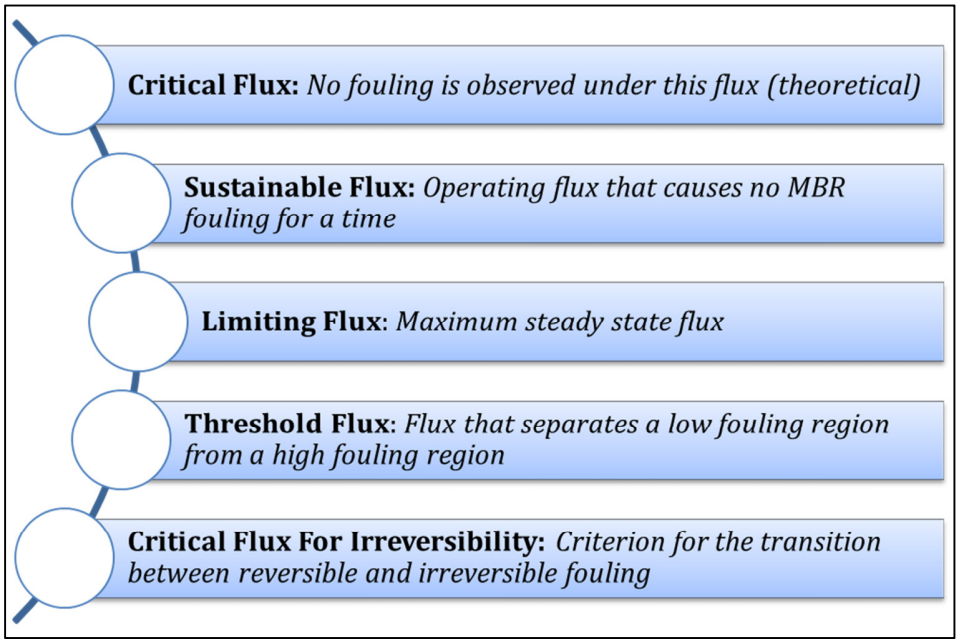

Figure 2.8. Fouling related flux types

The concept of critical flux, which was introduced by Field et al. (1995), may eventually be an important parameter in understanding membrane fouling in MBRs. critical flux (Figure 2.8 top) is defined as the permeate flux of a membrane system under which no or little fouling is observed. The region below the critical flux is known as sub-critical region. Filtration within this region is desirable for membrane fouling can be neglected. Thus, the membrane system could be operated in a totally clean regime.

Hence, membrane cleaning is not required and overall MBR plant design could be simplified (Judd 2006). Needless to say, operation above the critical flux causes fouling which reduces flux back to the critical value over time. Increasing TMP to compensate for flux decline only serve to increase the flux for a transient period with the stable flux eventually falling back to the critical flux. It is thus important to choose an adequate initial permeate flux.

Critical flux tends to depend on factors such as hydrodynamics, particle size, suspension properties (i.e. pH, salinity and conductivity) and interaction between colloids and membrane (Li et al. 2008). The hydrodynamics of the system especially are important in determining the critical fouling point (Muller et al. 1995, Gupta et al. 2008). True critical flux rarely exists in practical filtration because the feed water contains various foulants that can interact with the membrane surface even before water permeation begins (Judd 2006, Yoon 2015).

For example, macromolecules with very low back transport velocity continue to deposit at any flux condition (Zhang et al. 2006). Chang et al. (2002) further commented that while the critical flux concept has proven to be an invaluable tool in

conventional membrane process design, its validity is very questionable in MBR processes where fouling rates only approach zero at very low flux, and ultimately, impractical values.

Thus, the term sustainable flux is often used instead of critical flux to indicate a flux that can last a considerable amount of time without causing much membrane fouling (Fane 2002). The limiting flux is the maximum flux that can be achieved at steady state in an operation, and corresponds to a value of flux for which the critical flux is reached at all points of the membrane surface (Judd 2006, Jørgensen et al. 2014). As such, its value may be equal to that of critical flux.

As Field and Pearce (2011) broadly described it, threshold flux can be thought of to be the flux that divides a low fouling region from a high fouling region. This may be linked to both the critical and sustainable flux concepts (Field and Pearce 2011, Luo et al. 2013). In their research study, Luo et al. (2013) commented that threshold flux may be independent of membrane pore size, permeability and fouling. They further added that both limiting flux and flux fluctuations should be avoided in practical applications because they cause high fouling and flux declines.

Finally, critical flux for irreversibility is defined as a criterion for the transition between reversible and irreversible fouling (Luo et al. 2013). It seems, critical flux for irreversibility and threshold flux are more relevant to industrial applications as both extremely low flux with no fouling and high flux with awful fouling are not desirable (Bacchin et al. 2006, Luo et al. 2013).

2.1.3.2.2. EPS and SMP

There have been on-going debates on what truly causes fouling in MBRs but, amidst those debates, two terms have always been recurring. They are namely EPS and SMP, both of which are represented on Figure 2.9 by a simple diagram.

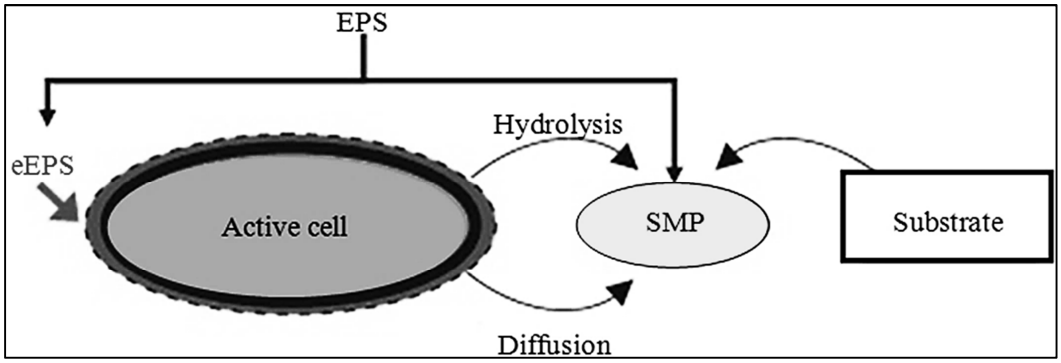

Figure 2.9. Fairly simplified schematic of EPS, extracted EPS (eEPS) and SMP (Le-Clech et al. 2006, Gkotsis et al. 2014)

EPS are commonly believed to be a very complex mixture of proteins, lipids, deoxyribonucleic acid, acid and polysaccharides (Le-Clech et al. 2006, Judd 2006). They surround cells, create a matrix for the microbial flocs and films, and allow the micro-organisms to live continuously at high cell densities in stable mixed population communities (Laspidou and Rittmann 2002).

EPS are further divided into two classes: bound EPS which are defined as fraction bound to the sludge flocs; and soluble EPS which are defined as fraction able to move freely between sludge flocs (Rosenberger and Kraume 2002). In MBRs, bound EPS co-deposit together with bacterial cells on filtration membranes and potentially form a compressible cake with high hydraulic resistance and consequently lead to membrane fouling (Ye et al. 2006).

With a bit of ambiguity, SMP are defined as soluble cellular components that are released during cell lysis, diffused through the cell membrane, are lost during synthesis, or are excreted for some purpose. Substrate utilisation, biomass decay, and EPS hydrolysis have been theorised to be the major processes contributing to SMP formation (Barker and Stuckey 1999, Fenu et al. 2010).

SMP have been found to lead to a decrease in membrane filterability (Nagaoka et al. 1996) and cause the so-called irreversible fouling, although not under all operating conditions (Drews et al. 2007). Typically, SMP are divided into two major categories (Namkung and Rittmann 1986) that are namely utilisation associated products (UAP) and biomass associated products (BAP).

UAP are SMP that are associated with substrate metabolism and biomass growth and are produced at a rate proportional to that of substrate utilisation. Conversely, BAP are SMP that are associated with biomass decay and are produced at a rate proportional to the concentration of biomass. This method of subdivision has been widely accepted (Fenu et al. 2010, Zuthi et al. 2012). There appears to be a general consensus on UAP formation and degradation mechanisms. According to Lu et al. (2001), UAP formation results from substrate utilisation and is proportional to the rate of substrate utilisation and biomass concentration.

In contrast, there are still many on-going discussions regarding the formation of BAP. Laspidou and Rittmann (2002) hypothesised that BAP are produced solely by EPS hydrolysis. This hypothesis was however shown to be quite weak (Zuthi et al. 2012). Hydrolysed (or soluble) EPS and BAP revealed different physico-chemical properties (Ramesh et al. 2006). Aquino and Stuckey (2008) argued that both soluble EPS and cell lysis products are the sources of BAP.

However, the main issue lies in the fact that there are still disagreement among researchers regarding the broad definition of EPS and SMP. For example, Patsios and Karabelas (2010) have defined soluble EPS and SMP as a biodegradable fraction of dissolved oxygen matter. There are also new terms that have come into use.

Biopolymers clusters or BPC (Wang et al. 2007, Lin et al. 2009a, Sun et al. 2011), transparent exopolymer particles or TEP (De la Torre et al. 2008) and especially sticky fraction of EPS, include such terms. Strictly speaking, all these compounds' group are created and excreted by micro-organisms.

Nevertheless, what is analysed as EPS, SMP, BPC or TEP by commonly agreed on methods is not only necessarily of microbial origin but can also be terrestrial (Judd 2006). It is worth noting that the location of the fouling relevant fraction of these fractions and also the conditions that shift it to different locations are still unknown (Zuthi et al. 2012).

Still, SMP and EPS have proven to accumulate in MBR systems as consequences of high membrane rejection and low biodegradability (Shin and Kang 2003, Drews et al. 2007, Liang et al. 2007). Their influence on fouling and their use as indirect indicators of fouling tendency through biomass deflocculation have been evaluated and recognised by many researchers (Le-Clech et al. 2006, Zhang et al. 2006, Wu et al. 2007, Janus and Ulanicki 2010).

2.1.3.3. Membrane Fouling in Rotating MBRs

Membrane fouling in RMBRs does not differ much from that of conventional MBRs. Jaffrin et al. (2004) described a formula for a rotating membrane disc that linked shear rate and flux. For some constant A_k and an exponent n_k, they defined the flux by Equation 2.29 as follows:

$$J = A_k . \dot{\gamma}_m^{n_k} \tag{2.29}$$

Where,
$\dot{\gamma}_m$, in s^{-1}, is the maximum shear rate of the membrane.

Although their formula does not depict the fouling mechanisms present within a MBR system, it appears to suggest that high exponent values n_k are associated with high viscosities, which in turn relates to solids concentrations. This seems to concur with some of the data provided by Zsirai et al. (2016) but has yet to hold ground. It has been shown that high viscosities are also associated with high MLSS (Yang et al. 2009, Basile et al. 2015). Therefore, it is possible that viscosity may also be a fouling factor in the membrane fouling of RMBRs.

Then again, the role of MLSS in fouling has been irregular (Basile et al. 2015), so the implication of that conjecture is still unknown. Stepping away from MLSS, it has been mentioned that fluid velocity is a small factor affecting membrane fouling in RMBRs. In the study conducted by Jiang et al. (2013), which involved the use of RMBR, their results suggested that the fluid's velocity has a slight impact on fouling.

Their assessment might not be totally unfounded as Engler and Wiesner (2000) before them, who examined the particles fouling of a RMBR, concluded that membrane fouling decreases with rotation rate. The same research argued that TMP may have an effect on membrane fouling in RMBRs. They concluded that membrane fouling increases with TMP. It also seems configuration may be a factor affecting membrane fouling in RMBRs as Liu et al. (2012), who used a rotating helical membrane, concluded that fouling reduction is affected by helical angles (e.g. best at 360°) of the membrane module.

Another factor that may instigate membrane fouling in SMBRs and RMBRs is the phenomenon known as concentration polarisation (Porter 1972). Deeply rooted into all membrane filtration processes, this phenomenon has been described as the accumulation of excess particles in a thin layer adjacent to the membrane surface (Mulder 1996).

Concentration polarisation increases resistance to solvent flow (i.e. continuous solutes accumulation on the membrane surface due to their rejection by membrane) and as a result reduces the permeate flux, which in turn limits the membrane's performance (Sarkar and Bhattacharjee 2008).

To further elaborate on this, it can be argued that membrane fouling generally starts with concentration polarisation. Due to the relentless transport of feed water and solutes to the membrane's surface and the selective retention of certain solutes, some solutes accumulate on and near the membrane surface.

Consequently, their concentration increases over the filtration time and results in a boundary layer of higher concentration with its peak being at the membrane's surface (Mulder 1996, Jiang 2007). The concentration build-up causes a particle back transport flux, a concentration gradient that directly opposes the permeate flux, into the bulk (Jiang 2007).

Back transport phenomenon can affect the fouling of membrane through diffusion mechanisms (see Equation 2.4 and 2.5). To understand it, one must first look at the system's fluid flow. During the course of fluid flow, particles that move near the membrane's surface are exposed to various forces.

Drag forces associated with the axial (i.e. tangential) and lateral (i.e. permeation) components of fluid flow tend to carry particulates along streamlines; meanwhile, particles are subjected to many forces that cause them to cross those streamlines (Yoon 2015). The forces (or mechanisms) which they are subjected to induce back transport velocities. Since many of those forces (in many cases, e.g. steady state) can be neglected (e.g. as settling velocity is negligible compared to that of convective flows, it can be ignored) or equated to one another, generally, only three amongst them tend to have significant impact on back transport.

They are namely Brownian diffusion, shear induced diffusion and inertial lift (Jiang 2007). Brownian diffusion is a direct result of random movement stemming from the bombardment of particles by water molecules. Particles with small radius such as colloids and micro-organisms are subjected to this mechanism (Jiang 2007). Therefore, Brownian diffusion increases with smaller particle size (Jørgensen et al. 2014).

The shear induced diffusion on the other hand, occurs due to individual particles undergoing random displacements from the streamlines in a shear flow as they interact with and collapse over other particles (Jiang 2007). Finally, inertial lift provides a lateral migration of solids, which transports particles away from the membrane (Green and Belfort 1980, Jiang 2007). Particles with radius typically bigger than 10 μm are more susceptible to the inertial lift mechanism.

2.2. State of the Art

RMBRs have been around for quite some time but have not been talked about and studied a lot (compared to conventional MBRs that is). In fact, the history of RMBRs can be traced as far back as the eighties. Since those days, their technologies have slowly but surely improved. Therefore, keeping up to date with their progress is a good exercise that ensures that the RMBR used to procure the filtration data found in this thesis is still viable.

2.2.1. Rotating MBRs

Kroner and Nissinen (1988) presented their so-called axially rotating filter, which was in fact a RMBR where the membranes rotated around a single shaft in a casing. Improved hydrodynamics meant that their RMBR system yielded high filtration performance. Its benefits were as clear as day. But, because it was also complex in structure, not everyone was keen about the idea.

During the Aqua Renaissance 90 project in Japan in the late eighties, the Japanese presented their own RMBR prototype (Yoon 2015). Equipped with 0.1 μm ceramic plate membranes, their RMBR prototype was tested with anaerobic digester broth. The rotating disc module was encapsulated in a pressure vessel and permeate was obtained by pressure.

Since the primary moving object was not wastewater, the energy cost of developing shear stress on the membrane surface was relatively low. However, the benefit of the energy cost savings was counterbalanced by the capital cost increases created by the complexity of the rotating disc module.

Since then, the majority of RMBRs researchers have used involved modified or bespoke systems into which a membrane mounted on a porous support rotates next to a wall that is stationary or rotating in the opposite direction to enhance shear (refer to Table 2.10 for the references). These systems are sometimes known as single shaft discs.

In the late nineties, SpinTeK was one of the few manufacturers that adopted such a configuration. Their SpinTek High Shear Rotary Filter (a RMBR) revealed stable filtration performance during experimentation due to boasting higher crossflow velocities than conventional crossflow systems (Reed et al. 1997). However, this system appears to have fallen out of fashion, most likely due to the complexity of its structure.

More recent manufacturers such as Kerafol, Novoflow and Grundfos BioBooster have implemented the same set-up but with some improvements. The membrane

discs are still housed in a pressurised vessel but their overall design is aesthetically more pleasing and the system's hydrodynamics have been improved a great deal, which is indicated through the pronounced usage of dynamic crossflow filtration.

Overall, high, stable filtration performance and versatility are to be expected from those RMBR systems. Yet, despite all that, those systems are not in high demands. The reasons for this may be the limited membrane area, the high manufacture cost (e.g. ceramic membranes are still used) and again the overall system's complexity.

Some RMBRs are also structured such that the membrane discs are mounted on two parallel shafts rotating in the same direction at the same speed and surrounded by a steel housing (i.e. overlapping multiple shaft discs, where the fluid is sheared between overlapping discs). Such designs were employed by Aaflowsystem and Westfalia.

They even made versions for research purposes (albeit very few). Unfortunately, despite their high, stable permeate production, those RMBRs are not very desirable. Perhaps a reason for this is the extra layer of complexity the multi-shaft gimmick adds to the overall system's structure.

Broadly speaking, as far RMBRs are concerned, Huber Technology's VRM technology has been around for at least a decade but, Huber Technology seems to focus more on industrial and municipal applications (e.g. WWTPs). In their RMBR, a single module with numerous membrane discs stacked together that is mounted and submerged in an open tank, rotates on a single shaft at very low speeds of about 1 to 2 rpm (at most). But at such low speeds hardly any shear is produced. Therefore, this RMBR seems to have been designed to allow for more efficient air scouring.

Recently, Avanti Membrane Technology has joined Huber Technology in adopting this type of configuration. Their RMBR unlike Huber Technology's however, boasts higher rotational speed (thus higher shear) and was made for research purposes. Preliminaries indicated that their RMBR has good filtration capabilities. Table 2.10 below gives a summary of currently available main RMBR types with references.

Table 2.10. List of researches conducted with RMBRs (and those currently available on the market)

	RMBR or manufacturer	References based on studies conducted or information	
Laboratory-based RMBRs	Bespoke or modified in some shape or form (e.g. filtration disc units).	Kroner and Nissinen 1988	Torras et al. 2006
		Aqua Renaissance 90 project Japan, late 1980s (Yoon 2015)	Frappart et al. 2008
		Aubert et al. 1993	Sarkar and Bhattacharjee 2008
		Reed et al. 1997	Luo et al. 2010
		Serra et al. 1999	Sarkar et al. 2011
		Serra and Wiesner 2000	Dutta et al. 2012
		Engler and Wiesner 2000	Liu et al. 2012 (RHM)[a]
		Ding et al. 2002	Ebrahimi et al. 2013
		Brou et al. 2003	Luo et al. 2013
		Bouzerar et al. 2003	Jørgensen et al. 2014
		Jaffrin et al. 2004	Zhu et al. 2016
		Bhattacharjee and Bhattacharya 2006	Ji et al. 2016 (CF + RTM)[b]
Commercialised RMBRs (e.g. pilot unit)	SpinTek	Reed et al. 1997	http://spintek.com/
	Aaflowsystems	Ding et al. 2006 (MSD)[c]	He et al. 2007 (modified)
	Westfalia	Espina et al. 2008 (modified)	Tu and Ding 2010 (MSD)
	Novoflow	Liebermann 2010	http://www.novoflow.com/
	Grundfos BioBooster	Bentzen et al. 2012	Ratkovich and Bentzen 2013 http://www.grundfos.com/
	Kerafol	http://www.kerafol.com/	
	VRM (Huber)	http://www.huber.de/ http://www.huber.co.uk/	http://www.huber-technology.com/
	Flexidisks (Avanti Membrane Technology)	http://www.avantimembrane.com/	

[a], RHM = rotating helical membrane; [b], CF + RTM = crossflow filtration + rotating tubular membrane; [c], MSD = multiple shaft discs

2.2.2. Modelling of Rotating MBRs

As far as modelling is concerned, only a couple of research studies, Jørgensen et al. (2014) and Bentzen et al. (2012), have been truly useful. However, their usefulness extends only as far as theory goes. Bentzen et al. (2012) in particular was useful in providing equations for activated sludge viscosity, which is a factor of shear that can be used in RMBR fouling models. Jørgensen et al. (2014) provided an overview of a system's mass balance formulation which is useful in understanding fouling and to some extent diffusion. As for RMBR models, theirs did not fully cover this thesis's author areas of interest.

Many of the other research studies were completely useless in terms of models as quite a few of them were not full-on modelling studies; and, those which undertook full-on modelling studies had models that were not extensive enough, were complex or did not cover this thesis's author areas of interest. The remaining few RMBR studies were full-on experimental (sometimes comparative) studies, and therefore were unusable as far modelling is concerned.

Aubert et al. (1993) used a rotating flat MF membrane to filter a colloidal suspension of actived carbon. They strived to determine the so-called critical shear stress of erosion, τ^* (Pa), which represents the minimal value of shear stress needed to create erosion. They concluded that as τ^* grows, so do the TMP and pore size. Reed et al. (1997) used a rotary UF system (i.e. SpinTek) to treat oil waste. Though they did not conduct a full modelling study, they created a relationship between permeate flux (gfd) and rotational speed, $N_{\omega r}$ (rpm): permeate flux equals $f(N_{\omega r})^{0.9}$. They found that permeate flux decreases and cake layer showed stability with increasing $N_{\omega r}$.

Serra et al. (1999) used a computational fluid dynamics (CFD) model to investigate the design of a RMBR. They run many simulations for the case of water permeating through a rotating membrane disc in a pressurised housing and concluded that the propensity for back pressure (i.e. negative local TMP due to the centrifugal force acting on the permeate) is higher when the membrane is more permeable but can be reduced by decreasing the membrane area.

Continuing with that same line of work, Serra and Wiesner (2000) compared a rotating membrane disc filter to a stationary membrane disc filter by means of CFD modelling. The authors concluded that operating conditions and design parameters should be carefully selected in order to minimise the back pressure phenomenon and maximise the effective membrane available for filtration.

In a totally separate study, Engler and Wiesner (2000) investigated the particle fouling of a RMBR. Though not modelling heavy, their study concluded that fouling decreases with rotation rate and increases with TMP (and therefore the initial permeate flux). They further went on to say that high rotational speed results in a

centrifugal induced back pressure that reduces or reverses the flow of permeate. In another research that was not modelling heavy, Brou et al. (2003) used a RMBR to investigate EPS produced by bacteria called Sinorhizobium meliloti. They claimed that permeate flux (in LMH) for various discs can be correlated with mean shear stress at the membrane, τ_{wm} (N/m^2), for a 30 °C broth, using the same function (i.e. permeate flux equates to $4.6.\tau_{wm}^{0.717}$).

In their shear related study, Jaffrin et al. (2004) compared the effects of various hydrodynamic parameters on the permeate flux for two different filtration systems, one of which was a RMBR. Their fairly simplistic model was based on the same generic formula linking flux and shear rate (see Equation 2.29). They noted that in a RMBR, membrane shear rate is very steady and increases with radius.

Bhattacharjee and Bhattacharya (2006) filtered black liquor using a UF rotating disc membrane. They wanted to minimise flux decline. Of interesting note in their study is the formulation of their free effective area available for UF which is denoted by Equation 2.30. Naturally (as the formulation dictates), the effective area available for transport in UF gradually decreases thanks to the pore blocking phenomenon.

$$A_{free}(t) = \left[1 - \frac{N_b}{N_0}\right].A_u \qquad (2.30)$$

Where,
A_{free}, in m^2, is the effective membrane area (pore opening) available at any t; and,
N_b, unitless (−), is the number of blocked pores.

Unfortunately, their unblocked membrane area model does not take into account the effect of pore blocking parameter and of pore size distribution. Results wise, they were consistent though. They concluded that the rotation of a membrane disc increases flux as an enhancement of 60% in flux was observed after a period of one hour of UF experimentation using rotating disc module when compared to a fixed disc one.

On the other hand, the shear stresses occurring near the surface of a rotating disc located adjacent to a stationary circular membrane encased in a cylindrical housing was modelled by means of CFD by Torras et al. (2006). They found their results to be somewhat satisfactory although they admitted more accurate measurements could have been taken. Sarkar and Bhattacharjee (2008) presented a semi analytical model based on the evaluation of the back transport flux phenomenon in a RMBR. Predictions from this model were found to be in good agreement with experimental data.

Wu et al. (2008) attempted to find the so-called critical TMP and to control reversible membrane fouling. They introduced the ratio of aeration intensity to permeate flux, A/F (-) and, estimated that increasing it, rotation speed, and stoppage of intermittent permeation time can help prevent reversible membrane fouling in a

RMBR. Though the fouling mechanisms were not analysed, they concluded that beyond the critical values of 60 rpm, 15 and 1 minute for every 10-minute cycle, for respectively rotation speed, A/F and stoppage of intermittent permeation time, fouling prevention is virtually naught.

Tu and Ding (2010) used a modified multiple shafts RMBR system (i.e. Westfalia) and ceramic membranes to perform MF of mineral suspension. Their study was once again not modelling orientated. They assessed the mean shear rates at the membrane so as to investigate their influence on filtrate flux, and their results showed that shear rate is the key parameter controlling filtrate flux. More on the modelling side, Sarkar et al. (2011) refined the semi analytical model presented by Sarkar and Bhattacharjee (2008) and concluded that their experimental data were in good agreement with their model with a deviation of ± 5%.

Dutta et al. (2012) examined the performance of UF rotating membrane disc. They focused on controlling flux decline. Through their results, they observed that a membrane rotation of 50 rpm was sufficient to alleviate membrane fouling and concentration polarisation. However, they did not fully detail and discuss the fouling mechanisms occurring within the rotating membrane itself.

Similarly Liu et al. (2012) endeavoured to reduce fouling in a RMBR. They utilised a rotating helical membrane. Their results revealed that flux enhancement and fouling reduction are affected by the membrane module helical angles (e.g. best at 360°). They further concluded that rotating a helical membrane is useful for stirring separations without aeration.

In a comparable study to Torras et al. (2006), Bentzen et al. (2012) performed modelling of Newtonian and non-Newtonian liquid for a rotational crossflow membrane by means of CFD. They made relationships for shear stress and area-weighted average shear stress and found that there was less than 8% error when they compared their results from relationships to those of CFD. As extension work to Bentzen et al. (2012), Ratkovich and Bentzen (2013) studied four different MBR systems, one of which was a RMBR (i.e. Grundfos BioBooster). They used CFD as a tool to develop and optimise them. They concluded that a RMBR without injection of air can generate more shear stresses than other systems.

Ebrahimi et al. (2013) investigated the application of rotating ceramic filter discs for the treatment of oily solutions. They concluded that an increase in membrane rotational speed minimises fouling by a significant amount. The modelling in their work was in small amount.

Luo et al. (2013) endeavoured to prove the existence of threshold flux. To that end, they treated raw chicory root extract using a rotating disc module equipped with MF and UF membranes, and then investigated the permeate flux behaviour at

high shear conditions. Their study was more experimental than it was modelling yet surprisingly had some interesting things to say.

They proposed a threshold flux to distinguish between low and high fouling rates; and, explained that below it, filtration resistance is independent of flux whilst above it, filtration resistance is flux dependent because membrane fouling increases with permeate flux.

They pointed out that their new threshold flux criterion was applicable to high shear MF and UF, and further added that threshold and limiting fluxes might be independent of membrane pore size, permeability and fouling condition. Finally, they argued the shift in size-dependent shear-induced and Brownian back diffusions may be the essential reason of threshold flux phenomenon.

In a different fouling related research, Jiang et al. (2013) investigated the relationships between mechanically induced hydrodynamics and membrane fouling using particle image velocimetry (PIV; flow visualisation technique that provides instantaneous velocity vector measurements in a cross-section of a flow). Their model simulations suggested that the fluid velocity has a slight impact on membrane fouling.

Using rotating ceramic membrane discs that were fouled by sludge, Jørgensen et al. (2014) showed the dependence of shear on fouling and ultimately presented a model that linked shear rate to limiting flux. They commented that the variations in the operational conditions of their RMBR unit were well simulated by their model, although said model only focused on one aspect of fouling.

Quite recently, Ji et al. (2016) employed a dynamic membrane filtration system that combines crossflow filtration and centrifugal separation in a rotating tubular ceramic membrane (0.14 μm nominal pore size) in an attempt to decrease fouling by buoyant particles (e.g. hollow glass microspheres). Their justification is that due to the no-slip boundary condition, membrane rotation leads to higher centripetal force near the lumen wall than introduction of a rotating flow.

The bulk of their modelling revolved around particle force balancing. According to those calculations, centripetal force should move particles with diameters exceeding 17 μm away from the lumen surface. Also, azimuthal and longitudinal shear stresses should likewise selectively remove larger particles from the membrane cake.

Their CFD simulations indicated that the rotational flow does not fully develop in the membrane and inertial effects may lead to deposition of particles even when their individual diameter exceeds 17 μm. Overall, their model seemed to have done a decent job at producing consistent results. Nonetheless, the lengthy particle force balancing and its derivatives add a layer of complexity to said model that makes its practicality, if any, very limited.

Unlike the above RMBR studies, there were researches that focused entirely on the experimental aspect of RMBRs. Such studies contained data reports (which allowed their authors to draw some kind of conclusion) and little to no modelling to speak of.

Kroner and Nissinen (1988) filtered microbial suspensions using an axially rotating filter. Their data showed that their rotating filter performed three times better than systems using other crossflow filtration techniques. Ding et al. (2002) performed UF of ultra-heat-treated skimmed milk using rotating disc modules. They noticed an increase in permeate flux of about 56% due to high fluid core velocity that resulted in high shear rates (of up to over 3×10^5 s^{-1}) at the membrane. Conversely, Bouzerar et al. (2003) filtered mineral suspensions and industrial effluent using MF, NF and UF rotating membrane discs and observed a permeate flux of 200 LMH at 40 bar.

Using Aaflowsystems, a multiple shaft discs system, Ding et al. (2006) performed MF of mineral suspensions while He et al. (2007) filtered the same solution but with a slightly modified version of the same RMBR system. In their version, the ceramic discs of one shaft were replaced by non-permeating metal discs of same size rotating at a speed different from that of membranes. They reported that raising the ceramic discs rotation speed had a larger effect on permeate flux than increasing the metal discs speed with permeate flux reaching values as high as 1790 LMH.

Espina et al. (2008) used a modified Westaflia RMBR to filter skimmed milk so as to separate caseins micelles from whey proteins. They reported maximum permeate fluxes of 120 LMH at 1930 rpm and 40 °C for the multiple shaft discs module, and 210 LMH at 2500 rpm and 45 °C for the rotating discs module. Frappart et al. (2008) performed RO of diluted skimmed milk using rotating disc modules. They obtained maximum permeate flux of 180 LMH at TMP of 4 Mega Pa (MPa).

Luo et al. (2010) treated dairy wastewater under hydraulic conditions with a NF rotating disc. They argued they were able to decrease membrane fouling by raising the pH above 9. Zuo et al. (2010) On the other hand, focused more on fouling mitigation methods. They chemically cleaned their rotating membrane module with water, NaOH and HCl, and recovered 90% of the operation's initial permeate flux. Liebermann (2010) gave an insight of Novoflow's RMBR.

Meyer et al. (2015) used UF rotating membranes to filter high concentrations of skimmed milk proteins. Their experimental data showed an increase in flux being almost linear up to a TMP of 100 kPa. Finally, Zhu et al. (2016) filtered sugar beet juice with the assistance of a UF rotating disc module. They observed that at TMP of 4 bar and rotation speed of 1000 rpm, flux was highest.

A conclusion that can be drawn from the state of the art for modelling of RMBRs is that a decent portion of RMBR studies containing models have relied on the use of CFD to draw conclusions in some shape or form about membrane shear stress. This

is not too surprising as encasing one's rotating membrane module in some kind housing is a good way to define boundaries for the fluid's flow. As a powerful modern tool, CFD can be used to diagnose and understand the two-phase flow (i.e. sludge-air or liquid-gas) in a MBR to a reasonable extent.

But, this may not always be true as MBRs involve manifold parameters that may all be too complex to define in CFD at once. Add to that the internal structure of the membrane and, the overall system's set-up might be a magnitude too great for CFD to overcome; especially if said membrane is fouled (with the formation of a biofilm as added bonus). After all, there are still on-going debates regarding various aspects of fouling.

However, it seems some researchers have gone back to roots as it appears first principle definitions may yet be the most effective way to explain certain facets of MBRs or at the very least, to ascertain some of the causes of fouling as shown by Sarkar and Bhattacharjee (2008) and Sarkar et al. (2011).

2.2.3. Membrane Fouling in Rotating MBRs

Regarding fouling models, almost none of the RMBR research studies that involved fouling in some shape or form have been useful modelling wise. This is because the majority of them focused more on mitigating fouling rather than explaining its mechanisms or internal aspects. Some studies amongst them had models that were either complex or not expansive enough to be of any use. The exceptions to these shortcomings have been Jørgensen et al. (2014) and Bentzen et al. (2012), but only because of the theories they presented.

Starting with Aubert et al. (1993), though their research was not fully fouling focused, they concluded that as τ^* grows, so do the TMP and pore size. As a result, fouling is more efficiently eliminated at high TMP and large pore size. Engler and Wiesner (2000) examined the particle fouling of a RMBR. They considered the possible effects of back transport on the particles yet did not perform sufficient modelling. However, their study concluded that fouling decreases with rotation rate and increases with TMP.

Bhattacharjee and Bhattacharya (2006) filtered black liquor using a UF rotating disc membrane. Their goal was to minimise flux decline. Pore blocking phenomenon was key in helping them determine their free effective area. They used the osmotic pressure model (see Equation 2.3) for their flux study. Evidently, their model did not take into account the effect of shear and cake filtration; as such, its depiction of fouling is limited. Despite this limitation, their results appeared consistent. They indicated that the rotation of a membrane disc increases flux as an enhancement of 60% in flux was observed after a period of one hour of UF experimentation using rotating disc module when compared to a fixed disc one.

With somewhat similar ideas, Wu et al. (2008) attempted to control reversible membrane fouling and determine the so-called critical TMP. They estimated that increasing rotation speed, A/F, and stoppage of intermittent permeation time can help prevent reversible fouling in a RMBR system. The fouling mechanisms were not analysed in full, but they concluded that beyond critical values 60 rpm, 15 and 1 minute for every 10-minute cycle, for respectively rotation speed, A/F and stoppage of intermittent permeation time, fouling prevention is virtually non-existent.

Dutta et al. (2012) inspected the performance of a UF rotating membrane disc. They set out to control flux decline. Through their results, they observed that a membrane rotation of 50 rpm was sufficient to lessen membrane fouling and also concentration polarisation. Their discussion of fouling however was lacking as they did not delved into its various aspects. Likewise, Liu et al. (2012) tried to reduce membrane fouling. To that end, they used a rotating helical membrane. Their results showed that flux enhancement and fouling reduction are affected by the membrane module helical angles (e.g. best at 360°).

Luo et al. (2013) studied the permeate flux behaviour in clarification of chicory juice at high shear conditions so as to prove the existence of threshold flux. They proposed a threshold flux to distinguish between low and high fouling rates; and, explained that below it, filtration resistance is independent of flux whilst above it, filtration resistance is flux dependent because membrane fouling increases with permeate flux.

They argued both limiting flux and flux fluctuations should be avoided in practical applications since they cause high fouling and flux decline. At the end of the day, their research focused far too much on experimental results to give any meaningful weight to their non-extensive modelling. Their model (i.e. similar to Equation 2.2), though sufficient for basic flux prediction, at large, is not well-developed enough to fully describe all classical fouling behaviours.

Jiang et al. (2013) investigated the relationships between mechanically induced hydrodynamics and membrane fouling using particle image velocimetry (PIV; flow visualisation technique that provides instantaneous velocity vector measurements in a cross-section of a flow). Their model simulations showed that the fluid velocity has a slight impact on membrane fouling. Overall, their model fairly accomplished what it set out to do; but, ultimately it is not rich enough to wholly explain complex fouling phenomena.

Jørgensen et al. (2014) studied the dependence of shear on fouling in RMBR. They used rotating ceramic membrane discs that were fouled by sludge. An interesting aspect of their research to note is the mass balance formulation from which they ultimately derived their flux model that linked shear rate (e.g. limiting flux, J_{LIM}).

Whilst taking into account back transport and diffusion terms, this mass balance was formulated for the development in amount of fouling, Ψ (kg/m^2), as shown by Equation 2.31. In this raw formulation, the back transport of foulants towards the membrane (J.ϕ) is affected by the migration of foulants due to surface interactions between the membrane and foulants surfaces p(ζ), Brownian diffusion, and shear induced diffusion.

$$\frac{d\Psi}{dt} = J.\phi - (D_S - D_B).\frac{d\phi}{dx} + p(\zeta) \qquad (2.31)$$

Where,
D_S, in m^2/s, is the shear-induced diffusion coefficient;
D_B, in m^2/s, is the Brownian diffusion coefficient;
ζ, in mV, is the zeta potential;
ϕ, in kg/m^3, is the volume fraction of foulants (relative to bulk concentration).

In their study, fouling was considered an effect of cake formation that is controlled by the mass balance and cake compression. Therefore, by assuming fouling was totally reversible, they eliminated (i.e. set to zero) p(ζ) from the above equation. Moreover, by solving the mass balance formulation for equilibrium, they were able to eventually derive the limiting flux, J_{LIM} (m/s).

They described it as the pressure-independent steady-state flux, above which the flux will always decline to the same value. Although their model rightfully took into account the non-Newtonian nature of activated sludge, in the end it focused far too much on the cake formation aspect of fouling while neglecting the others. As such, it is not succinct enough to describe in full all major fouling phenomena.

More recently, Ji et al. (2016) evaluated the effects of membrane rotation on the accumulation of particles at the membrane surface (e.g. fouling). They combined crossflow filtration with a rotating tubular ceramic membrane where hollow glass microspheres serve as model low-density, separate-phase foulants.

Early observations showed that at low crossflow rates, membrane rotation at 1725 rpm decreases fouling and shifts the microsphere size distribution in the membrane cake towards smaller diameters. Their modelling involved particle force balancing (for the majority) and some CFD. According to their force balance calculations, centripetal force should move particles with diameters exceeding 17 μm away from the lumen surface.

Their CFD simulations appeared consistent with experimental data; but, revealed that the rotational flow does not fully develop in the membrane and inertial effects may lead to deposition of particles even when their individual diameter exceeds 17 μm. All in all, their system model can for the most part, describe the cake formation facet of fouling. Nevertheless, the heavy particle force balancing and its derivatives

make said model, which does not fully account for all fouling mechanisms occurring in a RMBR, needlessly laborious.

As can be inferred from this sub-section (with a couple of exceptions), RMBRs are still in need of properly developed dynamic fouling models that can provide one an insight, even if small, of fouling mechanisms associated with membrane fouling in RMBRs.

2.3. Chapter Summary

This chapter documented the literature review of this thesis which of course serves as basis for the majority of the study undertaken here. State of the art studies have been done to ensure that latest technologies and techniques being used by other researchers in the field of RMBR are known as well as new methods used that may help improve the modelling aspect of RMBRs.

At large, membrane technologies have experienced an increase in usage for over a decade now not only in industrial and municipal WWTPs but also in many MBR related research areas. A reason for this is because though formerly expensive, cheaper alternatives with better operational conditions than older ones have entered the market. New membrane technologies are seeing the light of day and existing processes are being improved upon to enhance their physical and chemical performance along with economic competitiveness.

Since the emergence of submerged MBRs, which really started with Yamamoto et al. (1989) success, many major improvements have been made in various aspects of membrane technologies, including membrane materials (e.g. PVDFs are used as cheap alternatives for expensive ceramics), membrane module configurations (i.e. the widespread usage of flat sheets, hollow fibres or tubulars), modified membrane properties (i.e. the manipulation of pore sizes) and finally MBR configurations (i.e. MBR types such as vertical airlift or rotary systems are now optional).

Though submerged MBRs were found to be more efficient than the overly expensive side-stream MBRs over two decades ago; producing high volumes of permeate whilst maintaining consistent filtration performance, which sometimes is downright impossible due to fouling or concentration polarisation, still comes at the expense of huge costs.

This is where RMBRs are seemingly more useful. Not only do these systems with the right set-up (e.g. large radius and huge rotational speed) produce high volumes of permeate with dynamic crossflow filtration, but they also retain their high filtration performance for longer periods of time than conventional crossflow filtration MBRs (e.g. typical submerged MBRs)

Although RMBRs have been around for quite some time in some shape or form, the sad truth however, is that they have seemingly flown under the radar. This in part is due to their complex designs and intricate physics (e.g. hydrodynamic regimes); though, their associated costs might also be a contributing factor. Nevertheless, researches are still being conducted in this field; this PhD research work being one of them.

CHAPTER 3: EXPERIMENTAL METHODOLOGY

This chapter details the setting-up process of both MBR plants as well as how the filtration data were collected and experiments were performed. The data collection in particular is important as they are utilised to feed the fouling models in order to produce outputs for discussions. The experimental methodology section is divided into two main sub-sections:

i. *Pilot Plants*: This sub-section explores how both laboratory-based MBR rigs (i.e. RMBR and SMBR) were set-up.

ii. *Experimental Methods and data collection*: Details of experimentations that were used for data collection are outlined in this sub-section.

3.1. Pilot Plants

Both pilot units were used to run tests and collect data as needed, but not initially without some inconveniences that were eventually rectified. The RMBR unit in particular took quite some time to set up as the manual was originally in Chinese, but, fortunately alternatives were found.

3.1.1. Rotating MBR Unit

Manufactured in Taiwan, this bespoke laboratory-scale RMBR pilot unit which was designed as a research tool and included all data logging and measuring system interfaces, was used to perform required filtration operations. Figure 3.1 illustrates said RMBR unit, dubbed the RPU-185 RMBR, in operation on a typical day.

Figure 3.1. Set-up pictures of the RPU-185 RMBR in operation as the rotating membrane module is located in the batch tank (picture on the right) for filtration purposes. Equipped with a Human-Machine Interface (HMI) touch screen, most of its functionalities are automated

Originally, when this system was received, it was mostly assembled and did not take very long to install in the water sustainability laboratory; but, it occupied a good portion of the laboratory total space due to being large, thus giving little room to manoeuvre.

To guarantee the RPU-185 RMBR would function adequately when needed, such as for instance, leave it for an automated night-long run, additional equipment was added to it. To ensure sufficient amount of fluid would be fed to the batch tank after performing filtration operations (i.e. in cases where it was depleted and the fluid volume fell below required levels), a 1000-litre capacity feed tank was connected to it with the help of feed pipes.

To move the required fluid level from the feed tank to the batch tank in such cases, a peristaltic pump, which is generally ideal for transporting large amount of fluid of any kind, was used. It should be noted that due to the convenient positioning of the pipes and batch tank, the pump's maximum flow rate increased from 5×10^{-5} $m^3.s^{-1}$

to 8×10^{-5} $m^3.s^{-1}$. Though the batch tank has sensors to indicate that the fluid level in it is low, medium or high, they merely serve as warning.

To make sure the peristaltic pump picks up on this, and thereby automatically moves the fluid in the feed tank to top-up the batch tank to necessary levels when low, a float sensor gauged at three settings low, medium and high was added to it. With this arrangement of added equipment, the fluid flow from the feed tank was automatically controlled to ensure that the correct amount of fluid was circulated to the batch tank as required. The RPU-185 RMBR can be said to comprise three main parts. Figure 3.2 depicts the schematic of its complete piping and instrumentation diagram (PID).

(Please refer to **APPENDIX B.1** for more pictures pertaining to the RPU-185 RMBR)

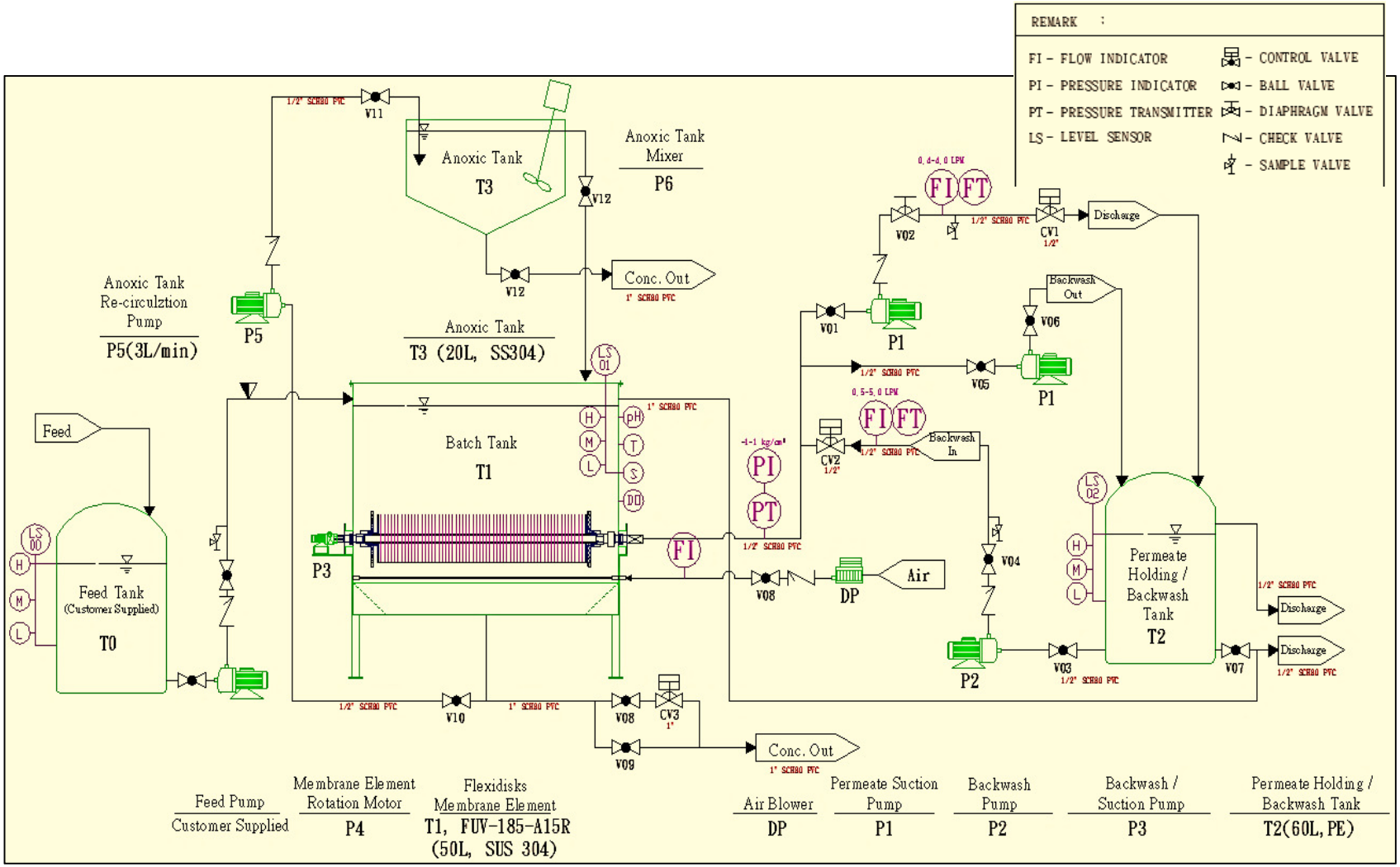

Figure 3.2. Piping and instrumentation diagram of RPU-185 RMBR

This laboratory-scale RMBR pilot unit (as shown on Figures 3.1 and 3.2) is an automated system that can be controlled as needed from the control panel. After first turning on the unit whilst following the manufacturer's instructions, the control panel is accessed and from its HMI touch screen and ten main buttons, experimental parameters are set to perform UF or backwash operations as required.

The three additional screens at the top of the control panel merely log pH, conductivity and DO levels; and, though they do have small buttons just underneath them to change these values, they are recommended not to be meddled with as the systems associated with them had already been calibrated by the manufacturer and set to required optimal values. Another part of this pilot unit that is worthy of note is the batch tank, which has a capacity of 50 litres, and houses the rotating membrane module. The quantity of fluid in the batch tank is gauged at 3 levels namely low, medium and high.

When the level of fluid in the batch tank is low, a warning alarm is heard and no filtration operation can take place (at which point the peristaltic pump will do its job). On the other hand, it is only when the batch tank is filled to just above medium level (i.e. about 42 litres of fluid which is the recommended level to avoid issues) with activated sludge fluid that is supplied by Thames Water (UK) or with other waste fluid types, and experimental parameters are set from the control panel, that the pilot unit is able to perform permeation successfully again.

To avoid spillage, hazard of coming into contact with potentially dangerous fluid substance or large energy consumption, filling the batch tank to high level is not recommended; and thus was not employed. The final important part of this RMBR unit is the permeate tank (i.e. with a capacity of 60 litres), which as the name suggests, holds the volume of fluid permeated after a filtration operation. When this tank is full, the sensor detects it, and a warning is sent out, at which point it must be emptied.

Fortunately the laboratory is equipped with pipes and huge water buckets to get the job done. During backwash operations, a calculated quantity of sodium hypochlorite (NaOCl) solution is added to the permeated fluid in the permeate tank to chemically flush the fouled membrane module. An anoxic tank was also included with the pilot unit for de-nitrification purposes but this option was unfortunately never used in this study due to lack of time.

Finally, during experimentations, TMP, DO levels, temperature, pH, permeate flux, and air scouring flow rates are all measured and logged automatically by the pilot unit (RPU-185 RMBR) itself. Figure 3.3 shows the HMI display screen with some experimental data.

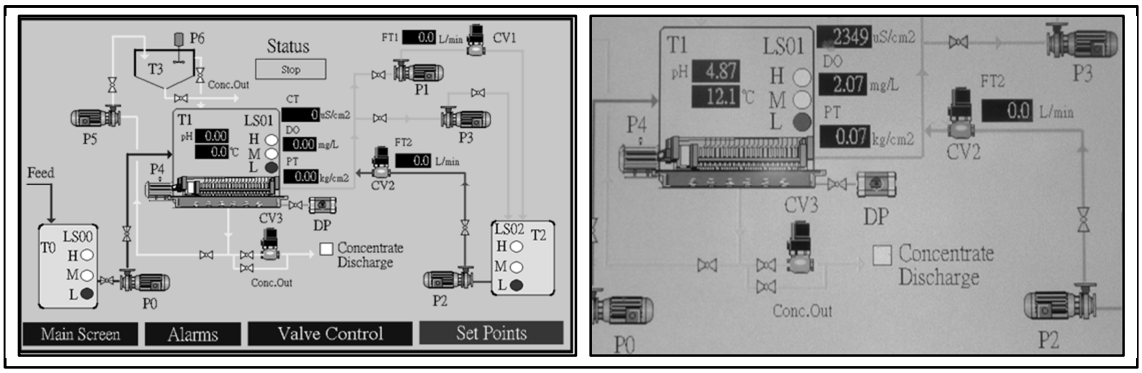

Figure 3.3. Pictures partially showing some data are automatically measured and displayed on the HMI touch screen. Other data types are internally logged within the RMBR system and accessible via USB

The operating conditions of the RPU-185 RMBR were fairly reasonable as experiments were optimally conducted with minimal issues. This is because it was ensured that they were in-line with the manufacturer's recommendations. Table 3.1 summarises the RPU-185 RMBR circular flat sheet membranes dimensions and operating conditions as provided by the manufacturer.

Table 3.1. RPU-185 RMBR circular membranes dimensions and operational data

Model	**RPU-185 Multi-Functional Pilot Unit**
Anti-fouling method	Chemical clean; Aeration (air scrub)
Operating temperature	5 – 50 °C
Operating pH range	1.5 – 12
Air scrubbing flow rate	8 – 22 L/min
TSS (Total suspended solids)	< 0.5 mg/L
TMP (Trans-membrane pressure)	(max) ≤ 2 bar
Batch tank	50 L
Permeate tank holding	60 L
Dimensions (Length x Width x Height)	130 cm (L) x 77 cm (W) x 125 cm (H)
Power supply	60 Hz/220 VAC
Specification	**FUV-185-A 15R Membrane Element**
Membrane type – Membrane material	Ultrafiltration (UF) – PVDF
Pore size	100,000 daltons (0.03 µm)
Membrane thickness	3 mm
Membrane outer diameter	0.177 m
Membrane inner diameter	0.055 m
Number of membranes	36
Total membrane area (module)	1.6006 m^2
Membrane module angular velocity	2.094 rad/s (20 rpm)

Having covered the RPU-185 RMBR, **sub-section 3.1.2** will cover the SMBR rig.

3.1.2. Static Square MBR Unit

This second MBR research rig, which was fabricated at Brunel University, uses a bespoke static square-shaped membrane module that was procured from Avanti Technology (USA). Said SMBR rig, in operation, is presented on Figure 3.4.

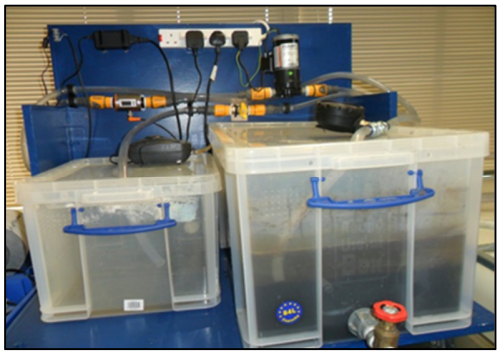

Figure 3.4. Picture of the constructed SMBR system in operation. The square membrane module is located in the larger tank on the right for filtration purposes

Similar to the RPU-185 RMBR, this SMBR utilises UF to produce permeate fluid, a process which can be automated via an on and off switch. The batch tank holds a capacity of 80 litres and houses the square-shaped membrane module but, unlike the RPU-185 RMBR, it does not have sensors to measure the fluid level so it has to be observed as experiments run and topped-up as required.

A diaphragm pump (Flojet brand) was installed to ensure that after UF of activated sludge (provided by Thames Water, UK), permeate water is collected from the membrane module and pumped to the permeate tank (which has a capacity of 40 litres). This tank also has to regularly be checked as filtration experiments go on so that it can be readily emptied when full. The permeate tank for this SMBR unit merely exists to hold collected permeate fluid volume. As such, no backwash can be performed. The fouled membrane module has to be physically removed from the batch tank and dipped into calculated solutions of NaOCl for chemical cleaning.

During filtration experiments, the SMBR rig was well aerated to recommended air scouring flow rate value similar to the RMBR case (since they are both from the same manufacturer) and DO level was kept at the usual 2 mg/L. Pressure gauges (DPI 104 Druck Digital Test Gauge by GE Company, USA) were also installed to ensure that TMP was kept to constant value as demanded per filtration experiment (see Equation 2.6).

Finally, the flow metre was used to record various flow rates as experiments went along. The dimensioning for the square-shaped membranes and operating conditions of the SMBR rig can be found summarised in Table 3.2.

Table 3.2. Square-shaped membranes dimensions and SMBR unit operating range

Model	**SMBR Pilot Unit**
Anti-fouling method	Chemical wash; Aeration
Operating temperature	~ 5 – 60 °C
Operating pH range	2 – 12
Air scrubbing flow rate	4.5 – 22 L/min
TSS (Total suspended solids)	< 1 mg/L
TMP (Trans-membrane pressure)	> 3 bar
Batch tank	80 L
Permeate tank holding	40 L
Power supply	60 Hz/220 VAC
Specification	**Square-shaped Membrane Element**
Membrane type – Membrane material	Ultrafiltration (UF) – PVDF
Pore size	100,000 daltons (0.03 μm)
Membrane thickness	6 mm
Individual membrane length	0.24 m
Individual membrane width	0.24 m
Number of membranes	20
Total membrane area (module)	1.152 m^2

Overall the operating conditions of the SMBR rig were ensured to be as close as possible to those of the RPU-185 RMBR. Experiments were optimally conducted with minimal issues and data collected were reasonable.

(Refer to **APPENDIX B.2** for more SMBR related pictures)

3.1.3. Polyvinylidene Difluoride (PVDF) Membrane Modules: Rotating and Static Square-Shaped

The rotating membrane module for the RPU-185 RMBR is an UF membrane module that allowed for short and medium term filtration data collection. The module comprises 36 circular flat sheet membranes that are attached to a single shaft rotating via an electrical motor with an operational speed of 20 rpm.

During filtration, the rotation of the membrane module generates a shear at the membrane surface that scours off the deposited particles, thereby reducing fouling whenever possible and/or providing stable permeate flow that is collected with the manifold located in the single shaft. Figure 3.5 displays a schematic of the rotating membrane module FUV-185-A15R (housed within the batch tank).

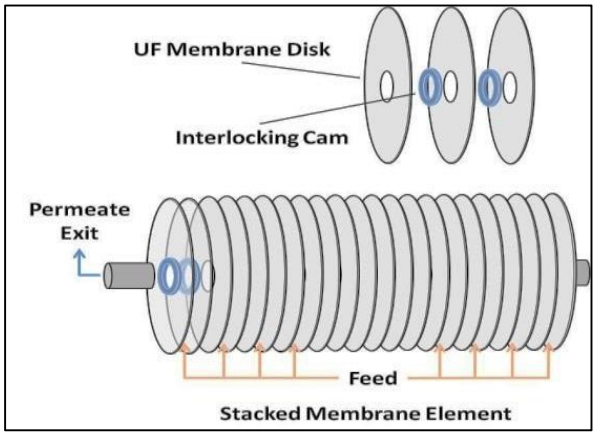

Figure 3.5. Schematic of rotating membrane module
FUV-185-A15R located within the batch tank of the RPU-185 RMBR

Individually, each flat sheet membrane disc (see Figure 3.5 top) is flexible and made of two circular membrane pieces welded together back-to-back with drainage cloth in the middle for permeation. Each is hydrophilic low fouling PVDF and therefore is a contributing factor though small to membrane fouling prevention.

The dimensioning for the rotating membrane module and conditions under which UFs are permissible are outlined in Table 3.1. Unsurprisingly, it was observed that running the RMBR pilot unit past recommended manufacturer's values, especially at fairly high TMPs, tends to damage the membrane module quicker as depicted on Figure 3.6 (Left).


Figure 3.6. (Left) Damaged membrane module at high TMP of over 75 kPa.
(Right) Easily removable membrane module that can be chemically washed

Because the RPU-185 RMBR was operated under a high TMP of over 75 kPa, the membrane module was fouled far quicker than usual, resulting in it being clogged-up. The clogging jammed the spars, and being unable to rotate, the membrane module was damaged. However, one of the benefits of having this RMBR is that because the membrane module is of push-fit configuration, it can easily be removed (as shown on Figure 3.6 Right) and dipped in NaOCl solution for chemical washing if heavily fouled; or, as in the above case

(see Figure 3.6 Left), it can be replaced with a brand new membrane module of similar properties to those of the damaged one (while it was in pristine condition of course).

The static square-shaped membrane module for the SMBR rig (see Figure 3.7) is an UF membrane module that permitted the collection of short and medium term filtration data. It consists of 20 static square-shaped membrane flat sheets that are mounted on a single shaft. Just as is the case for typical SMBRs, fouling prevention is done via air scouring.

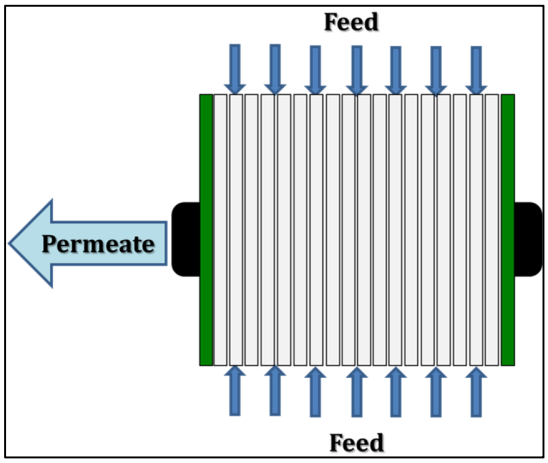

Figure 3.7. Schematic of static square-shaped membrane module that is located within the SMBR's batch tank

Each square-shaped flat sheet membrane is made of hydrophilic, low fouling PVDF with the manifold that collected permeate fluid being located in the single shaft. The dimensioning of this static membrane module and favourable conditions that allow UFs are highlighted in Table 3.2.

3.2. Experimental Methods and Data Collection

Amongst the experiments that were run, preparing the synthetic wastewater was the most worrisome task. On top of ensuring that the correct level of waste solution was produced as needed for the semi-batch feeding of activated sludge, this thesis' author had to ensure chemicals were ordered on time with the right quantity. Fortunately through tight time management, these issues were mitigated.

3.2.1. Synthetic Wastewater

Literature shows that synthetic wastewaters are typically prepared by researchers to meet specific study demands. For this thesis, a rich glucose (i.e. the main source of COD) based synthetic wastewater concentrate was required to feed the activated sludge so as to maintain it at required MLSS levels for data collection. The artificial wastewater did not need to emulate real domestic sewage hundred percent; it needed to be an average wastewater without its heavy protein components. This is because proteins can be naturally provided during activated sludge process via cannibalisation of dead micro-organisms.

To emulate said average domestic wastewater, chemical supplements are necessary. Actual domestic sewage contains a particulate fraction that is mineral (Nopens et al. 2001). This can be simulated by using salt compounds (e.g. Potassium Phosphate). Domestic sewage also contains some trace metals. This can be replicated by utilising trace metal compounds (e.g. Iron III chloride).

Following this route, the synthetic sewage that was used to feed the activated sludge of both MBR systems was a modified and richer version of the synthetic wastewater solution proposed by OECD (1992). This is because the proposed OECD (1992) synthetic sewage solution ticked most of the boxes needed to create a synthetic wastewater that imitated average domestic sewage (e.g. containing trace metals, minerals).

The usage of synthetic wastewater boasts many advantages; the first being availability. For locations that do not have a readily available real sewage source, synthetic wastewater is not only a better alternative option but also makes health and safety related issues more manageable, especially at laboratory-scale operations. Furthermore, when compared with real sewage, synthetic wastewater has better consistency for its composition is already known and is calculated beforehand to adhere to specific demands. With a consistent food source being used, fouling is largely independent of this external source.

Having selected the glucose-based synthetic wastewater, it was ensured that the right amount, acting as food source, semi-batch fed the activated sludge of both MBR systems (i.e. RMBR and SMBR). With food sufficiently limited, thus yielding low F/M values (i.e. typically as low as around 0.14) for both MBR plants, bacteria were able to develop thick

slime layers and clump together to form flocs that settled well. This thus augmented the MLSS level in the mixed liquor.

A protocol for producing the chosen synthetic wastewater (as shown on Figure 3.8) was created whilst taking into account its related health and safety and containment measures in cases of spillage. In order to create the synthetic wastewater, the following equipment was used:

- Personal protective equipment (PPE) which include: safety glasses, disposal gloves and face masks;
- Fume cupboard light (must be switched on);
- Measuring cylinder for distilled water (one litre);
- Weighing scales (positioned in fume cupboard);
- Containers with screw lid for synthetic wastewater;
- Weighing trays (8 – one for each chemical);
- Spatulas (9 – one for each chemical and one for mixing);
- Container with clip (must be sealed for used PPE)

The activated sludge semi-batch feeding process in both MBR plants necessitated 300 litres worth of synthetic wastewater to be made on an almost weekly basis. Table 3.3 depicts the chemical composition (in mass) needed to produce such synthetic wastewater volume.

Table 3.3. Synthetic wastewater chemical composition (in mass) for 300 litres

Chemical used	**Quantity (i.e. mass in g)**
D-glucose Anhydrous	280
Ammonium Chloride (NH_4Cl)	84
Potassium Phosphate (KH_2PO_4)	28
Sodium Hydrogen Carbonate ($NaHCO_3$)	168
Calcium Chloride ($CaCl_2$)	4.2
Magnesium Sulfate ($Mg_2S0_4.7H_2O$)	4.2
Iron (III) chloride ($FeCl_3.6H_2O$)	1.26
Magnesium Chloride ($MgCl_2$)	0.84

To make the synthetic sewage and its required volume, the below detailed procedure was meticulously followed:

- For every procedure apply PPE;
- Set-up equipment and move chemicals to fume cupboard;
- Measure 500 mL worth of distilled water into each container;
- Move containers to fume cupboard;
- For each chemical in turn weigh, add to distilled water and finally stir;

- Thoroughly clean-up;
- Switch on fume cupboard fan and light;
- Switch off weighing scales;
- Top-up synthetic wastewater concentrate to one litre with distilled water;
- Store synthetic wastewater concentrate in refrigerators;
- Remove PPE

Figure 3.8 illustrates how the synthetic wastewater was made.

Figure 3.8. Pictures of the production of synthetic wastewater in laboratory. After stirring-up the concentrate, 500 mL of it is poured into a beaker to top-up 500 mL of distilled water, making one litre of synthetic wastewater

The weekly storage of the synthetic wastewater comes from the fact that an initial test was performed so as to determine its storage limit. As such, in order to observe degradations (or precipitations) in the chemical waste solutions, meaning they would no longer be viable as food source; first, sample solutions of synthetic wastewater were created using the above method, and then were refrigerated (see Figure 3.9). After a seven-day observation, everything seemed fine; however, on the eighth day precipitations were discovered. COD measurements were carried out, its results reported in Table 3.4.

Table 3.4. COD test results for chemical waste solutions after 8 days

Chemical Solution	**Average COD – 7 days**	**COD – 8th Day**	**Unit**
NH_4Cl	13	-4	mg/L
$CaCl_2$	26	-9	mg/L
$Mg_2S0_4.7H_2O$	49	8	mg/L
$FeCl_3.6H_2O$	252	41	mg/L

Figure 3.9 below shows the stored chemical solutions in the refrigerator after they were produced fresh from the laboratory.

Figure 3.9. Refrigerated chemical solutions (from left to right respectively, NH_4Cl, $CaCl_2$, $Mg_2S0_4.7H_2O$, and $FeCl_3.6H_2O$)

After this experiment and few more testing runs of what was observed, and based on the chemical waste solutions' COD values in Table 3.4, it was concluded that the synthetic wastewater can be kept refrigerated for up to a week without formation of precipitation, meaning it would still be a viable food source for the activated sludge. It was also found that it can be stored for up to four days unrefrigerated without degradations forming. At the end of these tests, the chemical solutions were disposed of. The dilution method was used. They were diluted in a large water bucket filled with ten litres of tap water. The newly diluted solutions were poured down the sink.

(Please refer to **APPENDIX C.1** for chemicals hazards and health and safety measures)

3.2.2. COD Measurement

Finding the COD (which can be correlated to BOD) of the feed is an important measure that is needed to calculate the amount of food fed to the system, which in turn is necessary to determine the F/M. This is because adequate F/M values allow for better maintenance of the activated sludge in both MBR plants. As such, calculating the COD through the chemical formulation of the compounds (or degradations by extension) or measuring its value via conducting a test was necessary.

Preliminaries of both methods showed that doing a COD test was by far the most reliable method of the two and therefore was chosen. Conducting the COD test and measuring its value, though lengthy, was fairly easy to perform with Camlab test kits as the correct steps were squarely followed:

- Heat the HACH (COD test kit apparatus) thermostat up to 148 °C (typically takes 10 minutes);
- Pipette 2 mL of chemical sample into a COD cuvette;

- Invert the solution in several directions for up to 1 minute;
- Insert the mixed solution cuvette into the HACH COD test kit apparatus and run it for 2 hours;
- Upon completion, remove the cuvette and let it cool down to room temperature;
- Measure the COD using the DR 900 (device used to measure COD values)

Figure 3.10 below illustrates steps taken to carry out an efficient COD test. This process is not limited to the feed solution; it can also be used for the mixed liquor within the activated sludge process of the MBR plant.

Figure 3.10. Pictures of a COD test to be carried out. 2 mL of each sample solution is pipetted respectively into a cuvette. The HACH is then used to conduct the test and finally COD is measured with the DR 900. Images from left to right are sample solutions, HACH device and DR 900 measurement kit

3.2.3. MLSS and Activated Sludge

The activated sludge used for both MBR plants (i.e. RMBR and SMBR) filtration operations was supplied by Thames Water (UK) along with a small data sheet that listed typical values for the mean diameter of floc particles (i.e. d_{pi}). Parameter, d_{pi}, was averaged for each MLSS concentration range and kept constant during all model simulations for both MBR systems (i.e. RMBR and SMBR). Its estimated values were 0.26 µm for 3.34 – 4.26 g/L (RMBR only), 0.28 µm for 6.32 – 7.24 g/L and 0.28 µm for 8.22 – 9.35 g/L.

By feeding the collected activated sludge in a semi-batch process with laboratory fabricated wastewater for both MBR plants, it was ensured that MLSS concentration rose from an initial 2.35 g/L to a final 9.35 g/L for the RMBR and 5.48 g/L to 9.35 g/L for the SMBR. In the light of conducted literature research, laboratory-scale MBR pilot units are typically operated at MLSS values that do not exceed 12 g/L, therefore 9.35 g/L was an adequate MLSS concentration at which data was collected.

Before experimentations where concerned, periodic excess sludge wasting was done to ensure that both MBR rigs had correct MLSS levels. Measuring the MLSS is important in that if not checked and too low, the process will be wasting energy whilst not treating effluent (or permeate) effectively. On the other hand if overly too high, the process will be

prone to bulking of solids causing DO levels to drop. This means that excessive aeration will be required to compensate for the deficit, thus wasting energy.

Consequently, knowing the MLSS and ensuring that it falls within the correct range was necessary to running both MBR plants more efficiently. Initially to find the MLSS level, a 50 mL mixed liquor sample was filtered through a weighed glass-fibre filter. The residue that was left on the filter was dried in the oven for one hour at a temperature of 104 °C. The combined mass of the filter and dried residue was then weighed and the MLSS was simply calculated using Equation 3.1,

$$\text{MLSS}\left(\frac{\text{g}}{\text{L}}\right) = \frac{\text{combined mass of filter with dried residue (g)} - \text{mass of filter (g)}}{\text{Volume of sample (L)}} \qquad (3.1)$$

Eventually, in an attempt to seek better accuracy, a multi-purpose MLSS analyser was purchased and used to measure the MLSS, which was averaged on a daily basis. This device not only measures the MLSS with great accuracy (within ± 0.01) but can also measure the solids content (i.e. C_d). Parameter, C_d, was averaged for each MLSS concentration range and was kept constant during all model simulations for both MBR systems. The procedure for taking measurements (see Figure 3.11) with the GE-138 MLSS Suspended Solids Sludge Concentration Meter Analyser Monitor (A. Yite Technology Group, Wanchai, Hong Kong) is outlined as follows:

- Prepare a 500 mL mixed liquor sample at room temperature;
- Dip the GE-138 sensor fully submerged into the solution sample;
- Record value displayed onto the screen after the analyser is 100% done

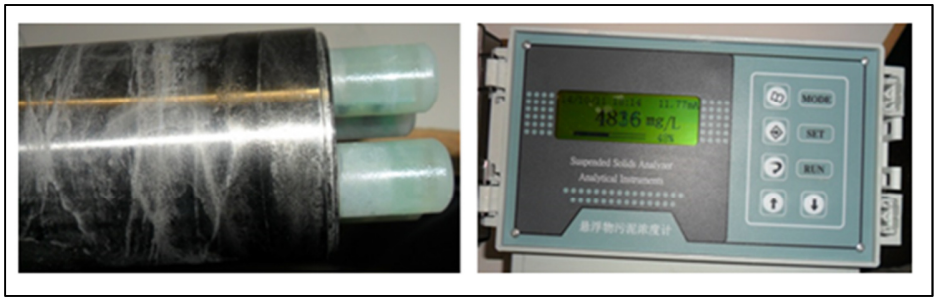

Figure 3.11. Pictures of MLSS Analyser in operation. The images from left to right are GE-138 sensor, GE-138 on-screen display after dipping its sensor inside solution sample

The recorded MLSS values for both MBR plants are shown on Figure 3.12. Each point on this graph represents the mean MLSS level that was calculated for a 3-day run period by averaging daily MLSS values. On the same figure, from the timeline axis, “Jul” means July, “Dec” means December, “Jan” means January and “Mar” means March.

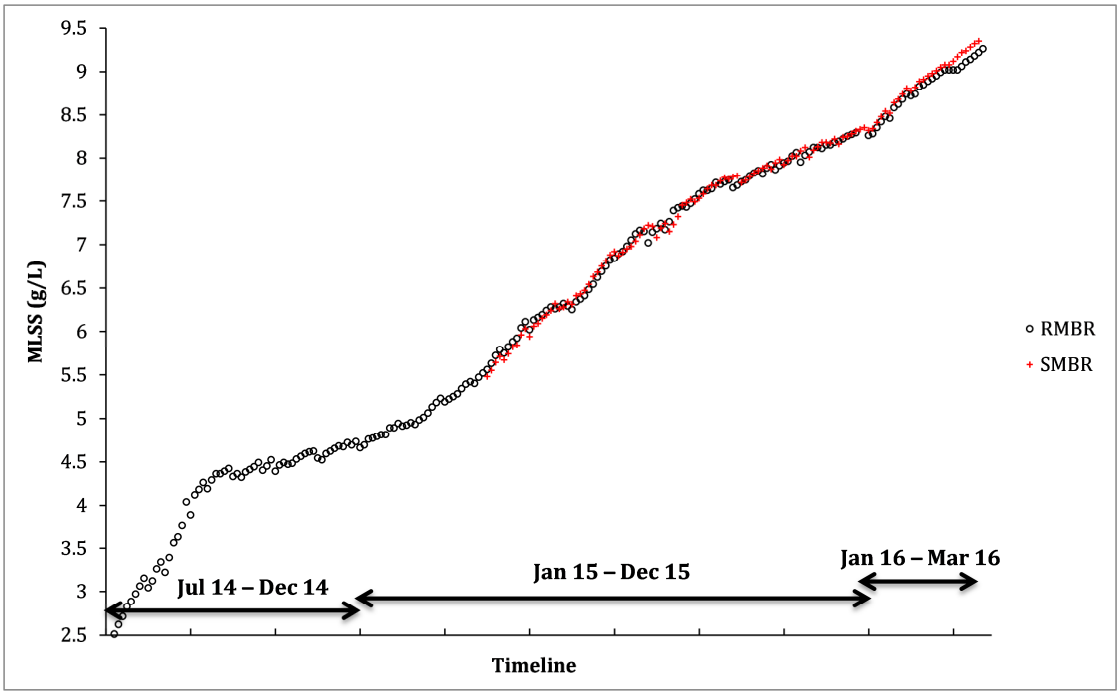

Figure 3.12. MLSS increases for the RMBR and SMBR system. Each MLSS point is averaged from a 3 day-run

From Figure 3.12 it can be said that both MBR plants were overall run within good MLSS range that fall in-line with other research studies. Despite the low starting point of 2.35 g/L for the RMBR system, the period of July to September 2014 experienced the biggest rise in MLSS concentration quickly reaching 4.42 g/L before finally being steady for the rest of the year. This is because early on in this research the activated sludge was less meddled with to allow the micro-organisms to grow when fed with adequate food.

However, after the TMP stepping experiments at MLSS level of 4.26 g/L, sludge wasting was done to keep the F/M ratio back to appropriate levels. Since then, due to daily runs to keep the RMBR plant functioning, MLSS increases had been slow but steady until the end of year 2014. At the beginning of 2015, once the laboratory became accessible (after its closure by the university due to holidays), further sludge wasting was done; and, after re-running the RMBR unit, MLSS levels decreased slightly.

By applying the usual feed, everything was back on track to a steady rate until finally in the month of April 2015, the SMBR rig was ready for usage (at which point the MLSS level had already reached 5.56 g/L). From there it was just a carry-over process. For the rest of the year after being fed at the same rate, it was observed that both MBR plants had reached agreeable MLSS values of 8.29 g/L (RMBR) and 8.35 g/L (SMBR). The same can be said for the first quarter of 2016 as both had reached MLSS value of 9.35 g/L, though noticeably sooner for the SMBR.

(Refer to **APPENDIX C.2** for the activated sludge handling, safety and collection protocol)

3.2.4. Membrane Resistance Tests

In order to obtain membrane properties data, which are used in both MBRs fouling models, membrane resistance tests for both MBR plants were carried out. The initial resistance tests for the RMBR were performed under the supervision of Mr Tzu-Lung Lin (Manager of Avanti Technology) who came all the way from the USA to lend a helping hand, and both PhD supervisors. Before conducting the irreversible and reversible resistance tests, first the clean membrane resistance test was carried out.

After ensuring that the water flux was steady (several UF tests through the membrane were run), the clean membrane resistance was determined based on UF of water at flow rate of 1×10^{-5} $m^3.s^{-1}$ and TMP of 3.92 kPa. The temperature of water was 21 °C. The clean membrane resistance was thus calculated in accordance with Darcy's law, Equation 3.2,

$$J = \frac{TMP}{\mu_w . R_m} = \frac{Q_w}{A_0}; \mu_w = 1.2182.10^{-6}[Pa.s].e^{\frac{16440.448\,[J.mol^{-1}]}{Rg.(T_w+273.15)}} \quad (3.2)$$

Where,
μ_w, in Pa.s, is the viscosity of water which is valid for water temperature, T_w (°C), between 0 and 100 °C;
R_m, in m^{-1}, is clean membrane resistance;
Q_w, in m^3/s, is the (permeate) water flow rate;
R_g, in $J.K^{-1}.mol^{-1}$ or $kJ.K^{-1}.mol^{-1}$, is the universal gas constant = 8.3145 ($J.K^{-1}.mol^{-1}$).

To confirm the pristine membrane resistance of the membrane module of the RMBR pilot unit, another test run with UF of water at flow rate of 2.33×10^{-5} $m^3.s^{-1}$ and TMP of 9.81 kPa was performed (the water temperature was 18 °C). Thus, from both runs, the calculated clean membrane resistance was found to be 6.26 (±0.03) × 10^{11} m^{-1}. For the reversible resistance test, the rotating membrane module was dipped in activated sludge for a couple of hours, and the batch tank was emptied.

The batch tank was refilled with water and UF was carried out for a period of 2 hours (until the permeate tank was full). Expectedly, since the membrane was fouled, the resistance value rose (when compared to that of the clean membrane resistance), and the calculated value was 8.93 (±0.01) × 10^{11} m^{-1}. A 58-second chemical backwash was then carried out with a 125 mg/L NaOCl solution, after which the irreversible resistance test was carried out. UF of water was run for a further 2 hours.

Since chemical backwash was carried out, it was within expectations that the resistance would go down but without a full recovery in effect. Indeed, the resistance had decreased and the calculated value was 7.67 (±0.01) × 10^{11} m^{-1}. Both resistance tests were ultimately carried out again to verify results. The reversible and irreversible membrane resistances were found to be respectively 8.95 (±0.02) × 10^{11} m^{-1} and 7.69 (±0.02) × 10^{11} m^{-1}, which were well within expected error margins. The membrane resistance loss was found to be roughly 25% and this is expected to never be recoverable.

For the constructed SMBR rig, in order to calculate the required resistances, the same tests procedures that were employed for the RMBR system were followed with an exception. After the reversible resistance test was over, since no backwash feature was available for this rig, the static membrane module was physically removed and then flushed through with a solution containing 625 mg/L of NaOCl. For the clean membrane resistance test, UF of water was conducted at flow rate of 1.25×10^{-5} $m^3.s^{-1}$ and TMP of 4.94 kPa (with water temperature of 20 °C). The membrane resistance tests results for both MBR systems are summarised in Table 3.5.

It should be noted that for calculations of irreversible and reversible resistances for both MBR plants, Equation 3.3, which is a modified form of Darcy's law, was used.

$$J = \frac{TMP}{\mu.(R_m + R_r + R_i)} \quad (3.3)$$

Where,
R_r, in m^{-1}, is the reversible membrane resistance; and,
R_i, in m^{-1}, is the irreversible membrane resistance.

Table 3.5. Membrane resistance experiments data for both MBR systems

Resistance type (m^{-1})	**RPU-185 RMBR**	**SMBR rig**
Clean membrane	$6.26\ (\pm 0.03) \times 10^{11}$	$4.55\ (\pm 0.02) \times 10^{11}$
Reversible	$8.93\ (\pm 0.01) \times 10^{11}$	$6.78\ (\pm 0.03) \times 10^{11}$
	$8.95\ (\pm 0.02) \times 10^{11}$ (2^{nd} run)	-
Irreversible	$7.67\ (\pm 0.01) \times 10^{11}$	$6.65\ (\pm 0.02) \times 10^{11}$
	$7.69\ (\pm 0.02) \times 10^{11}$ (2^{nd} run)	-

The data obtained from these experiments were fairly consistent and the clean membrane resistances of both MBR rigs were used and kept constant during model simulations where concerned.

3.2.5. Backwash and Chemical Clean

Only available for the RPU-185 RMBR, backwash is generally carried out depending on the number of experiments performed or how fouled the membrane is. This process is done automatically via the pilot unit by simply switching the backwash mode to auto and setting the flow rate to 5×10^{-5} $m^3.s^{-1}$ (or 3 L/min) as per the manufacturer's instructions.

The backwash time is typically between 1 to 3 minutes (maximum). It should be noted that several attempts at changing the backwash intensity to values more than 5×10^{-5} $m^3.s^{-1}$ or lower than 4.167×10^{-5} $m^3.s^{-1}$ (i.e. 2.5 L/min), or backwash running time above 3 minutes resulted in the pilot unit malfunctioning and the membrane module being jammed.

Thus, backwash was always carried out at the preferred 5×10^{-5} $m^3.s^{-1}$ for no more than 3 minutes. The chemical backwash requires a set amount of NaOCl concentration, C_{NaOCl} (mg/L), which is calculated using Equation 3.4,

$$C_{NaOCl} = \frac{(\text{Added volume (mL,@ 8\% NaOCl)} \times \text{Current permeate tank volume (L)} \times 0.0992)}{(\text{Permeate volume set point (L)})^2} \qquad (3.4)$$

Backwash was performed two ways after RMBR filtration operations:

i. *Normal backwash*: Automated, this process uses the permeate water to clean the rotating membrane module, and is typically done after minor experiments and/or normal daily RPU-185 pilot unit run-up. The change in total membrane resistance was relatively small when compared to chemical backwash since the colloids constricting the pores and particles adhering to the membrane surface could not be efficiently removed.

ii. *Chemical backwash*: This is generally done when the rotating membrane module is significantly fouled or after several TMP/flux stepping tests. The chemical agent as advised by the manufacturer is the sodium hypochlorite (NaOCl). Set amount of concentration of NaOCl solution depending on the permeate volume is added to and mixed with the permeate water for the backwash to automatically take place. The change in total membrane resistance was quite noticeable, which was mainly due to the fact that pore constriction was lessened to a small extent whilst the reversible resistance was vastly reduced.

However, even after chemical backwash, there were cases (i.e. MLSS value of 4.26 g/L and 7.24 g/L) where the total membrane resistance for most part remained unchanged. This meant that the membrane module was extremely fouled. In such cases, a chemical clean or bath of the membrane module was necessary. As per the manufacturer's instruction, the cleaning agent is NaOCl. The chemical dosage is typically 10 to 50 times the concentration required for a typical chemical backwash.

In practice, many industrial or municipal WWTPs use acid reagent for their chemical wash due to the large scale of their membrane modules, however for pilot units such as the RPU-185 RMBR or SMBR rig, the PVDF flat sheet membranes produce best results when used with solutions of NaOCl. The membrane module, either rotating or static, was removed whole and then dipped into a chemical bath with a high concentration of NaOCl.

The chemical bath comprised 30 litres worth of distilled water mixed with 900 mg/L of NaOCl that was poured into a big water bucket that contained either membrane module. The chemical clean lasted 42 hours and the membrane modules were refitted to their respective pilot unit in-situ. The changes in reversible and irreversible membrane resistances (Table 3.6) were fairly good and either MBR plant could resume UF operation again.

Table 3.6. Membrane resistance data after chemical clean (RMBR and SMBR)

	RPU-185 (RMBR)			SMBR Rig	
Membrane resistance (m^{-1})	**Original data**	**Chemical clean – 1st (4.26 g/L)**	**Chemical clean – 2nd (7.24 g/L)**	**Original data**	**Chemical clean – 1st (7.24 g/L)**
Reversible	8.93×10^{11}	9.17×10^{11}	9.22×10^{11}	6.78×10^{11}	6.97×10^{11}
Irreversible	7.67×10^{11}	7.89×10^{11}	7.93×10^{11}	6.65×10^{11}	6.86×10^{11}

Although an increase of 26% and 28% were observed respectively for the reversible and irreversible resistance for the RMBR system after the first chemical clean, they are still within the predicted 25% unrecoverable rate, consequently adequate data were collected after subsequent experiments were carried out. However, after the second chemical clean, build-up of colloids within the membrane pores and particles sticking to it, started to become prevalent as an increase set of 32% and 34% were observed for respectively the reversible and irreversible resistance.

Although not catastrophic for the filtration data collection that took place afterwards (e.g. still within acceptable range), the slow build-up of unrecoverable resistance is clear sign that performance wise the membrane module might no longer be reliable after a third chemical clean. The SMBR rig exhibited increase of 28% and 31% for respectively the reversible and irreversible resistance. These are still acceptable values as far obtaining filtration data are concerned, but the sharp rise in irreversible resistance proves that particles constricting the membrane pores are very hard to remove and the membrane might no longer be reliable after a second chemical clean.

3.2.6. Camlab Test Kits: Ammonium, Phosphate, Nitrate, Turbidity, Dissolved Oxygen, Total Dissolved Solids, Conductivity

As these are verification tests for the F/M (calculated using Equation 2.10), tests to check the permeate condition, or tests to obtain certain data points for both MBR rigs; and, the equipment used to conduct them are part of Camlab test kits, they will be described in one go in this section.

Broadly speaking Camlab test kits are cheap but, are inconsistent in terms of data output; and, more times than not, tests have had to be repeated a handful of time before getting trustworthy data. Needless to say, due to being less accurate when compared with a high technological process such as ion chromatography, it is generally accepted that these testing kits have a small deviation (e.g. as the HACH and DR900 are part of the kits, CODs are within ±4) on data being read, which could affect curves and analyses drawn. But, these deviations are not overly high enough to hamper the general the trend of these curves.

Consequently, good discussion and/or conclusion can be drawn out from them where necessary. Because the data for this sub-section were obtained via the usage of Camlab test kits, small deviations on calculated data points are to be expected.

Although not as accurate as the more advanced ion chromatography process, which is fairly expensive and somewhat time consuming with its methods and set-ups, Camlab test kits do have a great advantage in the sense that the methods designed for their tests are very easy to follow (usually). Hence, if anything goes wrong, the same experiment can be carried out several times until satisfactory data within reasonable boundaries are obtained.

The phosphate experiment was conducted as follows:

- Carefully remove the foil from the screwed-on Dosicap zip;
- Unscrew the Dosicap+;
- Pipette 0.5 mL of test sample into cuvette;
- Screw the Dosicap zip back tightly and firmly shake cuvette;
- Heat the cuvette in thermostat (HT 200 S) in standard program HT for 15 minutes;
- Allow it to cool to room temperature (23 °C) and shake firmly;
- Pipette into the cooled cuvette 0.2 mL reagent B (LCK 348 B) and close reagent B immediately after use;
- Screw a grey Dosicap C (LCK 348 C) onto the cuvette;
- Invert cuvette a few times, and after 10 minutes, invert it a few more times, then thoroughly clean the outside of the cuvette and evaluate

Determining the nitrate was fairly easy. Its experiment was performed as below:

- Slowly pipette 0.2 mL sample into the cuvette;
- Slowly pipette 1 mL of solution A (LCK 340 A) into the cuvette;
- Close cuvette and invert it a few times until no more streaks can be seen;
- After 15 minutes thoroughly clean the outside of the cuvette and evaluate

Most useful for nitrification and denitrification process (which were not covered in this research study), the ammonium level in permeate fluid is a good indicator of permeation quality. The ammonium test was done using the method below:

- Carefully remove the foil from the screwed-on Dosicap zip;
- Add 0.2 mL of sample to the cuvette;
- Screw the Dosicap zip back tightly, and firmly shake or invert cuvette for 1 minute;
- Cool the cuvette for 15 minutes;
- Read the value using the HACH DR 3900

Although not necessary, it is a good idea to check the permeate water DO level to ensure the correct level of DO is being fed to the MBR system. The DO test was performed using these simple steps as follows:

- Pipette 50 to 80 mL of solution sample into a beaker;
- Using HACH's HQd Field case (HQ 30d flexi), place the sensor (LDO HACH) into the solution sample totally submerged and wait until the evaluation is done

Turbidity (Figure 3.13 Left) measures the clarity of the permeate fluid, thus the smaller this value, the better the permeate water quality is. Conducting this test involved following the steps below:

- Using Palintest turbidity metre kit, take the 10 mL initial sample bottle (T0322) and place it into the holder to see if the turbidity reads 800 NTU ±80;
- Use one of the empty 10 mL test bottles and fill it with 10 mL of solution sample;
- Place said sample bottle into the holder and read

The good thing about measuring the total dissolved solids (TDS) and conductivity is that the device (Figure 3.13 Right) provides two useful parameters, temperature and fluid pH, alongside them. This is how temperature and pH levels for the SMBR rig were logged. Finding these values was accomplished through the method described below:

- Prepare 200 to 500 mL of solution sample beforehand;
- Using the HANNA H1 991300, dip the sensor into the solution sample to measure both TDS and conductivity (accomplished by simply switching functions from the menu). The temperature and pH will also be given

Figure 3.13. (Left) Turbidity read with Palintest turbidity metre. (Right) HANNA H1 991300 conductivity metre

(Please refer to **APPENDIX C.3** for their collected data including calculated values of F/M)

3.2.7. Cake Water Content, Porosity and Density

In order to accurately compute the cake thickness, a parameter dubbed cake water content, τ (-), was introduced. It was measured from filtration experiments. Averaged for specific MLSS level range, its values were used and kept constant during model simulations of both MBR rigs. Other than modelling purposes, the value of this factor gives a good indication of the cake layer particle size distribution.

Bigger cake water content would imply large particles formed a looser cake layer structure, and per this loose structure, the permeability of the cake layer would be relatively good. Conversely, with smaller cake water content, small particles would form compacter cake structure. With the assumption that τ is uniformly distributed throughout the cake layer, the procedure to calculate this parameter was fairly straight forward as per the method below:

- 5 mL of cake layer at predefined MLSS concentration (obtained from formed cake layer after UF experiments) dropped into a small glass jar (mass Mj) was accurately weighed together with the latter as Mi;
- It was then dried up in the oven at 103 °C for a period of two hours;
- This dried up mass (along with the small glass jar) was measured again as Mf;
- The cake water content, τ, was calculated using Equation 3.5,

$$\tau = {(\mathrm{Mi} - \mathrm{Mf})}\Big/{(\mathrm{Mi} - \mathrm{Mj})} \qquad (3.5)$$

Results obtained for τ are fairly reasonable as cake layers formed were not too dense or too loose; and, this is reflected in the fact that the bulk cake densities are not large. Table 3.7 outlines the measured values of τ for both MBR plants.

Table 3.7. τ determined at different MLSS concentrations used during the various UF of activated sludge

RPU-185 RMBR	**SMBR rig**	**RPU-185 RMBR**	**SMBR rig**
MLSS (g/L)	MLSS (g/L)	τ (–)	τ (–)
3.34	–	0.454	–
3.89	–	0.456	–
4.26	–	0.457	–
6.32	6.32	0.455	0.456
6.82	6.82	0.456	0.454
7.24	7.24	0.456	0.458
8.22	8.22	0.443	0.439
8.76	8.76	0.449	0.446
9.35	9.35	0.442	0.441

As such, an average τ of 0.456 was used for MLSS level range 3.34 – 4.26 g/L; 0.456 for MLSS level range 6.32 – 7.24 g/L; 0.445 and 0.442 for respectively RMBR and SMBR for MLSS level range 8.22 – 9.35 g/L.

Generally speaking, porosity, otherwise known as void fraction, is defined as a fraction of volume voids over the total volume and is between 0 and 1 (sometimes expressed as a percentage between 0 and 100%). As most of the empty space within the cake layer is considered filled with liquid, cake porosity, ε_c, can be calculated using Equation 3.6.

$$\varepsilon_c = (\text{bulk cake volume} - \text{dry cake volume}) \Big/ \text{bulk cake volume} \quad (3.6)$$

Thus, it can be said (and assumed) that cake porosity $\varepsilon_c \approx \tau$. This value was used and kept constant during model simulations of both MBR plants. In general literature research, porosity values used range from 0.4 to 0.5. For example, Jørgensen et al. (2014) used a porosity of 0.5 for his shear rate – viscosity model. Therefore, the values listed in Table 3.7 are fairly reasonable from a modelling standpoint.

The density of fluid, ρ_f (kg.m^{-3}), in both MBR systems fouling models is that of activated sludge. This value was calculated and kept constant within Matlab, and was used during model simulations of both MBR rigs. Some researchers have used 1040 kg.m^{-3} (Jørgensen et al. 2014) for their activated sludge density, however it can be better estimated with Equation 3.7 (Metcalf and Eddy 2003).

$$\rho_{sludge}\,[\text{kg.m}^{-3}] = \rho_{water} + 0.2.(\text{MLSS}\,[\text{g/L}]) \quad (3.7)$$

Where,
ρ_{water}, in kg.m^{-3}, is the water density; and,
ρ_{sludge}, in kg.m^{-3}, is the activated sludge density.

From simple mass over volume ratio, bulk cake density, ρ_b (kg.m^{-3}), was obtained alongside the cake water content. This value, averaged for specific MLSS concentration range, was used and kept constant during model simulations of both MBR systems. Therefore, ρ_b of 1128.23 kg.m^{-3} was used for MLSS level range 3.34 – 4.26 g/L; 1129.32 kg.m^{-3} for MLSS level range 6.32 – 7.24 g/L; and 1132.17 kg.m^{-3} for MLSS level range 8.22 – 9.35 g/L.

3.2.8. SMP Inclusion

Only done for the RMBR system, the original plan for the SMP inclusion model, was to try to measure protein and polysaccharide concentrations in the bioreactor's mixed liquor, and then by inference the amount sticking to the membrane. However, due to time constraints, a rougher and more direct approach was opted for.

Fairly straight forward, in order to study the implications of foulants (e.g. SMP) and cake formation in relation to MLSS concentration, after a filtration process, total cake thickness was measured (for desired bulk MLSS concentration used) then divided by initial total flux.

This value was later referred to as cake thickness ratio. MLSS concentrations used for cake thickness measurements initially varied from 1.2 to 4.3 g/L but later an additional data set for MLSS levels ranging from 5.96 to 9.35 g/L was collected. The starting flow rates for each MLSS concentration range were respectively 1×10^{-5} $m^3.s^{-1}$ and 1.15×10^{-5} $m^3.s^{-1}$.

Though nine data points were collected for each MLSS level range, data points at MLSS of 1.25 g/L, 2.82 g/L, 4.12 and 4.26 g/L, which could not be measured through experiments, were interpolated based on other experimentally measured cake thicknesses. Then, using Equation 4.17 for verification, final values were reached. All necessary experiments were carried out at constant room temperature (of 23 °C). The influents used had an average pH between 7.4 and 9.2.

3.2.9. Viscosity and Shear

The viscosity of activated sludge, which was tested at constant room temperature of 23 °C for the RMBR and SMBR system, is logged daily with the help of a viscometer (i.e. Rotary-Viscometer ASTM by PCE Instruments UK Ltd, Southampton, UK). To take measurements, first, a sample of fluid (e.g. mixed liquor) is collected (generally about 150 mL). With the machine turned on, one of the testing standards selected from the on-screen menu, and the recommended spindle type by the manufacturer chosen (as the device utilises the notion of torques for measurements), the viscosity is simply measured by having the spindle rotate through the fluid and wait until the testing standard is done analysing it.

The displayed value on-screen is the viscosity given in mPa.s (and accurate within ± 0.01). It should be noted that it was first ensured that the device was working adequately by reading water viscosity and ensuring that it was roughly equal to one mPa.s. In cases where viscosity could not be measured such as data with Coors (UK) and Duclos-Orsello et al. (2006), Equation 3.8 (Yang et al. 2009) was used.

$$\mu = 0.0126.\,(C_{MLSS})^{1.664}.\,e^{\frac{E}{Rg.(T_{room}+273.15)}} \qquad (3.8)$$

Where,
E, in $kJ.mol^{-1}$, is the activation energy for viscosity and normally = 9.217 ($kJ.mol^{-1}$); and,
T_{room}, in °C, is the room temperature.

When dealing with viscosity of activated sludge, which varies with shear rate (or torque) and affects the shear at the membrane surface, an extra step must be taken for the RMBR model. This is because shear is a key parameter promoting flux (where necessary) that may be significant in determining total available flux. Thus, another testing method involving

measuring viscosity at different shear rate so as to determine shearing effects parameters m and n was employed.

Even though full on sludge rheology tests were not conducted, the measurements still fell in-line with protocols by Yang et al. (2009) and Ratkovich et al. (2013). Following the exact same method described earlier in this sub-section for viscosity reading but, this time by changing torque thus shear rate (with corresponding values being read from a measuring sheet provided by the manufacturer), viscosities of fluid were measured at different shear rate for required MLSS concentration range.

The shear rate range was 10 – 350 s^{-1} for each MLSS level range of 3.34 – 4.26 g/L, 6.32 – 7.24 g/L and 8.22 – 9.35 g/L. Fourteen data points were collected for each MLSS level range. For verification the same viscosity reading tests were carried out using Brookfield rotating viscometer (High Shear CAP-2000+, by Brookfield Viscometers Ltd, Essex, UK). The exact same steps as described above were followed, except here for convenience, the device readily displayed the shear rate at which viscosity was read.

The readily available software of the viscometer was used for data collection (i.e. the same MLSS level range and shear rate range were used). While full on rheology tests were not carried on the activated sludge to precisely ascertain its properties, all collected data appeared consistent though small deviations of roughly 4% on data should be noted.

(Please refer to **APPENDIX C.4** for more information on viscosity)

3.2.10. TMP Stepping and Constant Flux

All experiments conducted here for both MBR rigs were UF of activated sludge at constant room temperature of 23 °C. The influents used had an average pH between the range of 7.4 and 9.2.

TMP stepping, which at its core concept is similar to flux stepping as it is a process of stepping up or down the TMP or flow rate (Le-Clech et al. 2003, Wu et al. 2008, Luo et al. 2013, Zhu et al. 2016), was used to gather filtration data sets for both MBR plants (i.e. RPU-185 RMBR and SMBR rig). These data were fed to the fouling models for simulations. The TMP steps that were used for performing the UF constant TMP experiments were 15, 30, 45 and 58 kPa. The MLSS concentrations at which each of these constant TMP experiments were conducted were: 3.34 and 4.26 g/L, 6.32 and 7.24 g/L, and 8.22 and 9.35 g/L.

The TMP steps up and their corresponding initial flow rates for these MLSS concentrations for both MBRs (i.e. RPU-185 RMBR and SMBR rig) are summarised in Table 3.8. For model calibration verifications (only carried out for the RMBR), only two TMP steps of 15 and 45 kPa were considered (so as to facilitate comparison) for each MLSS level of 3.89, 6.82 and 8.76 g/L (with each respectively falling within MLSS concentration range of 3.34 – 4.26 g/L, 6.32 – 7.24 g/L, and 8.22 – 9.35 g/L). Table 3.8 also summarises their starting flow rates.

Table 3.8. TMP steps up and their starting flow rate for both MBRs

	TMP step up (kPa)	RPU-185 RMBR	SMBR rig
		Initial flow rate ($m^3.s^{-1}$) × 10^{-5}	Initial flow rate ($m^3.s^{-1}$) × 10^{-5}
MLSS (g/L) 3.34 – 4.26	15	1.00	N/A
	30	1.83	
	45	2.25	
	58	2.75	
MLSS (g/L) 6.32 – 7.24	15	1.15	1.20
	30	2.017	2.03
	45	2.45	2.50
	58	2.93	3.02
MLSS (g/L) 8.22 – 9.35	15	1.28	1.32
	30	2.12	2.20
	45	2.60	2.62
	58	3.017	3.067
MLSS (g/L) 3.89 (Calibration verification)	15	1.067	N/A
	45	2.32	
MLSS (g/L) 6.82 (Calibration verification)	15	1.10	
	45	2.42	
MLSS (g/L) 8.76 (Calibration verification)	15	1.23	
	45	2.55	

During the constant flux experiments, which were only carried out for the RMBR, filtration data were recorded for each MLSS concentration of 3.34 and 4.26 g/L. The flow rate was 8.67 × 10^{-6} $m^3.s^{-1}$ whilst the corresponding starting TMP was 12 kPa. A final data set was collected for each MLSS level of 6.32 and 7.24 g/L. However, these were the absolute limits the RMBR could be pushed to without TMP reaching values too high that would harm the membrane module (i.e. there were after all limited rotating membrane modules available at the laboratory). The flow rate was 1.12 × 10^{-5} $m^3.s^{-1}$ whilst its corresponding initial TMP was 15 kPa.

For each carried out UF experiment, whether for the RMBR or SMBR, although filtration data was constantly being logged, to keep model computation time down to a minimum, only the average data point for every 5 min of filtration time was actually used in the simulation study with the total filtration period being two hours. This meant that a total of 25 data points were generated for each individual MLSS concentration. After each TMP step or constant flux experiment, a chemical backwash was done for the RMBR with 125 mg/L worth of NaOCl solution. For the SMBR rig, 185 mg/L of NaOCl solution was used to flush through the static membrane module.

3.3. Chapter Summary

This chapter covered the essentials on both pilot units (RMBR and SMBR). The RPU-185 RMBR appears to be a system with ease of access for most part and therefore can be used for experimentation where necessary while the SMBR rig on the other hand, requires some extra steps, such as having to remove the membrane module and flush through it with solutions of NaOCl since there is no backwash feature or relying on testing kits to log certain data.

Experimental or testing methods on how the models' constant parameters were obtained were outlined as well. One of these constant parameters was the pristine membrane's resistance. Its values were obtained through resistance testing of both membrane module types. Knowing the reversible and irreversible resistances from these tests, the effects of backwash as well as chemical wash on the membrane modules were discussed. Activated sludge was semi-batch fed with synthetic wastewater that was fabricated in laboratory.

This allowed the MLSS concentration to rise to a final 9.35 g/L for the RMBR and SMBR system. The protocol behind the creation of the synthetic sewage was explained and COD measurements were taken for the calculation of F/M. However, small deviations on the readings were acknowledged as the COD testing kits are part of the Camlab package.

The testing kits limitations were discussed as well. Viscosities were logged with the help of a viscometer and the shear's data were obtained. In cases where viscosity could not be determined, it was calculated using Equation 3.8. Finally, filtration experiments such as TMP stepping, constant flux and SMP inclusion, which yielded the necessary data that were fed to both MBRs' fouling models, were highlighted.

(Please refer to **APPENDIX C.5** for the simulations' constant parameters that were used to procure the Coors UK and Duclos-Orsello et al. 2006 curves)

CHAPTER 4: MODEL STRUCTURES

Demonstrating how the RMBR and square SMBR fouling models were developed is just as important as showing how they were implemented using Matlab. This section thus explores step by step derivations of the formulae and first principle definitions involved in the creation of the RMBR and SMBR fouling model. This chapter is divided into two main sub-sections:

i. *Development of Fouling Models*: This sub-section defines how the MBR fouling models were derived in full for both MBR systems.

ii. *Matlab Software, Genetic Algorithm and Optimisation of α_v and δ'*: This sub-section explains the usage of Genetic Algorithm in Matlab for simulations of the fouling models of both MBR plants, the optimisation of α_v (air scouring coefficient) and δ' (resistance distribution factor of cake layer), and the determination of shear effects and SMP inclusion model parameters.

4.1. Development of Fouling Models for Rotating and Static Square MBRs

As per Hermia (1982) model, traditionally four classical fouling mechanisms used to be considered. However, as intermediate blockage fouling mechanism essentially plays the same role as pore blocking fouling mechanism, three classical fouling mechanisms are nowadays the preferred option for studies (Duclos-Orsello et al. 2006, Gupta et al. 2008). These fouling mechanisms are namely pore blocking, pore constriction and cake filtration.

In this thesis, these three fouling mechanisms are chosen for study. Let us consider Figure 4.1a, b and c as the fouling mechanisms that occur during a typical filtration process (e.g. UF) for membranes that have been fouled for both MBRs (i.e. RMBR and SMBR). During the filtration timeline, fouling is observed with respect to the change in TMP (or flux), MLSS level, or a combination of both. The conditions under which these fouling mechanisms are dominant are discussed later in **Chapter 5** and **6** and summarised in **Chapter 8**.

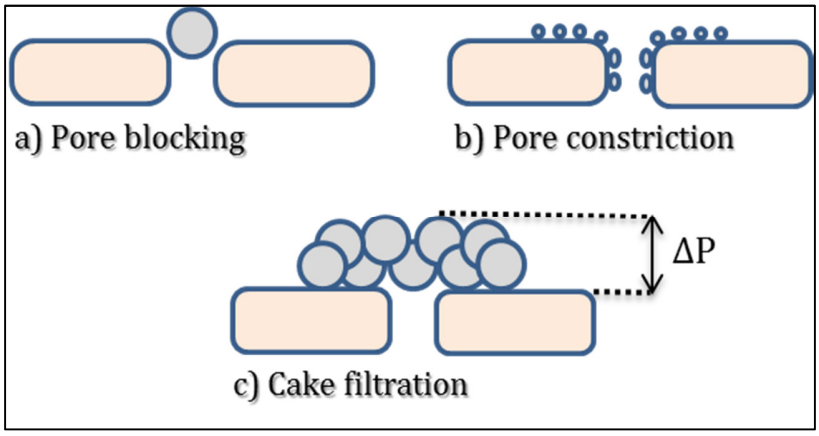

Figure 4.1. Diagram of the combined fouling mechanisms: Colloids or small particles constrict the pores while larger particles block them, and accumulate to form a cake

Firstly whilst referring to Figure 4.1a, b and c, it was assumed that the membrane's pores were cylindrical and uniformly distributed throughout the membrane, so that fluid flow could be described by Hagen-Poiseuille flow. Hence, pore constriction occurs through all open pores, and gradually the membrane surface becomes obstructed by aggregates forming a somewhat uneven blocked area. Once the pores are blocked by aggregates, pore constriction is stopped.

Consequently, a cake layer will form over any blocked area. The resistance of this deposit layer is time dependent with regions of greatest resistance delivering the smallest flux. However, in reality the actual membrane fouling process is extremely complex in nature with usually all effects simultaneously occurring. Nevertheless, to simplify the model the above assumptions are made as well as overlooking the effect of frictional forces and temperature (Paul and Jones 2015, Paul and Jones 2016).

4.1.1. Fouling Models for Rotating MBR

With the inclusion of shear effects, the fouling model for the RMBR rig needs to be handled with care when the system is operated under constant TMP mode. With this mode, as the filtration process goes on, the flux declines, indicating fouling. The ensuing sub-section shows how the fouling model for the RMBR was developed under such condition.

4.1.1.1. Constant TMP/Varying Flux

Since the RMBR is operated under constant TMP, its fouling model must be evaluated in terms of the varying flux. To assess the fouling in the RMBR, one must first look at two factors that affect its shear effects: the viscosity and MLSS. The viscosity of MLSS in a MBR plays a major role on mass transport and accordingly influences its hydrodynamic regimes, shear effects and overall performance.

Thus, its appearance in the fouling model formulation is a must. Using the power law for non-Newtonian fluids (as is activated sludge), the relationship between viscosity and shear rate is shown through Equation 4.1 (Yang et al. 2009, Bentzen et al. 2012) as follows:

$$\mu = m.\dot{\gamma}^{n-1} \tag{4.1}$$

Both m and n are parameters affecting viscosity with respect to shear rate; as such, they are referred to here as "shear effects parameters" which are, in effect, a combo of the fluid's flow consistency index (e.g. how consistent the fluid flow is) and the fluid's flow behaviour index (e.g. how the fluid behaves, for example pseudoplastic).

To calculate the shear rate over the rotating membrane, one must first consider the flow regime through the membrane module. The shear rate based on different flow regimes is computed using Equation 4.2 (Jaffrin 2008).

$$\text{if,} \begin{cases} Re_{r,NN} \leq 2.10^5, \text{laminar flow}, \dot{\gamma} = 1.81.(k_\omega.\omega)^{1.5}.r_o.\nu^{-0.5} \\ Re_{r,NN} > 2.10^5, \text{turbulent flow}, \dot{\gamma} = 0.057.(k_\omega.\omega)^{1.8}.{r_o}^{1.6}.\nu^{-0.8} \end{cases} \tag{4.2}$$

The shear rate in Equation 4.2 changes formula depending on flow regime (i.e. using $Re_{r,NN}$ values); where,
r_o, in m, is the membrane outer radius and r in original Equation 2.20 is represented by r_o.

The type of flow regime through the membrane for non-Newtonian fluids (as is the case for activated sludge) can be determined using Equation 2.21 (see **sub-section 2.1.2.2**).

The inclusion of the MLSS in the fouling model can be done in similar fashion to the reformulation of the Duclos-Orsello et al. (2006) model undertaken by Paul (2013). Thus, the bulk concentration, C_b (g/L), is replaced by the bulk MLSS concentration, C_{MLSS} (g/L).

Assuming the membrane rotates around a fixed axis (here defined as an imaginary straight line passing through the shaft) with angular velocity, ω (rad/s), and using the pore constriction model, unblocked flux (i.e. flux within the unblocked membrane area, A_u), J_u (m/s), defined as a function of (filtration) time, is shown in Equation 4.3 (Duclos-Orsello et al. 2006, Paul 2013) as follows:

$$\frac{J_u(t)}{J_0} = \frac{1}{(1+\beta.Q_0.C_{MLSS}.t)^2};\ \text{where}\ \beta = \frac{\sigma_a}{\pi.(r_p)^2.\delta_m} \rightarrow J_u(t) = \frac{r'_0.k_\omega.\omega}{(1+\beta.Q_0.C_{MLSS}.t)^2};\ \text{where}\ J_0 = r'_0.k_\omega.\omega \quad (4.3)$$

Where,
J_0, in m/s, is the initial flux of clean membrane;
Q_0, in m^3/s, is the initial flow rate;
r'_0, in m, is the distance radius from the spinning axis. Thus, $r'_0 = r_o - r_i$, with r_i (in m) being membrane inner radius;
β, in kg, is the pore constriction parameter (e.g. "amount of pore constriction" per unit of pore volume); and,
σ_a, in m^3.kg, is an adjustable parameter related to pore constriction or simply the "amount of pore constriction". This here represents the product of foulant deposited in pore interior, constricting it (i.e. pore constricted), and pore volume. As membrane thickness and pore radius should be known, it becomes a calculable value that varies based on the value of β (e.g. obtained from a simulation fit).

As the membrane fouls with time, the unblocked membrane area also decreases at the same rate, and the rate of unblocked membrane area reduction is given by Equation 4.4.

$$\frac{dA_u}{A_u} = \frac{-\alpha.C_{MLSS}.r'_0.k_\omega.\omega}{(1+\beta.Q_0.C_{MLSS}.t)^2}.dt \quad (4.4)$$

Assuming that at time t = 0, the initial unblocked membrane area relative to the membrane area is A_{u0} (m^2), by integrating Equation 4.4 between the filtration time boundaries, Equation 4.5 is derived.

$$\ln\left(\frac{A_u}{A_{u_0}}\right) = \frac{\alpha.r'_0.k_\omega.\omega}{\beta.Q_0}.\left(\frac{1}{1+\beta.Q_0.C_{MLSS}.t} - 1\right) \therefore A_u(t) = A_{u_0}.e^{\frac{\alpha.r'_0.k_\omega.\omega}{\beta.Q_0}.\left(\frac{1}{1+\beta.Q_0.C_{MLSS}.t}-1\right)} \quad (4.5)$$

By combining Equation 4.3 and 4.5, the flow rate through open (i.e. unblocked) pores, Q_u (m^3/s), can be calculated as shown in Equation 4.6.

$$Q_u(t) = \frac{A_{u_0}.r'_0.k_\omega.\omega}{(1+\beta.Q_0.C_{MLSS}.t)^2}.e^{\left\{\frac{\alpha.r'_0.k_\omega.\omega}{\beta.Q_0}.\left(\frac{1}{1+\beta.Q_0.C_{MLSS}.t}-1\right)\right\}} \quad (4.6)$$

The blocked flux (i.e. flux within the blocked membrane area), J_b (m/s), can be calculated from Equation 4.7 using Darcy's law and a resistance in-series approach, whilst the TMP can be expressed in terms of density and angular velocity in Equation 4.8 (Jaffrin 2008).

$$J_b = \frac{TMP}{\mu.(R_{in,b} + R_b)} \quad (4.7)$$

$$TMP = -PT - \left(\frac{1}{4}.\rho_f.(k_\omega.\omega.r_o)^2\right) \quad (4.8)$$

Where,
PT, in Pa, is the pressure at membrane periphery; and,
$R_{in,b}$, in m^{-1}, is the membrane resistance and resistance caused by pore constriction.

Once the pore constriction stops at time t_b (s), the time at which a membrane pore was first blocked, $R_{in,b}$ can be calculated from Equation 4.9 (Duclos-Orsello et al. 2006).

$$R_{in,b} = R_m.(1 + \beta.Q_0.C_{MLSS}.t_b)^2 \quad (4.9)$$

The resistance of particles dumped over a section of the membrane (assuming uniformity) increases with time due to the growth in mass (or thickness) of the cake layer. Using the cake filtration (or formation) model, this resistance R_b is determined in Equation 4.10.

$$\frac{dR_b}{dt} = f'.R'.J_b.C_{MLSS} \quad (4.10)$$

Assuming, no loss in area, the blocked membrane area, A_b (m^2), is given by Equation 4.11, and is directly proportional to the unblocked membrane area at time t_b.

$$\frac{dA_b}{dt_b} = -\frac{dA_u}{dt_b} \rightarrow$$
$$A_b(t_b) = \int_0^t \left(\frac{A_{u0}.\alpha.C_{MLSS}.r'_0.k_\omega.\omega}{(1+\beta.Q_0.C_{MLSS}.t_b)^2}.e^{\left\{\frac{\alpha.r'_0.k_\omega.\omega}{\beta.Q_0}.\left(\frac{1}{1+\beta.Q_0.C_{MLSS}.t_b}-1\right)\right\}}\right) dt_b \quad (4.11)$$

At low rotational speeds (such as that of the RMBR system here) the flow can be considered laminar, and thus by combining Equation 4.1, 4.2, 4.7 – 4.9 and 4.11, the flow rate through blocked pores, Q_b (m^3/s), is given by Equation 4.12.

$$Q_b(t)=\frac{-PT-\left(\frac{1}{4}.\rho_f.(k_\omega.\omega.r_o)^2\right)}{m.\left(1.81.(k_\omega.\omega)^{1.5}.r_o.\nu^{-0.5}\right)^{n-1}.\left(R_m.(1+\beta.Q_0.C_{MLSS}.t_b)^2+R_b\right)}.$$
$$\int_0^t\left(\frac{A_{u0}.\alpha.C_{MLSS}.r'_0.k_\omega.\omega}{(1+\beta.Q_0.C_{MLSS}.t_b)^2}.e^{\left\{\frac{\alpha.r'_0.k_\omega.\omega}{\beta.Q_0}.\left(\frac{1}{1+\beta.Q_0.C_{MLSS}.t_b}-1\right)\right\}}\right)dt_b \quad (4.12)$$

Thus, the total normalised flow rate through the membrane, Q_t (m^3/s), is expressed as the summation of the flow rate through open (i.e. unblocked) pores, Q_u, and flow rate through blocked pores, Q_b, respectively as shown in Equation 4.13.

$$Q_t(t)=\frac{A_{u_0}.r'_0.k_\omega.\omega}{(1+\beta.Q_0.C_{MLSS}.t)^2}.e^{\left\{\frac{\alpha.r'_0.k_\omega.\omega}{\beta.Q_0}.\left(\frac{1}{1+\beta.Q_0.C_{MLSS}.t}-1\right)\right\}}+$$
$$\frac{-PT-\left(\frac{1}{4}.\rho_f.(k_\omega.\omega.r_o)^2\right)}{m.(1.81.(k_\omega.\omega)^{1.5}.r_o.\nu^{-0.5})^{n-1}.(R_m.(1+\beta.Q_0.C_{MLSS}.t_b)^2+R_b)}. \quad (4.13)$$
$$\int_0^t\left(\frac{A_{u0}.\alpha.C_{MLSS}.r'_0.k_\omega.\omega}{(1+\beta.Q_0.C_{MLSS}.t_b)^2}.e^{\left\{\frac{\alpha.r'_0.k_\omega.\omega}{\beta.Q_0}.\left(\frac{1}{1+\beta.Q_0.C_{MLSS}.t_b}-1\right)\right\}}\right)dt_b$$

The accumulation of particles at the membrane surface results in the formation of a cake layer (or fouling layer) resistance that is represented here by the term R_b. In reality however, because this term is controlled by the system's hydrodynamics, the RMBR's hydrodynamics must be processed in order to ascertain its true value in the fouling model.

In terms of hydrodynamic regimes, air scouring flux (i.e. air flow rate divided by membrane area), J_{air} (m/s), plays an intrinsic role in the management and prevention of membrane fouling in most submerged MBR systems (as is the RMBR). As such, the cake layer growth rate depends on the scouring energy induced by the aeration. Furthermore, the rotation in RMBRs produces a torque which induces additional shear effects to reduce fouling on the membrane surface. Rightfully so, since the RMBR has a very low rotational speed of 2.09 rad/s (or 20 revolutions per minute), the aforementioned scenario and ensuing equations will be correct.

Nevertheless, it is worth mentioning that at very high rotational speeds there is a high possibility that the air scouring effects will be significantly much less than those induced by rotation. The net total effect on the membrane responsible for reducing fouling can tentatively be calculated by the summation of the air scouring and rotational effects. In hindsight however, at some point during the filtration process, these two effects work in opposite directions. This fact alone ultimately poses a physical limitation to the model since a completely isolated hydrodynamic study of the shear stresses will be required, which is not the scope of this study.

In the aforementioned scenario, the cake's resistance is consequently decreased to allow the system to gain flux due to these membrane cleaning effects. To account for these changes, an additional removal term was added to the rate of blocked membrane area as shown in Equation 4.14, and was defined as the flux induced by the air scouring flow

combined with rotational effects. This additional removal term is also in-line with Liang et al. (2006) cake's formulation equation which accounted for the change in reversible fouling due to cake build-up. An analogous reformulation is found in Equation 4.14 but includes air scouring and rotational effects.

$$\frac{dR_b}{dt} = f'.R'.J_b.C_{MLSS} - g_o.(\alpha_v.J_{air} - k_\omega.\omega.r_o).\delta'.(R'_c.\theta_c) \quad (4.14)$$

Where,
g_o, unitless (−), is the cake removal factor. This value dictates how much cake is removed by air scouring and rotational effects and is one of the factors controlling the decrease in cake layer formed;
R'_c, in m^{-2}, is the so-called specific cake resistance. It can be computed with the Carman–Kozeny Equation 4.15 (Giraldo and LeChevallier 2006);
α_v, unitless (−), is the air scouring coefficient;
δ', in m^{-1}, is the resistance distribution factor of cake layer; and,
θ_c, in m, is the cake's thickness.

$$R'_c = \frac{180.(1-\varepsilon_c)^2}{{d_{pi}}^2.{\varepsilon_c}^3} \quad (4.15)$$

A reduction in net cake layer growth rate means that the net blocked membrane area will reduce too. This ultimately gives the membrane module more unblocked membrane area to permeate. Subsequently, the blocked membrane area, A_b (m^2), is mathematically given by Equation 4.16.

$$\frac{dA_b}{dt} = \alpha.J_u.A_u.C_{MLSS} - k_{A_b}.(\alpha_v.J_{air} - k_\omega.\omega.r_o).\theta_c(t) \quad (4.16)$$

Where,
k_{Ab}, unitless (−), is the blocked pores area constant.

The net cake thickness increases steadily with filtration time (as the membrane gets more fouled) and can be calculated using Equation 4.17 (Li et al. 2012).

$$\theta_c(t) = \frac{Volume}{Area} = \frac{\frac{mass_{cake}}{(1-\tau).\rho_b}}{Area} = \frac{\frac{C_d.Area.J_{m_o}.t}{(1-\tau).\rho_b}}{Area} = \frac{C_d.J_{m_o}}{(1-\tau).\rho_b}.t \quad (4.17)$$

Where,
J_{mo}, in m/s, is the initial total flux within membrane.

4.1.1.2. SMP Inclusion Model

To account for variations in sludge properties and subsequent fouling agents as clogging particles (i.e. SMP) on the membrane surface, it was assumed that the MLSS concentration, C_{MLSS}, was directly proportional to the SMP's concentration, C_{SMP} (g/L). C_{SMP} is calculated in accordance with Giraldo and LeChevallier (2006) model as shown by Equation 4.18.

$$C_{SMP} = C'_{MLSS}.e^{\frac{k_i.\theta_c}{J_{m_o}}};\ C_{MLSS} = \epsilon_{smp}.C_{SMP} \tag{4.18}$$

Where,
C'_{MLSS}, in g/L, is the MLSS concentration factor;
k_i, in s^{-1}, is the first order particle removal coefficient; and,
ϵ_{smp}, unitless (−), is the SMP concentration factor.

Thus differentiating Equation 4.3, yields the unblocked flux expression as shown in Equation 4.19 with SMP effects included.

$$\frac{dJ_u}{dt} = -2.\beta.Au_0.\left(\epsilon_{smp}.C'_{MLSS}.e^{\frac{k_i.\theta_c}{J_{m_o}}}\right).(r'_0.k_\omega.\omega)^2.\left(\frac{1}{1+\beta.Q_0.\left(\epsilon_{smp}.C'_{MLSS}.e^{\frac{k_i.\theta_c}{J_{m_o}}}\right).t}\right)^3 \tag{4.19}$$

4.1.1.3. Constant Flux/Varying TMP

Since the system is operated under constant flux, the change in TMP with respect to filtration time must be modelled. This can be accomplished by deriving equations for the varying TMP with the assistance of Darcy's law and the resistance in-series approach. As the TMP increases (indicating fouled membranes), the total available area for permeate will decrease at a uniform rate such that there exists a time constant, t_c (s^{-1}) < 1/t, that yields Equation 4.20 where the time constant is proportional to the initial total flux (since flow rate is constant). It should be noted that this area formulation equation is somewhat similar to the one proposed by Hermia (1982).

$$A = A_0.(1 - t_c.t) = A_0.\left(1 - K_\alpha.J_{m_o}.t\right) \tag{4.20}$$

Where,
A, in m^2, is the remaining membrane area available for permeate; and,
K_α, in m^{-1}, is the area distribution density.

Using a Taylor's expansion of order 1 (as $\ln(1 - K_\alpha . J_{m_o} . t)$ at $t = 0$ is $\approx -K_\alpha . J_{m_o} . t$), Equation 3.20 reduces conveniently into Equation 4.21.

$$A = A_0 . \ln\left(e . \left(1 - K_\alpha . J_{m_o} . t\right)\right) \equiv A_0 . e^{(-K_\alpha . J_{m_o} . t)} \quad (4.21)$$

However, this reformulation has an extreme limitation in that simulated values for the remaining area will be under estimated after a certain period of time due to the truncation induced by the Taylor's expansion term. For the same K_α, both the reformulation and original area model will exhibit almost similar behaviour so long as the following is true:

$$0 < K_\alpha J_{m_o} . t \leq 0.1 \rightarrow K_\alpha \leq \frac{0.1}{J_{m_o} . t}$$

Outside this range, it is expected that large errors of more than 10% could occur. As such, determining the TMP using this area reformulation method will only be valid for short term filtration operations (i.e. up to two hours), and is not recommended that this approach be used for long term filtration data, where the original area formulation method should be used instead.

In this fouling model and as observed in practice, as the fouling of the membrane continues, the system experiences an exponential increase in TMP. Thus, total membrane resistance, R_{total} (m^{-1}), which is the summation of the cake's resistance and all other mechanisms' resistances, can be estimated using Equation 4.22 by introducing constant term φ.

$$R_{total} = \left(R_{in,b} + \varphi . (R'_c . \theta_c)\right) \quad (4.22)$$

Equation 4.23 is yielded by using Darcy's law and differentiating the TMP with respect to filtration time, t.

$$\frac{\mu}{A_0} . \left(\lim_{\Delta t \rightarrow 0} \left(\frac{\Delta Q}{\Delta t}\right)\right) = \frac{A}{A_0} . \left(\frac{d(TMP)}{dt} . \left(\frac{1}{R_{total}}\right) + TMP . \frac{d\left(\frac{1}{R_{total}}\right)}{dt}\right) \quad (4.23)$$

Since the flow rate through membrane, Q, is kept constant, $dQ/dt = 0$; and thus, combining Equations 4.20, 4.22 and 4.23, yields the TMP formulation model, model 1, which is denoted by Equation 4.24.

$$TMP(t) = TMP_0 . \frac{\left(R_m . ((1 + \beta . Q_0 . C_{MLSS} . t_b)^2 - 1) + \varphi . \left(\frac{180 . (1 - \varepsilon_c)^2}{{d_{pi}}^2 . {\varepsilon_c}^3} . \frac{C_d . J_{m_o}}{(1 - \tau) . \rho_b} . t\right) + R_{t0}\right)}{(1 - K_\alpha . J_{m_o} . t) . R_{t0}} \quad (4.24)$$

Where,
TMP_0, in Pa, is the initial trans-membrane pressure; and,

R_{t0}, in m^{-1}, is the initial total membrane's resistance at t = 0.

Additionally, combining Equations 4.21, 4.22 and 4.23, yields the TMP formulation model, model 2, which is denoted by Equation 4.25.

$$TMP(t) = TMP_0.\frac{\left(R_m.\left((1+\beta.Q_0.C_{MLSS}.t_b)^2-1\right)+\varphi.\left(\frac{180.(1-\varepsilon_C)^2}{{d_{pi}}^2.{\varepsilon_c}^3}.\frac{C_d.Jm_o}{(1-\tau).\rho_b}.t\right)+R_{t0}\right)}{e^{(-K\alpha.Jm_o.t)}.R_{t0}} \quad (4.25)$$

For the simulations of TMP variations, model 1 and model 2 were both used. This allowed conclusions to be better drawn regarding their limitations and on how well the system's fouling was represented. It is worth noting that Equation 4.24 and 4.25 include the specific cake resistance formulation via the Carman–Kozeny Equation (Giraldo and LeChevallier 2006).

This is because it was assumed that the particles forming the sludge floc are spherical in shape. In reality however, characteristics of activated sludge flocs structure viewed under the microscope show a varying difference in the particles' shape. Thus, this assumption induces a limitation to the derived models.

4.1.2. Fouling Model for Static Square MBR

The fouling model for the SMBR exists solely for comparative purposes against that of the RMBR. Thus, the SMP inclusion and constant flux/varying TMP model were not included as they are support models for the constant TMP/varying flux fouling model that was derived for the RMBR. Also, due to laboratory space and design constraints, the bespoke SMBR could only be set to constant TMP/varying flux operation mode. However, this was more than enough for comparative purposes as a fouling model for this mode of operation had already been derived for the RMBR.

Hence, it was not only assumed that the SMBR was fouled as per Figure 4.1a, b and c, but to obtain the fouling model for the SMBR under constant TMP/varying flux mode, the rotating functions in the RMBR fouling model were switched-off. In fairly similar fashion to **sub-section 4.1.1.1**, Equation 4.13 can be reduced to Equation 4.26, if the rotational switching functions are removed so that the model reverts to that of a submerged SMBR system that now simply includes the air scouring term.

$$Q_t(t) = \frac{A_{u_0}.J_0}{(1+\beta.Q_0.C_{MLSS}.t)^2}.e^{\left\{\frac{\alpha.J_0}{\beta.Q_0}.\left(\frac{1}{1+\beta.Q_0.C_{MLSS}.t}-1\right)\right\}}+ \frac{-PT}{\mu.(R_m.(1+\beta.Q_0.C_{MLSS}.t_b)^2+R_b)}.\int_0^t\left(\frac{A_{u0}.\alpha.C_{MLSS}.J_0}{(1+\beta.Q_0.C_{MLSS}.t_b)^2}.e^{\left\{\frac{\alpha.J_0}{\beta.Q_0}.\left(\frac{1}{1+\beta.Q_0.C_{MLSS}.t_b}-1\right)\right\}}\right)dt_b \quad (4.26)$$

The only prevalent hydrodynamic factor to take into account during operation of the constructed SMBR rig is the coarse bubble air scour that is mainly used to mitigate cake growth, and thus hamper fouling. Consequently, J_{air} also becomes a vital factor for the management of fouling in this SMBR system. Hereafter, this air scour removal term was added to the rate of membrane fouling resistance build up and the rate of increase in membrane blocked area. This is a comparable formulation that is also in-line with Liang et al. (2006) rate of membrane biomass build-up equation.

In a similar manner to the RMBR fouling model as seen in Equations 4.14 and 4.16, the hydrodynamics effect in form of air scour alone can be reduced simply to Equations 4.27 and 4.28.

$$\frac{dR_b}{dt} = f'.R'.J_b.C_{MLSS} - g_o.(\alpha_v.J_{air}).\delta'.(R'_c.\theta_c) \quad (4.27)$$

$$\frac{dA_b}{dt} = \alpha.J_u.A_u.C_{MLSS} - k_{A_b}.(\alpha_v.J_{air}).\theta_c(t) \quad (4.28)$$

An alternative fouling model for constant TMP/varying flux mode was derived for the square SMBR but due to lack of time was never implemented as it does not compromise the comparative purposes found in the thesis proper.

(Please refer to **APPENDIX D.1** for said SMBR fouling model)

4.2. Matlab Software, Genetic Algorithm and Optimisation of α_v and δ'

As seen from literature, various software packages are available for the modelling of wastewater treatment; however, the author of this thesis chose to work with Matlab (i.e. R2010a) as it is a good software package that is capable of simulating with great precision the behaviour of a system. Furthermore, the author's above than average proficiency with the software package was more than enough to be the deciding factor. Thus, the fouling models whether for the RMBR or SMBR were implemented using Matlab.

4.2.1. Simulation Best Fits in Matlab, Use of Genetic Algorithm

Using Matlab's innate functions, m-files were carefully constructed for the constant TMP/varying flux fouling models for both MBR rigs (i.e. RMBR and SMBR). An additional m-file for the constant flux/varying TMP fouling model was also constructed for the RMBR system. Matlab's debugging function run these m-files to ensure that they functioned properly. By feeding the collected experimental data that were obtained from both MBR plants to the fouling models, and running the m-files in Matlab proper, the required graphs including simulations best fits were produced. These results are used for discussions (see **Chapter 5** and **6**).

In every fouling model case, so as to avoid having manifold degrees of freedom, several model parameters are calculated (some of which are outlined in **sub-section 3.2**) before entering Matlab as they are readily available and kept constant during all simulations. This is because they do not vary much within their associated MLSS level range and therefore do not have significant effects on the fouling models in terms of describing fouling behaviour and parameters chosen for model fitting during simulations.

This works fine as the model parameters that pertain to the fouling mechanisms are the object of focus (since they are used to determine the weight of said fouling mechanisms), and should therefore be utilised as simulations' best fits and conducting necessary analyses. For the constant TMP/varying flux case for both MBR systems as well as to ensure model validity, six key parameters namely f'.R', α, β, R_{bo}/R_m, g_o and k_{Ab}, were used as simulations' calibrated best fit parameters. f' is a fraction of foulants contributing to particles deposit growth, and R' is the unit cake layer thickness formed per unit mass of fluid filtered.

They individually are factors associated with cake layer growth therefore their product can be considered a factor by itself that is also associated with cake layer growth. For this reason, f'.R' was chosen as one of the key parameters representing cake filtration. R_{bo} (m^{-1}) is the initial resistance of solids deposit where the actual cake growth begins; and, thus is a factor associated with cake growth (i.e. deposited solids form a cake layer that grows).

Therefore, it was chosen as another key parameter representing cake filtration. g_o, the cake removal factor, is a factor controlling the decrease in cake layer formed (i.e. cake growth) when accounting for hydrodynamic regimes. It was thus also a key parameter picked to represent cake filtration. The blocked pores area constant, k_{Ab}, gives an indication of how much cake layer is formed over a unit blocked area (when accounting for hydrodynamic regimes). It too was selected to represent cake filtration.

In light of the above, these four key parameters (i.e. f'.R', R_{bo}, g_o and k_{Ab}) were found to be the most fit to represent cake filtration. α is the membrane area blocked per unit mass of particles accumulation and indicates the amount of foulants that blocked pores. As such, it was chosen as key parameter contributing to pore blocking.

β (σ_a is directly proportional to β and is therefore less significant than the latter) on the other hand, is the amount of pore constriction per unit of pore volume, which essentially indicates the unit mass of foulants in pore interior. This implication means it was selected as key parameter contributing to pore constriction.

Implementing (using Matlab) the fouling models for both MBRs so as to quantify these key model parameters meant the use of Matlab function Genetic Algorithm (GA). Broadly speaking, GA is a process for solving both constrained and unconstrained optimisation problems based on a natural selection process that mimics biological evolution.

Using it, Matlab can tentatively solve complex problems to a reasonable degree of accuracy depending on the initial population size and nature of the system. Overall, GA is a fairly reliable simulation and fitting technique that has not only been used by many researchers in the field of engineering but has also been employed in other fields of science as well. So its usage here to simulate the fouling models was fair.

Best fits were obtained for every MLSS concentration range (3.34 – 4.26 g/L; 6.32 – 7.24 g/L; 8.22 – 9.35 g/L) and corresponding TMP steps for both MBRs (save the 3.34 – 4.26 g/L range for the SMBR). To ensure the best fits obtained were reliable, for each MLSS level range and TMP step, 50 GA simulations of the fouling model for either the RMBR or SMBR were run. The solution fits of these runs were individually averaged to finally give the best fit solutions (i.e. global optimum) recorded for said MLSS level range.

The reason for the number of runs is that GA can be tricky sometimes. GA parameters that can control model simulations either individually or through a combination thereof are population and generation number, and mutation rate, usually (e.g. crossover probability is often used as well). Run-of-the-mill values for these parameters vary from research to research and as Gutowski (2005) pointed out, it is rather hard to ascertain a "working" standard set from literature.

For this thesis, the biggest worry with GA in Matlab was the population size (as the other GA parameters can be auto-set from in-built options). Some commonly observed values in literature for population number range from 30 to 200. Naturally, it came as no surprise

that they did produce terrible fits for the fouling models. From there on, adjustments had to be made so as to achieve the desired performance.

To help speed up the process, the least squared residual between the simulated data and experimental data was introduced alongside the curves as visual aid. If the solution fit was obtained then, it stands to reason that this residual must be minimised and converge to a value closer to zero (i.e. experimental and simulated nearly match, and the fouling model optimised). In doing so, the curves, which contain both experimental and simulated data points will also (or nearly) match, thereby obtaining the global optimum solutions for GA.

By manipulating (i.e. changing the GA parameters values in increments) these aspects (including the visual), which needless to say took many trials, the correct GA parameters for all around fitting were obtained. To perform GA, in the upper bound (UB) matrix of GA, a 1 by 6 matrix that could be anything, a 6-entry initial guess is first entered.

The objective or fitness function then uses the information in UB and the population size (ultimately found to be large through the adjustments) in conjunction with the collected experimental data (e.g. fluxes for constant TMP) to try to match said experimental data with simulated data by converging them to the lowest possible error. The m-file generates graphs (used for discussions) along with best fits.

Going a step further with calibration, a set of experimental data in specific MLSS level range (3.89 g/L for 3.34 – 4.26 g/L; 6.82 g/L for 6.32 – 7.24 g/L; and, 8.76 g/L for 8.22 – 9.35 g/L) for the RBMR rig were used to verify that the calibrated best fit parameters obtained for said MLSS level range during GA simulations were reasonable.

For the constant flux/varying TMP case for the RMBR system, there were only three key parameters namely K_α, β and φ that were used for fitting and analyses. Model parameter β accounted for pore constriction fouling mechanism whilst K_α and φ both represented comparative terms for the models. To obtain the simulations best fits, the same steps used for the constant TMP/varying flux case were followed as GA was also utilised. However, instead of a 1 by 6 matrix, a 3-entry initial guess was entered in a 1 by 3 matrix.

(Please refer to **APPENDIX D.2** for all Matlab m-codes and **APPENDIX D.2.1** for simplified results concerning obtained GA factors and convergence of least squared residuals)

4.2.2. Fitting of SMP Inclusion Model and Shear Effects in Matlab

The fitting parameters for the SMP inclusion model and shearing effects parameters m and n were obtained using Matlab functions *"polyfit" and "polyval"*. The outputted curves of the SMP inclusion model and those of the shear effects were obtained via Matlab's *"plot"* function (see **sub-section 5.1** and **5.2.4**).

For the SMP inclusion model, by taking the logarithm of C_{MLSS} in the C_{SMP} Equation 4.18, it follows that,

$$\ln(C_{MLSS}) = \ln\left(\epsilon_{smp}.C'_{MLSS}\right) + k_i.\ln\left(e^{\frac{\theta_c}{Jm_o}}\right) \quad (4.29)$$

And this derived Equation 4.29 is that of a polynomial of order one (i.e. straight line) in the form y = b.x + c, where, y = ln(C_{MLSS}), x = ln($e^{(\theta c/Jmo)}$), b (−) is the line's gradient, and c (−) is the line's constant. Thus, by plotting the logarithm of MLSS concentration against the cake thickness ratio (i.e. cake thickness divided by total flux) whilst also doing a linear fit in Matlab, the values of k_i and $\epsilon_{SMP}.C'_{MLSS}$ were obtained. Gradient b corresponded to the value of k_i whilst the value of $\epsilon_{SMP}.C'_{MLSS}$ was e^c.

To find the shearing effects parameters m and n, a fairly similar method to the SMP inclusion model was employed. Since the shear's equation (Equation 4.1) obeys a power law, it naturally follows that the logarithm of said equation would produce a polynomial of order one (i.e. straight line) in the form y = b.x + c, such that, y = ln(μ) and x = ln(γ̇). Consequently, parameters m and n were determined by plotting the logarithm of viscosity against the logarithm of the shear rate using a linear curve fitting process in Matlab. Gradient b + 1 was the value of n whilst the value of m was e^c.

The determined parameters m and n for each specific MLSS level range (i.e. 3.34 − 4.26 g/L, 6.32 − 7.24 g/L and 8.22 − 9.35) were used and kept constant during model simulations of the RMBR rig. It is worth noting that m and n are only prevalent in the RMBR fouling model as they govern the shear effects (including rotation) and viscosity. Conversely, since the SMBR unit was not operated under rotation, these shearing effects parameters were removed and not utilised during its model simulations.

4.2.3. Optimisation of α_v and δ'

In essence, the determination of α_v and δ' simplifies the MBR fouling models without undermining the integrity of the fouling mechanisms occurring during the filtration processes. This is because these constants do not fluctuate a lot during RMBR and SMBR filtration operations. For instance, since the operational air flow rates for both MBRs vary in small increments, their coefficient of proportionality, α_v, can be assumed to be near constant at almost all times.

This early stage of optimisation is more of a trial and error to find the appropriate values for the air scouring coefficient, α_v (−), and the resistance distribution factor of cake layer, δ' (m^{-1}). Whilst ensuring that all other model parameters were correctly determined, this optimisation method was accomplished by starting with initial guesses for both parameters (i.e. α_v and δ') then run several simulations.

After each simulation, the final value (i.e. best fit value) that was provided by Matlab was recorded; and, as this value was initially too big, the initial guesses were increased by small increments and simulations were run anew. As these initial guesses increased, the simulations' final values got smaller. This signified that α_v and δ' were being optimised. This process of increasing the initial guesses was repeated until the final values settled to a steady state.

At this point the fitting curves were all fairly adequate. The values of α_v and δ' found at steady state for the RMBR system were respectively 0.0292 and 4.6×10^{-4} m^{-1}. These newly determined values were used and kept constant in all subsequent simulations to calculate the best fit solutions for the fouling models.

The aeration rate for all collected data sets for the SMBR rig was similar in scale to that of the RMBR system operated under laboratory scale conditions. Thus, the same values of α_v and δ' that were determined for the RMBR system were used and kept constant during all simulations of the SMBR fouling model.

As the air scouring flow rate of 3.55×10^{-4} $m^3.s^{-1}$, which was kept the same during all simulations of both the SMBR and RMBR, is a typically recommended value by MBR manufacturers to run laboratory-scale MBR plants optimally, RMBR's values for α_v and δ' were used for simulations of the Coors (UK) and Duclos-Orsello et al. (2006) filtration data. In practice however, this may not be always true as certain MBR plants are more demanding than others but as estimates, these values were fairly reasonable.

(Refer to **APPENDIX D.3** for the simulations' final values)

4.3. Chapter Summary

Fouling, a phenomenon that membrane is subjected to over time that either decreases flux or augments TMP depending on the system's mode of operation, has been modelled for two MBR systems: RMBR and SMBR. This chapter thus, detailed the methodologies that went into their development. These fouling models were soundly made whilst making suitable, grounded assumptions.

For the RMBR under constant TMP, the effects of shear (by extension rotational effects too) were included into the fouling model whilst also acknowledging limitation such as not including into it a completely isolated hydrodynamic study of the shear stresses, which is not the scope of this research. For the RMBR under constant flux, two TMP models were created: one which included the Taylor's expansion and the other not.

Taylor's expansion inherent limitation on model 2 for TMP formulation as well as Carman-Kozeny limitation on both TMP models which assumes that particles forming sludge floc are spherical in shape were acknowledge. To account for clogging materials, a SMP related model in terms of MLSS was created using a more "direct" approach.

For the SMBR, its fouling model was constructed under constant TMP by switching off the rotational parameters from the RMBR fouling model. This model was later used for comparative purposes. Overall, all these constructed models were implemented using software program of choice, Matlab (i.e. R2010a) whilst GA was used for simulations and obtaining best fit model parameters. Finally, constant parameters α_v and δ' were optimised early on.

CHAPTER 5: FOULING MODEL STUDY OF THE ROTATING MBR

This segment not only covers results obtained from RMBR related experiments and from simulations of the fouling models (i.e. constant TMP and flux) for the RMBR but also includes their full discussions as well. Results are displayed in forms of graphs and table summarising model simulation best fit parameters. This chapter is divided into two main sub-sections:

i. *Shear Effects (Shear Rate versus Viscosity)*: A fairly short sub-section, it displays graphs attained from the viscosity and shear experiments and discusses them.

ii. *Model Validation (with Hydrodynamic Effects)*: This sub-section outlines validation of fouling model (i.e. constant TMP) for RMBR which includes the hydrodynamics effects in form of curves and discusses them. Solution best fits from GA simulations are shown in table form and discussed as well. Additionally, this sub-section also highlights validation of TMP models (i.e. constant flux) for RMBR in form of graphs, RMBR model calibration verification curves, and SMP inclusion model curves with discussions.

5.1. Shear Effects (Shear Rate versus Viscosity)

Data outputted from shear experiments (viscosities measurement at different shear rates) that were plotted are shown on Figure 5.1, 5.2 and 5.3 in this sub-section and discussed. On each of these figures, y represents the values of y-axis (vertical axis), and x represents the values of x-axis (horizontal axis); and, experimental data are either small crosses or circles whilst simulated ones are solid lines.

Shear parameters m and n were broadly obtained by plotting logarithm of viscosity against logarithm of shear rate using a linear curve fitting process in Matlab. The gradient of the line + 1 equaled the value of n whilst the value of m was exponential of the line's constant (see **sub-section 4.2.2** for details). It is worth noting that while RMBR systems can handle shear rates up of to over 2×10^5 s^{-1}, the range of shear rates used during tests were kept minimal since the RPU-185 RMBR unit only operated at very low rotational speed (though it should be mentioned that a 20 rpm spindle equated to a shear of 26 s^{-1}).

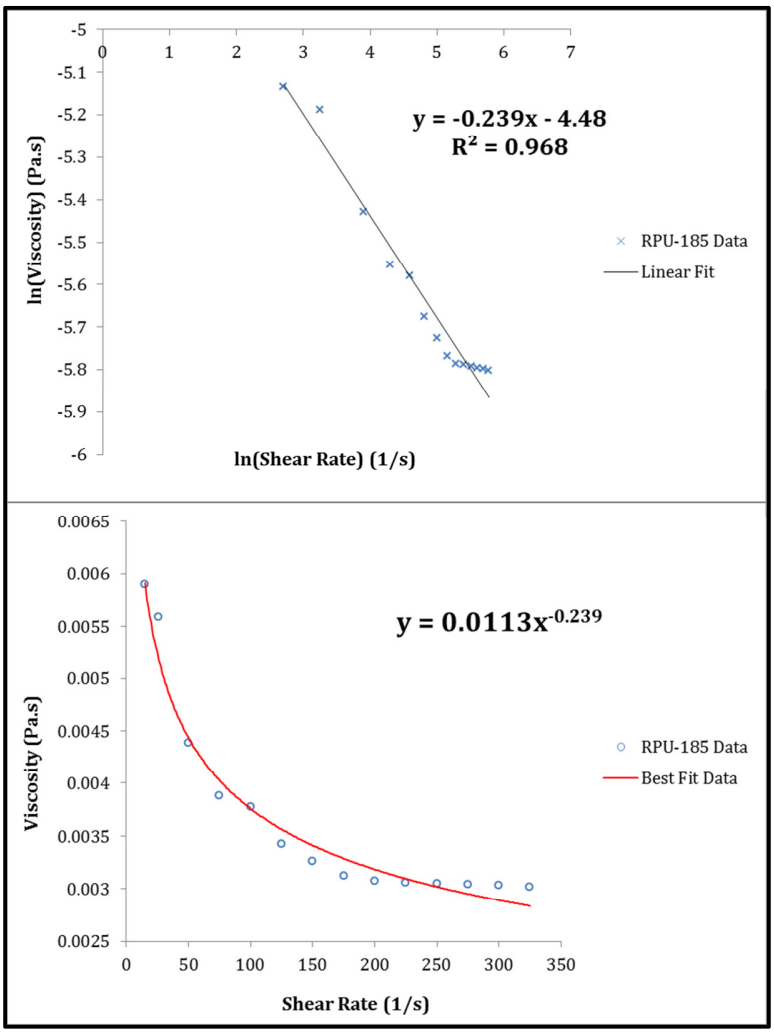

Figure 5.1. Viscosity plotted against shear rate for MLSS level range 3.34 – 4.26 g/L

Figure 5.1 shows the viscosity plotted against the shear rate (with the solid line being the best fit) for MLSS concentration range of 3.34 – 4.26 g/L for RPU-185 RMBR. Results indicated that the fluid's viscosity had declined much faster at higher shear rate (by almost 56%). This was expected since the calculated radial Reynolds number ($Re_{r,NN}$) showed that the flow regime was laminar.

Additionally, it should be mentioned that since activated sludge is a shear thinning fluid (as seen in literature), the rheological measurements (which pertain to shear rates) must be kept in the laminar regime otherwise the outcome of the viscometer (or rheometer) becomes increasingly difficult to interpret.

The coefficient of determination, R^2 (–), for the linear fit procedure was found to be 0.968. This indicated a respectable fit for the power law model since the sum of the squared residuals were also minimised. Parameter m was found to be 0.0113 whilst n gave a value of 0.761. Expectedly, the value of n was less than one. This was a clear indication that the fluid had deviated from Newtonian behaviour, thus earning its shear thinning status. The value of m was considered reasonable for this type of MBR operated at a relatively low MLSS of 4.26 g/L.

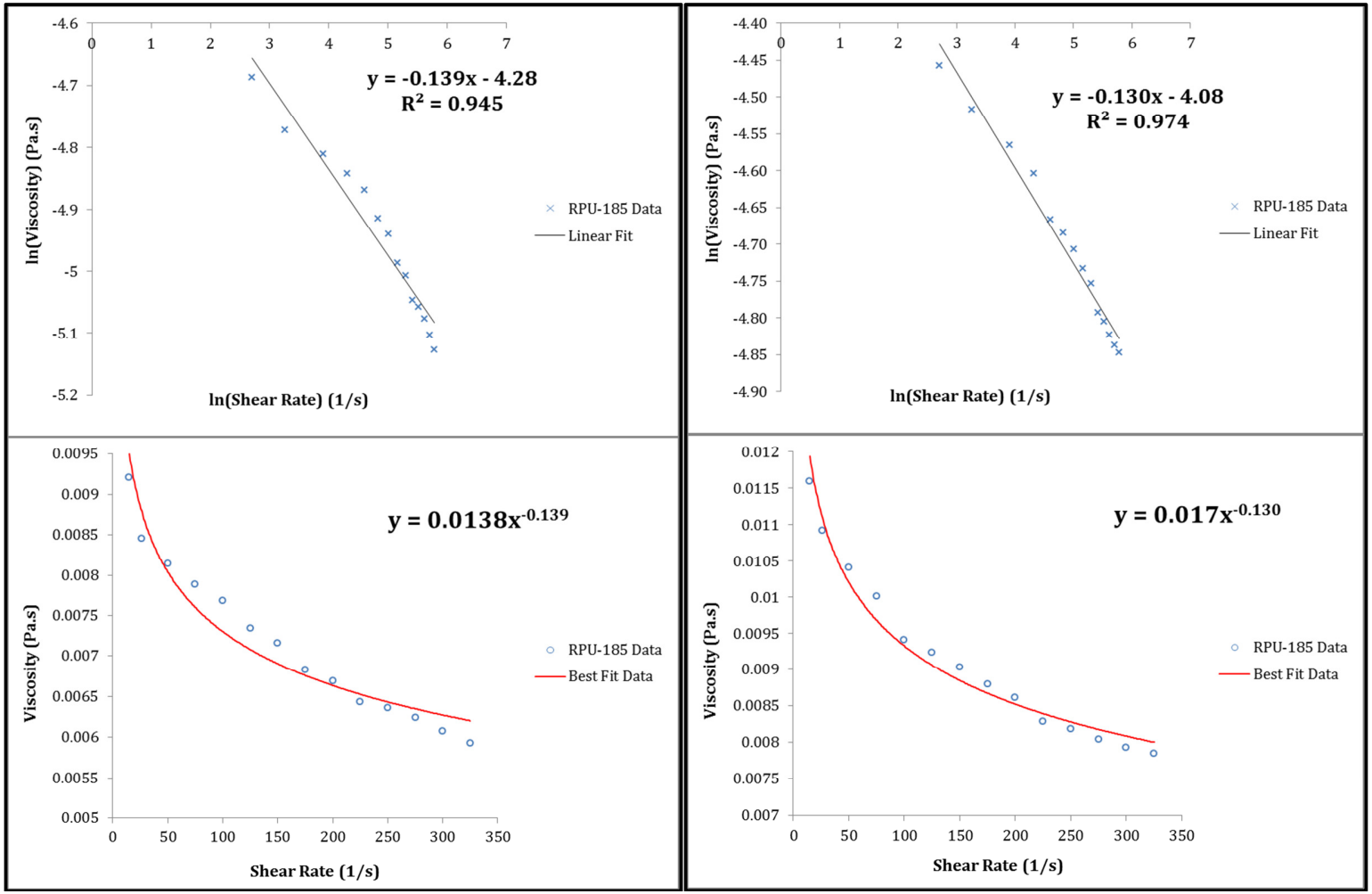

Figure 5.2. Left – Viscosity plotted against shear rate for MLSS level range 6.32 – 7.24 g/L
Figure 5.3. Right – Viscosity plotted against shear rate for MLSS level range 8.22 – 9.35 g/L

Figure 5.2 and 5.3 each shows the viscosity plotted against the shear rate (with the solid line on each being the best fit) for respectively MLSS concentration range of 6.32 – 7.24 g/L and of 8.22 – 9.35 g/L for RPU-185 RMBR. Results indicated that for every MLSS concentration range, the fluid's viscosity had decreased much faster at higher shear rate (by over 30%), which came as no surprise since calculated radial Reynolds number showed that the flow was laminar during RMBR operations (i.e. $R_{er,NN}$ was less than 2×10^5).

Furthermore, it should be noted that since activated sludge is a shear thinning fluid (as seen in literature), the rheological measurements (which pertain to shear rates) must be kept in the laminar regime otherwise the outcome of the viscometer (or rheometer) becomes increasingly hard to interpret.

For each of these MLSS concentration ranges the coefficient of determination for the linear fits were respectively 0.945 and 0.974, indicating respectable model fits since the sum of the squared residuals were also minimised. The coefficients m were found to be 0.0138 and 0.0170 whilst n gave values of 0.861 and 0.870 for respectively each MLSS concentration range.

This can be interpreted as higher MLSS levels are prone to inconsistent fluid flow whilst at the same time said fluid deviate from Newtonian behaviour (as the values of n were less than one). This is because higher MLSS levels are associated with high viscosities that in turn strongly hinder mass transfer leading to extended and increases in membrane fouling (Yang et al. 2009).

In summary, the values of shear effect parameters m and n are within acceptable range as they are in-line with those found in earlier work (Paul and Jones 2015); however, these values appear to change at a steady rate (from experiments that have been conducted so far) depending on the range of MLSS concentrations used and since high viscosities are associated with high MLSS, the likelihood of cake filtration (cake formation) occurring is drastically increased at high TMPs.

5.2. Model Validation (Hydrodynamic Effects)

The results obtained from simulations of RMBR fouling models are discussed in full and displayed here in a summarised table and in graph forms. The figures (from **sub-sections 5.2.1** to **5.2.3**) contain experimental data which are represented by small asterisks, circles, or triangles, and simulated data which are either solid or dashed lines.

All the curves were created and the simulations best fits were determined as detailed in **sub-section 4.2.1** and **4.2.2**. Broadly speaking, the m-files that were created in Matlab for the fouling models also contain sub-routines that plot best fits figures after GA simulation has terminated (that of course means the experimental data must have been fed to said implemented m-files). Lastly, on all these graphs C_b is the same as C_{MLSS}.

5.2.1. Constant TMP/Varying Flux

The developed fouling model for RMBR under constant TMP regime was validated using data generated from the unique hydrodynamic regime employed by the RPU-185 RMBR. The bulk MLSS concentration ranges used for all the TMP steps (i.e. 15, 30, 45 and 58 kPa) were 3.34 – 4.26 g/L, 6.32 – 7.24 g/L and 8.22 – 9.35 g/L. The flow regimes were laminar which were well within expectations since calculated $Re_{r,NN}$ values were much less than 2×10^5.

The air scouring coefficient, α_v, and the resistance distribution factor of cake layer, δ', were obtained as discussed in **sub-section 4.2.3.** Their values were respectively 0.0292 for α_v and 4.6×10^{-4} m^{-1} for δ'. These aforementioned and determined values were used in all subsequent GA simulations to obtain the best fit values for the developed fouling model.

For every MLSS concentration range and TMP step, 50 GA simulations of the fouling model for the RPU-185 RMBR (rig) were run. The solution parameters of these runs were each averaged, giving the best fit parameters ($f'.R'$, α, β, R_{bo}/R_m, g_o and k_{Ab}) that are summarised in Table 5.1 for all four TMP steps. The term σ_a was determined upon obtaining the fitting value of β since the membrane pore size was known whilst k_ω though initially obtained via sensitivity analysis, was eventually calculated within Matlab (with known fluxes). Both terms are acceptable for their range and fluxes they operated on during experimentations.

Table 5.1. Averaged best fit fouling model parameters including hydrodynamic effects for the RPU-185 (RMBR) after 50 GA runs for each TMP step and MLSS concentration range

	TMP step up (kPa)	**Averaged optimised parameters**							
		$f'.R' \times 10^9$ (m/kg)	α (m^2/kg)	β (kg)	R_{bo}/R_m (–)	g_o (–)	k_{Ab} (–)	$\sigma_a \times 10^{-17}$ ($kg.m^3$)	$k_\omega \times 10^{-5}$ (–)
MLSS (g/L) 3.34 – 4.26	15	489.04	0.332	2.342	0.174	21.79	29.79	1.788	2.446
	30	435.88	0.0579	0.856	0.867	3.178	229.77	6.535	4.484
	45	490.67	4.929	1.751	0.239	70.63	29.27	1.336	5.503
	58	65.72	0.670	0.472	0.390	35.67	0.382	3.601	6.725
MLSS (g/L) 6.32 – 7.24	15	0.248	0.118	0.893	0.206	79.59	0.025	6.816	2.812
	30	15.50	0.179	0.662	0.574	66.30	0.874	1.367	4.931
	45	199.73	1.157	0.589	0.324	24.76	26.57	4.497	5.991
	58	28.07	0.262	0.242	0.525	35.41	0.402	1.847	7.172
MLSS (g/L) 8.22 – 9.35	15	24.73	0.122	0.499	0.305	89.97	4.459	3.808	3.138
	30	210.96	0.105	0.232	0.616	78.25	1.346	1.769	5.175
	45	76.55	1.012	0.487	0.450	38.72	19.208	3.720	6.357
	58	10.42	0.153	0.148	0.419	39.52	0.130	1.132	7.376

Overall, fitting parameters $f'.R'$, α, β, R_{bo}/R_m, g_o and k_{Ab} are fairly reasonable as optimisation and calibration fitting sets for they are in-line with former work completed by Paul and Jones (2015).

From Table 5.1, when comparing pore blocking parameter, α, at different data sets, its lowest value of 0.0579 is found at MLSS concentration range of 3.34 – 4.26 g/L for TMP step of 30 kPa. This suggests that the pore blocking's effect on fouling was minimal during filtration. Moreover, this is justified since its corresponding pore constriction parameter, β, is much bigger. Thus, a possible interpretation is that at lower TMPs, pore blocking is less likely to dominate fouling.

In contrast, the highest value of the pore blocking parameter, α, is 4.929 and is found at MLSS concentration range of 3.34 – 4.26 g/L for TMP step of 45 kPa. It implies that pore blocking was one of the dominant fouling mechanisms during filtration which is reasonable since its corresponding pore constriction parameter, β, is much smaller. Therefore an inference is that at very high TMPs, pore blocking is more likely to be one of the dominant fouling mechanisms.

When comparing pore constriction parameter, β, at various data sets, its lowest value of 0.148 is found at MLSS concentration range of 8.22 – 9.35 g/L for TMP step of 58 kPa (see Table 5.1). Hence, it can be inferred that pore constriction had lesser impact on fouling since its equivalent pore blocking parameter, α, is almost double that of β. Consequently, a conclusion that can be drawn is that at higher TMPs, pore constriction is less likely to be dominant.

On the other hand, the highest value of pore constriction, β, is 2.342 and is found at MLSS concentration range of 3.34 – 4.26 g/L for TMP step of 15 kPa. This therefore implies that pore constriction was one of the dominant fouling mechanisms during filtration. This is justified since its corresponding pore blocking parameter, α, is almost seven times smaller. Accordingly, it can be concluded that at lower TMPs, pore constriction is more likely to dominate fouling.

When comparing the combination of parameters f'.R' (a fraction of foulants of total foulants multiplied by unit cake layer thickness formed per unit mass of fluid filtered), R_{bo} (initial resistance of solids deposit), g_o (cake removal factor) and k_{Ab} (blocked pores area constant), which all pertained to cake filtration, its lowest combination is found at MLSS concentration range of 3.34 – 4.26 g/L for TMP step of 15 kPa. This suggests that cake formation (by extension cake filtration) was fairly weak and less influential during fouling. Therefore, at lower TMPs, cake filtration is expected to be less dominant but not uncommon during fouling of membrane.

Conversely, the highest combination of parameters f'.R', R_{bo}, g_o and k_{Ab}, is found at MLSS concentration range 6.32 – 7.24 g/L for TMP step of 45 kPa. It implies that cake formation (by extension cake filtration) was significant during fouling. As such, it can be deduced that at high TMPs, cake filtration is expected to be one of the dominant fouling mechanisms or at the very least, cake formation is nearly, if not, as persistent as the other fouling mechanisms.

Although three MLSS level ranges were used for curve fitting, all subsequent discussions in this sub-section will only focus on one range: 8.22 – 9.35 g/L (with all four TMP steps). The reason for this is that the other two MLSS level ranges with the same TMP steps provide fairly similar analyses and therefore are not needed to draw initial conclusions. On each of the following figures within this sub-section, the legend applies to both curves (i.e. top and bottom).

(For the figures not included here, which are for the other two MLSS level ranges for all TMP steps, please refer to **Appendix E.1**)

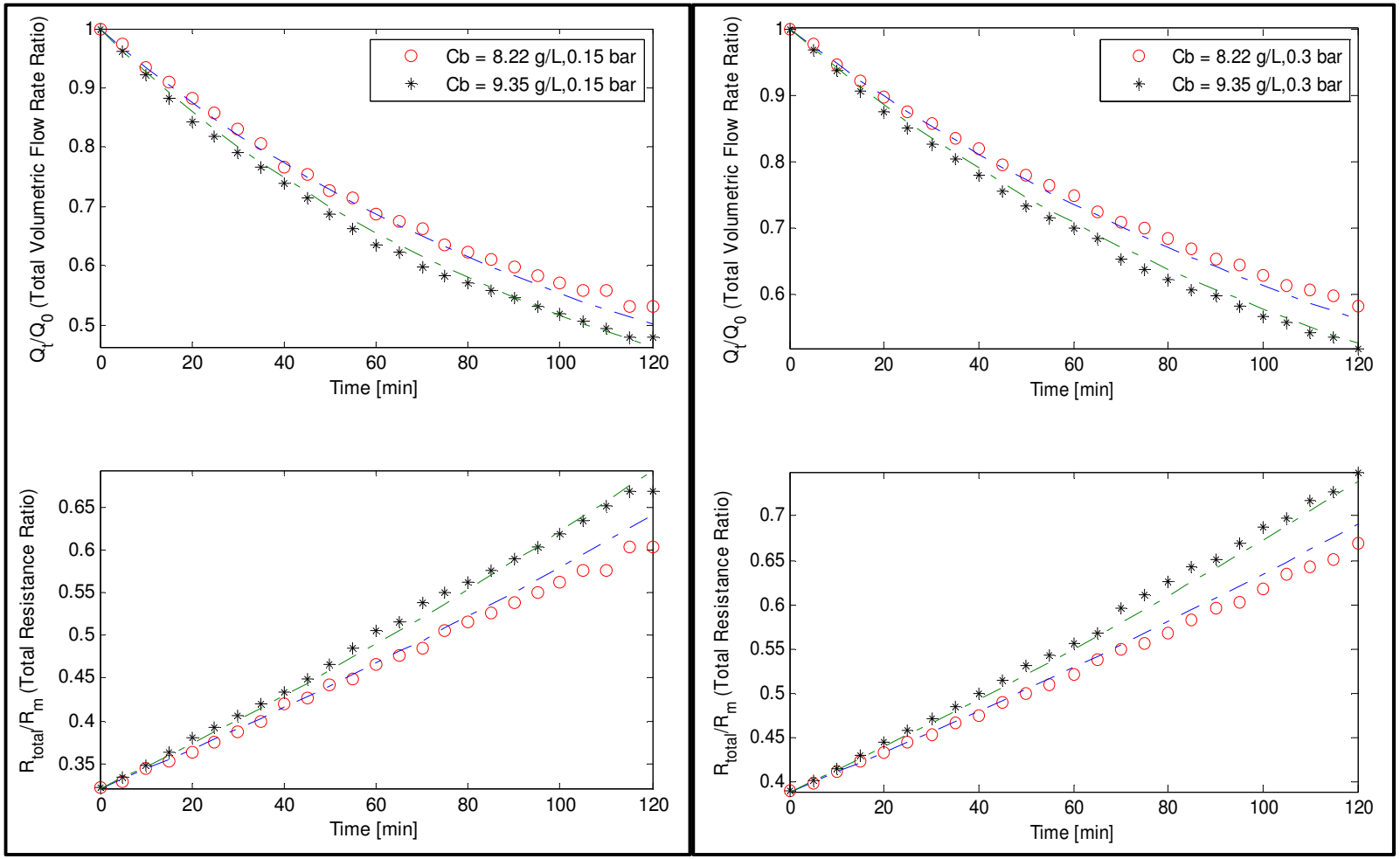

Figure 5.4. Left - Flux decline and total resistance for TMP step at 15 kPa for MLSS levels of 8.22 and 9.35 g/L
Figure 5.5. Right - Flux decline and total resistance for TMP step at 30 kPa for MLSS levels of 8.22 and 9.35 g/L

Figure 5.4 depicts the effects of the fouling behaviour of RPU-185 RMBR, using both the normalised flow rates and total resistance ratios for MLSS concentrations of 8.22 and 9.35 g/L at a constant TMP of 15 kPa (with the dashed lines representing the best fit simulation data). The total resistance was calculated using Darcy's law (see Equation 2.2). An averaged reasonable decrease in flux of about 52% can be observed at roughly both MLSS concentrations.

This is in-line with the results from the earlier study by Paul and Jones (2015) that found that the rate of decrease in flux is consistent and steady unless the TMP is dramatically increased. Furthermore, this gradual drop in flux is as expected and in-line with critical flux theory. The trend shown by the fluxes curves for both MLSS concentrations is sufficient to suggest that fouling occurring during filtration was caused by a combination of all three classical fouling mechanisms.

This is further supported by the fact that the total resistances' curves for said MLSS levels displayed linear best fits. However, as seen in Table 5.1, it is found upon closer inspection that small R_{b0} and big cake removal factor, g_0, indicated weak cake layer formation.

Consequently, this implies that cake filtration was less prevalent which was actually anticipated since at low TMP of 15 kPa, cake formation is expected to be less dominant (Paul and Jones 2015). Furthermore, pore constriction parameter, β, being roughly four times bigger than pore blocking parameter, α, ultimately suggested that fouling was dominated by pore constriction (as $\beta >> \alpha$).

Figures 5.5 shows the normalised flow rates and the total resistance ratios plotted against the filtration time at constant TMP of 30 kPa for MLSS concentrations 8.22 and 9.35 g/L for RPU-185 RMBR (with the solid dashed lines representing the best fits simulation data). The total resistance was calculated using Darcy's law (see Equation 2.2). Here a fair and steady decrease in flux (averaged) of nearly 48% was sustained at roughly both MLSS levels.

Again this gradual drop in flux is as expected although not as much as theory would predict. The near linear best fits of the total resistances' curves for both MLSS concentrations seemingly suggests that fouling occurring during filtration was caused by a combination of all three classical fouling mechanisms.

But upon closer look, it can be observed from Table 5.1 that pore constriction fouling mechanism was a dominant fouling mechanism as β, pore constriction parameter was bigger than pore blocking parameter, α. This is still acceptable because as described by Paul and Jones (2016), at lower TMPs (i.e. 30 kPa is still barely in range) pore constriction fouling mechanism tends to be dominant during membrane fouling.

Furthermore, R_{b0} being almost half R_m and the somewhat big cake removal factor, g_0, implied that caking layer was weak. Thus, pore constriction fouling mechanism dominated fouling overall.

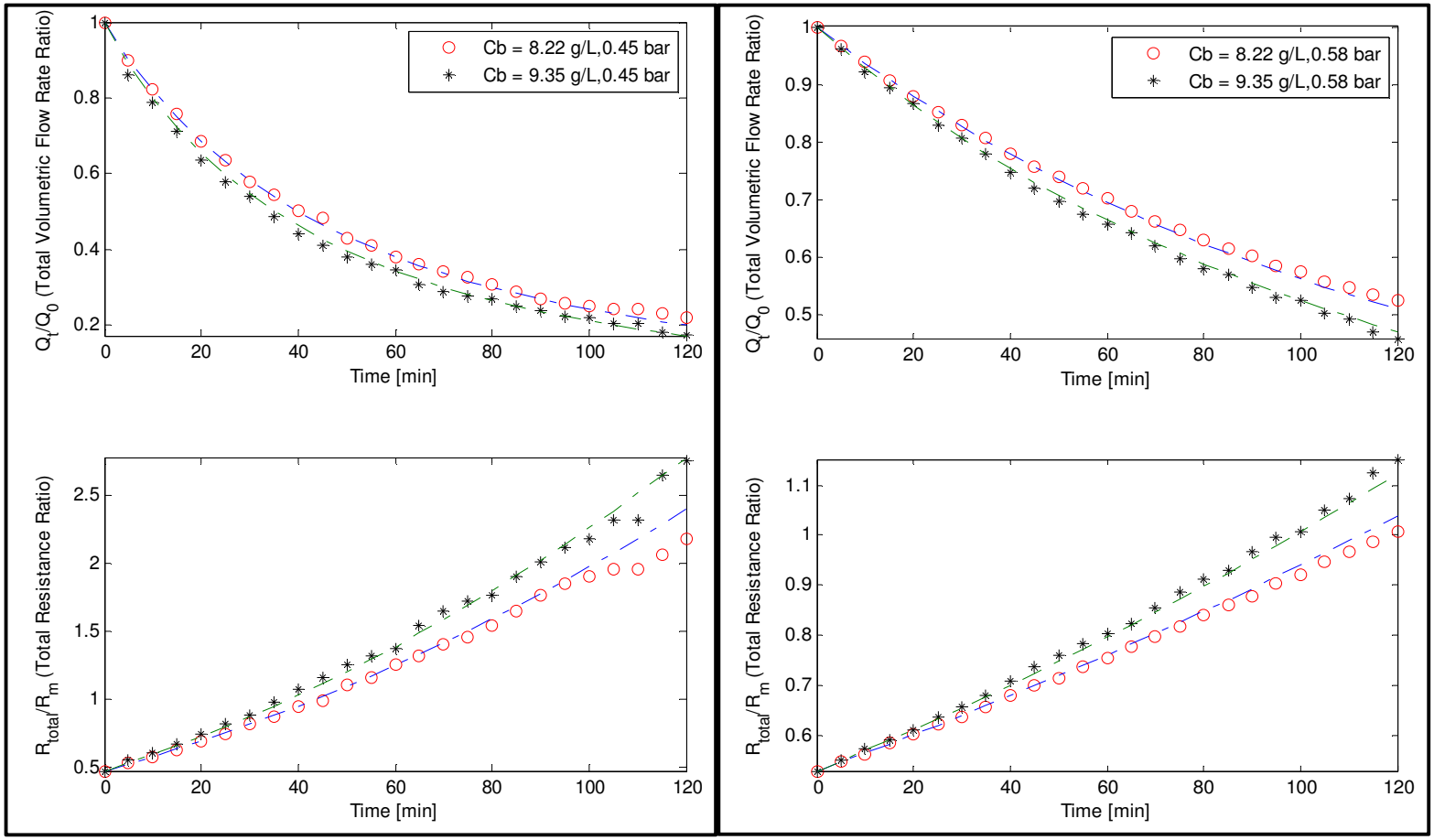

Figure 5.6. Left - Flux decline and total resistance for TMP step at 45 kPa for MLSS levels of 8.22 and 9.35 g/L
Figure 5.7. Right - Flux decline and total resistance for TMP step at 58 kPa for MLSS levels of 8.22 and 9.35 g/L

Figure 5.6 displays the TMP step data as normalised flow rates and the total resistance ratios plotted against the filtration time at a constant TMP of 45 kPa for MLSS concentrations of 8.22 and 9.35 g/L for the RPU-185 RMBR (with the dashed lines representing the best fit simulation data). The total resistance was calculated using Darcy's law (see Equation 2.2). Experimental data showed that severe drop in flux of over 75% was experienced at almost both MLSS concentrations.

This meant that not only had the initial flux increased at higher TMPs, but also that the flux decline rate had increased at greater pressure when compared to that at constant TMP of 15 and 30 kPa. These findings are in-line with theory since a membrane is likely to foul more quickly when approaching or exceeding critical flux (Judd 2006, Paul and Jones 2015). The massive drop in flux also resulted in the total resistances increasing exponentially for both MLSS concentrations.

This strongly indicates that the fouling in these cases was dominated for most part by both pore blocking and cake filtration although the combined effect of all three fouling mechanisms on the total fouling cannot be precisely extrapolated. Again as per Table 5.1, with the pore blocking parameter, α, being roughly two times bigger than the pore constriction parameter, β, the pore blocking fouling mechanism must have had a significant impact on fouling.

For this MLSS concentration range, a bigger R_{b0} and f'.R' coupled with a much lower cake removal factor, $g_{0,}$ when compared to data of same MLSS level range at constant TMP of 15 kPa, indicated that a reasonably strong cake layer was formed. Thus, it is thought that the bulk of the fouling was dominated by both pore blocking and cake filtration.

Figure 5.7 portrays the TMP step data as normalised flow rates and the total resistance ratios plotted against the filtration time at a constant TMP of 58 kPa for MLSS concentrations of 8.22 and 9.35 g/L for the RPU-185 RMBR (with the dashed lines representing the best fit simulation data). The total resistance was calculated using Darcy's law (see Equation 2.2).

A decline in flux of over 60% at a rate that is consistent with the 45 kPa cases was noticed for both MLSS concentrations. The total resistances for both MLSS concentrations seemed to intrinsically increase linearly with filtration time, albeit at a much higher rate. This is arguably because fouling was caused by a combined effect of the three fouling mechanisms.

As viewed in Table 5.1, pore blocking parameter, α, is almost of equal value to pore constriction parameter β (though α is slightly above β). This suggests that neither of the two fouling mechanisms was really dominant (although strictly speaking, pore blocking fouling mechanism has slightly the edge in terms of fouling dominance between the both).

Furthermore, with this MLSS concentration range, a bigger R_{b0} coupled with a lower cake removal factor, g_0 (e.g. over two times smaller) when compared to data of said MLSS level range at constant TMP of 15 kPa along with a small blocked pore area constant, k_{Ab},

signified that a fair cake layer size was formed. Consequently, all three fouling mechanisms were almost of equally great importance during fouling.

In the light of the above analyses conducted for the RPU-185 RMBR fouling model, focused interpretations on MLSS concentrations of 3.34 g/L to 9.35 g/L can be summarised as seen below:

i. At constant TMP of 15 kPa, the pore constriction fouling mechanism is dominant without fail during membrane fouling for all MLSS levels.

ii. At constant TMP of 30 kPa, pore constriction is still a dominant fouling mechanism for all MLSS levels but it is possible for cake filtration to be fairly relevant though occasionally.

iii. At constant TMP of 45 kPa, pore blocking and cake filtration (cake formation by extension) fouling mechanisms both typically dominate fouling but only at high MLSS levels. At low MLSS concentration range of 3.34 – 4.26 g/L, cake filtration seems meeker as pore blocking fouling mechanism dominates.

iv. At constant TMP of 58 kPa, even though pore blocking and cake filtration fouling mechanisms still dominate during membrane fouling for all MLSS concentrations, pore constriction is fairly relevant as well. Consequently, it can generally be said that all three fouling mechanisms are of equally great importance during fouling.

Overall, the simulations calculated data (using the RMBR fouling model) are seemingly in reasonable agreement with the experimentally collected data, with deviations of up to about 25% (sometimes a bit more) on total resistances (by extension total fluxes declines) data being sustained (e.g. fairly noticeable for MLSS concentration of 9.35 g/L at constant TMP of 45 kPa).

This could be attributed to permeate restart being needed before TMP steps experiments could carry on again due to low batch tank fluid levels. As a short conclusion, it was noticed that viscosity indirectly affects fouling which is in-line with study carried by Jaffrin et al. (2004) and data provided by Zsirai et al. (2016). A less viscous mixed liquor under the same operating conditions as those experienced by more viscous mixed liquor will most likely foul less (i.e. flux likely to drop slower). This is because, typically, higher viscosities are associated to high MLSS concentrations.

5.2.2. Model Calibration Verification Curves (Constant TMP/Varying Flux)

For a specific MLSS concentration range, a set of calibrated best fit parameters (see Table 5.1) were obtained; therefore, it stands to reason that using said best fit parameters, any MLSS level within said MLSS concentration range can be fitted to a reasonable degree. This of course assumes that the MLSS level within said MLSS concentration range will undergo similar fouling phenomena as concluded at the end of **sub-section 5.2.1**. Thus, the chosen MLSS levels will all be manoeuvred under the same RMBR fouling model that was derived for constant TMP (varying flux).

The usual fouling model constants still apply (e.g. chosen within each MLSS concentration range where appropriate). Three MLSS levels (each in a MLSS concentration range) were used for model verification: 3.89 g/L for 3.34 – 4.26 g/L; 6.82 g/L for 6.32 – 7.24 g/L; and, 8.76 g/L for 8.22 – 9.35 g/L. They were each tested at constant TMP step of 15 and 45 kPa.

The simulation data for each of these MLSS levels were computed in Matlab (i.e. using the best fit parameters for MLSS concentration range each belongs to), and then plotted against its corresponding experimental data (see **sub-section 3.2.10** for experimental details). These results are displayed below. Once again, since all of these MLSS levels with the same TMP step provide similar analyses, only 3 sets of data will be the objects focus: MLSS level of 3.89 g/L at constant TMP of 15 kPa (due to its aeration level being changed) and MLSS level of 8.76 g/L at each TMP of 15 and 45 kPa. Finally, on each of the subsequent figures within this sub-section, the legend applies to both curves (i.e. top and bottom).

(For the verification curves that are not included here, which are for the other two MLSS levels save MLSS level of 3.89 g/L at constant TMP of 15 kPa, please refer to **APPENDIX E.1.1**)

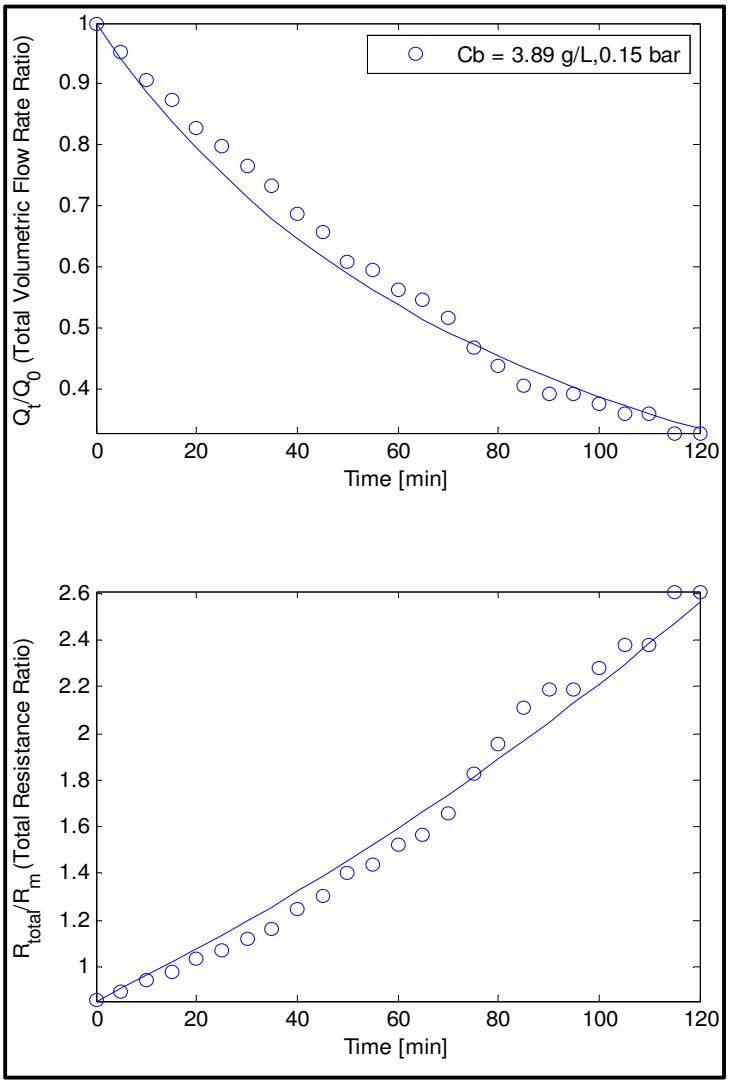

Figure 5.8. Model calibration curve verification for TMP step at 15 kPa for MLSS level of 3.89 g/L

Figure 5.8 depicts the normalised flow rates and the total resistance ratios plotted against filtration time at constant TMP of 15 kPa for respectively MLSS level of 3.89 g/L for the RPU-185 RMBR (with the solid lines representing the best fits simulation data). The general curves trend and flux decline rate are to be expected for this low a MLSS, however, the fitting curves are not very good with a fair bit of deviation.

This is most possibly attributed to the fact that TMP step at that particular MLSS level was conducted under fairly different aeration intensity than that of its corresponding MLSS concentration range (of 3.34 – 4.26 g/L). This was done so in order to view the effects of change in aeration intensity for a RMBR. Though the changes in aeration intensity were not huge, they were still fair enough to affect the data, seemingly, though not much. It should be mentioned that for all the other data sets (chosen MLSS levels along with both TMP steps) the aeration intensity was set back to normal level as per usual.

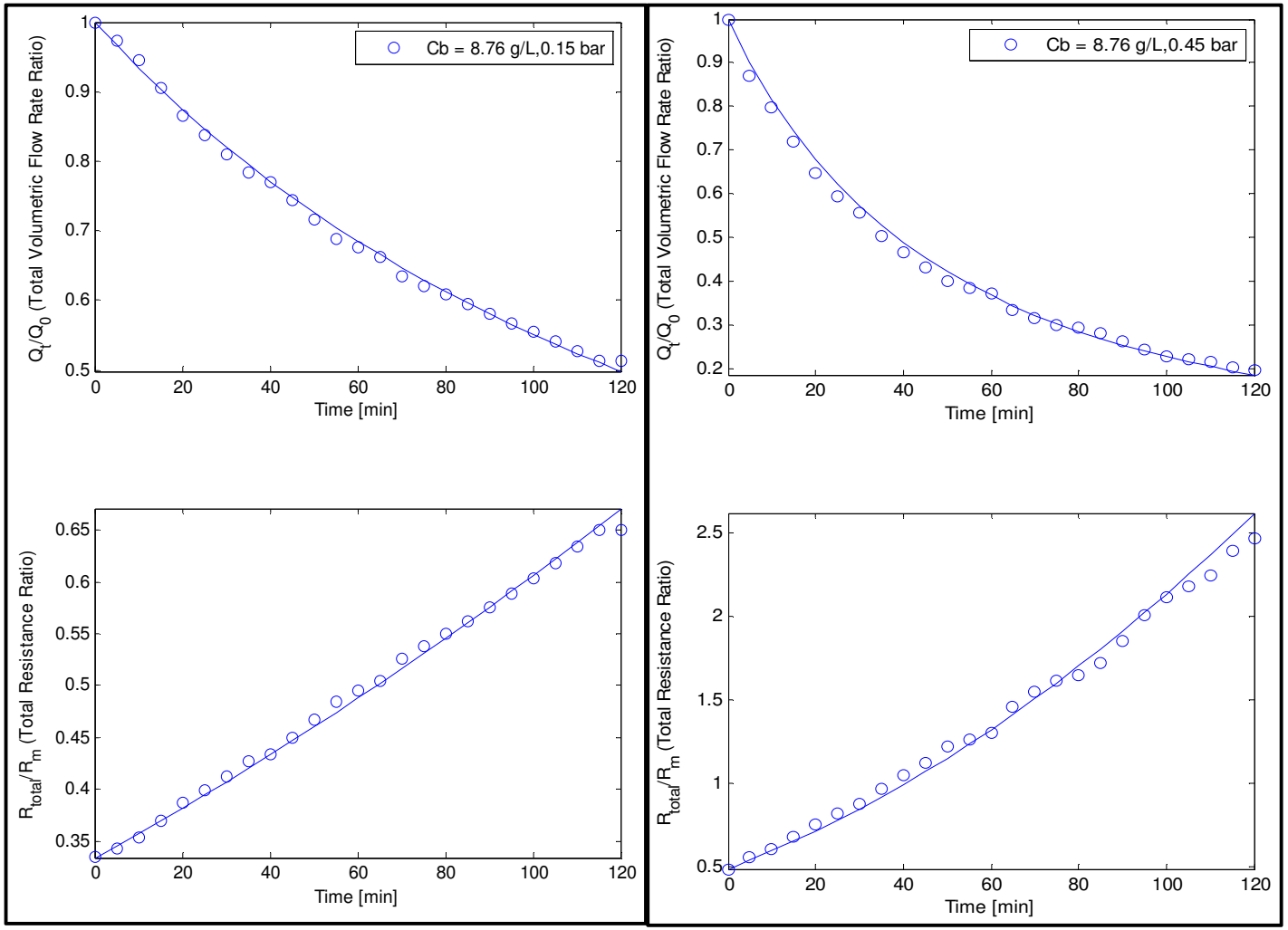

Figure 5.9. Left – Model calibration curve verification for TMP step at 15 kPa for MLSS level of 8.76 g/L
Figure 5.10. Right – Model calibration curve verification for TMP step at 45 kPa for MLSS level of 8.76 g/L

Figure 5.9 shows the normalised flow rates and the total resistance ratios plotted against filtration time at constant TMP of 15 kPa for respectively MLSS level of 8.76 g/L for the RPU-185 RMBR (with the solid lines representing the best fits simulation data). The fitting curves for this MLSS level are fairly good and their overall trend is in-line with those of its upper and lower bound MLSS concentration range.

Figure 5.10 presents the normalised flow rates and the total resistance ratios plotted against filtration time at constant TMP of 45 kPa for respectively MLSS level of 8.76 g/L for the RPU-185 RMBR (with the solid lines representing the best fits simulation data). The general curves trend and flux decline rate are to be expected for this high a MLSS and TMP and are in-line with theory (Paul and Jones 2015).

The fitting curves are really good for this MLSS level and are in reasonable agreement with its upper and lower bound MLSS concentration range (i.e. 8.22 − 9.35 g/L), although few data points seemingly do not follow that trend (especially the near end filtration points). This is likely attributed to permeate restart being needed before the TMP stepping experiments could continue again because of low batch tank fluid levels.

Overall, the fouling model verification fitting curves for chosen MLSS levels looked good when compared with their original validation curves (i.e. each within their respective MLSS concentration range). This gives further validity to the sets of calibrated best fit parameters for the RMBR fouling model found in Table 5.1. However, few points are to be noted for the RPU-185 RMBR (rig):

- A change in aeration intensity could potentially affect data, though in small amounts.
- Permeate restart could potentially affect collected data yet not disastrous.
- Fouling models for constant TMP/Varying flux can produce well calibrated fitting parameters sets provided data collected at a specific MLSS level is within modelled MLSS concentration range.

5.2.3. Constant Flux/Varying TMP

The created TMP models for RMBR under constant flux were validated using data produced from the RPU-185 RMBR. MLSS concentrations utilised for the constant fluxes were 3.34, 4.26, 6.32 and 7.24 g/L. Constant flow rates used (i.e. corresponds to fluxes if divided by area) were respectively 8.67×10^{-6} $m^3.s^{-1}$ for MLSS levels of 3.34 and 4.26 g/L and 1.12×10^{-5} $m^3.s^{-1}$ for 6.32 and 7.24 g/L.

Model simulations were carried out via GA as described in **sub-section 4.2.1**. The results obtained were represented in form of graphs. On those graphs, model 1 characterises Equation 4.24 (i.e. model using formulation area Equation 4.20); and, model 2, which relies on truncated Taylor's expansion (area Equation 4.21), characterises Equation 4.25.

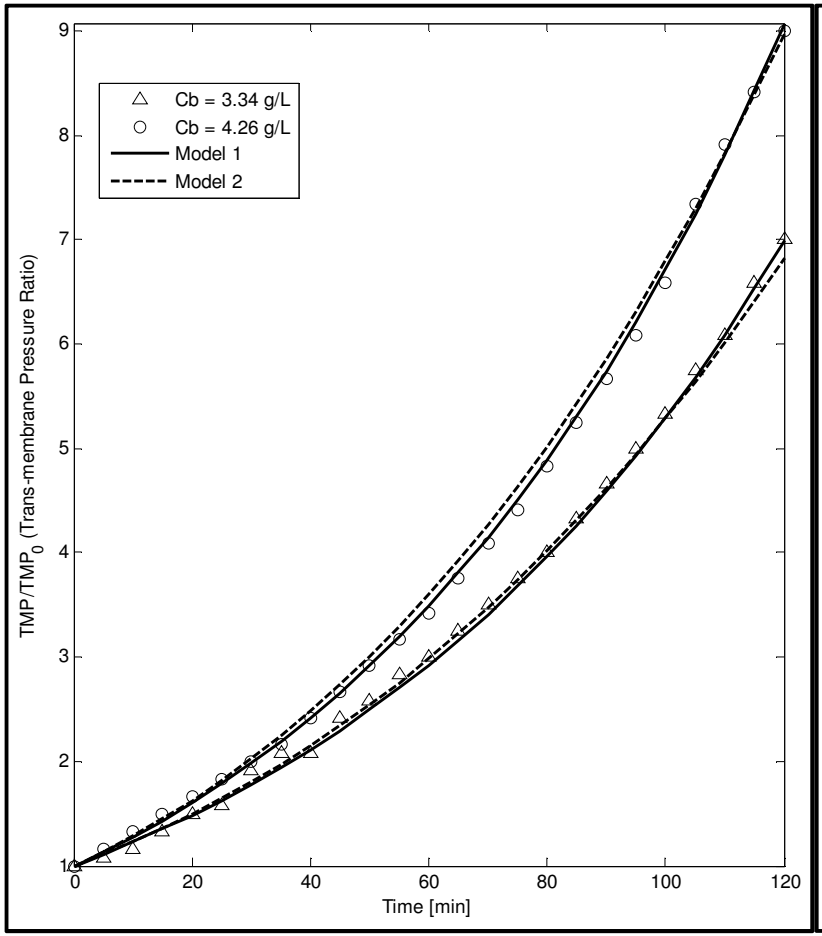

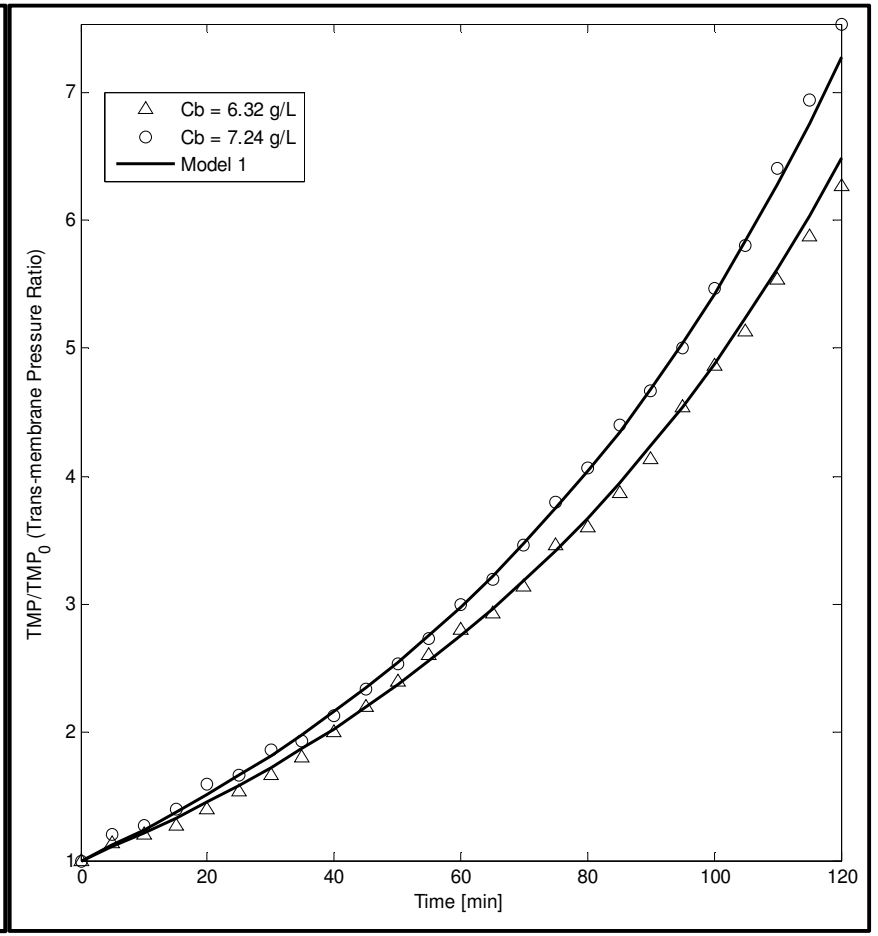

Figure 5.11. Left - TMP rise at constant flow rate of 8.67×10^{-6} $m^3.s^{-1}$ for MLSS levels of 3.34 and 4.26 g/L
Figure 5.12. Right - TMP rise at constant flow rate of 1.12×10^{-5} $m^3.s^{-1}$ for MLSS levels of 6.32 and 7.24 g/L

Figure 5.11 and 5.12 each displays TMP rise plotted against filtration time at constant flow rate of respectively 8.67×10^{-6} $m^3.s^{-1}$ and 1.12×10^{-5} $m^3.s^{-1}$ for corresponding MLSS level of 3.34 and 4.26 g/L, and 6.32 and 7.24 g/L for RPU-185 RMBR (rig). Figure 5.11 boasts two models (model 1 is shown by solid lines and model 2 is represented by dashed lines) while Figure 5.12 relies on one (model 1 represented by solid lines).

Experimentally collected data indicated that TMP had increased on average by over 70% for all MLSS concentrations, and noticeably so at higher MLSS levels. The fouling rate thus increased with bigger MLSS concentration, as seen by higher TMP readings at higher MLSS concentration on each figure. As already explained, this is likely due to the fact that at higher MLSS concentrations more caking is observed due to the higher solids content in the mixed liquor, causing more clogging of the membrane and thus progressively increasing the TMP over time.

On Figure 5.11, model 1 is derived from Equation 4.20 whilst model 2 is derived from Equation 4.21 which relies on the truncated Taylor's expansion. Between time intervals from 30 to 90 min for MLSS concentration of 4.26 g/L, model 2 had an error deviation of 9% on simulated data when compared with Model 1. This is a direct consequence of the Taylor's expansion truncation error.

Thus, model 2 predicted the available remaining filtration area to be much lower than expected and with it determined slightly higher TMP values than model 1. This is directly reflected in parameter K_α where for model 2 it had a value of 10.53 whilst for model 1 it had a value of 9.975. The bigger this value the higher the predicted TMP will be with more subsequent fouling.

For that reason, model 1 was utilised with Figure 5.12 to interpolate its predicted TMPs value for tighter curve fitting. The found K_α value for model 1 for MLSS level of 6.32 and 7.24 g/L (Figure 5.12) was 9.26. The shape of the curves of TMP versus time for both figures indicate that fouling was likely caused by cake filtration although initially induced by pore constriction fouling mechanism effects, with β found to be 16.308 and 17.58 for respectively model 1 and 2 for MLSS level of 3.34 and 4.26 g/L, and 2.325 for MLSS concentration of 6.32 and 7.24 g/L.

It was found that for both models, k_ω, amounted to 1.404×10^{-5} for MLSS concentration of 3.34 and 4.26 g/L while for model 1 for MLSS concentration of 6.32 and 7.24 g/L, its value was 2.911×10^{-5}. Conversely, φ was 0.0939 and 0.06 for respectively model 1 and 2 for MLSS level of 3.34 and 4.26 g/L, and 5.13×10^{-6} for MLSS level of 6.32 and 7.24 g/L. Finally, terms k_ω and φ are reasonable for their range and the filtration conditions experiments were carried on.

Overall, fouling model simulations are in good agreement with experimentally collected data but with some deviations of between 9 to 15% on simulations that are acknowledged. It can thus be concluded for RPU-185 RMBR fouling model for MLSS concentration range of 3.34 to 7.24 g/L at constant flow rate range of 8.67×10^{-6} to 1.12×10^{-5} $m^3.s^{-1}$ that:

i. Higher fouling rates are experienced at higher MLSS, thus rapidly increasing TMP.

ii. Two fouling models, one of which utilises Taylor's expansion, can be used to predict fouling behaviour for sudden rise in TMP. Though they are both equally as correct, one interpolates TMPs while the other with Taylor's expansion extrapolates TMP values by 9%.

5.2.4. SMP Inclusion Model

The role of SMP in membrane fouling has been pretty irregular to say the least. The goal of this SMP inclusion model was not to conduct a full on SMP study but rather to give broad approximation of its effect on fouling in RMBR. Since MLSS has some relationship with SMP, a rough model (see Equation 4.18) was used for estimations.

To that end after every filtration experiment (i.e. RPU-185 RMBR), the total cake thickness was measured. This was value was divided by the initial total flux within the membrane. The new value obtained is what was referred to as "cake thickness ratio" or cake thickness per unit flux. All experimental details are as outlined in **sub-section 3.2.8**.

It should be noted that as per Equation 4.18 cake thickness ratio was needed for the linear fit process so as to procure the model's best fit; hence, the need to obtain it either experimentally or through interpolation in cases where it could not be directly obtained. The involvement of cake thickness is not surprising here since a fraction of foulants forming the cake can indeed be SMP.

The MLSS level ranges used for model validation were 1.2 – 4.3 g/L and 5.96 – 9.35 g/L. The best fits and curves were obtained as discussed in **sub-section 4.2.2**. From the model fit parameters that were yielded from Matlab linear fits (i.e. the line gradient corresponded to value of k_i whilst the value of $\epsilon_{SMP}.C'_{MLSS}$ was exponential of line's constant), simulation curves were plotted. The experimental data points were added to them for comparison.

On the ensuing figures within this sub-section, experimental data are represented by small crosses or circles whilst simulated ones are represented by solid lines. Also, C_b here holds the same value as C_{MLSS}. Finally, on each of these figures, y represents the values of y-axis (vertical axis), and x represents the values of x-axis (horizontal axis).

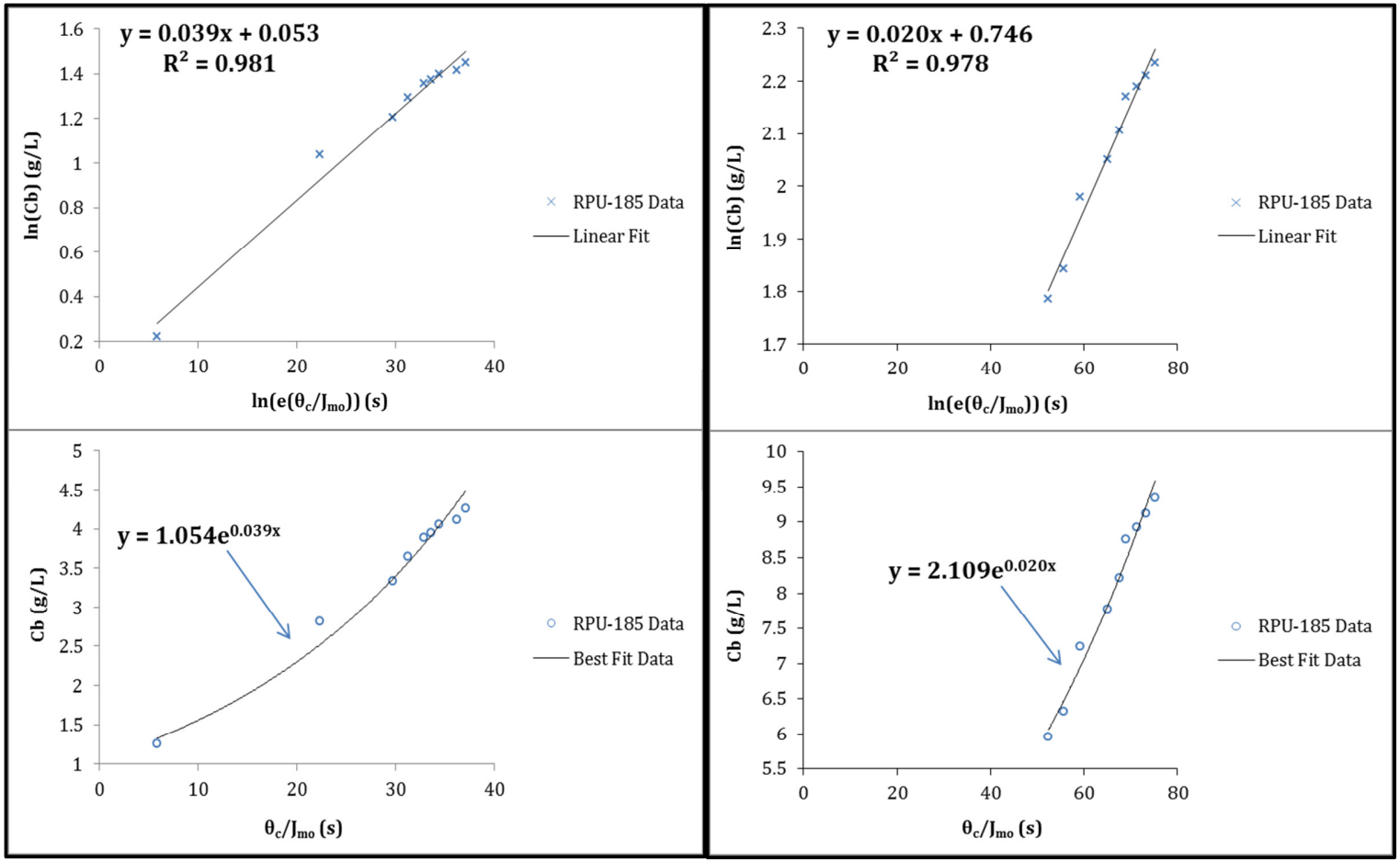

Figure 5.13. Left – MLSS versus cake thickness ratio for MLSS levels of 1.2 to 4.3 g/L
Figure 5.14. Right – MLSS versus cake thickness ratio for MLSS levels of 5.96 to 9.35 g/L

Figures 5.13 and 5.14 each respectively portrays MLSS levels plotted against cake thickness ratios for MLSS concentration range of 1.2 – 4.3 g/L and of 5.96 – 9.35 g/L for RPU-185 RMBR (with the solid line on each being the best fit for a two-hour filtration period). The coefficients of determination, R^2, for each MLSS concentration range are respectively 0.981 and 0.978, suggesting the fittings values are quite respectable.

Simulation best fit values for $\epsilon_{SMP.}C'_{MLSS}$ (g/L) and k_i (s^{-1}) for each MLSS level range were respectively 1.054 and 0.039, and 2.109 and 0.020. This can be interpreted as at higher MLSS levels, SMP levels are likely to increase with cake build-up. As such, during filtration process one likely scenario is that the SMP deposit inside the membrane pores, and then constrict the membrane pores area, thereby increasing the overall membrane resistance and fouling rate.

On both figures at first glance, the exponential fits appear to not accurately predict SMP concentration for few MLSS levels. For instance on Figure 5.13, MLSS concentrations of 2.82, 4.12 and 4.26 g/L are guilty of not falling in range. A reason for this is likely because their matching cake thickness values were interpolated based on other experimentally measured cake thicknesses. However, upon closer inspection of both graphs, the fits seem to succinctly describe the fouling behaviour of the membrane.

Thus, the model predicts that for a bigger thickness cake to form, an exponentially bigger MLSS concentration is required and with it, a subsequent increase in SMP concentration on the membrane surface (as proven by parameter $\epsilon_{SMP.}C'_{MLSS}$, the product of SMP and MLSS concentration factor, being bigger at higher MLSS level range). This appears to explain why higher MLSS levels give rise to faster total flux decline whilst membrane resistances climb rapidly at the same rate. This finding is in-line with Yuan et al. (2002) study.

5.3. Chapter Summary

This chapter fully detailed the results obtained from model simulations of RMBR system (fouling models or otherwise) as well as outlined necessary discussions for them. For the RMBR, the shear effect parameters m and n appeared consistent as they were in line with previous carried out studies. While discussing the curves and fouling mechanisms for the RMBR, one thing of interesting note was the versatility in fouling mechanisms occurring under specific conditions such as TMP or MLSS.

For instance, if TMP were too high, there was a chance of cake filtration being prevalent or at the very least persistent. The calibration verification curves seemed good, however permeate restart somewhat had a slight adverse effect on some end filtration data points whilst varied aeration was a small issue affecting filtration data collected for MLSS level of 3.89 g/L at constant TMP of 15 kPa.

Fouling models for the rise in TMP gave good analysis in that though the Taylor's expansion model is as good as the other model, it ultimately extrapolates TMP values by a deviation of 9% which should be acknowledged whilst the other model interpolates them. Although not most ideal, the SMP inclusion gave some interesting insight from its predictive model.

CHAPTER 6: FOULING MODEL STUDY OF THE STATIC SQUARE MBR

This part not only contains results attained from SMBR related experiments and from simulations of SMBR fouling model but also includes their discussions in full. Results are presented in forms of figures and table summarising model simulation best fit parameters. However, before that the SMBR fouling model is tested with two external data sources. This chapter is divided into two main sub-sections:

i. *Model Fitting using External Data (Validation)*: Two external data sources, one from SMBR operated at Coors (UK) and the other from Duclos-Orsello et al. (2006) are added for discussion (as they are used for verification).

ii. *Model Validation using the Square Static MBR:* This sub-section depicts validation of fouling model for SMBR which includes the hydrodynamics effects in curves form and discusses them. Solution best fits from GA simulations are shown in table form and discussed as well.

6.1. Model Fitting using External Data (Validation)

In order to verify and validate the SMBR fouling model, two external distinct sets of data were first used. The first set was collected from the study carried out by Duclos-Orsello et al. (2006), and the other was data procured from a pilot MBR plant operated at Coors UK (Paul 2013). It is worth mentioning that, for the Coors (UK) data, the viscosity (Pa.s) was calculated from the MLSS data provided and by using Equation 3.8. The flow regimes were laminar.

There were clearly no induced rotational shear effects to take into account. This simplified the entire simulation procedure since only the hydrodynamics effects were included with appropriate parameters and coefficients used during GA simulation runs.

Simulations' best fits parameters are highlighted in Table 6.1 whilst the graphs for analyses are portrayed in this sub-section as Figure 6.1 and 6.2. On these graphs, experimental data are represented by small asterisks, crosses, circles, or triangles and simulated data are displayed as solid lines. Additionally, on all of them C_b is the same as C_{MLSS}. On each of the ensuing figures within this sub-section, the legend applies to both curves (i.e. top and bottom).

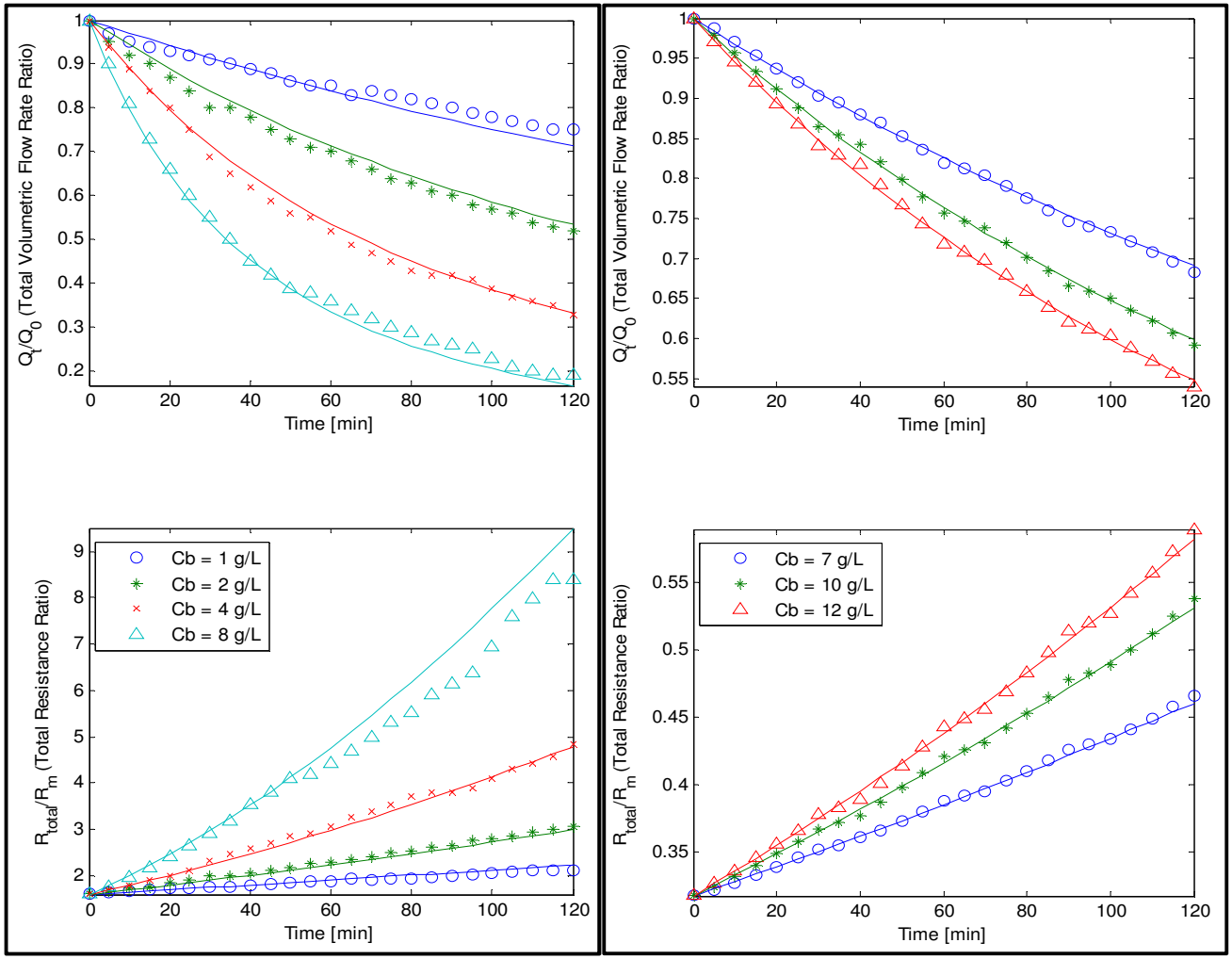

Figure 6.1. Left - Flux decline and total resistance data obtained from Duclos-Orsello et al. (2006) with best model fits

Figure 6.2. Right - Flux decline and total resistance data obtained from SMBR plant located at Coors UK with best model fits

Figure 6.1 displays the TMP step data as normalised flow rates and the total membrane resistance ratios plotted against the filtration time at a constant TMP of 14 kPa for MLSS concentrations varying from 1 to 8 g/L based upon the Duclos-Orsello et al. (2006) data; with the solid lines representing the best fit simulation solutions. The total resistance was obtained using Darcy's law (Equation 2.2).

It was immediately noticeable that at the highest MLSS concentration of 8 g/L, the flux decline was much greater than for all lesser MLSS concentrations. In fact it was an actual decrease of about 84% making the total membrane resistance climb steeply for this entire filtration event. This indicated that fouling was dominated by pore constriction even though all three types of fouling mechanisms were in operation to a greater or lesser extent.

This conclusion appears justifiable since the calculated pore constriction parameter, β, was found to be roughly four times the size of the pore blockage parameter, α (see Table 6.1). Additionally, a weak deposit layer as depicted by R_{b0}, and a big cake removal factor, g_0, indicated a fairly weak cake layer formation which is reinforced by a smaller f'.R' factor and a small blocked pores area constant, k_{Ab}.

Thus, the combination of parameters f'.R', R_{bo}, g_o and k_{Ab}, implied that cake filtration was relatively less significant during fouling which was expected for such low TMP operations. These finding seem to concur with the results found in the original study by Duclos-Orsello et al. (2006). As with the original study, at bulk concentrations of 1 and 2 g/L the resistances and the volumetric flow rates seemed essentially linear.

Figure 6.2 shows the normalised flow rates and the total resistance ratios versus the filtration time at a constant TMP of 18 kPa with initial flow rate of 1.24×10^{-5} $m^3.s^{-1}$, for normalised MLSS bulk concentrations of 7, 10 and 12 g/L respectively for the data supplied by the pilot MBR unit operated at Coors UK (Paul 2013); with the solid lines representing the best fit simulation solutions.

This MBR system's data set had typically high MLSS values that are usually associated with high overall fluid viscosities. This suggested that the flux was expected to decline rapidly at the highest MLSS concentrations. Indeed it is found that at a MLSS concentration of 12 g/L, the flux had declined almost linearly by 63%.

High MLSS concentrations at respectively 7 and 10 g/L exhibited this similar declining behaviour albeit at slightly reduced rates of 59 and 61% respectively. Although slightly below theoretical expectations due to arguably a low TMP regime, the linear increase in resistances was probably caused by the combined effect of all three fouling mechanisms occurring simultaneously with pore constriction fouling being slightly more dominant.

As seen in Table 6.1, and expectedly for low TMP operations, an analysis of the combination of parameters f'.R', R_{bo}, g_o and k_{Ab}, indicated that cake formation was moderately weak.

Moreover, a bigger pore constriction parameter, β, than the pore blockage parameter, α, suggested that pore constriction was somewhat more prevalent in fouling.

In conclusion, simulations produced respectable results when compared with experimental data although extreme MLSS concentrations values of 8 and 12 g/L respectively for the Duclos-Orsello et al. (2006), and the Coors (UK) data (Paul 2013), gave rather poor fits. Interpretations of these analyses can be summarised on MLSS level range of 1 to 12 g/L for TMP range of 14 to 18 kPa as follows:

i. The SMBR fouling model for constant TMP/varying flux can fit to a good degree external data sources for SMBR units provided the right assumptions are made. Some anomalous or poor fits can be expected at high MLSS in cases where sludge or other high viscous fluid is used.

ii. The SMBR fouling model for constant TMP/varying flux can also give a pretty fair indication of the fouling mechanisms occurring during the filtration process of said external SMBR units though some unpredictability is to be expected.

6.2. *Model Validation using the Square Static MBR*

So as to fully validate the SMBR fouling model, data collected from the SMBR rig that was made at the laboratory were used. The MLSS level ranges used for all the TMP steps (15, 30, 45 and 58 kPa) were 6.32 − 7.24 g/L and 8.22 − 9.35 g/L. Expectedly, the flow regimes during filtration processes were all laminar (as Re values were much less than 2×10^5). The aeration rates for all the data sets for the SMBR rig were similar in scale to that of RMBR system operated under lab-scale conditions.

Hence, similar constant values for air scouring coefficient, α_v, (i.e. 0.0292), and resistance distribution factor of cake layer, δ', (i.e. 4.6×10^{-4} m^{-1}) were used during all GA simulations. Additionally, since the SMBR system was not operated under rotation (but still affected by air scouring effects), the shear effects parameters m and n, and factor k_ω were removed and not used during all GA simulations.

For each MLSS level range and TMP step, 50 GA simulations of the fouling model for the SMBR rig were run. The same procedure was applied to the two external data sources individually. The solution fits of these simulations were each averaged, giving the SMBR fouling model's best fit parameters (in form of f'.R', α, β, R_{bo}/R_m, g_o and k_{Ab}). These best fit solutions are summarised in Table 6.1 for all TMPs. The term σ_a was determined upon obtaining the fitting value of β since the membrane pore size was known and its found values are fairly reasonable for their range. In Table 6.1 D-O stands for Duclos-Orsello.

Table 6.1. Averaged best fit fouling model parameters including hydrodynamic effects for all SMBRs after 50 GA simulations for each TMP step and MLSS concentration range

	TMP (kPa)	Averaged optimised parameters						
		f'R' ×10^{11} (m/kg)	α (m^2/kg)	β (kg)	R_{bo}/R_m (–)	g_o (–)	k_{Ab} (–)	$\sigma_a \times 10^{-17}$ ($kg.m^3$)
External Data	D-O et al. 2006 – 14	1.81	0.576	2.538	0.168	24.58	1.46	-
	Coors (UK) – 18	1.76	0.122	0.289	0.159	27.24	0.108	-
- SMBR Rig - MLSS (g/L) 6.32 – 7.24	15	0.834	0.094	0.492	0.126	63.75	9.36	3.79
	30	0.947	0.184	0.305	0.692	10.99	2.032	2.33
	45	108.8	0.907	0.486	0.526	15.36	14.23	3.78
	58	32.01	0.221	0.212	0.457	29.66	1.26	1.62
- SMBR Rig - MLSS (g/L) 8.22 – 9.35	15	0.373	0.174	0.444	0.207	87.79	3.437	3.77
	30	0.661	0.144	0.299	0.408	12.84	6.293	1.687
	45	59.63	1.039	0.468	0.598	19.20	17.95	3.976
	58	7.499	0.194	0.130	0.564	32.95	0.006	1.106

Best fit parameters f'.R', α, β, R_{bo}/R_m, g_o and k_{Ab} as presented in Table 6.1 all appear to be in sensible agreement with prior conducted work (Duclos-Orsello et al. 2006, Paul and Jones 2015) and in-line with Table 5.1 results. A justification for this is that despite variations depending on the TMP used, these fitted values remained constant within simulated specific MLSS concentration range.

Though three MLSS concentration ranges were used for curve fitting, all subsequent discussions in this sub-section will only focus on one range: 8.22 – 9.35 g/L (with all four TMP steps). The reason for this is that the other two MLSS level ranges with the same TMP steps provide fairly similar analyses and therefore are not needed to draw initial conclusions. Also, on each of the ensuing figures within this sub-section, the legend applies to both curves (i.e. top and bottom).

On all ensuing figures that will be used for discussions, C_b is the same as C_{MLSS}. On these graphs, experimental data are denoted by small asterisks or circles whilst simulated data are represented by solid lines.

(For the figures not included here, which are for the other MLSS level range, please refer to **Appendix E.2**)

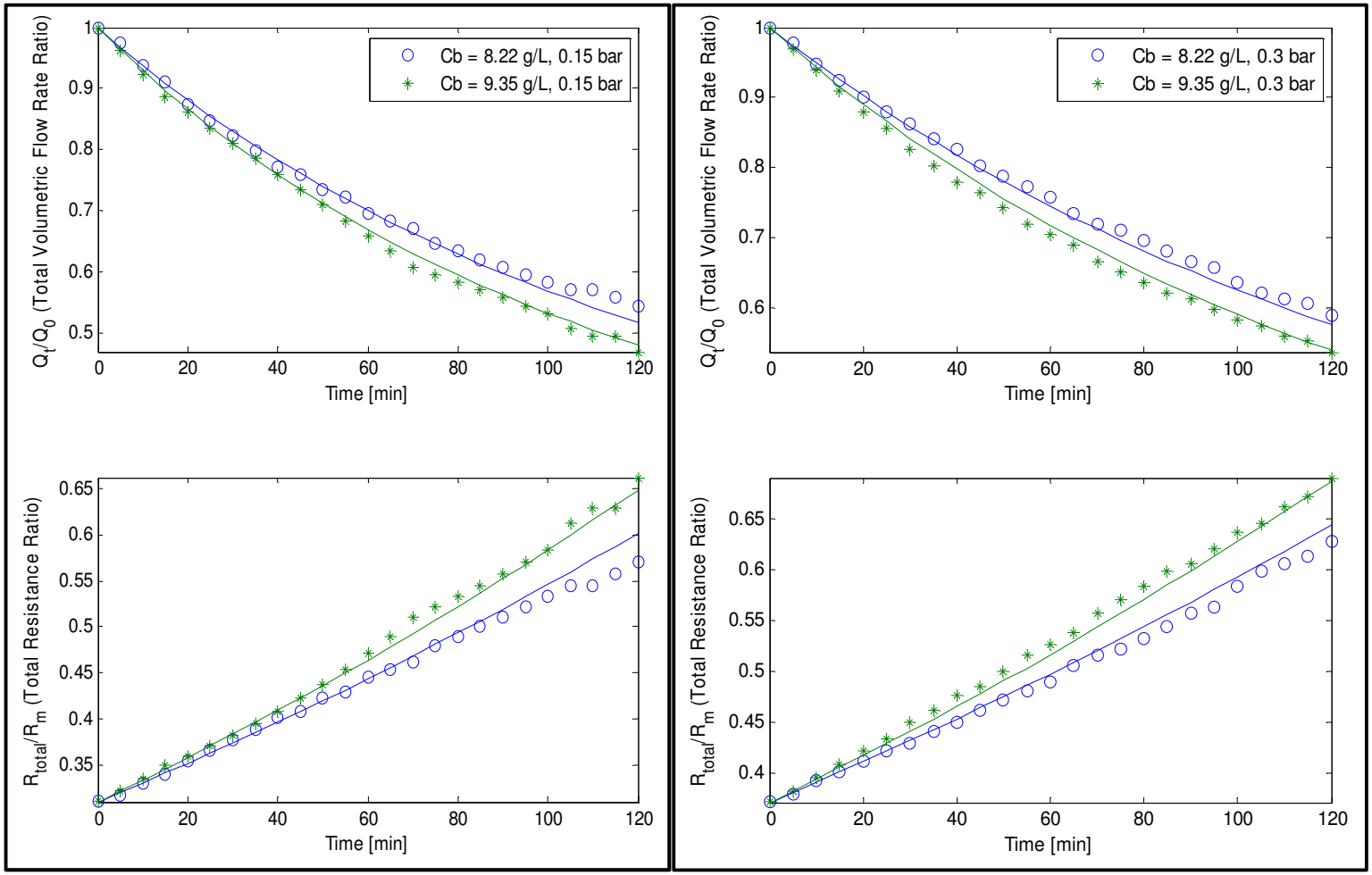

Figure 6.3. Left - Flux decline and total resistance for TMP step at 15 kPa for MLSS levels of 8.22 and 9.35 g/L
Figure 6.4. Right - Flux decline and total resistance for TMP step at 30 kPa for MLSS levels of 8.22 and 9.35 g/L

Figure 6.3 represents the normalised flow rates and the total resistance ratios plotted against the filtration time at constant TMP of 15 kPa (TMP step data), for MLSS concentrations of 8.22 and 9.35 g/L for the constructed SMBR rig; with the solid lines representing the best fits simulation data. The total resistance was calculated using Darcy's law (see Equation 2.2). Collected data showed that flux had declined at a steady rate by roughly 55% for both MLSS levels.

For both MLSS levels the total resistances' curves displayed an almost linear trend, suggesting fouling was caused by the combination of all three fouling mechanisms. As shown in Table 6.1, a fairly small R_{b0} factor and a big cake removal factor, g_0, indicated the formation of a weak cake layer which is further reinforced by a smaller f'.R' and a small k_{Ab}.

As a result, the combination of parameters f'.R', R_{bo}, g_o and k_{Ab}, suggested that cake filtration was less dominant during fouling which was anticipated since at low TMP of 15 kPa, cake formation is expected to be less prevalent (Paul and Jones 2015). Furthermore, pore constriction parameter, β, being roughly three times bigger than pore blocking parameter, α, ultimately suggested that fouling was dominated by pore constriction (as $\beta >> \alpha$).

Figure 6.4 depicts the normalised flow rates and the total resistance ratios plotted against the filtration time at constant TMP of 30 kPa (TMP step data), for MLSS concentrations of 8.22 and 9.35 g/L for the constructed SMBR rig; with the solid lines representing the best fits simulation data. The total resistance was calculated using Darcy's law (see Equation 2.2).

A similar flux decline comparable in number to the 15 kPa TMP case was observed for both MLSS levels. The rate of decline was steady and this gradual drop was expected since it was in-line with critical flux theory (Judd 2006). The total resistances' curves for both MLSS levels, yet again, seem to indicate that fouling could be attributed to the combined effect of all three mechanisms.

As seen from Table 6.1, for this MLSS concentration range, a fairly big R_{b0} and a small cake removal factor, g_o, indicates a fair amount of cake layer formed which is supported by a bigger f'.R' factor when compared to data of said MLSS level range at constant TMP of 15 kPa, and a small blocked pores area constant, k_{Ab}.

Consequently, the combination of parameters f'.R', R_{bo}, g_o and k_{Ab}, suggested that cake formation (by extension cake filtration) was sufficiently prevalent during fouling. In addition, the pore blocking parameter, α, being much smaller than the pore constriction parameter, β, all seemingly implied that the bulk of fouling was dominated by both pore constriction and cake filtration.

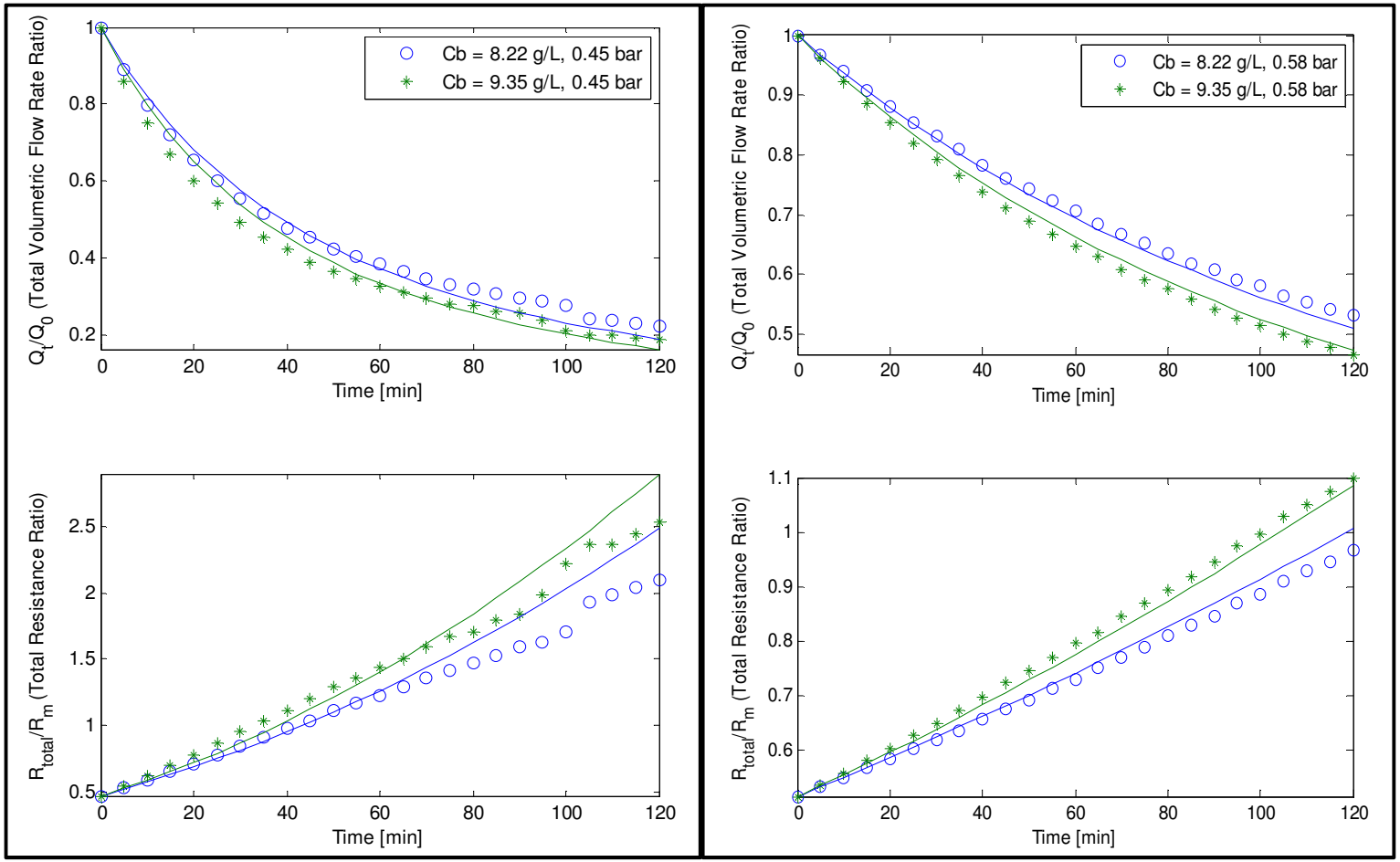

Figure 6.5. Left - Flux decline and total resistance for TMP step at 45 kPa for SMBR rig for MLSS levels of 8.22 and 9.35 g/L
Figure 6.6. Right - Flux decline and total resistance for TMP step at 58 kPa for SMBR rig for MLSS levels of 8.22 and 9.35 g/L

Figure 6.5 displays the normalised flow rate and the total resistance ratios plotted against the filtration time at constant TMP of 45 kPa (TMP step data), for MLSS concentrations of 8.22 and 9.35 g/L for the constructed SMBR rig; with the solid lines representing the best fits simulation data. The total resistance was calculated using Darcy's law (see Equation 2.2). Due to a colossal drop in flux at this high TMP, the total resistance increases at an exponential rate for both MLSS concentrations.

It is noticeable that the best fit curves at this high TMP are extremely poor (especially after 80 minutes), however, the curves' trend are of the right scale and in the right direction to allow an analysis of the fouling behaviour that is occurring. At first glance, analysis would suggest that fouling may be due to all three fouling mechanisms, but it can be argued that fouling was mainly dominated by cake filtration and pore blocking.

For this MLSS concentration range, a relatively bigger R_{b0} and f'.R' when compared to data of said MLSS level range at constant TMP of 15 kPa, coupled with similar sized cake removal factor, g_0, and blocked pore area constant, k_{Ab}, all strongly indicated that a fairly big cake layer was formed (see Table 6.1). However, with the pore blocking parameter, α, being roughly twice as big as the pore constriction parameter, β, it can be inferred that the pore blocking fouling mechanism was also prevalent during fouling. Hence, the bulk of the fouling was dominated by both cake filtration and pore blocking.

Figure 6.6 displays the normalised flow rate and the total resistance ratios plotted against the filtration time at constant TMP of 58 kPa (TMP step data), for MLSS concentrations of 8.22 and 9.35 g/L for the constructed SMBR rig; with the solid lines representing the best fits simulation data. Again, the total resistance was calculated using Darcy's law (see Equation 2.2).

The total resistance for each MLSS concentration seemingly increases in a linear fashion with filtration time albeit at a high rate. This is probably because fouling was caused by all three mechanisms happening simultaneously. As can be seen from Table 6.1, pore blocking parameter, α, and pore constriction parameter, β, are of almost equal value. This suggested that neither of the two mechanisms was dominant.

Furthermore, for this MLSS levels range, a fairly big R_{b0} and f'.R', and smaller (e.g. over two times) cake removal factor, g_0 when compared to data of said MLSS concentration range at constant TMP of 15 kPa, coupled with a small blocked pore area constant, k_{Ab}, all indicated that a decent amount of cake layer was formed. Consequently, all three fouling mechanisms can be said to have been of equally great importance during fouling.

As such, in the light of the above conducted analyses for the SMBR fouling model, focused interpretations can be summarised on MLSS levels range of 6.32 to 9.35 g/L as follows:

i. At constant TMP of 15 kPa, pore constriction fouling mechanism is dominant during membrane fouling for all MLSS levels.

ii. At constant TMP of 30 kPa, pore constriction and cake filtration fouling mechanisms both typically dominate fouling for all MLSS levels.

iii. At constant TMP of 45 kPa, pore blocking and cake filtration (cake formation by extension) fouling mechanisms dominate fouling for all MLSS levels. The biological activities taking place at high MLSS are very active; therefore fits can be expected to be poor or irregular but can still be fair enough in trend to give a good analysis.

iv. At constant TMP of 58 kPa, all three fouling mechanisms are fairly relevant and can be said to be of equally great importance during fouling for all MLSS levels. The biological activities happening at high MLSS are very lively; consequently fits can be expected to be irregular though they should still be good enough to give analysis.

Overall, modelling simulations (using the SMBR fouling model) are in fairly respectable agreement with experimentally collected data for the constructed SMBR rig. However, it can be seen that at higher TMPs, the simulation fit progressively deteriorated as the flux rapidly declined. Thus, at a TMP step of constant TMP of 45 kPa, the simulations fitting curves were extremely poor, and by extension, were a bit poor for the 58 kPa cases as well (though marginally better than the cases involving the TMP step of 45 kPa). This situation is less prevalent for the RMBR system, as both air scouring and rotational shear contribute to the reductions in fouling.

6.3. Chapter Summary

This chapter presented the necessary discussion for the SMBR as far as its fouling model was concerned. Two data sets, one from Duclos-Orsello et al. (2006) and another from Coors (UK) were tested to validate the fouling model. Even though some assumptions had to be made, the end results for the simulation of these data sets were satisfactory. Having said that though, some deviation at high MLSS are to be expected when fitting non-local data.

Overall, model simulations for SMBR simulated experimental data reasonably. However, there were some rather poor fits as well. This was largely the case for high TMPs. Yet, despite that the general trend of these simulations remained consistent, thus allowing for fouling mechanisms analyses. One thing of note here is the flexibility in fouling mechanisms occurring under explicit conditions (e.g. TMP, MLSS), which were almost similar to those of the SMBR system but the change in fouling rate was the difference.

CHAPTER 7: COMPARATIVE STUDY AND FUTURE OF ROTATING MBR

In this chapter, a comparative study as analysis between the RMBR and SMBR is conducted. Table and graphs are used to emphasise on some of these analytical points. Moreover, an analysis of activated sludge for the RMBR viewed under microscope is outlined. Finally, a closing discussion is given on RMBRs' future. This chapter is divided into three main sub-sections:

i. *Comparison of Static MBR against Rotating MBR – An Analysis*: A small comparative study is conducted between the RMBR and SMBR in this sub-section to find out the better performer.

ii. *Microscopic View of Activated Sludge*: Pictures taken under the microscope for the activated sludge for the RMBR are discussed in this sub-section.

iii. *Are Rotating MBR Systems the Future? – A Discussion*: A small discussion about the next step RMBRs might take is given in this section.

7.1. Comparison of Static MBR against Rotating MBR – An Analysis

After every simulation done in Matlab, a mean of minimised residuals or sum of the least squared residuals (i.e. mean fitness) and the best minimised residuals or sum of the least squared residuals (i.e. final value or best fitness) are automatically calculated. These can in turn be used to accurately and aptly determine how well a simulation fit was conducted. Needless to say, the smaller these values, the better analysis can be conducted. Using these facts, a comparison between both MBR models (static and rotating) and their fitness values will be conducted and some conclusions drawn.

When comparing and fitting the data obtained from the RMBR system to that obtained from the square-shaped SMBR system, the most prominent difference found for the latter case is the somewhat poor fit between the experimental data and the simulations run (especially at constant TMP of 45 kPa). Table 7.1 summarises the best fitness values after simulations for both MBR rigs for the same two TMP steps at constant TMPs of 15 and 45 kPa for MLSS levels of 6.32 and 7.24 g/L.

Table 7.1. Statistic with fitness values from simulations as seen in Matlab for MLSS levels of 6.32 and 7.24 g/L at constant TMPs of 15 and 45 kPa for the RMBR and SMBR system

	Avanti RMBR		**Constructed SMBR rig**	
Fit Parameters	**15 kPa TMP**	**45 kPa TMP**	**15 kPa TMP**	**45 kPa TMP**
Best fitness (−)	0.0361	0.0294	0.346	1.293
Mean fitness (−)	0.0849	0.0672	0.968	4.541

As can be seen, the best fitness values for the RMBR system are all much smaller than those for the square-shaped SMBR system. In fact, the best fitness value for the latter is roughly ten times greater than that of the RMBR system for TMP of 15 kPa (and even greater for TMP of 45 kPa, at over 40 times). The difference here can be probably attributed to the fact that the shear effects are instrumental in reducing the overall fouling for the RMBR system while the square-shaped SMBR system is only aided by standard air scour alone.

This concurs with critical flux theory and the area-loss model that explains any rapid TMP jump phenomenon (Judd 2006), since greater fouling will lead to greater uneven cake build up, leading to loss of clean membrane surface. This means that locally critical flux could be exceeded, thus promoting the likelihood of rapid declines in fluxes at higher TMPs at unpredictable rates. In simple terms, this means that for the same constant TMP regime for both MBR systems, the fouling build up expected on the RMBR system would be less with a reduced likelihood of local critical flux being exceeded.

This is depicted through Figure 7.1 Left, where, it can be observed that the fouling rate (which is equal to change in flow rate, dQ in L/h, divided by change in filtration time, dt in h) for the RMBR system at each TMP is of much lower magnitude than that of the SMBR system.

In practice, because the static membrane module has less area than the rotating membrane module, for the same flow rate under the same conditions, the SMBR rig should be gaining more flux and thereby produce more permeate volume.

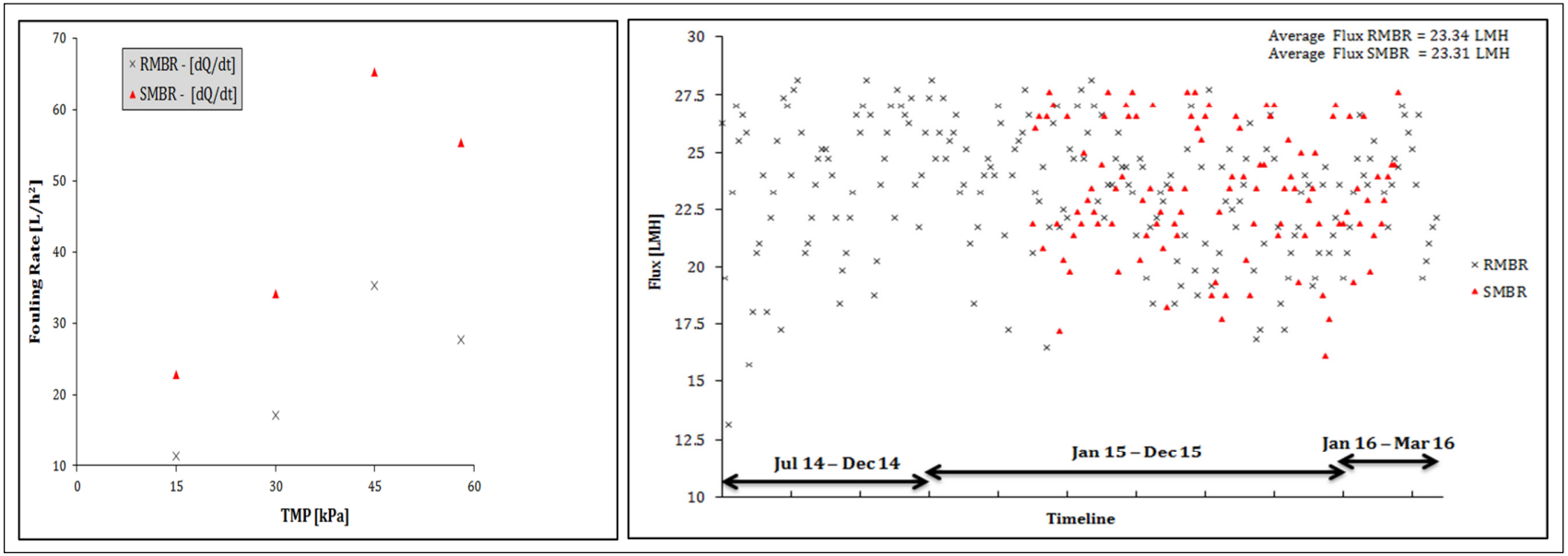

Figure 7.1. (Left) Fouling rates at different TMPs for both MBR systems for MLSS levels range of 6.32 - 7.24 g/L. (Right) 3-day average points fluxes profile for both MBR plants; average flux for RMBR = 23.34 LMH and average flux for SMBR = 23.31 LMH

On Figure 7.1 (Right), from the timeline axis, “Jul” is July, “Jan” is January, “Dec” is December and “Mar” is March.

However, this is not the case as the huge increases in fouling rates cause it to lose flux in the long run. This can be seen on Figure 7.1 Right, whereon, the average flux for the SMBR system is lower than that of the RMBR system. The SMBR system is thus losing flux whilst the RMBR system can seemingly increase flux throughput. As such, data sets obtained under the latter system would be expected to have flux declines occurring in more predictable, consistent ways, and at reduced levels even at higher TMPs when compared to the SMBR system.

Consequently, it would be expected that more consistent and less variable data would give arise to better simulation fits for the RMBR system, and conversely produce a much less reasonable and agreeable fit for the SMBR system even though both were manufactured by the same company, using the same materials, pore sizes, and spacing between individual membrane sheets.

A logical conclusion for these all these results is that for the RMBR system, its additional rotation shear evens out the cake formation on the membrane surface while for the square-shaped SMBR system, the cake distribution is highly uneven and less predictable. In physical terms this hypothesis can be confirmed, since it is very evident when carrying out membrane autopsies for both system types, it is clear that huge cake build up occurs on the membrane surface for the SMBR system.

Figure 7.2 Left and Right show the actual typical caking patterns observed on both types of membrane sheets when they were individually removed from the bioreactor. These simulation results and actual physical observations indicate that the RMBR system may be a more preferable option if reduced fouling was a key need in the system design.

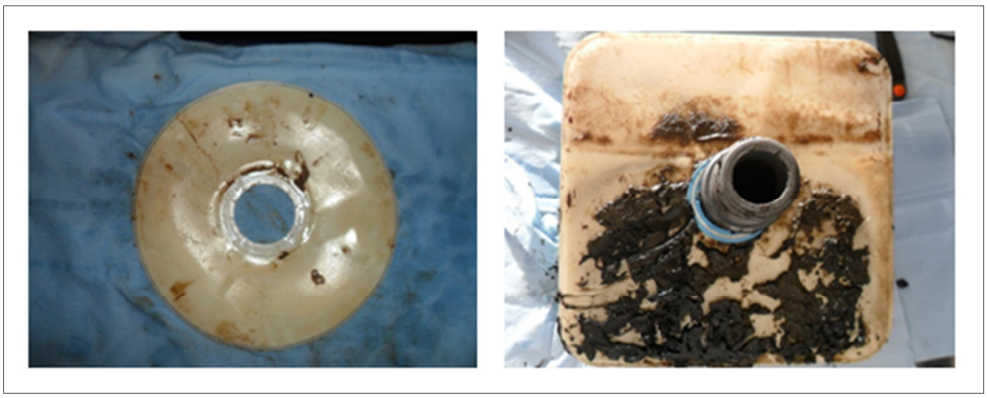

Figure 7.2. (Left) Impact of fouling on the RMBR system - Even caking is observed. (Right) Impact of fouling on the SMBR system - Uneven caking is observed

Interpretations of these results can thus be summarised as follows:

i. RMBR rig boasts lower fouling rates when compared to SMBR system. TMP of 45 kPa produces the largest decline in flux for both systems.

ii. SMBR system loses flux in the long run whilst RMBR system can seemingly increase flux throughput by significant amount although there may be additional capital and operational costs implications.

iii. RMBR produces more consistent filtration data output even at higher TMPs when compared to the SMBR system.

iv. Even though the slowly rotating spindle induce a weak crossflow shear, it can still even out cake build-up across membrane surface (i.e. sweep effect), thus reducing the likelihood of localised critical flux being exceeded, which would lead to dramatic loss of flux.

(For more pictures concerning caking formed on the membranes of both MBR rigs, please refer to **APPENDIX F.1**, which also includes the cake compressibility tests for the RMBR system and a small section that briefly talks about membrane autopsy)

7.2. Microscopic View of Activated Sludge (Rotating MBR)

Observing the activated sludge to study its properties under the microscope though not performed by most, is not exactly a new art either. In fact, there are several advanced, accurate and expensive sludge microscopic techniques out there ranging from phase-contrast and bright-field to (epi)fluorescence and confocal laser scanning that can provide a plethora of information about the sludge.

Lopeza et al. (2005) determined the application limits of these microscopic techniques through image analysis while Mesquitaetal et al. (2013) not only made an extensive review on characterisation of activated sludge through these microscopic techniques but also covered more traditional approaches as well.

The issue with these techniques is that not only can they be lengthy and often time consuming with their set-ups but they also require lengthy quantitative image analysis that might provide a cluster of data that might not be relevant to a plant operator who is concerned with knowing the performance of his or her system through F/M, ML(V)SS, and SRT, which can all be adjusted for better system performance by simple analysis of flocs formed.

Basic floc formation is required for activated sludge operations; as such, examining the flocs formed in the activated sludge is a good way to gauge the system's performance in terms of MLSS augmentation. Good floc formation generally occurs at lower growth rates and at lower nutrient levels, essentially starvation or stationary growth.

Mainly, floc forming species utilise the formation of extracellular polysaccharides (carbohydrate, CHO, whose molecules consist of a number of sugar molecules bonded together), proteins and cellulose fibrils to cement bacteria together to form floc. For this reason, it is a good idea and important to feed the activated sludge with glucose-based synthetic wastewater. When all is said and done, for this type of floc analysis, expensive and/or advanced microscopy is not necessary; an adequate laboratory-scale microscope with the right magnifications suffices.

Thus, 100 µL worth of activated sludge sample taken from the RMBR system was viewed under the microscope to identify early system issues if any. In doing so, activated sludge flocs were imaged using ten times magnification on the microscope so that a good portion of flocs' structure formed as whole could be evaluated; and then later on, observe bacterial and/or protozoans activities. The results for microscopy are shown on Figure 7.3 below,

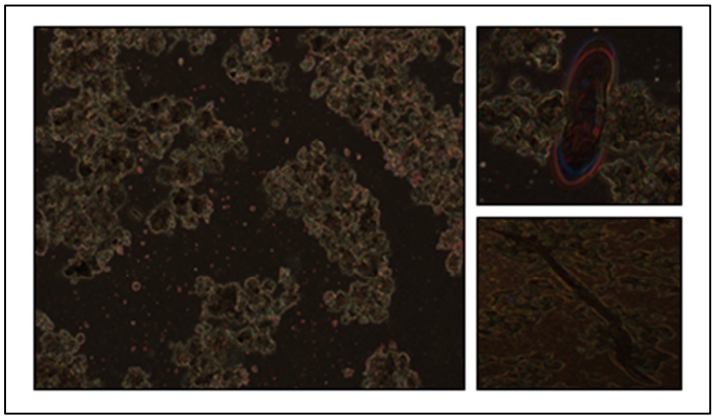

Figure 7.3. (Left) - Part of an activated sludge flocs structure observed under lab-scale microscopy at ten times magnification. (Right) - Rotifers and Annelids protozoans observed

What was found was that individually for the most part flocs were strong, kind of round in shape and compact which are positive signs for good settling and MLSS rise (production of quality effluent by extension). However, as structure they did not seem to mesh quite well together (as depicted on Figure 7.3 Left), signifying there were still slight balancing issues.

This was not unexpected as this test was conducted early on when the activated sludge was received from Thames Water (UK) and started being fed synthetic wastewater as the MLSS concentration hardly exceeded two thousand five hundred mg/L. With this, adjustments to the RMBR system were made, such as reducing the amount of food and regulating the wasting of sludge to balance F/M, to produce better sludge and MLSS levels that were later on used for filtration data collection.

The average floc size calculated from the experiment was 365 μm which was in-line with data provided by Thames Water (UK). Although some bacterial activities (e.g. filaments) were noticed at higher magnifications, protozoan activities are equally as important if not more. In fact, in wastewater treatment, protozoans are higher life forms above bacteria. This is in part because they are indicators of biomass health and effluent quality (in full on activated sludge systems).

Additionally, these single-celled microscopic animals perform three important roles in activated sludge processes; floc formation, cropping of bacteria and removal of suspended material. Various protozoan groups develop in activated sludge according to growth conditions. Through observations under the microscope, Rotifers (e.g. varied in shapes and more complex than other protozoans) were found. This is good as a healthy abundance of these protozoans and free-swimming ciliates (oval in shape) indicate good floc formation and system operation.

Next, Annelids or worms were seen as well, however these protozoans are at their most useful role during nitrification, a process which unfortunately was not carried out due to lack of time.

In conclusion, by observing the flocs population and structure of a sample activated sludge under microscope, it is possible to identify early issues, thereby make adjustments to the system as needed for better control and performance.

(Please refer to **APPENDIX F.2** for the activated sludge flocs pictures that were taken under 40 and 100 times magnification and some general experimental information)

7.3. Are Rotating MBR Systems the Future? – A Discussion

To answer this question one must first look at Figure 7.4, where the mitigation percentage of fouling in the RPU-185 RMBR is shown.

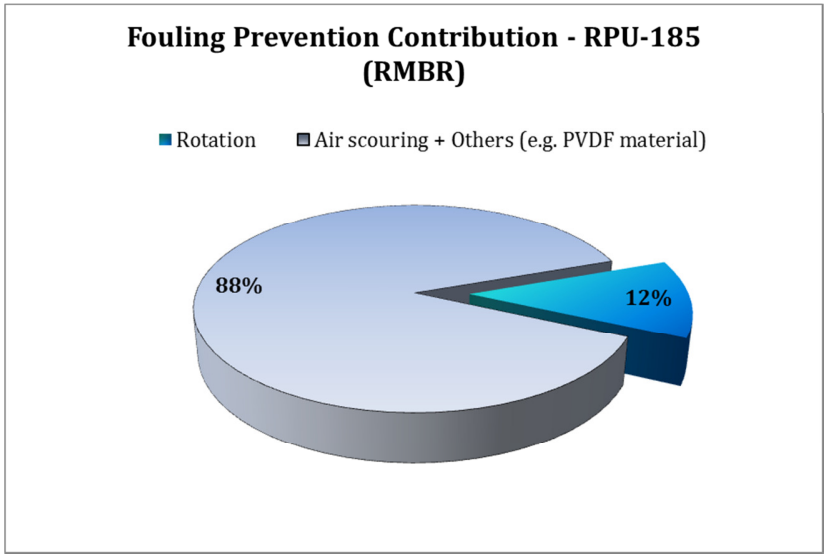

Figure 7.4. Estimated fouling prevention partition for the RPU-185 RMBR

The above estimations were obtained through "data mining" of filtration data collected at the laboratory for the RMBR. What this is saying is that weak crossflow induced by coarse bubble aeration causes an even weaker shear induced crossflow due to rotating spindle. This means that the RMBR's low twenty rpm rotational speed causes cake build-up to even across the membrane surface during fouling, something akin to a "sweep" effect.

It is one of the defining mechanisms behind this system that other RMBRs seem to also employ. A direct consequence of this is that the synergistic interaction of air scouring and rotation reduces fouling far better and produces consistent filtration data when compared to the SMBR rig which relies on air scouring alone to get the job done. Indeed, the twelve percent fouling prevention by rotation alone does not seem like much at first (and really is not), but, together with air scouring it makes a world worth of difference in terms of fouling control and uniformity, and performance.

Even Huber Technology's VRM (RMBR) system which utilises ridiculously lower rotational speeds (i.e. one to two rpm) that hardly produce any shear uses this "effect" to allow for more efficient air scouring. This is one of the advantages RMBRs with low rpms boasts. Furthermore, with the introduction of dynamic crossflow filtration, which is ever more so present in Kerafol and Grundfos BioBooster RMBR systems, it is safe to say RMBR systems are marginally better than conventional SMBR systems as the former boast better filtration performance whilst controlling fouling better.

So, why are they not more widespread? One may ask. After all as Jaffrin (2008) mentioned, on top of the above explained advantages, RMBR systems do tend to reduce energy consumption. There are few reasons for this, starting with the most obvious one, system complexity. Throughout this thesis, presented fouling models, which in themselves have some degree of complexity, produced fine results as fouling mechanisms were described but they are not perfect.

Many assumptions had to be made about the rotation and the end product was something that describes the singular rather than the plural. That is to say if one was to truly model the rotation of RMBRs and all that it entails, unlike SMBRs, the three-dimensional rotation of every single particle attached to the membrane would have to be studied as well. But, that is a myriad of particles each with different angular momentum, thus adding a further level of complexity to their dimension matrices, which have to be summed to describe or make the plural.

Even with a powerful computational package such as CFD it is virtually impossible to be that precise let alone simulate for every case. And that is only one aspect of rotation. The other reason that is perhaps more crucial as to why they are not as widespread as conventional SMBRs is cost related. But, the root of this problem is a combination of short-sightedness, lack of available long term data and everything in between.

Then again, when looking at the short term benefit, it is not hard to see why. A single manufactured RMBR unit even at laboratory scale will cost tens of thousands of pounds while a SMBR of same scale will be about a third or fourth of said price, or sometimes even as low as a tenth if it is a fabricated MBR rig. But, therein lies the problem.

One may have a system that produces a decent amount of and quality permeate fluid; however, it will foul quicker leaving one with high maintenance costs and eventually having to replace it whole. This is a nightmare for industrial or municipal WWTPs who utilise large membrane modules for permeation whilst trying to adhere to tight regulations.

In such cases, when membranes are fouled and if they are of ceramic types, the chemical cleaning and/or maintenance costs incurred will be ridiculous. Meanwhile, with a system like the RPU-185 RMBR, for example, because its rotating membrane module uses low fouling PVDF, is robust, easy to clean, and has excellent chemical resistance, its chemical cleaning and/or maintenance costs will be significantly reduced when compared to most SMBRs.

Thus, in the long term if both MBR systems were to be operated side by side, the reduced operational (e.g. less energy consumed due to low SAD) and maintenance costs of the RMBR combined with its high performance will counterbalance its initial high capital costs.

To conclude, whilst RMBRs might be more desirable options than conventional SMBRs if reduced fouling was a key need in MBR system design, understanding their long term benefits and implications might just be the first step towards its widespread usage. In

addition, once there is better understanding of the rotational processes and researches and designs into this sector broaden; RMBRs may become the systems of first choice. Interpretations of this discussion can be summarised as follows:

i. The rotational mechanisms in terms of fouling prevention for the RPU-185 RMBR account for only twelve percent of cake removal, with the rest being mostly accomplished through the air scouring mechanism.

ii. Even though RMBRs have complex rotational processes, the system can be made to describe the singular for better results rather than the plural, which as the only possible alternative can have ruinous effects on the model as whole.

iii. RMBRs have long term benefits that can offset their initial high capital costs.

iv. RMBRs are first-rate MBR systems that might be more desirable in the future.

7.4. Chapter Summary

This chapter described through comparative study performance difference between RMBR and SMBR. The RMBR outperformed the SMBR in terms of filtration stability and data collection. Furthermore, it was shown that the SMBR unit fouled quicker at higher rates than the RMBR system.

Through the same chapter, activated sludge was viewed under the microscope to observe bacterial activities and flocs formation. Early system problems with sludge were identified and the right adjustments were made accordingly. Indeed, not just for RMBRs, but for any other treatment system running activated sludge, it is a good idea to study flocs formation at an early stage. In doing so, the system can be better managed.

Finally, the future of RMBRs was discussed. The system has not been as widespread as its good performance suggests. Amongst possible reasons for this happening are associated costs and system complexity. Therefore, the only way to advance forward is to be more far-sighted and broaden understanding of this field more.

CHAPTER 8: CONCLUSIONS AND RECOMMENDATIONS

This chapter finalises this PhD research study. All findings are listed here in the general conclusion and final closing words are given. Areas of future studies that might be useful to further researches in this field are listed as well as slightly discussed where necessary.

8.1. General Conclusion

Long before this research, many researchers had conducted studies of almost all kinds with MBRs whether external or internal in structure, and most likely several will still continue to do so long after the completion of this research. While this is a good thing for the field of membrane research in general, the issue lies in the "gap" that was created as a result of focusing more researches on one particular group of MBRs, static and immersed generally, due to their ease of access and initial reduced capital costs.

Consequently, a disparity in knowledge in understanding the inner workings of RMBRs, especially on the modelling side, and well-studied SMBRs was created. This research work attempted to bridge some of that gap. In this endeavour, unique and comprehensive fouling model for initially the RPU-185 RMBR then later constructed SMBR rig, were formulated to understand, or rather, attempt to explain the fouling mechanisms that occur during membrane fouling.

Using short and medium term filtration data sets collected from both MBR rigs, these fouling models were extensively validated. The SMBR fouling model in particular was initially tested using medium term filtration data obtained from a similar SMBR pilot unit operated at Coors (UK). In general, fairly good agreements were reached between experimentally collected filtration data and the simulations outputs but deviations of up to 25% in some cases are to be acknowledged.

The SMBR system in particular whose results were largely respectable, gave a couple of poor fits especially at high TMPs and MLSS levels that were attributed to the unpredictable nature of SMBRs at high MLSS, especially those operated at high TMPs where biological activities tend to be more active, but, only after the fact. The findings and outcomes of the fouling models for both MBR rigs including the shear effects for the RMBR are outlined as follows:

- Higher MLSS levels are prone to inconsistent fluid flows whilst at the same time said fluids deviate from Newtonian behavior. This is based on the read values of "shear effects parameters" m and n.

- High viscosities are associated with high MLSS, thus the likelihood of cake filtration (cake formation) occurring is drastically increased at high TMPs.

- The fouling mechanisms occurring in a RMBR that is operated on MLSS level range of 3.34 to 9.35 g/L under constant TMP ranging from 15 to 58 kPa can be broken down as listed below:

  - Constant TMP of 15 kPa: Pore constriction fouling mechanism is dominant without fail during membrane fouling for all MLSS levels.

  - Constant TMP of 30 kPa: Pore constriction is still a dominant fouling mechanism for all MLSS levels but it is possible for cake filtration to be fairly relevant though occasionally.

  - Constant TMP of 45 kPa: Pore blocking and cake filtration (cake formation by extension) fouling mechanisms both typically dominate fouling but only at high MLSS levels. At low MLSS concentration range of 3.34 – 4.26 g/L, cake formation (or filtration by extension) is seemingly meeker as pore blocking fouling mechanism dominates.

  - Constant TMP of 58 kPa: Even though pore blocking and cake filtration fouling mechanisms still dominate during membrane fouling for all MLSS concentrations, pore constriction is fairly relevant as well. Accordingly, it can be generally said that all three fouling mechanisms are of equally great importance during fouling.

- The SMBR fouling model for constant TMP/varying flux can fit to a good degree external data sources for SMBR units provided the right assumptions are made. Some anomalous or poor fits can be expected at high MLSS in cases where sludge or other high viscous fluid is used.

  The fouling model can additionally give a pretty fair indication of the fouling mechanisms occurring during the filtration process of said external SMBR units though some unpredictability is to be expected. MLSS levels and TMP range are respectively 1 to 12 g/L and 14 to 18 kPa. However, since the same fouling model was able to fit the constructed SMBR rig, TMP range is broaden to 14 to 58 kPa.

- The fouling mechanisms occurring in a SMBR that is operated on MLSS level range of 6.32 to 9.35 g/L under constant TMP ranging from 15 to 58 kPa can be broken down as follows:

  - Constant TMP of 15 kPa: Pore constriction fouling mechanism is dominant during membrane fouling for all MLSS levels.

  - Constant TMP of 30 kPa: Pore constriction and cake filtration (or formation) fouling mechanisms both typically dominate fouling for all MLSS levels.

- Constant TMP of 45 kPa: Pore blocking and cake filtration (cake formation by extension) fouling mechanisms dominate fouling for all MLSS levels. The biological activities taking place at high MLSS are very active, so fits can be expected to be poor or irregular but they can still be fair enough in trend to give good analysis.

- Constant TMP of 58 kPa: All three fouling mechanisms are fairly relevant and can be said to be of equally great importance during fouling for all MLSS levels. The biological activities taking place at high MLSS are very lively; therefore fits can be expected to be irregular though they should still be good enough to give analysis.

For the RMBR system, further steps were taken. First the parameters best fits for the fouling model which were calibrated values obtained from Matlab GA were verified by using additional sets of filtration data at specific MLSS concentration that fell into modelling MLSS level ranges. The fitting calibration curves for RMBR fouling model were remarkably good when compared with their original MLSS concentration range validation curves. This gave validity to the sets of calibrated fitting solutions for the RMBR fouling model.

What was found was that a change in aeration intensity could potentially affect data though often in small amounts (i.e. the MLSS level of 3.89 g/L at constant TMP 15 kPa case), and that permeate restart could potentially affect collected filtration data though not to catastrophic levels. As for the SMP inclusion model, results were generally adequate and findings indicated that bigger MLSS concentrations give rise to bigger cake thicknesses, and with it an increase in SMP levels on the membrane surface is sustained.

This explains why higher MLSS levels give rise to faster total flux decline whilst membrane resistances climb rapidly at the same rate. A constant flux/Varying TMP fouling model was also created for the RMBR to further verify its fouling behaviour. Simulated data were in good agreement with experimentally collected filtration data though with deviations of between 9 to 15% on simulations data observed.

It was found that higher fouling rates are experienced at higher MLSS, thus rapidly increasing TMP. Additionally, two fouling models one of which utilises Taylor's expansion can be used to predict fouling behaviour for sudden rise in TMP. Even though they are both equally as correct, one interpolates TMPs while the other with Taylor's expansion, extrapolates TMP values by 9%. A comparative study between the SMBR and RMBR system was conducted to shed some much needed on light on why RMBRs could be useful.

Analysis showed that whilst the SMBR system incurred increases in fouling rates the RMBR system boasted lower fouling rates. Because of this the SMBR system lost flux in the long run as opposed to the RMBR which could increase flux throughput. And while all the above listed findings may be useful for researchers and/or industry practitioners, the most salient ones are highlighted as follows:

- Even though the slowly rotating spindle of the RPU-185 RMBR induce a weak crossflow shear, it can still even out cake build-up across membrane surface (i.e. like a sweep effect), thus reducing the likelihood of localised critical flux being exceeded, which would lead to dramatic loss of flux.

- The rotational mechanisms in terms of fouling prevention for the RPU-185 RMBR account for only 12% of cake removal, with the rest being mostly accomplished through the air scouring mechanism.

- Although RMBRs have complex rotational processes, the system can be made to describe the singular for better results rather than the plural, which as the only possible alternative can produce catastrophic outcomes.

The first two points in particular are interesting to note as they have good implications. That is to say, RMBR systems produce far more consistent filtration data output even at higher TMPs when compared to SMBR systems. This makes them very efficient systems that are by all accounts viable alternatives to and should be more desirable options than conventional SMBRs. This is because more often than not, reduced fouling is a key need in MBR design, something municipal and industrial WWTPs actively seek for their MBR plants. To address the pricing issue one has to look at the long-term benefits.

While on their initial approach RMBRs are a bit pricy, one has to remember that some of them (the RPU-185 RMBR for instance) utilise cheap and efficient low fouling PVDF membrane material that are robust and easy to clean. What this means is that compared to most conventional SMBRs their maintenance costs are significantly reduced, thus eventually offsetting their initial high capital costs in long term, something municipal and industrial WWTPs need to look into a bit deeper.

As for the last point, in future, once there is better understanding of the rotating processes and researches and designs into this sector broaden; RMBRs may become the systems of first choice, which leads to concluding note knowledge. Knowledge can be as bottomless as a sea of infinite depth even within a single field of research. The more one achieves mastery of “knowledge” in said field the more one realises he or she has not truly learnt much.

That is to say though what is presented here is a substantial amount of information and it is, in the grand scheme of things, it is but a droplet of water that is trying to cleanse a near endless ocean of the unknown that is this yet to be fully explored field of engineering. In the end, only after using, absorbing and wielding this knowledge along with predecessors’ to create new ones to add to the collective can RMBRs truly move forward in the right direction.

8.2. Areas of Future Studies

Although an unprecedented amount of work was uncovered here in this thesis, there are still more studies that could be carried out to advance this field of engineering even further. Future study areas should thus focus on:

i. Whether the forces acting on an activated sludge particle during rotation have a significant effect on the fouling or the shear hydrodynamic regimes: *Absolutely. More RMBRs related this is to further expand understanding of their hydrodynamic regimes and rotational aspects. One of the key steps towards achieving that is the incorporation of this kind of study in RMBR modelling where possible. This could and has the potential to lead to new ways to model fouling in not only RMBRs but MBRs (by of course switching-off the rotating terms) in general as well.*

ii. Whether activated sludge and benchmark models could be created for RMBRs whilst including the shear effects and hydrodynamic regimes: *This has to be done or tried at some point. Again, most activated sludge and benchmark models are studied as is, and even those that are presented for SMBRs only add a couple of additional processes (most prevalent in activated sludge model 3). What needs to be looked at is how to make amendments with these models to allow for RMBRs in order to further expand this area of study.*

iii. Whether model predictive control using these developed RMBR models would enhance efficiency gains within an operational plant: *Using control systems are good and efficient ways to optimise almost any given system, which of course includes all MBRs. The fact that they are mostly utilised in benchmark models for SMBRs and not broadly practiced for other MBR types is a problem, disparity in knowledge. The field of RMBRs could benefit from these types of studies not only from an optimisation stance but also from a fouling mitigation perspective. This could potentially lead to new ways to look at membrane fouling.*

iv. Whether the real measured SMP concentrations could be used to create an even better SMP predictive model that accurately explains fouling behaviour: *Currently what we are lacking in the field of MBRs in general is a true predictive SMP model that can accurately describe fouling phenomena or compute SMP levels. By making one, not only will membrane studies in general benefit from it from a fouling standpoint but it could hypothetically clear over a decade worth of debate that is still on-going about SMP and their involvement in membrane fouling.*

REFERENCES

All cited references that were used during this thesis (including the appendices) are listed in this segment with general style APA Fifth Edition (Number of references: **227**).

Abdel-Kader, A. M. (2013). Studying the efficiency of grey water treatment by using rotating biological contactors system. *Journal of King Saud University - Engineering Sciences, 25*(2), 89–95.

Ahn, Y., Choi, Y., Jeong, H., & Shin, S. (2006). Modeling of extracellular polymeric substances and soluble microbial products production in a submerged MBR at various SRTs. *Water Sci. Technol., 53*, 209–216.

Andersson, H., De Korte, E., & Meland, R. (2001). Flow of a power-law fluid over a rotating disk revisited. *Fluid Dynamics Research, 28*(2), 75-88.

Aquino, S., & Stuckey, D. (2008). Integrated model of the production of soluble microbial products (SMP) and extracellular polymeric substances (EPS) in anaerobic chemostats during transient conditions. *Biochemical Engineering Journal, 38*(2), 138-146.

Ardern, E., & Lockett, W. T. (1914). Experiments on the oxidation of sewage without the aid of filters. *J. Chem. Technol. Biotechnol., 33*, 523–539.

Aubert, M., Elluard, M., & Barnier, H. (1993). Shear stress induced erosion of filtration cake studied by a flat rotating disk method. Determination of the critical shear stress of erosion. *Journal of membrane science, 84*(3).

Avanti Membrane Technology. (2013). *Flexidisks® Ultra Filtration MBR System (Technical Data and Report).*

Bacchin, P., Aimar, P., & Field, R. (2006). Critical and sustainable fluxes: theory, experiments and applications. *Journal of Membrane Science, 28*(1), 42-69.

Baghapour, M. A., Jabbari, E., & Baskaran, K. (2011). Reducing of excess sludge production in wastewater treatment using combined anaerobic/aerobic submerged biological filters. *Iran. J. Environ. Health. Sci. Eng., 8*(3), 207-218.

Baker, K., Hegarty, J., Redmond, B., Reed, N., & Herson, D. (2002). Effect of Oxidizing Disinfectants (Chlorine, Monochloramine, and Ozone) on Helicobacter pylori. *Applied and Environmental Microbiology, 68*(2), 981–984.

Barker, D., & Stuckey, D. (1999). A review of soluble microbial products (SMP) in wastewater treatment. *Water research, 33*(14), 3062-3082.

Basile, A., Cassano, A., & Rastogi, N. (2015). *Advances in Membrane Technologies for Water Treatment: Materials, Processes and Applications.* Elsevier.

Baxter, & Woodman. (2009). *Calculations Used in the Daily Operations of a Wastewater Treatment Facility.*

Benidickson, J. (2011). *The Culture of Flushing: A Social and Legal History of Sewage.* UBC Press.

Bentzen, T., Ratkovich, N., Madsen, S., Jensen, J., Bak, S., & Rasmussen, M. (2012). Analytical and numerical modelling of Newtonian and non-Newtonian liquid in a rotational cross-flow MBR. *Water Science & Technology, 66*(11), 2318-2327.

Bertera, R., Steven, H., & Metcalfe, M. (1984). Development Studies of crossflow microfiltration. *The Chemical Engineer, 401*, 10-14.

Berube, P., & Hall, E. (2001). Fate and removal kinetics of contaminants contained in evaporator condensate during treatment for reuse using a high-temperature membrane bioreactor. *Journal of Pulp and Paper Science, 27*(2), 41-45.

Beychok, M. R. (1967). *Aqueous Wastes from Petroleum and Petrochemical Plants* (1st ed.). John Wiley & Sons Ltd.

Bhattacharjee, C., & Bhattacharya, P. (2006). Ultrafiltration of black liquor using rotating disk membrane module. *Separation and Purification Technology, 49*(3), 281–290.

Bian, R., Yamamoto, K., & Watanabe, Y. (2000). The effect of shear rate on controlling the concentration polarization and membrane fouling. *Desalination, 131* (1–3), 225-236.

Bitton, G. (1997). *Formula Handbook for Environmental Engineers and Scientists.* Wiley-Interscience.

Böhm, L., Drews, A., Prieske, H., Bérubé, P., & Kraume, M. (2012). The importance of fluid dynamics for MBR fouling mitigation. *Bioresource technology, 122*, 50-61.

Bouhabila, E., Aïm, R., & Buisson, H. (1998). Microfiltration of activated sludge using submerged membrane with air bubbling. *Desalination, 118*(1), 315–322.

Bouhabila, E., Aïm, R., & Buisson, H. (2001). Fouling characterisation in membrane bioreactors. *Separation and Purification Technology, 22*, 123-132.

Bouzerar, R., Paullier, P., & Jaffrin, M. (2003). Concentration of mineral suspensions and industrial effluent using a rotating disk dynamic filtration module. *Desalination, 158*(1), 79–85.

Braak, E., Alliet, M., Schetrite, S., & Albasi, C. (2011). Aeration and hydrodynamics in submerged membrane bioreactors. *Journal of Membrane Science, 379*(1-2), 1–18.

Brepols, C. (2010). *Operating Large Scale Membrane Bioreactors for Municipal Wastewater Treatment.* IWA Publishing.

Brou, A., Jaffrin, M., Ding, L., & Courtois, J. (2003). Microfiltration and ultrafiltration of polysaccharides produced by fermentation using a rotating disk dynamic filtration system. *Biotechnology and bioengineering, 82*(4), 429-437.

Buer, T., & Cumin, J. (2010). MBR module design and operation. *Desalination, 250*(3), 1073–1077.

Buisson, H., Cote, P., Praderie, M., & Paillard, H. (1998). The use of immersed membranes for upgrading wastewater treatment plants. ,. *Water Science and Technology, 37*(9), 89-95.

Cabassud, C., Laborie, S., Durand-Bourlier, L., & Laine, J. (2001). Air sparging in ultrafiltration hollow fiber: relationship between flux enhancement, cake characteristics and hydrodynamic parameters. *Journal of Membrane Science, 181*(1), 57–69.

Carlsson, B. (1998). *An introduction to sedimentation theory in wastewater.* Uppsala, Sweden: Systems and Control Group (Uppsala University).

Chang, I.-S., & Judd, S. J. (2002). Air sparging of a submerged MBR for municipal wastewater treatment. *Process Biochemistry, 37*(8), 915–920.

Chang, I.-S., Le-Clech, P., Jefferson, B., & Judd, S. (2002). Membrane Fouling in Membrane Bioreactors for Wastewater Treatment. *Journal of environmental engineering, 128*(11), 1018-1029.

Chaudhary, D., Vigneswaran, S., Ngo, H., Shim, W., & Moon, H. (2003). Biofilter in water and wastewater treatment. *The Korean Journal of Chemical Engeneering, 20*(6), 1054-1065.

Cicek, N. (2003). A review of membrane bioreactors and their potential application in the treatment of agricultural wastewater. *Canadian Biosystems Engineering, 45*, 6.37 - 6.49.

Cicek, N., Franco, J., Suidan, M., Urbain, V., & Manem, J. (1999). Characterization and comparison of a membrane bioreactor and a conventional activated-sludge system in the treatment of wastewater containing high-molecular-weight compounds. *Water Environment Research, 71*(1), 64-70.

Cicek, N., Winnen, H., Suidan, M., Wrenn, B., Urbain, V., & Manem, J. (1998). Effectiveness of the membrane bioreactor in the biodegradation of high molecular weight compounds. *Water Research, 32*(5), 1553-1563.

Copp, J. (2002). *The COST Simulation Benchmark: Description and Simulator Manual.* Office for Official Publications of the European Communities, Luxembourg.

Côté, P., Buisson, H., & Praderie, M. (1998). Immersed membranes activated sludge process applied to the treatment of municipal wastewater. *Water Science and Technology, 38*(4-5), 437-442.

Côté, P., Masini, M., & Mourato, D. (2004). Comparison of membrane options for water reuse and reclamation. *Desalination, 167*, 1–11.

Cui, Z., Chang, S., & Fane, A. (2003). The use of gas bubbling to enhance membrane processes. *Journal of Membrane Science, 221*(1), 1-35.

Davis, R., & Sherwood, J. (1990). A similarity solution for steady state crossflow microfiltration. *Chemical Engineering Science, 45*(11), 3203-3209.

De la Torre, T., Lesjean, B., Drews, A., & Kraume, M. (2008). Monitoring of transparent exopolymer particles (TEP) in a membrane bioreactor (MBR) and correlation with other fouling indicators. *Water Sci. Technol., 58*(10), 1903–1909.

Ding, L., Al-Akoum, O., Abraham, A., & Jaffrin, M. (2002). Milk protein concentration by ultrafiltration with rotating disk modules. *Desalination, 144*(1), 307-311.

Ding, L., Jaffrin, M., Mellal, M., & He, G. (2006). Investigation of performances of a multishaft disk (MSD) system with overlapping ceramic membranes in microfiltration of mineral suspensions. *Journal of membrane science, 276*(1), 232-240.

Doble, M., & Kumar, A. (2005). *Biotreatment of Industrial Effluents.* Butterworth-Heinemann.

Drews, A. (2010). Membrane fouling in membrane bioreactors - characterization, contradiction, causes and cures. *Journal of membrane science, 363*(1), 1–28.

Drews, A., Mante, J., Iversen, V., Vocks, M., Lesjean, B., & Kraume, M. (2007). Impact of ambient conditions on SMP elimination and rejection in MBRs. *Water Research, 41*(17), 3850-3858.

Duclos-Orsello, C., Li, W., & Hob, C.-C. (2006). A three mechanism model to describe fouling of microfiltration membranes. *Journal of Membrane Science, 280*(1-2), 856–866.

Dudley, L., & Darton, E. (1996). Membrane autopsy — a case study. *Desalination, 105*(1–2), 135-141.

Dutta, S., Sarkar, P., Bhattacharjee, C., & Datta, S. (2012). Performance comparison of rotating disk ultrafiltration membrane module, a high shear device with cross-flow module. *International Journal of Environment and Pollution , 49*(3-4), 197 - 209.

Ebrahimi, M., Schmitz, O., Kerker, S., Liebermann, F., & Czermak, P. (2013). Dynamic cross-flow filtration of oilfield produced water by rotating ceramic filter discs. Desalination and Water Treatment. *51*(7-9), 1762-1768.

Engler, J., & Wiesner, M. (2000). Particle fouling of a rotating membrane disk. *Water Research, 34*(2), 557-565.

EPA. (1976). *Process Design Manual for Phosphorus Removal (EPA 625/1-76-001a).* United States Environmental Protection Agency.

EPA. (1989). *Design Manual: Fine Pore (Fine Bubble) Aeration Systems (EPA/625/1-89/023).* United States Environmental Protection Agency.

EPA. (2004). *Primer for Municipal Wastewater Treatment Systems (EPA 832-R-04-001).* United States Environmental Protection Agency.

EPA. (2005). *Membrane Filtration Guidance Manual (EPA 815-R-06-009).* United States Environmental Protection Agency.

Espina, V., Jaffrin, M., Frappart, M., & Ding, L. (2008). Separation of casein micelles from whey proteins by high shear microfiltration of skim milk using rotating ceramic membranes and organic membranes in a rotating disk module. *Journal of Membrane Science, 325*(2), 872-879.

Fane, A. (2002). Membrane bioreactors: design and operational options. *Filtration and Separation, 39*(5), 26-29.

Fenu, A., Guglielmi, G., Jimenez, J., Sperandio, M., Saroj, D., Lesjean, B., et al. (2010). Activated sludge model (ASM) based modelling of membrane bioreactor (MBR)

processes: A critical review with special regard to MBR specificities. *Water research, 44*(15), 4272- 4294.

Field, R. W., & Pearce, G. K. (2011). Critical, sustainable and threshold fluxes for membrane filtration with water industry applications. *Adv Colloid Interface Sci., 164*(1-2), 38-44.

Field, R., Wu, D., Howell, J., & Gupta, B. (1995). Critical flux concept for microfiltration fouling. *Journal of Membrane Science, 100*(3), 259–272.

Fitzgerald, K. S. (2008). *Membrane Bioreactors.* TSG Technologies, Inc.

Frappart, M., Jaffrin, M., & Ding, L. (2008). Reverse osmosis of diluted skim milk: comparison of results obtained from vibratory and rotating disk modules. *Separation and Purification Technology, 60*(3), 321–329.

Futselaar, H., Schonewille, H., Vente, D. d., & Broens, L. (2007). NORIT AirLift MBR: side-stream system for municipal waste water treatment. *Desalination, 204*(1-3), 1-7.

Gernaey, K., van Loosdrecht, M., Henze, M., Lind, M., & Jørgensen, S. (2004). Activated sludge wastewater treatment plant modelling and simulation: state of the art. *Environmental Modelling & Software, 19*(9), 763–783.

Giraldo, E., & LeChevallier, M. (2006). Dynamic mathematical modeling of membrane fouling in submerged membrane bioreactors. "Proceedings of Water Environment Foundation, WEFTEC". 4895-4913.

Gkotsis, P. K., Banti, D. C., Peleka, E. N., Zouboulis, A. I., & Samaras, P. E. (2014). Fouling Issues in Membrane Bioreactors (MBRs) for Wastewater Treatment: Major Mechanisms, Prevention and Control Strategies. *Processes, 2*, 795-86.

Green, G., & Belfort, G. (1980). Fouling of ultrafiltration membranes: lateral migration and the particle trajectory model. *Desalination, 35*, 129-147.

Guglielmi, G., Saroj, D., Chiarani, D., & Andreottola, G. (2007). Sub-critical fouling in a membrane bioreactor for municipal wastewater treatment: experimental investigation and mathematical modelling. *Water research, 41*(17), 3903-3914.

Guibert, D., Aim, R., Rabie, H., & Cote, P. (2002). Aeration performance of immersed hollow-fiber membranes in a bentonite suspension. *Desalination , 148*(1), 395-400.

Günder, B., & Krauth, K. (1998). Replacement of secondary clarification by membrane separation – results with plate and hollow fibre modules. *Water Science and Technology, 38*(4-5), 383-393.

Gupta, N., Jana, N., & Majumder, C. (2008). Submerged membrane bioreactor system for municipal wastewater treatment process: an overview. *Indian Journal of Chemical Technology, 15*(6), 604-613.

Gutowski, W. M. (2005). *Biology, Physics, Small Worlds and Genetic Algorithms (in Leading Edge Computer Science Research: chap 6, pp. 165-218).* Nova Science Publishers, Inc.

Hai, F., & Yamamoto, K. (2011). *Membrane Biological Reactors. In P. Wilderer (Eds.), Treatise on Water Science.* UK: Elsevier.

Hammer, M. J. (1975). *Water and Wastewater Technology.* John Wiley & Sons.

He, G., Ding, L., Paullier, P., & Jaffrin, M. (2007). Experimental study of a dynamic filtration system with overlapping ceramic membranes and non-permeating disks rotating at independent speeds. *Journal of Membrane Science, 300*(1), 63-70.

Henze, M., Grady Jr, C., Gujer, W., Marais, G., & Matsuo, T. (1987). *Activated Sludge model no. 1. IAWQ Scientific and Technical Report No. 1 .* London, United Kingdom: IAWQ.

Henze, M., van Loosdrecht, M. C., Ekama, G., & Brdjanovic, D. (2008). *Biological wastewater treatment: principles, modelling and design.* IWA Publishing.

Hermia, J. (1982). Constant pressure blocking filtration law: application to power law non-Newtonian fluids. *Trans. Inst. Chem. Eng, 60*, 183-187.

Ho, C., & Zydney, A. (2000). A combined pore blockage and cake filtration model for protein fouling during microfiltration. *J. Colloid Interface Sci., 232*, 389–399.

Ho, C., & Zydney, A. (2002). Transmembrane pressure profiles during constant flux microfiltration of bovine serum albumin. *Journal of Membrane Science, 209*(2), 363-377.

Holdich, R. (2002). *Fundamentals of Particle Technology ("Filtration of Liquids").* Nottingham, UK: Midland Information Technology & Publishing.

Holenda, B., Domokos, E., Redey, A., & Fazakas, J. (2008). Dissolved oxygen control of the activated sludge wastewater treatment process using model predictive control. *Computers and Chemical Engineering, 32*(6), 1270–1278.

Hou, Y.-p., Peng, D.-c., Wang, B.-b., Zhang, X.-y., & Xue, X.-d. (2014). Effects of stirring strategies on the sludge granulation in anaerobic CSTR reactor. *Desalination and Water Treatment, 52*, 6348–6355.

Hwang, B., Lee, W., Yeon, K., Park, P., Lee, C., Chang, I., et al. (2008). Correlating TMP increases with microbial characteristics in the biocake on the membrane surface in a membrane bioreactor. *Environ. Sci. Technol., 42*, 3963-3968.

Imasaka, T., Kanekuni, N., So, H., & Yoshino, S. (1989). Cross-flow filtration of methane fermentation broth by ceramic membranes. *Journal of Fermentation and Bioengineering, 68*, 200-206.

Jaffrin, M. (2008). Dynamic shear-enhanced membrane filtration: A review of rotating disks, rotating membranes and vibrating systems. *Journal of Membrane Science , 324*(1), 7–25.

Jaffrin, M., Ding, L., Akoum, O., & Brou, A. (2004). A Hydrodynamic Comparison Between Rotating Disk and Vibratory Dynamic Filtration Systems. *Journal of Membrane Science, 242*(1-2), 155–167.

Janocha, H. (1999). *Adaptronics and Smart Structures: Basics, Materials, Design, and Applications* (2 ed.). Springer-Verlag Berlin Heidelberg.

Janus, T., & Ulanicki, B. (2010). Modelling SMP and EPS formation and degradation kinetics with an extended ASM3 model. *Desalination, 261*(1), 117–125.

Jefferson, B., Laine, A., Judd, S., & Stephenson, T. (2000). Membrane bioreactors and their role in wastewater reuse. *Water Science and Technology, 41*(1), 197-204.

Jeppsson, U. (1996). *Modelling aspects of wastewater treatment processes.* Lund University, Industrial Electrical Engineering and Automation (IEA), Lund Institute of Technology (LTH). IEA, LTH, Box 118, SE-221 00 Lund, Sweden.

Ji, J., Liu, F., Hashim, N. A., Abed, M. M., & Li, K. (2015). Poly(vinylidene fluoride) (PVDF) Membranes for Fluid Separation. *Reactive and Functional Polymers, 86*, 134–153.

Ji, P., Motin, A., Shan, W., Bénard, A., Bruening, M., & Tarabara, V. (2016). 2016. Dynamic crossflow filtration with a rotating tubular membrane: Using centripetal force to decrease fouling by buoyant particles. *Chemical Engineering Research and Design, 106*, 101-114.

Jiang, T. (2007). *Characterization and Modelling of Soluble Microbial Products in Membrane Bioreactors .* PhD Thesis, University of Ghent, Belgium.

Jiang, T., Myngheer, S., De Pauw, D., Spanjers, H., Nopens, I., Kennedy, M., et al. (2008). Modelling the production and degradation of soluble microbial products (SMP) in membrane bioreactors (MBR). *Water Research, 42*(20), 4955-4964.

Jiang, T., Zhang, H., Yang, F., Gao, D., & Du, H. (2013). Relationships between mechanically induced hydrodynamics and membrane fouling in a novel rotating membrane bioreactor. *Desalination and Water Treatment, 51*(13-15), 2850-2861.

Jørgensen, M., Pedersen, M., Christensen, M., & Bentzen, T. (2014). Dependence of shear and concentration on fouling in a membrane bioreactor with rotating membrane discs. *AIChE Journal, 60*(2), 706-715.

Judd, S. (2006). *The MBR Book: Principles and Applications of Membrane Bioreactors for Water and Wastewater Treatment* (1st ed.). Amsterdam: Elsevier.

Judd, S. (2011). *The MBR Book: principles and applications of membrane bioreactors in water and wastewater treatment* (2nd ed.). Oxford, United Kingdom: Elsevier science & technology.

Kawai, H. (1969). The Piezoelectricity of Poly (vinylidene Fluoride). *Japanese Journal of Applied Physics, 8*(7), 975.

Kedem, O., & Katchalsky, A. (1958). Thermodynamic analysis of the permeability of biological membranes to non-electrolytes. *Biochimica et Biophysica Acta, 27*, 229-246.

Kimura, S. (1991). Japan's aqua renaissance '90 project. *Water Science and Technology, 23*(7-9), 1573-1582.

Koros, W., Ma, Y., & Shimidzu, T. (1996). Terminology for membranes and membrane processes (IUPAC Recommendations 1996). *Pure and Applied Chemistry, 68*(7), 1479–1489.

Kothandaraman, V., & Evans, R. (1972). *Removal of Algae from Waste Stabilization Pond Effluents - A State of the Art.* Illinois State Water Survey.

Kroner, K., & Nissinen, V. (1988). Dynamic filtration of microbial suspensions using an axially rotating filter. *Journal of Membrane Science, 36*, 85-100.

Laera, G., Giordano, C., Pollice, A., Saturno, D., & Mininni, G. (2007). Membrane bioreactor sludge rheology at different solid retention times. *Water Research, 41*(18), 4197-4203.

Laspidou, C., & Rittmann, B. (2002). A unified theory for EPS, SMPs, and active and inert biomass. *Water Research, 36*(11), 2711-2720.

Latimer, R., Pitt, P., Hocking, C., Williams, P., Suwanarpa, K., & Shukla, O. (2008). Advanced BioWin Modeling for MBR Process Design Optimization: A Case Study of a Split

Conventional/MBR Design. *Proceedings of the Water Environment Federation, WEFTEC 2008: Session 81 through Session 90*, *2008(9)*, pp. 6491-6499.

Le-Clech, P., Chen, V., & Fane, T. (2006). Fouling in membrane bioreactors used in wastewater treatment. *Journal of membrane science, 284*(1-2), 17-53.

Le-Clech, P., Jefferson, B., & Judd, S. J. (2005). A comparison of submerged and sidestream tubular membrane bioreactor configurations. *Desalination, 173*(2), 113-122.

Le-Clech, P., Jefferson, B., Chang, I., & Judd, S. (2003). Critical flux determination by the flux-step method in a submerged membrane bioreactor. *J. Membr. Sci., 227*, 81–93.

Lee, S. A., Fane, A. G., Amal, R., & Waite, T. D. (2003). The effect of floc size and structure on specific cake resistance and compressibility in dead-end microfiltration. *Separation Science and Technology, 38*(4), 869-887.

Lee, S., & Gagnon, G. (2015). The rate and efficiency of iron generation in an electrocoagulation system. *Environmental Technology*, 1-9.

Leitea, J., Fernandesa, B., Pozzia, E., Barbozab, M., & Zaiata, M. (2008). Application of an anaerobic packed-bed bioreactor for the production of hydrogen and organic acid. *International journal of Hydrogen Energy, 33* , 579 – 586.

Léonard, D., Mercier-Bonin, M., Lindley, N., & Lafforgue, C. (1998). Novel Membrane Bioreactor with Gas/Liquid Two-Phase Flow for High-Performance Degradation of Phenol. *Biotechnology Progress , 14*(5), 680-688.

Lesjean, B., Rosenberger, S., Schrotter, J., & Recherche, A. (2004). Membrane-aided biological wastewater treatment - an overview of applied systems. *Membrane Technology , 2004*(8), 5-10.

Li, M., Lu, J., Heijman, B., & Rietveld, L. (2012). *Effect of cake layer characteristics on fouling control in long time filtration without backwash for submerged ceramic MF membrane in surface water treatment.* Delft University of Technology, Delft, The Netherlands.

Li, N. N., Fane, A. G., Ho, W. S., & Matsuura, T. (2008). *Advanced Membrane Technology and Applications.* Wiley-Blackwell.

Liang, S., Liu, C., & Song, L. (2007). Soluble microbial products in membrane bioreactor operation: behaviors, characteristics, and fouling potential. *Water Research, 41*(1), 95-101.

Liang, S., Song, L., Tao, G., Kekre, K., & Seah, H. (2006). A modeling study of fouling development in membrane bioreactors for wastewater treatment. *Water Environ. Res., 78*(8), 857–863.

Liebermann, F. (2010). Dynamic cross flow filtration with Novoflow's single shaft disk filters. *Desalination, 250*(3), 1087-1090.

Lin, H., Xie, K., Mahendran, B., Bagley, D., Leung, K., Liss, S., et al. (2009a). Sludge properties and their effects on membrane fouling in submerged anaerobic membrane bioreactors (SAnMBRs). *Water Research, 43*(15), 3827–3837.

Lin, Y., Tay, J., Liu, Y., & Hung, Y. (2009b). *Biological Nitrification and Denitrification Processes. In Biological treatment processes* (Vol. 8). Humana Press.

Lindberg, C. F., & Carlsson, B. (1996). Nonlinear and set-point control of the dissolved oxygen concentration in an activated sludge process. *Water Science and Technology, 34*(3-4), 135–142.

Listiarini, K., Sun, D., & Leckie, J. (2009). Organic fouling of nanofiltration membranes: Evaluating the effects of humic acid, calcium, alum coagulant and their combinations on the specific cake resistance. *Journal of Membrane Science, 332*(1-2), 56-62.

Liu, L., Gao, B., Liu, J., & Yang, F. (2012). Rotating a helical membrane for turbulence enhancement and fouling reduction. *Chemical Engineering Journal, 181*, 486-493.

Lu, S., Imai, T., Ukita, M., Sekine, M., Higuchi, T., & Fukagawa, M. (2001). A model for membrane bioreactor process based on the concept of formation and degradation of soluble microbial products. *Water Research, 35*(8), 2038-2048.

Luo, J., Ding, L., Wan, Y., Paullier, P., & Jaffrin, M. (2010). Application of NF-RDM (nanofiltration rotating disk membrane) module under extreme hydraulic conditions for the treatment of dairy wastewater. *Chemical Engineering Journal, 163*(3), 307-316.

Luo, J., Zhu, Z., Ding, L., Bals, O., Wan, Y., Jaffrin, M., et al. (2013). Flux behavior in clarification of chicory juice by high-shear membrane filtration: evidence for threshold flux. *Journal of membrane science, 435*, 120-129.

Makowska, M., Spychała, M., & Mazur, R. (2013). Removal of Carbon and Nitrogen Compounds in Hybrid Bioreactors, Biomass Now - Cultivation and Utilization. *InTech*.

Manem, J., & Sanderson, R. D. (1996). *Membrane bioreactors. In Mallevialle, J., Odendaal, P.E. and Wiesner, M.R. (eds.) Water Treatment Membrane Processes.* New York: McGraw Hill.

Marcucci, M., Nosenzo, G., Capannelli, G., Ciabatti, I., Corrieri, D., & Ciardelli, G. (2001). Treatment and reuse of textile effluents based on new ultra filtration and other membrane technologies. *Desalination, 138*(1), 75-82.

Meijer, S., Van Loosdrecht, M., & Heijnen, J. (2001). Metabolic modelling of full-scale biological nitrogen and phosphorus removing WWTP's. *Water Research, 35*(11), 2711–2723.

Meng, F., Zhang, H., Li, Y., Zhang, X., & Yang, F. (2005). Application of fractal permeation model to investigate membrane fouling in membrane bioreactor. *Journal of Membrane Science, 262*, 107–116.

Mercier, M., Fonade, C., & Lafforgue-Delorme, C. (1997). How slug flow can enhance the ultrafiltration flux in mineral tubular membranes. *Journal of Membrane Science, 128*(1), 103-113.

Metcalf, & Eddy. (1972). *Wastewater Engineering: Collection, Treatment, Disposal* (1st ed.). McGraw-Hill.

Metcalf, & Eddy. (1991). *Wastewater Engineering: Treatment, Disposal, Reuse* (3rd ed.). (G. Tchobanoglous, & F. L. Burton, Eds.) New York: McGraw-Hill.

Metcalf, & Eddy. (2003). *Wastewater Engineering: Treatment, Disposal, Reuse* (4th ed.). (G. Tchobanoglous, & F. L. Burton, Eds.) New York: McGraw-Hill.

Meyer, P., Mayer, A., & Kulozik, U. (2015). High concentration of skim milk proteins by ultrafiltration: characterisation of a dynamic membrane system with a rotating membrane in comparison with a spiral wound membrane. *International Dairy Journal, 51*, 75-83.

Mulder, J. (1996). *Basic Principles of Membrane Technology* (2nd ed.). Springer.

Muller, E., Stouthamer, A., van Verseveld, H., & Eikelboom, D. (1995). Aerobic domestic wastewater treatment in a pilot plant with complete sludge retention by crossflow filtration. *Water Research, 29*(4), 1179-1189.

Murkes, J., & Carlsson, C. (1988). *Crossflow filtration: Theory and practice.* John Wiley & Sons.

Nagaoka, H., Ueda, S., & Miya, A. (1996). Influence of bacterial extracellular polymers on the membrane separation activated sludge process. *Water Science and Technology, 34* (9), 165–172.

Namkung, E., & Rittmann, B. (1986). Soluble microbial products (SMP) formation kinetics by biofilms. *Water Research, 20*(6), 795-806.

Nasr, M., Moustafa, M., Seif, H., & El Kobrosy, G. (2011). Modelling and simulation of German BIOGEST/EL-AGAMY wastewater treatment plants – Egypt using GPS-X simulator. *Alexandria Engineering Journal, 50*(4), 351–357.

NESC. (2003). Explaining the Activated Sludge Process. *Pipeline (National Environmental Services Center), 14*(2).

Nghiem, L., & Schäfer, A. (2006). Fouling autopsy of hollow-fibre MF membranes in wastewater reclamation. *Desalination, 188*(1-3), 113-121.

Nopens, I., Capalozza, C., & Vanrolleghem, P. (2001). *Stability analysis of a synthetic municipal Wastewater.* BIOMETRICS AND PROCESS CONTROL, BIOMATH, Universiteit Gent.

OECD. (1992). *Guideline For The Testing Of Chemicals: Adopted by the Council.*

Olsson, G., & Newell, B. (1999). *Wastewater treatment systems : Modelling, Diagnosis and Control.* London, UK: IWA Publishing.

Parr, J., Smith, M., & Shaw, R. (2002). Technical brief no. 64 : wastewater treatment options. *Waterlines: journal of appropriate water supply and sanitation technologies, 21*(1), 15-18.

Patsios, S., & Karabelas, A. (2010). A review of modeling bioprocesses in membrane bioreactors (MBR) with emphasis on membrane fouling predictions. *Desalination and Water Treatment, 21*(1-3), 189–201.

Paul, P. (2013). Development and Testing of a Fully Adaptable Membrane Bioreactor Fouling Model for a Sidestream Configuration System. *Membranes 2013, 3*, 24-43.

Paul, P., & Jones, F. A. (2015). Development of a Comprehensive Fouling Model for a Novel Rotating Membrane Bioreactor System. *Water, 7*(2), 377-397.

Paul, P., & Jones, F. A. (2016). Advanced Wastewater Treatment Engineering – Investigating Membrane Fouling in both Rotational and Static Membrane Bioreactor Systems Using Empirical Modelling. *Int. J. Environ. Res. Public Health, 13*(1), 100.

Petersen, B. (2000). *Calibration, identifiability and optimal experimental design of activated sludge models.* PhD Thesis, Ghent University.

Petersen, B., Vanrolleghem, P., Gernaey, K., & Henze, M. (2002). Evaluation of an ASM1 model calibration procedure on a municipal–industrial wastewater treatment plant. *Journal of Hydroinformatics, 4*(1), 15–38.

Pinnekamp, J., & Friedrich, H. (2006). *Municipal water and waste management (Volume 2): Membrane technology for wastewate treatment.* Aachen: FIW Verlag.

Porter, M. (1972). Concentration Polarization with Membrane Ultrafiltration. *Industrial & Engineering Chemistry Product Research and Development, 11*(3), 234-248.

Pulefou, T., Jegatheesan, V., Steicke, C., & Kim, S. (2008). Application of submerged membrane bioreactor for aquaculture effluent reuse. *Desalination , 221*(1), 534-542.

Radjenovic, J., Matosic, M., Mijatovic, I., Petrovic, M., & Barceló, D. (2008). *Membrane Bioreactor (MBR) as an Advanced wastewater treatment technology. In Handbook of Environmental Chemistry, Emerging Contaminants from Industrial and Municipal Waste: Removal Technologies* (Vol. 5 S/2). Springer Berlin Heidelberg.

Ramesh, A., Lee, D., & Hong, S. (2006). Soluble microbial products (SMP) and soluble extracellular polymeric substances (EPS) fromwastewater sludge. *Applied microbiology and biotechnology, 73*(1), 219-225.

Ratkovich, N., & Bentzen, T. (2013). Comparison of four types of membrane bioreactor systems in terms of shear stress over the membrane surface using computational fluid dynamics. *Water Science and Technology, 68*(12), 2534-2544.

Ratkovich, N., Horn, W., Helmus, F., Rosenberger, S., Naessens, W., Nopens, I., et al. (2013). Activated Sludge Rheology: A critical review on data collection and modelling. *Water Res., 47*, 463–482.

Reed, B., Viadero Jr, R., Young, J., & Lin, W. (1997). Treatment of oily wastes using high-shear rotary ultrafiltration. *Journal of Environmental Engineering, 123*(12), 1234-1242.

Rosenberger, S., & Kraume, M. (2002). Filterability of activated sludge in membrane bioreactors. *Desalination, 146*, 373-379.

Rosenberger, S., Helmus, F., Krause, S., Bareth, A., & Meyer-Blumenroth, U. (2011). Principles of an enhanced MBR-process with mechanical cleaning. *Water Science & Technology, 64*(10), 1951-1958.

Rosenberger, S., Kubin, K., & Kraume, M. (2002). Rheology of activated sludge in membrane bioreactors. *Engineering in life sciences, 2*(9), 269-275.

Rosenberger, S., Laabs, C., Lesjean, B., Gnirss, R., Amy, G., Jekel, M., et al. (2006). Impact of colloidal and soluble organic material on membrane performance in membrane bioreactors for municipal wastewater treatment. *Water Research, 40*(4), 710-720.

Sarkar, D., & Bhattacharjee, C. (2008). Modeling and analytical simulation of rotating disk ultra filtration module. *Journal of Membrane Science, 320*(1), 344-355.

Sarkar, D., Datta, D., Sen, D., & Bhattacharjee, C. (2011). Simulation of continuous stirred rotating disk-membrane module: An approach based on surface renewal theory. *Chemical engineering science, 66*(12), 2554–2567.

Schuler, S. (2009). *Operating Experience with Rotating Membrane Bioreactors in MEMBRANES a Supplement to WaterWorld.* PennWell Corporation/Huber Technology.

Serra, C., & Wiesner, M. (2000). A comparison of rotating and stationary membrane disk filters using computational fluid dynamics. *Journal of Membrane Science, 165*(1), 19-29.

Serra, C., Wiesner, M., & La□né, J. (1999). Rotating membrane disk filters: design evaluation using computational fluid dynamics. *Chemical Engineering Journal , 72*(1), 1-17.

Seyssiecq, I., Ferrasse, J.-H., & Roche, N. (2003). State-of-the-art: rheological characterization of wastewater treatment sludge, Biochemical Engineering Journal . *16*(1).

Shim, S. N., Kim, S.-R., Jo, S. J., Yeon, K.-M., & Lee, C.-H. (2015). Evaluation of mechanical membrane cleaning with moving beads in MBR using Box–Behnken response surface methodology. *Desalination and Water Treatment , 56*(11).

Shimizu, Y., Rokudai, M., Thoya, S., Tanaka, H., & Eghchi, K. (1990). Effect of membrane resistance on filtration characteristics for methanogenic wastes. *Kakaku Kogaku Ronbunshu, 16*, 145.

Shin, H., & Kang, S. (2003). Characteristics and fates of soluble microbial products in ceramic membrane bioreactor at various sludge retention times. *Water Research, 37*(1), 121-127.

Smith Jr, C. V., Di Gregorio, D., & Talcott, R. M. (1969). The Use of Ultrafiltration Membranes for Activated Sludge Separation. Proceedings of the 24th Industrial waste Conference, Purdue Uni., Indiana, USA.

Steffe, J. (1996). *Rheological Methods in Food Process Engineering* (2nd ed.). Freeman Press.

Stenstrom, M. K., & Rosso, D. (2010). *Aeration.* University of California.

Stephenson, T., Brindle, K., Judd, S., & Jefferson, B. (2000). *Membrane Bioreactors for Wastewater Treatment.* London, United Kingdom: IWA.

Subramanian, S., Kumar, N., Murthy, S., & Novak, J. (2007). Effect of anaerobic digestion and anaerobic/aerobic digestion processes on sludge dewatering. *Journal of Residuals Science and Technology, 4*(1), 17-23.

Sun, F., Wang, X., & Li, X. (2011). Effect of biopolymer clusters on the fouling propertyof sludge from a membrane bioreactor (MBR) and its control by ozonation. *Process Biochemistry, 46*(1), 162–167.

Sustarsic, M. (2009). Wastewater Treatment: Understanding the Activated Sludge Process. *Chemical engineering progress, 105*(11), 26-29.

Sutton, P. (2006). Membrane bioreactors for industrial wastewater treatment: Applicability and selection of optimal system configuration. *Proceedings of the Water Environment Federation (WEF)*, *2006(9)*, pp. 3233-3248.

Sutton, P. M., Li, A., Evans, R. R., & Korchin, S. R. (1983). Dorr-Oliver Fixed Film and Suspended Growth Anaerobic Systems for Industrial Wastewater Treatment and Energy Recovery. (pp. 667-675). Proceedings of the 37th Industrial Waste Conference, Purdue Uni., Indiana, USA.

Tarabaraa, V., Koyuncub, I., & Wiesner, M. R. (2004). Effect of hydrodynamics and solution ionic strength on permeate flux in cross-flow filtration: direct experimental observation of filter cake cross-sections. *Journal of Membrane Science, 241*(1), 65-78.

TEA. (1995). *Water Quality, Chapter 2, Toxics in Texas wastewater discharges.* Texas Environmental Almanac.

Templeton, M. R., & Butler, D. (2011). *Introduction to Wastewater Treatment.* Ventus Publishing ApS.

Tiller, R. (1953). The role of porosity in filtration. *Chem. Eng. Prog., 49*(9), 467-479.

Tolkou, A., Zouboulis, A., & Samaras, P. (2014). The Incorporation of Ceramic Membranes in MBR Systems for Wastewater Treatment: Advantages and Patented New Developments. *Recent Patents on Engineering, 8* (1), 1-9.

Torras, C., Pallarès, J., Garcia-Valls, R., & Jaffrin, M. (2006). CFD simulation of a rotating disk flat membrane module. *Desalination, 200*(1), 453–455.

Torres, M.P., López, J.C., & Chaparro, T.R. (2013). Removal of organic matter and toxicity in an upflow immobilized biomass anaerobic reactor treatin. *Dyna rev.fac.nac.minas, 80*(182), 124-130.

Tu, Z., & Ding, L. (2010). Microfiltration of mineral suspensions using a MSD module with rotating ceramic and polymeric membranes. Separation and Purification Technology. *73*(3), 363-370.

Ueda, T., Hata, K., Kikuoka, Y., & Seino, O. (1997). Effects of aeration on suction pressure in a submerged membrane bioreactor. *Water Research, 31*(3), 489-494.

Urbain, V., Mobarry, B., De Silva, V., Stahl, D., Rittmann, B., & Manem, J. (1998). Integration of performance, molecular biology and modeling to describe the activated sludge process. *Water Science and Technology, 37*(4), 223-229.

van Veldhuizen, H., van Loosdrecht, M., & Heijnen, J. (1999). Modelling biological phosphorus and nitrogen removal in a full scale activated sludge process. *Water Res., 33*, 3459–3468.

Vanrolleghem, P., Insel, G., Petersen, B., Sin, G., De Pauw, D., Nopens, I., et al. (2003). A comprehensive model calibration procedure for activated sludge models. *Proceedings of the Water Environment Federation*, *2003(9)*, pp. 210-237.

Viessman Jr, W., Hammer, M. J., Perez, E. M., & Chadik, P. A. (2008). *Water Supply and Pollution Control* (8th ed.). Prentice Hall.

Visvanathan, C., Aim, R., & Parameshwaran, K. (2000). Membrane separation bioreactors for wastewater treatment. *Critical Reviews in Environmental Science and Technology, 30*(1), 1-48.

von Sperling, M. (2007). *Activated Sludge and Aerobic Biofilm Reactors* (Vol. 5). IWA Publications.

Wang, X., Li, X., & Huang, X. (2007). Membrane fouling in a submerged membrane bioreactor (SMBR): characterisation of the sludge cake and its high filtration resistance. *Separation and Purification Technology, 52*(3), 439–445.

Ward, B. (1996). Nitrification and Denitrification: Probing the Nitrogen Cycle in Aquatic Environments. *Microbial Ecology, 32*(3), 247-261.

Wilén, B.-M., & Balmér, P. (1999). The effect of dissolved oxygen concentration on the structure, size and size distribution of activated sludge flocs. *Water Research, 33*(2), 391–400.

Wintgens, T., Rosen, J., Melin, T., Brepols, C., Drensla, K., & Engelhardt, N. (2003). Modelling of a membrane bioreactor system for municipal wastewater treatment. *J. Membr. Sci., 216*(1-2), 55-65.

Wu, G., Cui, L., & Xu, Y. (2008). A novel submerged rotating membrane bioreactor and reversible membrane fouling control. *Desalination, 228*(1), 255-262.

Wu, J., Chen, F., Huang, X., Geng, W., & Wen, X. (2006). Using inorganic coagulants to control membrane fouling in a submerged membrane bioreactor. *Desalination ., 197*(1), 124-136.

Wu, Z., Wang, Z., Zhou, Z., Yu, G., & Gu, G. (2007). Sludge rheological and physiological characteristics in a pilot-scale submerged membrane bioreactor. *Desalination, 212*(1-3), 152-164.

Xu, N., Xing, W., Xu, N., & Shi, J. (2002). Preliminary Study on Airlift Membrane-Bioreactor . *Chinese Journal of Chemical Engineering, 10*(3), 347-348.

Yamamoto, K., Hiasa, M., Mahmood, T., & Matsuo, T. (1989). Direct solid-liquid separation using hollow fiber membrane in an activated sludge aeration tank. *Water Science and Technology, 21*(4-5), 43-54.

Yang, F., Bick, A., Shandalov, S., Brenner, A., & Oron, G. (2009). Yield stress and rheological characteristics of activated sludge in an airlift membrane bioreactor. *J. Membr. Sci, 334*, 83–90.

Ye, Y., Chen, V., & Fane, A. (2006). Modeling long-term subcritical filtration of model EPS solutions. *Desalination, 191*(1), 318-327.

Yoon, S., Lee, C., Kim, K., & Fane, A. (1999). Three-dimensional simulation of the deposition of multi-dispersed charged particles and prediction of resulting flux during cross-flow microfiltration. *Journal of Membrane Science, 161*(1-2), 7-20.

Yoon, S.-H. (2015). *Membrane Bioreactor Processes: Principles and Applications.* CRC Press.

Yuan, W., Kocic, A., & Zydney, A. L. (2002). Analysis of humic acid fouling during microfiltration using a pore blockage–cake filtration model. *Journal of Membrane Science, 198*, 51–62.

Zeng, M., Soric, A., & Roche, N. (2013). Calibration of hydrodynamic behavior and biokinetics for TOC removal modeling in biofilm reactors under different hydraulic conditions. *Bioresource Technology, 144*, 202–209.

Zhang, J., Chua, H., Zhou, J., & Fane, A. (2006). Factors affecting the membrane performance in submerged membrane bioreactors. *Journal of Membrane Science, 284*, 54-66.

Zhang, Y., Love, N., & Edwards, M. (2009). Nitrification in Drinking Water Systems. *Critical Reviews in Environmental Science and Technology, 39*(3), 153-208.

Zhu, T., Xie, Y. H., Jiang, J., Wang, Y. T., Zhang, H. J., & Nozaki., T. (2009). Comparative study of polyvinylidene fluoride and PES flat membranes in submerged MBRs to treat domestic wastewater. *59*(3), 399-405.

Zhu, Z., Mhemdi, H., Zhang, W., Ding, L., Bals, O., Jaffrin, M., et al. (2016). Rotating Disk-Assisted Cross-Flow Ultrafiltration of Sugar Beet Juice. *Food and Bioprocess Technology, 9*(3), 493-500.

Zsirai, T., Qiblawey, H., A-Marri, M., & Judd, S. (2016). The impact of mechanical shear on membrane flux and energy demand. *Journal of Membrane Science, 516*, 56–63.

Zuo, D.-Y., Li, H.-J., Liu, H.-T., & Wu, G.-P. (2010). A study on submerged rotating MBR for wastewater treatment and membrane cleaning. *Korean Journal of Chemical Engineering, 27*(3), 881-885.

Zuthi, M., Ngo, H., & Guo, W. (2012). Modelling bioprocesses and membrane fouling in membrane bioreactor (MBR): A review towards finding an integrated model framework. *Bioresource Technology, 122*, 119–129.

APPENDICES

This section depicts all the appendices or extras that were not included in the text proper of this thesis. It is divided into six main sub-sections as follows:

i. *APPENDIX A*: The time management for this PhD research work is shown here and only covers key tasks that were undertaken. This sub-section is part of **Chapter 1 sub-section 1.7**.

ii. *APPENDIX B*: Various pictures pertaining to both MBR rigs (RMBR and SMBR) are shown here. This sub-section concerns itself with **Chapter 3 sub-section 3.1.1 and 3.1.2**.

iii. *APPENDIX C*: This sub-section contains various experimental information; hazard of chemicals used in synthetic wastewater and safety, sludge handling, safety and collection protocol, some Camlab collected data and F/M, information on viscosity, and simulations' constant parameters used to procure the Coors UK and Duclos-Orsello et al. 2006 curves. This sub-section is part of **Chapter 3 sub-section 3.2.1, 3.2.3, 3.2.6, 3.2.9 and 3.3**.

iv. *APPENDIX D*: Mainly for **Chapter 4 sub-section 4.1.2, 4.2.1 and 4.2.3**, this sub-section presents an alternative fouling model (constant TMP/varying flux mode) derived for the SMBR, Matlab m-codes used for the implemented MBR fouling models (RMBR and SMBR), the optimisation of simulations' final values for α_v and δ' and the simplified GA factors results from adjustments made along with least squared residuals.

v. *APPENDIX E*: This sub-section concerns itself with **Chapter 5 sub-section 5.2.1 and 5.2.2, and Chapter 6 sub-section 6.2**. The discussion graphs that are not present in these chapters are shown here (verification curves and TMP steps curves for RMBR and TMP steps curves for SMBR).

vi. *APPENDIX F*: Dealing with **Chapter 7 sub-section 7.1 and 7.2**, this sub-section contains additional pictures regarding the caking formed on the RMBR and SMBR membranes (comparative purposes), cake compressibility test for the RMBR, a small section that briefly talks about membrane autopsy, and activated sludge flocs pictures taken under 40 and 100 times magnification as well as some general microscopy experimental information.

In this whole section, concerned tables and figures are denoted, first by a prefix AP (=APPENDIX), followed by a suffix denoted by the APPENDIX sub-section letter and figure number (e.g. AP.B.1).

APPENDIX A

Table AP.A.1. Time management for this research work with key tasks along with their respective time-scale shown

Main tasks undertaken	Description	Completion time (expected)
Year 1		
Familiarisation with MBR field + Initial Literature Review + Setting-up of RMBR and Water Laboratory	Trying to familiarise with water techniques, MBRs in general and conducting a general literature review for topic while waiting for the RMBR unit to arrive; set-up the pilot unit as per manufacturer instructions and getting the water laboratory ready for future tests	July 2013 – January 2014
Membrane Resistance Tests + Conference: 15th National Young Water Professionals Conference, Manchester	Carry out membrane resistance tests; collect initial activated sludge in small quantity just for this conference; make necessary preparations including writing conference paper	February 2014 – End April 2014
Recollection of Activated Sludge to Grow MLSS + Collection of Data for RMBR + Writing of 1st Journal Paper	Start the real activated sludge maintenance; production of synthetic wastewater as needed including initial tests; start collecting filtration data from RMBR rig; Write first journal paper and getting it ready for peer review	May 2014 – August 2014
Conference: 15th Aachen Membrane Colloquium, Department of Chemical Engineering, RWTH Aachen University, Germany	Getting ready for the conference (writing conference paper, preparing a poster) and attending it; this also includes collecting more data for the RMBR plant; send journal paper for peer review	September 2014 – End November 2014
Data Collection for RMBR + Corrections to be Made for 1st Journal Paper	Collect more filtration data from the RMBR pilot unit and getting changes for the first journal paper as per feedback of reviewers ready	December 2014

Year 2		
Published first Journal Paper	Getting final revisions from editors ready and ensure that the paper is published	January 2015
Checking of Activated Sludge + Start Construction for SMBR rig + Layout for 2nd Journal Paper	Checking activated sludge health; conduct wasting of sludge if necessary, etc; start writing-up making layout for another journal paper; finally, ensure construction of SMBR rig is going well	February 2015
Conference: 12th IWA Leading Edge Conference on Water and Wastewater Technologies, Hong Kong	Preparing for the conference (including writing conference paper, preparing a poster) and attending it; this also includes collecting data for the SMBR rig	March 2015 – End May 2015, 5th June 2015
Finish Write-up of 2nd Journal paper + More Data Collection for both MBR rigs (RMBR and SMBR)	Getting the final script for second journal paper ready, sending it for peer review and make changes as needed after feedback from reviewers/editors; ensuring that more filtration data are collected for the both MBR rigs	7th June 2015 – December 2015
Year 3 (Mostly thesis write-up)		
Published second Journal Paper	Getting final revisions ready and ensure that the paper is published	January 2016
Data Collection for both MBR plants (The Final Sets)	Running the pilot units still, producing more synthetic wastewater, collecting filtration data and conducting some Camlab tests to check for consistency	February 2016 – April2016
(Thesis Write-up Begins in Earnest) **–** **Chapter 1**: INTRODUCTION	The thesis introduction. Focus on aim and objectives, research rationale, publications, time management, etc; abstract and acknowledgements written	May 2016 – June 2016
Chapter 2: LITERATURE REVIEW	As this thesis covers a range of inter-disciplinary areas such as, mathematical modelling, etc, it is appropriate that this section provides fundamental theories for unfamiliar readers	July 2016 – October 2016

Chapter 3: METHODOLOGY	This chapter explores all the methodologies used throughout this thesis to complete all the required tasks. The setting-up of both pilot units (i.e. rotating and bespoke) are fully described as well	November 2016 – December 2016
Chapter 4: RESULTS	This section entirely focuses on displaying the outputted results from the various models of both MBRs (e.g. graphs and tables)	January 2017
Year 4 (Thesis write-up continued)		
Chapter 5: DISCUSSIONS	Discussions and analyses of the results are done at this stage. Thus, everything that was found or discovered is presented here	February 2017
Chapter 6: CONCLUSIONS AND RECOMMENDATIONS	The general conclusions of this thesis, what have been learnt by the author and future studies that could be used to further broaden this specific field of engineering are summarised and detailed in this chapter	March 2017
THESIS SUBMISSION DATE	Proof-reading and submission	End March 2017

APPENDIX B

This appendix section outlines the pictures taken for both MBR rigs. It is therefore related to Chapter 3 **sub-section 3.1**. Appendix B1 (for **sub-section 3.1.1**) contains pictures for the RMBR whilst Appendix B.2 (for **sub-section 3.1.2)** presents to the constructed SMBR rig pictures.

APPENDIX B.1

Various pictures pertaining to the RPU-185 RMBR can be found below on Figure AP.B.1,

Figure AP.B.1. (Left) – RPU-185 RMBR pilot unit being operated by PhD author; and, below this is an overview of control panel;
(Right) – Non-fouled and fouled rotating membrane module; respectively on image below them are: pH, Conductivity and D.O. meter

APPENDIX B.2

Several pictures pertaining to the laboratory constructed SMBR rig can be found below on Figure AP.B.2,

Figure AP.B.2. (Left) – SMBR rig flow meter being used;
(Right) – Diaphragm pump and a pressure gauge in operation

APPENDIX C

This appendix section contains various elements and data regarding experimental data that were undertaken for both MBR plants, and is overall still related to Chapter 3 but only **sub-section 3.2**. Appendix C1 (for **sub-section 3.2.1**) has details regarding chemical hazards for synthetic wastewater, and Appendix C2 (for **sub-section 3.2.3**) contains sludge handling, safety and collection protocol.

Appendix C3 (for **sub-section 3.2.6**) entails some Camlab collected data and F/M whilst Appendix C4 (for **sub-section 3.2.9**) outlines viscosity related information. Finally, Appendix C5 (for **sub-section 3.3**) presents simulations' constant parameters that were used to produce the Coors UK and Duclos-Orsello et al. 2006 curves.

APPENDIX C.1

Chemicals Hazards

Synthetic wastewater ingredients [All]:

D-Glucose anhydrous, Ammonium Chloride NH_4Cl

Causes serious eye irritation
May cause slight skin irritation
Harmful if swallowed
May cause irritation if inhaled

Potassium Phosphate KH_2PO_4

May cause eye irritation
May cause skin irritation
May cause irritation if swallowed
May cause irritation if inhaled

Sodium Hydrogen Carbonate $NaHCO_3$

May cause eye irritation
May cause skin irritation
May cause irritation if swallowed
May cause irritation if inhaled

Calcium Chloride $CaCl_2$

May cause eye irritation
May cause skin irritation
May cause irritation if swallowed
May cause irritation if inhaled

Magnesium Sulfate Mg_2SO_4

Causes eye irritation

May cause slight skin irritation
Harmful if swallowed
Causes irritation if inhaled

Iron III chloride $FeCl_3$
Dangerous substance, beware!
Causes serious eye irritation
Causes serious skin irritation
Harmful if swallowed
Harmful if inhaled

Magnesium Chloride $MgCl_2$
May cause eye irritation
May cause skin irritation
Harmful if swallowed
Causes irritation if inhaled

Control and safety measures

- All mixing must take place in the fume cupboard in TD013 (=Tower D 013, Brunel University);
- Fume cupboard fan must be switched on;
- Fume cupboard light must be switched on;
- PPE: Safety glasses, disposable gloves and face masks

APPENDIX C.2

The safety, handling and collection of the activated sludge as well as control measures for the water laboratory are presented below as follows:

Activated Sludge Hazards

Activated sludge and river water contain:

- pathogenic viruses;
- bacteria;
- protozoa;
- fungi;
- parasitic eggs

Through contact with activated sludge or river water, personnel may be exposed to various infectious diseases. The gateway may be through:

- ingestion;
- inhalation of wastewater sludge in the form of aerosols;
- inhalation of dried sludge;
- the eye and other mucous membranes;
- cuts and abrasions and puncture wounds (needlestick injury);
- intact skin

Transportation of activated sludge from Hogsmill STW to Brunel University – Control measures and procedures

- All personnel using the Water Process Laboratory must read these procedures;
- All procedures must be reviewed on an annual basis

At Thames Water (UK, Hogsmill STW):

- activated sludge to be filled into 4-litre containers by trained Thames Water personnel;
- containers to have handles;
- containers to be clearly marked to show contents;
- firm snap on lid to be fitted to each container;
- four containers to be placed in a box [box to act as a bund];
- box to have integral handles;
- box to be clearly marked to show contents;
- located lid to be fitted to box;

- box to be loaded into motor vehicle by two trained Brunel personnel

PPE to be worn at Hogsmill STW:

- disposable safety gloves;
- eye protection;
- face masks;
- safety boots;
- safety helmets;
- high visibility vests

Equipment to be carried in motor vehicle:

- eye wash station;
- cleaning kit [including disinfectant, paper towels and bin for hazardous waste];
- disposable safety gloves

At Brunel:

- box to be moved from vehicle to the Water Process Laboratory must be two trained Brunel personnel

PPE to be worn at Brunel:

- safety gloves;
- eye protection;
- face masks;
- safety boots;
- safety helmets;
- high visibility vests

In Water Process Laboratory:

- lid to be removed from box;
- containers [with lids still fitted] to be removed from box;
- if spillage has occurred in transit, containers to be cleaned with disinfectant;
- containers to be stored [with lids still fitted] in refrigerator;
- if spillage has occurred in transit, containers to be cleaned with disinfectant

PPE to be worn in Water Process Laboratory:

- safety gloves;
- eye protection;
- face masks;

- overalls

Personnel

i. All Brunel personnel will be fully trained.

ii. All Brunel personnel will be instructed to:

- always thoroughly wash, hands, forearms and face, at the end of the procedure or before food, drink or cigarettes are handled;
- always keep cuts and skin scratches clean and covered with a waterproof plaster;
- always change all wound dressings at the end of the procedure;
- always avoid rubbing the nose, mouth or eyes during the procedure;
- always wear the personal protective equipment (PPE) prescribed for the procedure;
- always remove all PPE at the end of the procedure or before eating;
- always clearly identify all dirty PPE for cleaning or disposal;
- never take home PPE

Water Process Laboratory – Control measures and procedures

- All personnel using the Water Process Laboratory must read these procedures;
- All procedures must be reviewed on an annual basis;
- All personnel must leave both coats and bags in lockers outside entrance to laboratory;
- Access to laboratory must be controlled;
- All signage must conform to European Standards

Water Process Laboratory – Procedure including emergency response plan for fire and for other emergencies

- Planning for emergencies must be communicated through written procedures;
- Laboratory has one entrance, one exit and two emergency exits;
- Entrance must be clearly labelled externally;
- Exit must be clearly labelled internally;
- Emergency exits must be clearly labelled internally;
- Entrance Zone, Clean Zone, Central Storage Zone, Analytical Zone and Dirty Zone must all be clearly labelled;

- Chemical cupboard, Clean Zone storage cupboard and Dirty Zone storage cupboard must all be clearly labelled;
- Movement direction for curtains separating zones must be clearly labelled;
- Security phone number, emergency phone number, phone numbers for first aiders and number for named person must all be posted next to telephone;
- All personnel must receive training for handling sharps. Sharps must never be bent or sheared;
- All personnel must receive training in dispensing biohazard material from a pipette by allowing the material to run down the receiving container wall;
- All personnel must receive training for minimising spills

External to entrance, the following must be posted:

- name and phone number of a named person who is to be contacted in the event of a fire, accident or spill;
- phone number of security;
- list of hazards that may be encountered in laboratory (including chemical and biological material);
- safety instructions for personnel entering laboratory (including requirement to wear PPE and to wash hands before leaving);
- "coats and bags to be left in lockers";
- "smocks must be warn";
- "food, drink, applying cosmetics, handling contact lenses, wearing open toed shoes and mouth pipetting are all prohibited"

Internal to entrance, the following must be posted:

- location of PPE, eye washing station, first aid station, spill control kit and fire extinguishers;
- location of dustbins for hazardous waste, dust bin for micro biological waste, dust bin for used PPE and laundry basket for dirty smocks;
- location of telephone;
- location of emergency exits;
- "walkways must be kept clear"

Adjacent to the exit and emergency exits, the following must be posted:

- location of alarm activation points;
- exit routes from building;
- location of fire assembly points;
- names, phone numbers and locations of first aiders;
- "wash hands before leaving laboratory";

- "removal of smocks and used PPE from laboratory is prohibited"

Above bench in both Clean and Dirty Zone, the following must be posted:

- "sharps must not be carried around"

Above hand washing sink in Entrance Zone, the following must be posted:

- "hands must be washed frequently, even after wearing gloves";
- "hands must be scrubbed vigorously with soap and water for a full 30 seconds"

Procedure for contact with a named person

- Named person must be present on Brunel University Campus;
- If no named person is present on campus, laboratory must not be used

Procedure for medical emergencies

i. If possible, injured or exposed personnel must be helped by administering immediate first aid.

ii. Injured personnel must only be moved if this is necessary in order to prevent exposure to further harm.

iii. Spills affecting a small area of skin must immediately be flushed with flowing water for at least 15 minutes. If no visible burn exists, skin must be washed with warm water and soap. Jewellery must be removed to facilitate proper decontamination.

iv. If the spill affects clothing, contaminated clothing must immediately be removed. If necessary, clothing must be cut off in order to prevent contamination of eyes. Contaminated clothing must either be discarded or decontaminated using a contracted laundry service. Contaminated clothing must not be taken home.

v. Creams and lotions must only be used to neutralise spilled material.

vi. If the splash is into the eyes, eyes must be immediately irrigated at the eye wash station for at least 15 minutes. Eyelids must be held away from the eyeball, eyes must be moved in all directions to wash thoroughly behind the eyelids.

vii. If necessary, artificial respiration must be administered. When possible, those administering must be CRP trained.

viii. First aider must be contacted.

ix. If necessary, paramedics must be contacted. Safety information must accompany injured personnel leaving the laboratory.

x. Named person must be notified.

Procedure for clearing up after spillages

i. All personnel must receive spill response training.

ii. Spill hazard warning signs must be set up.

iii. Personnel in the immediate area of spill must be notified.

iv. Nonessential personnel must be evacuated from spill area.

v. Any personnel who have been exposed to contamination must be attended to.

vi. If spilled material is biological, laboratory must be vacated for at least 30 minutes to allow time for aerosolised material to settle.

vii. If spilled material is flammable, ignition and heat sources must be turned off.

viii. Breathing vapours from spilled material must be avoided, face masks must be used.

ix. Exposure to spilled materials must be minimise, appropriate safety glasses and disposable gloves, must be used.

x. Appropriate steps to confine and limit spillage must be taken without risking injury or contamination.

xi. If spilled material is chemical, laboratory spill control kit must be used.

xii. Sharp contaminated objects including broken glass must be removed by using mechanical means, hands must never be used.

xiii. Spill area must be neutralised or disinfected. Adequate contact time must be allowed to ensure complete neutralisation or disinfection.

xiv. If spilled material is biological, paper towels must be placed on spilled material. Disinfectant must be poured carefully around the edges of spill. Care must be taken to avoid splashing.

xv. Spread of contamination must be minimised, spilled material must be cleaned by working from the outside of spill towards the middle.

xvi. Spill clean-up debris must be disposed of in accordance with procedure for disposal of used PPE, hazardous waste, microbiological waste and chemical waste.

xvii. If spilled material is biological, after initial clean up, paper towels must again be placed on spill area, flooded with disinfectant, and left to soak for at least 15 minutes or in accordance with manufacturer's instructions. A final wipe-down must be done with clean paper towels soaked with disinfectant.

xviii. Any equipment, walls or other areas splashed by spill must be disinfected.

xix. After completing clean up, hands and other exposed skin must be washed.

xx. Named person must be notified.

Procedure for storage of chemical and biological materials

All materials must be:

- stored in lockable chemical cupboard, Clean Zone lockable storage cupboard or Dirty Zone lockable storage cupboard;
- stored in accordance with manufacturer's instructions;
- stored in containers that are in good condition, closed and clearly labelled;
- stored in cupboards that are compatible with the material and hazard;
- stored in cupboards secured to prevent tipping;
- stored in cupboards that are dry, adequately vented and away from heat sources;
- stored below a height of 1.75 metres;
- entered into an inventory

Safety data sheets for materials must be stored in folders adjacent to lockable chemical cupboard, Clean Zone lockable storage cupboard or Dirty Zone lockable storage cupboard.

Procedure for disposal of used PPE, hazardous waste, microbiological waste, chemical waste, needles and syringes

i. Waste for disposal must be prepared in tightly sealed, leak proof containers. When two third full the container must be considered to be full.

ii. Metal sharps: needles, blades and syringes must all be disposed of in a puncture resistant container. To prevent needle sticks, needles must not be recapped or removed from syringes.

iii. Plastic sharps must be disposed of in a puncture resistant container.

iv. Broken glass must be disposed of in a puncture resistant container.

v. Containers must be in good condition.

vi. Puncture resistant containers must not be reused.

vii. Containers must be clearly labelled. Full chemical names must be shown.

viii. If possible, a chemical should be disposed of in the container in which that chemical was purchased.

ix. Chemicals must not be mixed in containers.

x. All biohazard solid waste must be decontaminated before disposal by using a chemical disinfectant.

xi. All biohazard liquid waste must be decontaminated before disposal, by using a chemical disinfectant.

Procedure for cleaning laboratory, equipment and safety glasses

i. Appropriate chemical disinfectants must be identified. Sufficient contact time must be allowed.

ii. Laboratory floors and walls must be regularly cleaned with a chemical disinfectant.

iii. Work surfaces must be cleaned, at least once a day and after every spill, with a chemical disinfectant.

iv. Equipment must be regularly cleaned, according to the manufacturer's instructions, with a chemical disinfectant.

v. Phone must be cleaned regularly and after every emergency use, with a chemical disinfectant.

vi. After use, pipettes must be placed horizontally in a pan filled with enough disinfectant to completely cover the pipettes.

vii. A cleaning procedure must be displayed next to each piece of equipment.

viii. Soap and towel dispenser, at hand washing sink in Entrance Zone, must be kept topped up.

ix. Safety glasses must be regularly washed in warm soapy water and wiped over with a solution very low in alcohol.

x. Cleaning procedures must be held in a file with cleaning records.

xi. All cleaning must be recorded in the cleaning records.

xii. Chemical disinfectant must be:

- used with safety glasses, disposable glasses and face masks.
- used in accordance with product safety instructions;
- appropriate in volume for number of organisms present;
- compatible with equipment being decontaminated;
- compatible with work surfaces;
- compatible with glassware;
- suitable for use on surfaces contaminated by organic matter;
- used within shelf life

Procedure for cleaning smocks

i. Smocks must be sent for commercial laundering.

ii. Smocks must be properly contained and labelled. Name of the biological agent of potential exposure must be shown.

Compiled by Gerald Edwardson and Franck Anderson Jones

APPENDIX C.3

Table AP.C.1. Some collected Camlab testing kits data for both MBR rigs and F/M values

RPU-185 (RMBR)						
MLSS (mg/L)	Ammonia (mg/L)	Nitrate (mg/L)	Phosphorous (mg/L)	Turbidity (NTU)	COD - Feed (mg/L)	F/M
5827	4.52	4.06	0.86	1.49	633	0.141
5846	4.08	4.29	0.68	1.45	644	0.152
5853	4.86	4.52	0.76	1.56	686	0.144
5872	4.25	4.68	0.98	1.72	693	0.134
5892	5.52	4.59	1.02	1.86	702	0.139
5903	4.02	5.63	1.16	2.03	713	0.142
5918	4.66	5.26	0.79	1.96	661	0.136
6003	4.76	4.31	1.11	1.42	616	0.147
6047	4.32	4.53	0.92	1.33	627	0.154
6123	5.04	4.76	0.96	1.49	669	0.145
6199	4.49	4.92	1.22	1.65	676	0.135
6275	5.76	4.83	1.26	1.79	686	0.137
6351	4.26	5.87	1.44	1.96	700	0.135
6427	4.92	5.57	1.09	1.89	644	0.143
SMBR Rig						
5832	4.58	4.15	0.97	1.78	See RMBR	0.145
5851	4.33	4.49	0.76	1.65	-	0.155
5862	4.94	4.72	0.88	1.54	-	0.147
5879	4.65	4.88	1.09	1.89	-	0.136
5909	5.82	4.69	1.35	1.91	-	0.142
5928	4.45	5.82	1.42	1.98	-	0.145
5946	4.89	5.48	0.84	2.13	-	0.133
6009	4.46	4.36	1.19	1.81	-	0.143
6053	4.92	4.99	0.97	1.86	-	0.152
6129	5.23	5.29	0.99	1.64	-	0.139
6205	4.66	4.78	1.51	1.95	-	0.144
6281	5.91	5.95	1.72	1.98	-	0.138
6357	4.48	6.12	1.48	2.02	-	0.137
6433	5.94	5.89	1.63	1.94	-	0.139

F/M is calculated using Equation 2.10. Like all other filtration experiments, the DO level is 2 mg/L and the air scouring flow rate is 21.3 L/min; SRT levels are usually kept between 10 to 20 days.

APPENDIX C.4

With known torques and angles, viscosities can be calculated from formulae seen below (Brookfield guidebook, manufacturer's booklet):

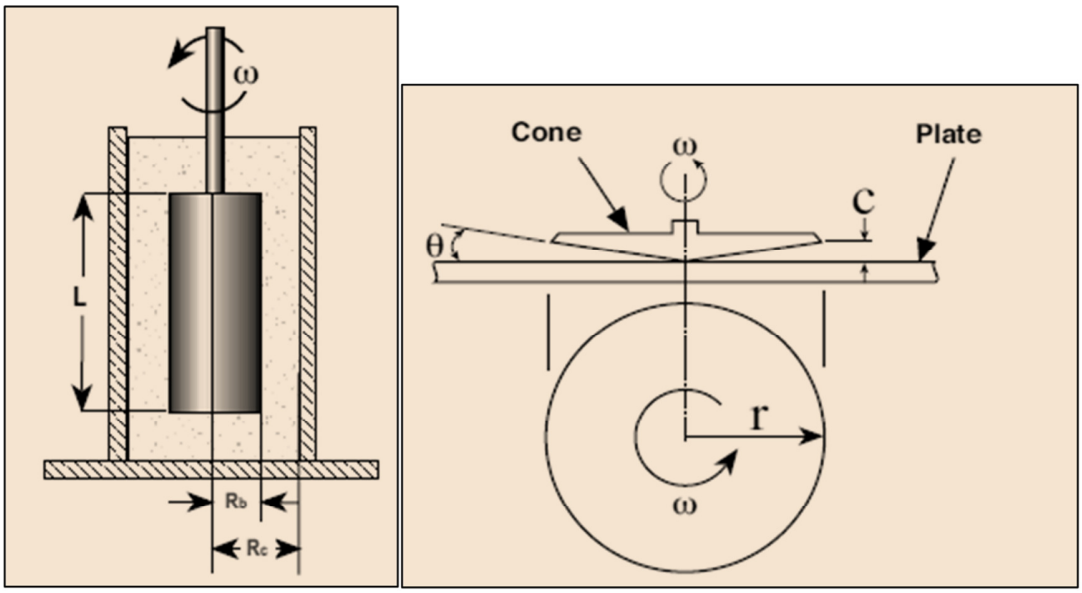

Figure AP.C.1. (Left) – Spindle types, cylindrical spindles. (Right) – Cone and plate

<u>Viscosity determination</u> (using spindle types/cylindrical spindles)

Figure AP.C.1 (Left) and Equation AP.C.1,

$$\begin{cases} \text{Shear Rate } (\dot{\gamma}) = \frac{2.\omega.R_C^2.R_b^2}{(x')^2.(R_C^2 - R_b^2)} \\ \text{Shear Stress } (\tau') = \frac{M'}{2.\pi.R_b^2.L} \\ \text{Viscosity } (\mu, \text{poise}) = \frac{\tau'}{\dot{\gamma}} \end{cases} \qquad \text{(AP.C.1)}$$

Where, ω (in rad/s) is angular velocity of spindle; R_c (in cm) is radius of container; R_b (in cm) is radius of spindle; x' (in cm) is the radius at which shear rate is being calculated; M' [in dyne.cm, with 1 N (Newton) = 10^5 dyn (dyne)] is the torque input; and, L is effective length of spindle (cm); **Note:** *To convert poise to cP = centipoise = 1 mPa.s, multiply it by 100*.

<u>Viscosity determination</u> (using cone and plate)

Figure AP.C.1 (Right) and Equation AP.C.2,

$$\begin{cases} \text{Shear Rate } (\dot{\gamma}) = \dfrac{\omega}{\sin(\theta)} \\ \text{Shear Stress } (\tau') = \dfrac{M'}{\frac{2}{3}.\pi.r^3} \\ \text{Viscosity } (\mu, \text{poise}) = \dfrac{\tau'}{\dot{\gamma}} \end{cases} \qquad \text{(AP.C.2)}$$

Where, r (in cm) is the cone radius; and, θ (in arc degree) is the cone angle;

The rotary viscometer, which can be used to read viscosities on a daily basis, is displayed below on Figure AP.C.2 as follows:

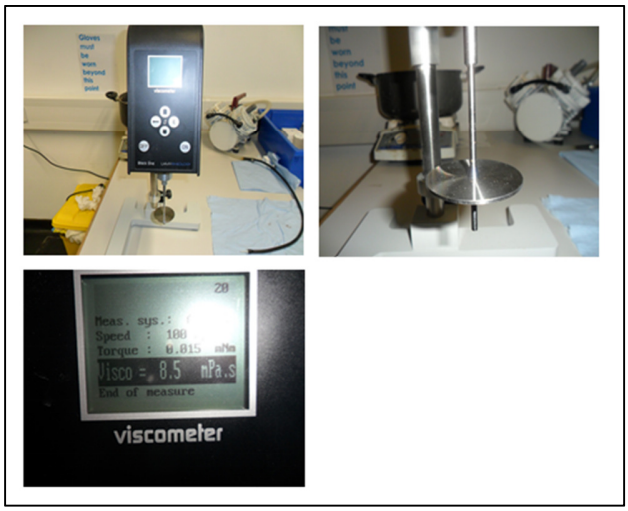

Figure AP.C.2. The rotary viscometer being used with one of the spindles shown

APPENDIX C.5

A lot of the values presented in Table AP.C.2 are extrapolated or interpolated based on SMBR rig data and are fairly respectable in terms of range within the context of SMBR fouling model.

Table AP.C.2. List of simulations' constant parameters used to obtain Coors (UK) and Duclos-Orsello et al. (2006) curves

	Avg C_d (g/L)	Avg d_{pi} (μm)	Avg τ (–)	ρ_b (kg/m^3)
Duclos-Orsello et al. 2006	[1 – 2 g/L] 0.89 [4 – 8 g/L] 3.82	0.26	[1 – 2 g/L] 0.446 [4 – 8 g/L] 0.448	1126.83
Coors (UK)	[7 – 10 g/L] 6.63 [10 – 12 g/L] 7.26	0.28	[7 – 10 g/L] 0.442 [10 – 12 g/L] 0.447	1137.42

Avg = Average

The cake porosity value is assumed to be equal to that of the cake water content. As for the terminologies, please refer to **NOMENCLATURE**.

APPENDIX D

This appendix section provides additional information related to Chapter 4. Appendix D.1 (for **sub-section 4.1.2**) shows an optional fouling model (i.e. constant TMP) that was created for the SMBR. Appendix D2 (for **sub-section 4.2.1**) on the other hand, displays the m-codes used to implement the MBRs fouling models using Matlab and also displays obtained GA factors after adjustments in Appendix D.2.1. Appendix D3 (for **sub-section 4.2.3**) shows optimisation results of simulations final values for α_v and δ'.

APPENDIX D.1

An alternative fouling model for constant TMP/varying flux mode was derived for the square SMBR that is presented below as follows:

Activated sludge in MBR systems is classified as non-Newtonian fluid that can be expressed as a function of MLSS. This was studied in depth by Yang et al. (2009). From their study, viscosity (μ, Pa.s) is proportional to MLSS as seen in Equation AP.D.1 such that:

$$\mu = 0.0126.\left(C_{MLSS}\right)^{1.664}.e^{\frac{E}{Rg.(T_{room}+273.15)}} \quad \text{(AP.D.1)}$$

During UF, as the membrane becomes fouled and flux gradually decreases, the total available area for permeate will decrease at a uniform rate such that, there exist a time constant t_c (s^{-1}) < 1/t that yields area formulation Equation AP.D.2. Assuming time constant, t_c (s^{-1}), is proportional to the initial flux (as TMP is constant), the area formula Equation AP.D.2 can be further expanded such that:

$$A = A_0(1 - t_c.t) = A_0(1 - K_\alpha.Jm_0.t) \quad \text{(AP.D.2)}$$

As can be observed from the above equation, it is quite similar to Hermia (1982) area formulation. A Taylor's expansion of order 1 of $\ln(1 - K_\alpha.Jm_o.t)$ at t = 0 is $\approx -K_\alpha.Jm_o.t$. This reduces the area formulation to Equation AP.D.3.

$$A = A_0.\ln\left(e.(1 - K_\alpha.Jm_o.t)\right) \equiv A_0.e^{(-K_\alpha.Jm_o.t)} \quad \text{(AP.D.3)}$$

Due to caking observed during UF process, the total resistance will increase with the membrane area available for filtration. According to the in-series resistance approach, the total membrane resistance is defined as the summation of the cake's resistance and all other mechanisms' resistances. As such, by including the pore constriction mechanism and constant φ, R_{total} (m^{-1}), can be can be computed as seen in Equation AP.D.4.

$$R_{total} = \left(R_{in,b} + \varphi.R_b\right) \quad \text{(AP.D.4)}$$

At time t_b (s), once the pore constriction stops, the time at which a pore was first blocked, resistance $R_{in,b}$ can be calculated by Equation AP.D.5 (Duclos-Orsello et al. 2006),

$$R_{in,b} = R_m(1 + \beta . Q_0 . C_{MLSS} . t_b)^2 \quad \text{(AP.D.5)}$$

The resistance of the particles deposit increases with time due to the growth in mass (or thickness) of the cake layer, and with the cake filtration model, resistance, R_b, (m^{-1}) is given by Equation AP.D.6.

$$\frac{dR_b}{dt} = f' . R' . J . C_{MLSS} \quad \text{(AP.D.6)}$$

The flux, J ($m.s^{-1}$), can be calculated from Equation AP.D.7 using Darcy's law at constant TMP and the in-series resistance approach.

$$J = \frac{TMP}{\mu.(R_{in,b}+\varphi.R_b)} \quad \text{(AP.D.7)}$$

Thus, by combining Equations AP.D.1 to AP.D.7, the total normalised flow rate through membrane, Q_t ($m^3.s^{-1}$), for the square SMBR is expressed in Equation AP.D.8 as the product of the available area and the flux.

$$Q_t(t) = \frac{TMP}{0.0126.(C_{MLSS})^{1.664}.e^{\frac{E}{R_g.(T_{room}+273.15)}}.(R_m(1+\beta.Q_0.C_{MLSS}.t_b)^2+\varphi.R_b)} . A_0 . e^{(-K_\alpha . Jm_o . t)} \quad \text{(AP.D.8)}$$

Where, R_g is the universal gas constant ($R_g = 8.3145 \times 10^{-3}$ $kJ.K^{-1}.mol^{-1}$), E is the so-called activation energy which according to Yang et al. (2009) is 9.217 ($kJ.mol^{-1}$) for the viscosity of sludge, T_{room} is the room temperature in °C.

The only prevalent hydrodynamic factor to take into account during operation of the square MBR is the air scouring which is mainly in charge of mitigation cake growth and thus reduce fouling. Additionally, air scouring flux, J_{air} ($m.s^{-1}$), is a key parameter for the management and prevention of membrane fouling in most submerged MBR systems.

Thus, an additional removal term defined as the flux induced by the air scouring flow effects was added. This supplementary removal term is also in-line with Liang et al. (2006), cake's formulation equation. An analogous reformulation is found in Equation AP.D.9 but includes the air scouring effects.

$$\frac{dR_b}{dt} = f' . R' . J . C_{MLSS} - g_o . (\alpha_v . J_{air}) . \delta' . (R'_c . \theta_c) \quad \text{(AP.D.9)}$$

For the terminologies, please refer to **NOMENCLATURE**.

APPENDIX D.2

The Matlab m-codes that were used to implement both MBRs (i.e. RMBR and SMBR) fouling models are presented below (the green texts are comments and everything else execution lines).

```
function Constant_Flux_FoulingModel_RMBR(~)

% just a formality!
clear all; close all; clc;

% ga algorithm stars,
Si_pop=1.2e3;  % population size - bigger, better or something like
that!
numb_vars=3;   % number of fitting variables

LB=[0 0 0]; UB=[30 30 0.5]; % initial guess matrix UB = [k_alpha beta
phi_i] in that order!
ini_population=repmat(LB,Si_pop,1) + repmat((UB-
LB),Si_pop,1).*rand(Si_pop,numb_vars); % initial random population

% optimisation starts:
options=gaoptimset('PopulationSize',Si_pop,...
                   'TimeLimit',inf,...
                   'StallTimeLimit',inf,...
                   'TolFun',1e-10,...
                   'Generations',6000,...
                   'MigrationFraction',0.25,...
                   'InitialPopulation',ini_population,...
                   'MutationFcn',@mutationadaptfeasible,...
                   'PlotFcns',@gaplotbestf,...
                   'CreationFcn',@createfunktionfueroptimierung);
[xi,fval]=ga(@simulate_TMP,numb_vars,[],[],[],[],LB,UB,[],options);

% compute adjustable parameter for beta, model parameter:
memb_thick=(3*36)/1000; % thickness of membrane in (m)
rp=(0.03/2)*1e-6; %
sigma_a=xi(2)*pi*(rp)^2*memb_thick; % adjustable parameter for model

% re-run with optimised data points for fitted curves
best_fit_data(xi);

display (['Optimised Parameters: ' num2str([xi fval])]); %
display (['Blockage Parameters: ' num2str([rp sigma_a])]); %

end %%%

function [TMP_meas,Opt_val]=Obj_func_mini(TMP,TMP0)

% call for measured data in bar:
TMP_cal1=[0.15
0.17
0.18
```

```
0.19
0.21
0.23
0.25
0.27
0.30
0.33
0.36
0.39
0.42
0.44
0.47
0.52
0.54
0.58
0.62
0.68
0.73
0.77
0.83
0.88
0.94]; % lower mlss goes here
TMP_cal1=TMP_cal1';
TMP_cal2=[0.15
0.18
0.19
0.21
0.24
0.25
0.28
0.29
0.32
0.35
0.38
0.41
0.45
0.48
0.52
0.57
0.61
0.66
0.70
0.75
0.82
0.86
0.95
1.03
1.12]; % higher mlss goes here
TMP_cal2=TMP_cal2';

% we need our Pa! for those TMPs
TMP_meas=([TMP_cal1;TMP_cal2]*1e5)';
% TMP0=15000;

% sum-difference calculation between real flow and computed
sd1    = (TMP(:,1).^1 -  TMP_meas(:,1).^1)./TMP0;
```

```
sd2    = (TMP(:,2).^1 -  TMP_meas(:,2).^1)./TMP0;

Opt_val=sum(sd1.^2) + sum(sd2.^2); % minimisation of sum of the
squares, note: sum(sd1.^2) = sd1*sd'1!, bingo!

end %%%

%%% _____________________ SUBFUNCTION
function Obj_val=simulate_TMP(xin)

% define  persistent or global variables
global CNTg val_final

% just a little trick! for counter
if isempty(CNTg)
CNTg = 1;
else
CNTg = CNTg + 1;
end %

% changeable parameters used in optimisation!
k_alpha=xin(1);          %
beta   =xin(2);          %
phi_i  =xin(3);          % parameter for resistance

% initial unchangeable parameters
Q0    =0.67/60000;   % iniial volumetric flow rate in m^3/s
TMP0  =15000;        % initial starting TMP in Pa
bulk  =[6.32 7.24];  % mlss concentration g/L
epsilon=0.456;       % average water content for specific mlss range
Cporo =epsilon;      % void fraction
dpi   =0.28*1e-6;    % particle diameter taken from thames water
Cd    =4.89;         % solids content for specific mlss range in g/L
(kg/m^3)
rho_b =1129.32;      % Average bulk cake layer density for specific
mlss range in kg/m^3
visc_ii=0.0074;      % avg visc in Pa.s,
A     =1.6006;       % membrane area (m^2),
Au0   =A;            % initial unblocked area of clean membrane in m^2
at t=0
J0    =Q0/Au0;       % flux in m/s
Rm    =6.262e11;     % clean membrane resistance in 1/m
Rtot_i=TMP0/(visc_ii*J0); % well, we need to start somewhere!

%%% computing unblocked flow Qu:
ti=0;          % simul start 0.8e-20
tstep=60*5;    % time steps
tj=60*120;     % end of simul in sec or filtration time
t=ti:tstep:tj; % time vector

tp=t.*0.39; % small time factor no more than 1/2.56

% initialize data
RCi=(180*(1 - Cporo)^2)/(dpi^2*Cporo^3); % specific cake resistance
```

```
depth=(Cd*J0)/((1 - epsilon)*rho_b);     % depth or thickness

% note at this stage you can go two ways, model 1 or model 2 (the ones
I derived), they're both almost equally valid!
% Taylor's expansion model uses the exponential version but has small
truncations that one might need to be wary of.
% In any even if you want to plot both, you'll have to find the best
fits of both models first,
% you can individually do this by interchanging Tmp_ratio (i.e.
Tmp_ratio=(TMP0./(1-k_alpha*J0*t)) for model 1 or
% Tmp_ratio=(TMP0./exp(-k_alpha*J0*t)) for model 2). As for the rest,
well
% you can follow the methods here, then use plot and legend (i.e.
legend('Cb = 3.34 g/L','Cb = 4.26g/L','Model 1','Model 2');
% for this m-file I'll go ahead and use model 1.
Tmp_ratio=(TMP0./(1-k_alpha*J0*t));       % or (TMP0./exp(-
k_alpha*J0*t)) for model 2;
% moving on ...
TMP=zeros(length(t),length(bulk));
Rtot_m=zeros(length(t),length(bulk));
Rinb=zeros(size(TMP));
Rcake=zeros(size(TMP));
 j=0; %%%
for i=bulk % bulk concentration values
    j=j+1;
   Cb=i;    % concentration in g/L

% TMP increasing over decreasing area:
    %%%
    Rinb(:,j)=Rm.*((1 + beta*Q0*Cb*tp).^2-1);
    Rcake(:,j)=depth*RCi.*t;
    Rtot_m(:,j)=Rinb(:,j)+phi_i*Rcake(:,j)+Rtot_i;
    TMP(:,j)=Tmp_ratio'.*(Rtot_m(:,j)/Rtot_i);
end

% minimisation difference
[TMP_meas,Opt_val]=Obj_func_mini(TMP,TMP0);%#ok<ASGLU,> %
Obj_val=Opt_val;

% part of your data so far goes here!
val_final(CNTg,:)=[bulk TMP0 CNTg Obj_val xin];

% don't forget to save once in the blue moon!
if ~isempty(find(CNTg==0:300:CNTg+301,1))
    % a rainy day perhaps!?
    save Sim_run_ConstantFlux.mat val_final -mat
end %

end %%%

%%% _____________________ SUBFUNCTION
function best_fit_data(xin)

%%%=================================================================
====
```

```
% changeable parameters used in optimisation and some rounding up!
k_alpha=xin(1);          %
beta   =xin(2);          %
phi_i  =xin(3);          % parameter for resistance

% initial unchangeable parameters
Q0    =0.67/60000;   % iniial volumetric flow rate in m^3/s
TMP0  =15000;        % initial starting TMP in Pa
bulk  =[6.32 7.24];  % mlss concentration g/L
epsilon=0.456;       % average water content for specific mlss range
Cporo =epsilon;      % void fraction
dpi   =0.26*1e-6;    % particle diameter taken from thames water
Cd    =4.89;         % solids content for specific mlss range in g/L
(kg/m^3)
rho_b =1129.32;      % Average bulk cake layer density for specific
mlss range in kg/m^3
visc_ii=0.0074;      % avg visc in Pa.s,
A     =1.6006;       % membrane area (m^2),
Au0   =A;            % initial unblocked area of clean membrane in m^2
at t=0
J0    =Q0/Au0;       % flux in m/s
Rm    =6.262e11;     % clean membrane resistance in 1/m
Rtot_i=TMP0/(visc_ii*J0); % well, we need to start somewhere!

%%% computing unblocked flow Qu:
ti=0;          % simul start 0.8e-20
tstep=60*5;    % time steps
tj=60*120;     % end of simul in sec or filtration time
t=ti:tstep:tj; % time vector

tp=t.*0.39; %

% initialize data
RCi=(180*(1 - Cporo)^2)/(dpi^2*Cporo^3); % specific cake resistance
depth=(Cd*J0)/((1 - epsilon)*rho_b);     % depth or thickness
Tmp_ratio=(TMP0./(1-k_alpha*J0*t));      % (TMP0./exp(-k_alpha*J0*t));
TMP=zeros(length(t),length(bulk));
Rtot_m=zeros(length(t),length(bulk));
Rinb=zeros(size(TMP));
Rcake=zeros(size(TMP));
 j=0; %%%
for i=bulk % bulk concentration values
    j=j+1;
   Cb=i;    % concentration in g/L

% TMP increasing over decreasing area:
    %%%
    Rinb(:,j)=Rm.*((1 + beta*Q0*Cb*tp).^2-1);
    Rcake(:,j)=depth*RCi.*t;
    Rtot_m(:,j)=Rinb(:,j)+phi_i*Rcake(:,j)+Rtot_i;
    TMP(:,j)=Tmp_ratio'.*(Rtot_m(:,j)/Rtot_i);
end

%%%=================================================================
====
```

```
%%% figures & graphs
figure; % call figure window
t_xi =0:5:120; % time interval for real data

% lab data goes here:
[TMP_meas,Opt_val]=Obj_func_mini(TMP,TMP0); %#ok<NASGU> %

% plotting tmps 'MarkerFaceColor','k'
plot(t_xi,TMP_meas(:,1)./TMP0,'^k','MarkerEdgeColor','k','MarkerSize',6
)

hold on;

plot(t_xi,TMP_meas(:,2)./TMP0,'ok','MarkerEdgeColor','k','MarkerSize',6
);

% labels and legends
xlabel('Time [min]'); %
ylabel('TMP/TMP0 (Transmembrane Pressure Ratio)'); %

plot(t./60,TMP(:,1)./TMP0,'-k','LineWidth',2);  % I like '--k' better
plot(t./60,TMP(:,2)./TMP0,'-k','LineWidth',2); hold off; % fitted
values for Qt
legend(['Cb = ' num2str(bulk(1)) ' g/L'],['Cb = ' num2str(bulk(2)) '
g/L'], 'Model 1');

axis tight; % fit max values or % axis square;

end %%%
```

```
function Constant_TMP_FoulingModel_RMBR(~)

% just a formality!
clear all; close all; clc;

% measuring elapsed or execution time {% t_ini=clock; @function
;t_elp=etime(clock,t); ===> method 1 instead of tic toc}
t_ini=tic; % simulation start time

%%% ga algorithm stars,
Si_pop=1.2e3;   % population size - don't take my word for it but
someone once said bigger is better ... who knew!
numb_vars=6;    % number of fitting parameters

LB=[0 0 0 0 0 0]; UB=[0.9 1.5 0.8 500 90 50]; % initial guess matrix in
order [Rp0Rmi alpha  beta fiRi go kab],
ini_population=repmat(LB,Si_pop,1) + repmat((UB-
LB),Si_pop,1).*rand(Si_pop,numb_vars); % initial random population

% optimisation starts:
options=gaoptimset('PopulationSize',Si_pop,...
                   'TimeLimit',inf,...
```

```
                    'StallTimeLimit',inf,...
                    'TolFun',1e-10,...
                    'Generations',6000,...
                    'MigrationFraction',0.25,...
                    'InitialPopulation',ini_population,...
                    'MutationFcn',@mutationadaptfeasible,...
                    'PlotFcns',@gaplotbestf,...
                    'CreationFcn',@createfunktionfueroptimierung);
[xi,fval]=ga(@simulate_shear_effect,numb_vars,[],[],[],[],LB,UB,[],opti
ons);

% compute adjustable parameter for beta, model parameter:
memb_thick=(3*36)/1000; % total thickness of membrane in (m)
rp=(0.03/2)*1e-6; %
sigma_a=xi(3)*pi*(rp)^2*memb_thick; % adjustable parameter for model

% re-run with optimised data points for fitted curves
best_fit_data(xi);

t_elp=toc(t_ini); % end simulation

display (['Simulation Time (sec): ' num2str(t_elp)]); %
display (['Optimised Parameters: ' num2str([xi fval])]); %
display (['Blockage Parameters: ' num2str([rp sigma_a])]); %

end %%%

%%% _____________________ SUBFUNCTION
function
[m,n,rho_f,ReNN,kw]=mncoefficientfit(MLSS,visc_i,shear_R,omega,R0,Ri,Q0
,A0) %Q0,A0

% let's determine m and n, shall we!?, (you can cross ref with
calculated values in Excel, it'll be and should be the same!)
p=polyfit(log(shear_R),log(visc_i),1);
m=exp(p(2)); n=p(1)+1; %%

% flow regime:
r=R0-Ri; % radial distance
rho_f=1000 + 0.2*(sum((MLSS/1000))/length(MLSS)); % AS density
calculation kg/m^3, some researcher take rho_f=1040 kg/m^3!
ReNN=(rho_f*omega^(2-n)*r^2)/m; % ReNN , varargout(1)=rho_f

%%% getting kw
kw=(Q0/A0)/(r*omega);

end % mncoefficientfit

%%% _____________________ SUBFUNCTION
function [Qi,Ri]=Lab_flows_data(A,miu,TMP) %Ri,Qi

% flow rate at # bulk concentrations values, in L/min (just the values
read raw from lab in original unit)
Qt_1=[1.27
```

```
1.24
1.20
1.17
1.14
1.11
1.09
1.06
1.04
1.01
0.99
0.97
0.95
0.92
0.90
0.89
0.87
0.85
0.83
0.82
0.80
0.78
0.77
0.76
0.74]; % intervals of 5 min, (i.e. for 8.22-9.35, this will be for 8.22
g/L)
Qt_1=Qt_1';
Qt_2=[1.27
1.23
1.19
1.15
1.11
1.08
1.05
1.02
0.99
0.96
0.93
0.91
0.89
0.87
0.83
0.81
0.79
0.77
0.76
0.74
0.72
0.71
0.69
0.68
0.66]; % enter higher Mlss Q decline for same tmp (i.e. for 8.22-9.35,
this will be for 9.35 g/L)
Qt_2=Qt_2';

Qr=([Qt_1;Qt_2])';
Qi=Qr/60000; % m^3/s, they are converted here to standard unit!
```

```
Ri=(TMP*A)./(miu.*Qi); % total resistance m^-1

end %%%

function Opt_val=Obj_func_mini(Qt,Q0,A,miu,TMP)

% call for measured data:
[Q,R]=Lab_flows_data(A,miu,TMP);  %#ok<NASGU>

% sum-difference calculation between real flow and computed
sd1    =(Qt(:,1) -  Q(:,1))./Q0;
sd2    =(Qt(:,2) -  Q(:,2))./Q0;

Opt_val=sum(sd1.^2) + sum(sd2.^2); % minimisation of sum of the
squares, note: sum(sd1.^2) = sd1*sd'1!, bingo!

end %%%

%%% _____________________ SUBFUNCTION
function Obj_val=simulate_shear_effect(xin)

% define  persistent or global variables
global CNTg val_final

% just a little trick! for counter
if isempty(CNTg)
CNTg = 1;
else
CNTg = CNTg + 1;
end %

% Optional but will be useful - file containing specific mlss range,
shear rate and viscosity measured from experiment (MLSS shear_R
visc_i),
% create a matrix for each (all must be of same matrix size) that'll
display in the workspace, then
% use the save function (i.e. save RPU185_MBR_MLSS(8220n9350).mat MLSS
shear_R visc_i -mat, bingo!),
% it'll be used for calculation verification of m and n values but will
also calculate rho_f, ReNN and kw ...
% alternatively you may choose not to have the file and enter those
matlab calculated values yourself. that is
% assuming you have calculated those values before hand and you should!
- change adequately as needed in this subfunction!
load RPU185_MBR_MLSS(8220n9350) -mat;

% changeable parameters used in optimisation!
Rp0Rmi =xin(1);          % ratio of initial resistances
alpha  =xin(2);          % pore blockage parameter
beta   =xin(3);          % pore constriction parameter in kg
fiRi   =xin(4)*1e9;      % combined parameter for cake build up
go     =xin(5);          % cake removal coefficient
kab    =xin(6);          % Area constant, adjustable
```

```
% initial unchangeable parameters [must be inputted as needed]
Q0    =1.27/60000;   % iniial volumetric flow rate converted in m^3/s
PT    =-30000;       % PT, negative sign of initial tmp (Pa)
Qair  =21.3/60000;   % 21.3 L/min in m^3/s, air scouring flow rate
Sig_i =0.00046;      % resistance constant in m^-1
bulk  =[8.22 9.35];  % MLSS concentration g/L, must be in this order
[smaller value bigger value]
epsilon=0.445;       % average cake water content for specific mlss
range
Cporo =epsilon;      % void fraction, some researchers use 0.5
dpi   =0.28*1e-6;    % average particle diameter for each mlss specific
range taken from thames water in m,
Cd    =6.32;         % average solids content for each mlss range in
kg/m^3 (or just g/L works as well),
rho_b =1132.17;      % bulk cake layer density in kg/m^3, averaged for
each mlss range
alpha_v=0.0292;      % air scouring coefficient
visc_ii=0.0093;      % avg visc (Pa.s),
A     =1.6006;       % membrane area (m^2)
Au0   =A;            % initial unblocked area of clean membrane in m^2
at t=0;
Ab0   =0;            % initial blocked area (m^2)
R0    =0.177;        %%% membrane outer radius (m);
Ri    =0.055;        %%% membrane inner radius (m);
RPM   =20;           %%% revolution per min for membrane module
rotation;
omega =(RPM*2*pi)/60;% angluar velocity in rad/s
Rm    =6.262e11;     % clean membrane resistance in 1/m
Rp0   =Rp0Rmi*Rm;    % Rm computed in 1/m, just a bit of rearranging
Jair  =Qair/Au0;     % air scouring flux in m/s
Jm    =Q0/Au0;       %

% invoke this function to determine flow regime and m & n coefficients,
etc ...
% or input them manually if you haven't loaded the file earlier for
specific mlss range
% (i.e. m=0.0170; n=0.870 for [8.22 9.35], etc ...)
[m,n,rho_f,ReNN,kw]=mncoefficientfit(MLSS,visc_i,shear_R,omega,R0,Ri,Q0
,Au0);

%%% computing unblocked flow Qu:
ti=0.8e-20;    % simul start
tstep=60*5;    % time steps
tj=60*120;     % end of simul in sec or filtration time
t=ti:tstep:tj; % time vector

tp=t.*0.39; %%% small time factor, no more than 1/2.56

% initialize data
Qu=zeros(length(t),length(bulk));
Au=zeros(size(Qu));
 j=0; %%%
for i=bulk % bulk concentration values
    j=j+1;
   Cb=i;    % concentration in g/L
```

```
% unblocked flow and area:
    Qu(:,j)=((Au0*Jm)./(1+beta*Q0*Cb*t).^2).*exp(-
alpha*Cb*Jm*t./(1+beta*Q0*Cb*t));
    %%%
    depth=(Cd*Jm)/((1 - epsilon)*rho_b);      % depth or thickness
    Au(:,j)=-alpha*Cb*Qu(:,j)'.*t.^1 + kab*(alpha_v*Jair +
kw*omega*R0)*1/2*depth*t.^2 + Au0; % m^2
end

%%% computing the blocked flow Qb:
TMPi     =-PT-(0.25*rho_f*(kw*omega*R0)^2); % real tmp
kine_visc=visc_ii/rho_f; % kine_visc = dyna_visc/rho

if ReNN<=2e5
    flow_type='laminar';
else
    flow_type='turbulent';
end %

switch flow_type
   case 'laminar'
   % initialize data
   Qb=zeros(length(t),length(bulk));
   Ab=zeros(size(Qb));
   Rp=zeros(size(Ab));
   j=0; %%%

   for i=bulk % bulk concentration value
    j=j+1;
   Cb=i;       % concentration in g/L

   % unblocked flow and area:
   % reformulated Ab
   RCi=(180*(1 - Cporo)^2)/(dpi^2*Cporo^3); % specific cake resistance
   depth=(Cd*Jm)/((1 - epsilon)*rho_b);     % depth or thickness
   Ab(:,j)=alpha*Cb*Qu(:,j)'.*t.^1 - kab*(alpha_v*Jair +
kw*omega*R0)*1/2*depth*t.^2 + Ab0;
   Rp(:,j)=fiRi*Cb*(Jm-(Qu(:,j)'./Au(:,j)')).*t.^1 -
go*Sig_i*(alpha_v*Jair + kw*omega*R0)*1/2*(RCi*depth).*t.^2 + Rp0;
   Qb(:,j)=(TMPi./((m.*(1.81*(kw*omega)^1.5*R0*kine_visc^(-0.5))^(n-
1)).*(Rm.*(1 + beta*Q0*Cb*tp).^2 + Rp(:,j)'.^1))).*...
           (alpha*Cb*Qu(:,j)'.*t.^1 - kab*(alpha_v*Jair +
kw*omega*R0)*1/2*depth*t.^2 + Ab0);
   Qb(1,j)=ti;                                % note, when t tends to
zero, Qb becomes zero, thus Qt=Qu!
   end

   case 'turbulent'
   % initialize data
   Qb=zeros(length(t),length(bulk));
   Ab=zeros(size(Qb));
   Rp=zeros(size(Ab));
   j=0; %%%
```

```
   for i=bulk % bulk concentration value
    j=j+1;
   Cb=i;       % concentration in g/L

   % unblocked flow and area:
   % reformulated Ab
   RCi=(180*(1 - Cporo)^2)/(dpi^2*Cporo^3); % specific cake resistance
   depth=(Cd*Jm)/((1 - epsilon)*rho_b);     % depth or thickness
   Ab(:,j)=alpha*Cb*Qu(:,j)'.*t.^1 - kab*(alpha_v*Jair +
kw*omega*R0)*1/2*depth*t.^2 + Ab0;
   Rp(:,j)=fiRi*Cb*(Jm-(Qu(:,j)'./Au(:,j))).*t.^1 -
go*Sig_i*(alpha_v*Jair + kw*omega*R0)*1/2*(RCi*depth).*t.^2 + Rp0;
   Qb(:,j)=(TMPi./((m.*(0.057*(kw*omega)^1.8*R0^1.6*kine_visc^(-
0.8))^(n-1)).*(Rm.*(1 + beta*Q0*Cb*tp).^2 + Rp(:,j)'.^1))).*...
           (alpha*Cb*Qu(:,j)'.*t.^1 - kab*(alpha_v*Jair +
kw*omega*R0)*1/2*depth*t.^2 + Ab0);
   Qb(1,j)=ti;    % note, when t tends to zero, Qb becomes zero, thus
Qt=Qu!
   end

end

%%% total flow is the sum of blocked and unblocked; and calculation of
Rtotal
% initialize data
   Qt=zeros(length(t),length(bulk));
   Rtot=zeros(size(Qt));
 for k=1:length(bulk) %
   Qt(:,k)=Qu(:,k)+Qb(:,k); % total volumetric flow rate
   Rtot(:,k)=(TMPi*Au0)./(visc_ii.*(Qu(:,k)+Qb(:,k))); % Rtotal
 end %

% call for minimisation difference function!
Obj_val=Obj_func_mini(Qt,Q0,Au0,visc_ii,TMPi); %

% simulation data thus far to be used for save
val_final(CNTg,:)=[m n ReNN kw bulk -PT CNTg Obj_val xin];

% save your simulations data every now and then - optional
if ~isempty(find(CNTg==0:300:CNTg+301,1))
    %%% save as '.dat' or '.mat' file, for maybe a rainy day!
    save Simu_Run_RotatingMBR.mat val_final -mat
end %

end %%%

%%% _____________________ SUBFUNCTION - Evaluate the best fit in graph
form
function best_fit_data(xin)

%%%
=========================================================================
load RPU185_MBR_MLSS(8220n9350) -mat; % why hello there, we meet again!
```

```
% changeable parameters used in optimisation!
Rp0Rmi =xin(1);         % ration of initial protein resistance ratio
alpha  =xin(2);         % pore blockage parameter
beta   =xin(3);         % pore constriction parameter in kg
fiRi   =xin(4)*1e9;     % combined parameter for cake build up
go     =xin(5);         % cake removal coefficient
kab    =xin(6);         % Area constant, adjustable

% initial unchangeable parameters [must be inputted as needed]
Q0    =1.27/60000;   % iniial volumetric flow rate converted in m^3/s
PT    =-30000;       % PT, negative sign of initial tmp (Pa)
Qair  =21.3/60000;   % 21.3 L/min in m^3/s, air scouring flow rate
Sig_i =0.00046;      % resistance constant in m^-1
bulk  =[8.22 9.35];  % MLSS concentration g/L, must be in this order
[smaller value bigger value]
epsilon=0.445;       % average cake water content for specific mlss
range
Cporo =epsilon;      % void fraction, some researchers use 0.5
dpi   =0.28*1e-6;    % average particle diameter for each mlss specific
range taken from thames water in m,
Cd    =6.32;         % average solids content for each mlss in kg/m^3
(or just g/L works as well),
rho_b =1132.17;      % bulk cake layer density in kg/m^3, averaged for
each mlss range
alpha_v=0.0292;      % air scouring coefficient
visc_ii=0.0093;      % avg visc (Pa.s),
A     =1.6006;       % membrane area (m^2)
Au0   =A;            % initial unblocked area of clean membrane in m^2
at t=0;
Ab0   =0;            % initial blocked area (m^2)
R0    =0.177;        %%% membrane outer radius (m);
Ri    =0.055;        %%% membrane inner radius (m);
RPM   =20;           %%% revolution per min for membrane module
rotation;
omega =(RPM*2*pi)/60;% angluar velocity in rad/s
Rm    =6.262e11;     % clean membrane resistance in 1/m
Rp0   =Rp0Rmi*Rm;    % Rm computed in 1/m, just a bit of rearranging
Jair  =Qair/Au0;     % air scouring flux in m/s
Jm    =Q0/Au0;       %

% invoke this function to determine flow regime and m & n coefficients,
etc ...
% or input them manually if you haven't loaded the file earlier for
specific mlss range
% (i.e. m=0.0170; n=0.870 for [8.22 9.35], etc ...)
[m,n,rho_f,ReNN,kw]=mncoefficientfit(MLSS,visc_i,shear_R,omega,R0,Ri,Q0
,Au0);

%%% computing unblocked flow Qu:
ti=0.8e-20;    % simul start
tstep=60*5;    % time steps
tj=60*120;     % end of simul in sec or filtration time
t=ti:tstep:tj; % time vector

tp=t.*0.39; %%%
```

```
% initialize data
Qu=zeros(length(t),length(bulk));
Au=zeros(size(Qu));
 j=0; %%%
for i=bulk % bulk concentration values
    j=j+1;
   Cb=i;    % concentration in g/L

% unblocked flow and area:
    Qu(:,j)=((Au0*Jm)./(1+beta*Q0*Cb*t).^2).*exp(-
alpha*Cb*Jm*t./(1+beta*Q0*Cb*t));
    %%%
    depth=(Cd*Jm)/((1 - epsilon)*rho_b);      % depth or thickness
    Au(:,j)=-alpha*Cb*Qu(:,j)'.*t.^1 + kab*(alpha_v*Jair +
kw*omega*R0)*1/2*depth*t.^2 + Au0; % m^2
end

%%% computing the blocked flow Qb:
TMPi     =-PT-(0.25*rho_f*(kw*omega*R0)^2); % real tmp
kine_visc=visc_ii/rho_f; % kine_visc = dyna_visc/rho

if ReNN<=2e5
    flow_type='laminar';
else
    flow_type='turbulent';
end %

switch flow_type
   case 'laminar'
   % initialize data
   Qb=zeros(length(t),length(bulk));
   Ab=zeros(size(Qb));
   Rp=zeros(size(Ab));
   j=0; %%%

   for i=bulk % bulk concentration value
    j=j+1;
   Cb=i;       % concentration in g/L

   % unblocked flow and area:
   % reformulated Ab
   RCi=(180*(1 - Cporo)^2)/(dpi^2*Cporo^3); % specific cake resistance
   depth=(Cd*Jm)/((1 - epsilon)*rho_b);     % depth or thickness
   Ab(:,j)=alpha*Cb*Qu(:,j)'.*t.^1 - kab*(alpha_v*Jair +
kw*omega*R0)*1/2*depth*t.^2 + Ab0;
   Rp(:,j)=fiRi*Cb*(Jm-(Qu(:,j)'./Au(:,j)')).*t.^1 -
go*Sig_i*(alpha_v*Jair + kw*omega*R0)*1/2*(RCi*depth).*t.^2 + Rp0;
   Qb(:,j)=(TMPi./((m.*(1.81*(kw*omega)^1.5*R0*kine_visc^(-0.5))^(n-
1)).*(Rm.*(1 + beta*Q0*Cb*tp).^2 + Rp(:,j)'.^1))).*...
           (alpha*Cb*Qu(:,j)'.*t.^1 - kab*(alpha_v*Jair +
kw*omega*R0)*1/2*depth*t.^2 + Ab0);
   Qb(1,j)=ti;                              % note, when t tends to
zero, Qb becomes zero, thus Qt=Qu!
   end
```

```
   case 'turbulent'
   % initialize data
   Qb=zeros(length(t),length(bulk));
   Ab=zeros(size(Qb));
   Rp=zeros(size(Ab));
   j=0; %%%

   for i=bulk % bulk concentration value
    j=j+1;
   Cb=i;       % concentration in g/L

   % unblocked flow and area:
   % reformulated Ab
   RCi=(180*(1 - Cporo)^2)/(dpi^2*Cporo^3); % specific cake resistance
   depth=(Cd*Jm)/((1 - epsilon)*rho_b);     % depth or thickness
   Ab(:,j)=alpha*Cb*Qu(:,j)'.*t.^1 - kab*(alpha_v*Jair +
kw*omega*R0)*1/2*depth*t.^2 + Ab0;
   Rp(:,j)=fiRi*Cb*(Jm-(Qu(:,j)'./Au(:,j))).*t.^1 -
go*Sig_i*(alpha_v*Jair + kw*omega*R0)*1/2*(RCi*depth).*t.^2 + Rp0;
   Qb(:,j)=(TMPi./((m.*(0.057*(kw*omega)^1.8*R0^1.6*kine_visc^(-
0.8))^(n-1)).*(Rm.*(1 + beta*Q0*Cb*tp).^2 + Rp(:,j)'.^1))).*...
           (alpha*Cb*Qu(:,j)'.*t.^1 - kab*(alpha_v*Jair +
kw*omega*R0)*1/2*depth*t.^2 + Ab0);
   Qb(1,j)=ti;    % note, when t tends to zero, Qb becomes zero, thus
Qt=Qu!
   end

end

%%% total flow is the sum of blocked and unblocked; and calculation of
Rtotal
% initialize data
   Qt=zeros(length(t),length(bulk));
   Rtot=zeros(size(Qt));
 for k=1:length(bulk) %
   Qt(:,k)=Qu(:,k)+Qb(:,k); % total volumetric flow rate
   Rtot(:,k)=(TMPi*Au0)./(visc_ii.*(Qu(:,k)+Qb(:,k))); % Rtotal
 end %
%%%
=========================================================================

%%% figures & graphs
figure; % call figure window
t_xi =0:5:120; % time interval for real data

% lab data goes here:
[Qa,Ra]=Lab_flows_data(Au0,visc_ii,TMPi); %

subplot(2,1,1) % plotting flow rates
plot(t_xi,Qa(:,1)./Q0,'or',...
     t_xi,Qa(:,2)./Q0,'*k');

% labels and legends
```

```
xlabel('Time [min]'); %
ylabel('Q_t/Q_0 (Total Volumetric Flow Rate Ratio)'); %
legend(['Cb = ' num2str(bulk(1)) ' g/L, ' num2str(-PT/1e5) ' bar'],['Cb
= ' num2str(bulk(2)) ' g/L, ' num2str(-PT/1e5) ' bar']);

hold on;
plot(t./60,Qt./Q0,'-.'); hold off; % fitted values for Qt

axis tight; % fit max values or % axis square;

subplot(2,1,2) % plotting total resistances
plot(t_xi,Ra(:,1)./(Rm),'or',...
     t_xi,Ra(:,2)./(Rm),'*k');

% labels and legends
xlabel('Time [min]'); %
ylabel('R_t_o_t_a_l/R_m (Total Resistance Ratio)'); %
legend(['Cb = ' num2str(bulk(1)) ' g/L, ' num2str(-PT/1e5) ' bar'],['Cb
= ' num2str(bulk(2)) ' g/L, ' num2str(-PT/1e5) ' bar']);

hold on;

plot(t./60,Rtot./(Rm),'-.'); hold off; % fitted values for Rtot

axis tight; % fit max values or axis square;

display (['[ReNN m n]: ' num2str([ReNN m n])]); %%% optional, never
hurts to double check!

end %%%
```

```
function Constant_TMP_FoulingModel_SMBR(~)

% just a formality!
clear all; close all; clc;

%%% measuring elapsed or execution time {% t_ini=clock; @function
;t_elp=etime(clock,t); ===> method 1}
t_ini=tic; % simulation start time

% ga algorithm stars,
Si_pop=1.2e3;  % population size - need large
numb_vars=6;  % number of fitting variables

LB=[0 0 0 0 0 0]; UB=[0.9 2.5 0.5 300 90 30]; % guess matrix must be in
order [Rp0Rmi alpha  beta   fiRi go kab]
ini_population=repmat(LB,Si_pop,1) + repmat((UB-
LB),Si_pop,1).*rand(Si_pop,numb_vars); % initial random population

% optimisation starts:
options=gaoptimset('PopulationSize',Si_pop,...
                   'TimeLimit',inf,...
                   'StallTimeLimit',inf,...
                   'TolFun',1e-10,...
```

```
                    'Generations',6000,...
                    'MigrationFraction',0.25,...
                    'InitialPopulation',ini_population,...
                    'MutationFcn',@mutationadaptfeasible,...
                    'PlotFcns',@gaplotbestf,...
                    'CreationFcn',@createfunktionfueroptimierung);
[xi,fval]=ga(@simulate_shear_effect,numb_vars,[],[],[],[],LB,UB,[],opti
ons);

% compute adjustable parameter for beta, model parameter:
memb_thick=(6*20)/1000; % thickness of membrane in (m)
rp=(0.03/2)*1e-6; %
sigma_a=xi(3)*pi*(rp)^2*memb_thick; % adjustable parameter for model

% re-run with optimised data points for fitted curves
best_fit_data(xi);

t_elp=toc(t_ini); % end simulation

display (['Simulation Time (sec): ' num2str(t_elp)]); %
display (['Optimised Parameters: ' num2str([xi fval])]); %
display (['Blockage Parameters: ' num2str([rp sigma_a])]); %

end %%%

%%% _____________________ SUBFUNCTION
function [Qi,Ri]=Lab_flows_data(A,miu,TMP) %Ri,Qi

% flow rate at # bulk concentrations values %
Qt_1=[1.84
1.78
1.73
1.67
1.62
1.57
1.53
1.49
1.44
1.40
1.37
1.33
1.30
1.26
1.23
1.20
1.17
1.14
1.12
1.09
1.07
1.04
1.02
1.00
0.98]; % lower value mlss goes here
Qt_1=Qt_1';
```

```
Qt_2=[1.84
1.77
1.70
1.63
1.57
1.51
1.46
1.41
1.36
1.31
1.27
1.23
1.19
1.16
1.12
1.09
1.06
1.03
1.00
0.97
0.95
0.92
0.90
0.88
0.86]; % higher value mlss goes here
Qt_2=Qt_2';

Qr=([Qt_1;Qt_2])';
Qi=Qr/60000; % m^3/s
Ri=(TMP*A)./(miu.*Qi); % total resistance m^-1

end %%%

function Opt_val=Obj_func_mini(Qt,Q0,A,miu,TMP)

% call for measured data:
[Q,R]=Lab_flows_data(A,miu,TMP);  %#ok<NASGU>

% sum-difference calculation between real flow and computed
sd1    =(Qt(:,1) -  Q(:,1))./Q0;
sd2    =(Qt(:,2) -  Q(:,2))./Q0;

Opt_val=sum(sd1.^2) + sum(sd2.^2); % minimisation of sum of the
squares, note: sum(sd1.^2) = sd1*sd'1!, bingo!

end %%%


%%% _____________________ SUBFUNCTION
function Obj_val=simulate_shear_effect(xin)

% define  persistent or global variables
global CNTg val_final
```

```
% just a little trick! for counter
if isempty(CNTg)
CNTg = 1;
else
CNTg = CNTg + 1;
end %

% changeable parameters used in optimisation!
Rp0Rmi =xin(1);          % ratio of initial resistance
alpha  =xin(2);          % pore blockage parameter
beta   =xin(3);          % pore constriction parameter in kg
fiRi   =xin(4)*1e9;      % combined parameter for cake build up
go     =xin(5);          % cake removal coefficient
kab    =xin(6);          % Area constant, adjustable

% initial unchangeable parameters
Q0     =1.84/60000;    % iniial volumetric flow rate in m^3/s
PT     =-58000;        % PT, negative sign of initial tmp (Pa)
Qair   =21.3/60000;    % 21.3 L/min in m^3/s
Sig_i  =0.00046;       % resistance constant in m^-1
bulk   =[8.22 9.35];   % mlss concentration g/L
epsilon=0.442;         % average cake water content for specific mlss
range
Cporo  =epsilon;       % void fraction
dpi    =0.28*1e-6;     % average particle diameter for each mlss specific
range taken from thames water in m,
Cd     =6.32;          % average solids content in kg/m^3 (or just g/L
works as well),
rho_b  =1132.17;       % Average bulk cake layer density for each mlss
range in kg/m^3
alpha_v=0.0292;        % air scouring coefficient
visc_ii=0.0093;        % avg visc in Pa.s,
A      =1.152;         % membrane area (m^2)
Au0    =A;             % initial unblocked area of clean membrane in m^2
at t=0;
Ab0    =0;             % initial blocked area (m^2)
Rm     =4.55e11;       % clean static membrane module resistance in 1/m
Rp0    =Rp0Rmi*Rm;     % Rm computed in 1/m
Jair   =Qair/Au0;      % air scouring flux in m/s
Jm     =Q0/Au0;        %

%%% computing unblocked flow Qu:
ti=0.8e-20;     % simul start
tstep=60*5;     % time steps
tj=60*120;      % end of simul in sec or filtration time
t=ti:tstep:tj; % time vector

tp=t.*0.39; %%%

% initialize data
Qu=zeros(length(t),length(bulk));
Au=zeros(size(Qu));
 j=0; %%%
for i=bulk % bulk concentration values
    j=j+1;
```

```
   Cb=i;    % concentration in g/L

% unblocked flow and area:
    Qu(:,j)=((Au0*Jm)./(1+beta*Q0*Cb*t).^2).*exp(-
alpha*Cb*Jm*t./(1+beta*Q0*Cb*t));
    %%%
    depth=(Cd*Jm)/((1 - epsilon)*rho_b);      % depth or thickness
    Au(:,j)=-alpha*Cb*Qu(:,j)'.*t.^1 +
kab*(alpha_v*Jair)*1/2*depth*t.^2 + Au0; % m^2
end

%%% computing the blocked flow Qb:
TMPi     =-PT;  %%% tmp

%%% a bit restructuring ....
 % initialize data
 Qb=zeros(length(t),length(bulk));
 Ab=zeros(size(Qb));
 Rp=zeros(size(Ab));
 j=0; %%%

   for i=bulk % bulk concentration value
    j=j+1;
   Cb=i;       % concentration in g/L

   % unblocked flow and area:
   % reformulated Ab
   RCi=(180*(1 - Cporo)^2)/(dpi^2*Cporo^3); % specific cake resistance
   depth=(Cd*Jm)/((1 - epsilon)*rho_b);     % depth or thickness
   Ab(:,j)=alpha*Cb*Qu(:,j)'.*t.^1 - kab*(alpha_v*Jair)*1/2*depth*t.^2
+ Ab0;
   Rp(:,j)=fiRi*Cb*(Jm-(Qu(:,j)'./Au(:,j)')).*t.^1 -
go*Sig_i*(alpha_v*Jair)*1/2*(RCi*depth).*t.^2 + Rp0;
   Qb(:,j)=(TMPi./(visc_ii.*(Rm.*(1 + beta*Q0*Cb*tp).^2 +
Rp(:,j)'.^1))).*...
          (alpha*Cb*Qu(:,j)'.*t.^1 - kab*(alpha_v*Jair)*1/2*depth*t.^2
+ Ab0);
   Qb(1,j)=ti;                                % note, when t tends to
zero, Qb becomes zero, thus Qt=Qu!
   end
%

%%% total flow is the sum of blocked and unblocked; and calculation of
Rtotal
% initialize data
   Qt=zeros(length(t),length(bulk));
   Rtot=zeros(size(Qt));
 for k=1:length(bulk) %
   Qt(:,k)=Qu(:,k)+Qb(:,k); % total volumetric flow rate
   Rtot(:,k)=(TMPi*Au0)./(visc_ii.*(Qu(:,k)+Qb(:,k))); % Rtotal
 end %

% minimisation difference
Obj_val=Obj_func_mini(Qt,Q0,Au0,visc_ii,TMPi); %
```

```
% simulation data thus far to be used for save
val_final(CNTg,:)=[bulk -PT CNTg Obj_val xin];

% save your simulations data every now and then - optional
if ~isempty(find(CNTg==0:300:CNTg+301,1))
    %%% save as '.dat' or '.mat' file, for maybe a rainy day!
    save Simu_Run_StaticMBR.mat val_final -mat
end %

end %%%

%%% ____________________ SUBFUNCTION
function best_fit_data(xin)

%=========================================================================
====
% changeable parameters used in optimisation and some rounding up!
Rp0Rmi =xin(1);         % ration of initial protein resistance ratio
alpha  =xin(2);         % pore blockage parameter
beta   =xin(3);         % pore constriction parameter in kg
fiRi   =xin(4)*1e9;     % combined parameter for cake build up
go     =xin(5);         % cake removal coefficient
kab    =xin(6);         % Area constant, adjustable

% initial unchangeable parameters
Q0    =1.84/60000;   % iniial volumetric flow rate in m^3/s
PT    =-58000;       % PT, negative sign of initial tmp (Pa)
Qair  =21.3/60000;   % 21.3 L/min in m^3/s
Sig_i =0.00046;      % resistance constant in m^-1
bulk  =[8.22 9.35];  % mlss concentration g/L
epsilon=0.442;       % average cake water content for specific mlss
range
Cporo =epsilon;      % void fraction
dpi   =0.28*1e-6;    % average particle diameter for each mlss specific
range taken from thames water in m,
Cd    =6.32;         % average solids content in kg/m^3 (or just g/L
works as well),
rho_b =1132.17;      % Average bulk cake layer density for each mlss
range in kg/m^3
alpha_v=0.0292;      % air scouring coefficient
visc_ii=0.0093;      % avg visc in Pa.s,
A     =1.152;        % membrane area (m^2)
Au0   =A;            % initial unblocked area of clean membrane in m^2
at t=0;
Ab0   =0;            % initial blocked area (m^2)
Rm    =4.55e11;      % clean static membrane module resistance in 1/m
Rp0   =Rp0Rmi*Rm;    % Rm computed in 1/m
Jair  =Qair/Au0;     % air scouring flux in m/s
Jm    =Q0/Au0;       %

%%% computing unblocked flow Qu:
ti=0.8e-20;    % simul start
tstep=60*5;    % time steps
tj=60*120;     % end of simul in sec or filtration time
t=ti:tstep:tj; % time vector
```

```
tp=t.*0.39; %%%

% initialize data
Qu=zeros(length(t),length(bulk));
Au=zeros(size(Qu));
 j=0; %%%
for i=bulk % bulk concentration values
    j=j+1;
   Cb=i;    % concentration in g/L

% unblocked flow and area:
    Qu(:,j)=((Au0*Jm)./(1+beta*Q0*Cb*t).^2).*exp(-
alpha*Cb*Jm*t./(1+beta*Q0*Cb*t));
    %%%
    depth=(Cd*Jm)/((1 - epsilon)*rho_b);      % depth or thickness
    Au(:,j)=-alpha*Cb*Qu(:,j)'.*t.^1 +
kab*(alpha_v*Jair)*1/2*depth*t.^2 + Au0; % m^2
end

%%% computing the blocked flow Qb:
TMPi     =-PT;  %%% tmp

%%% a bit restructuring ....
 % initialize data
 Qb=zeros(length(t),length(bulk));
 Ab=zeros(size(Qb));
 Rp=zeros(size(Ab));
 j=0; %%%

   for i=bulk % bulk concentration value
    j=j+1;
   Cb=i;       % concentration in g/L

   % unblocked flow and area:
   % reformulated Ab
   RCi=(180*(1 - Cporo)^2)/(dpi^2*Cporo^3); % specific cake resistance
   depth=(Cd*Jm)/((1 - epsilon)*rho_b);     % depth or thickness
   Ab(:,j)=alpha*Cb*Qu(:,j)'.*t.^1 - kab*(alpha_v*Jair)*1/2*depth*t.^2
+ Ab0;
   Rp(:,j)=fiRi*Cb*(Jm-(Qu(:,j)'./Au(:,j)')).*t.^1 -
go*Sig_i*(alpha_v*Jair)*1/2*(RCi*depth).*t.^2 + Rp0;
   Qb(:,j)=(TMPi./(visc_ii.*(Rm.*(1 + beta*Q0*Cb*tp).^2 +
Rp(:,j)'.^1))).*...
           (alpha*Cb*Qu(:,j)'.*t.^1 - kab*(alpha_v*Jair)*1/2*depth*t.^2
+ Ab0);
   Qb(1,j)=ti;                                % note, when t tends to
zero, Qb becomes zero, thus Qt=Qu!
   end
%

%%% total flow is the sum of blocked and unblocked; and calculation of
Rtotal
% initialize data
   Qt=zeros(length(t),length(bulk));
```

```
   Rtot=zeros(size(Qt));
 for k=1:length(bulk) %
   Qt(:,k)=Qu(:,k)+Qb(:,k); % total volumetric flow rate
   Rtot(:,k)=(TMPi*Au0)./(visc_ii.*(Qu(:,k)+Qb(:,k))); % Rtotal
 end %
%=========================================================================
====

%%% figures & graphs
figure; % call figure window
t_xi =0:5:120; % time interval for real data

% lab data goes here:
[Qa,Ra]=Lab_flows_data(Au0,visc_ii,TMPi); %

subplot(2,1,1) % plotting flow rates
plot(t_xi,Qa(:,1)./Q0,'o',...
     t_xi,Qa(:,2)./Q0,'*');

% labels and legends
xlabel('Time [min]'); %
ylabel('Q_t/Q_0 (Total Volumetric Flow Rate Ratio)'); %
legend(['Cb = ' num2str(bulk(1)) ' g/L, ' num2str(-PT/1e5) ' bar'],['Cb
= ' num2str(bulk(2)) ' g/L, ' num2str(-PT/1e5) ' bar']);

hold on;
plot(t./60,Qt./Q0); hold off; % fitted values for Qt

axis tight; % fit max values or % axis square;

subplot(2,1,2) % plotting total resistances
plot(t_xi,Ra(:,1)./(Rm),'o',...
     t_xi,Ra(:,2)./(Rm),'*');

% labels and legends
xlabel('Time [min]'); %
ylabel('R_t_o_t_a_l/R_m (Total Resistance Ratio)'); %
legend(['Cb = ' num2str(bulk(1)) ' g/L, ' num2str(-PT/1e5) ' bar'],['Cb
= ' num2str(bulk(2)) ' g/L, ' num2str(-PT/1e5) ' bar']);

hold on;
plot(t./60,Rtot./(Rm)); hold off; % fitted values for Rtot
axis tight; % fit max values or axis square;

end %%%
```

APPENDIX D.2.1

The small adjustments made to obtain GA factors are summarised in Table AP.D.1 as simplified results (the least squared residuals are also included).

Table AP.D.1. Simplified GA factors results from adjustments made along with least squared residuals

Least squared residual convergence	Population size	Number of generations
154.457	60	100
151.346	115	120
147.123	170	240
120.458	215	525
100.765	265	715
92.671	300	900
81.896	355	1350
70.343	425	1800
63.567	475	2050
52.269	525	2350
45.672	575	2650
32.423	625	2850
25.621	675	3000
21.092	720	3200
18.354	780	3500
15.658	835	3825
10.642	900	4150
3.126	1015	5000
2.164	1075	5600
0.103	1200	6000
0.326	1250	6000
0.968	1285	6000
2.457	1340	7000
2.346	1390	6065

Population size: 1.2×10^3 [roughly a range of 1200 – 1500]
Number of generations: 6000
Migration fraction: 0.25

Having a fairly large population does not always necessarily equate to a better set of solutions, but in this case it was. In the end, a hands-on approach (obviously not the most expert way to do it) worked for this author but it might not necessarily work for the next.

APPENDIX D.3

The optimisation of simulation final values for parameters α_v and δ' are summarised in Table AP.D.2.

Table AP.D.2. Determined parameters α_v and δ' after optimisation

Guesses for parameters		**Matlab**
α_v (-)	δ' (m^{-1})	Simulation Final Values
0.0084	3.0×10^{-4}	1.4667
0.0097	3.1×10^{-4}	1.1856
0.0110	3.2×10^{-4}	1.0092
0.0123	3.3×10^{-4}	0.8489
0.0136	3.4×10^{-4}	0.7092
0.0149	3.5×10^{-4}	0.6245
0.0162	3.6×10^{-4}	0.4126
0.0175	3.7×10^{-4}	0.3955
0.0188	3.8×10^{-4}	0.3692
0.0201	3.9×10^{-4}	0.3417
0.0214	4.0×10^{-4}	0.2763
0.0227	4.1×10^{-4}	0.2511
0.0240	4.2×10^{-4}	0.2134
0.0253	4.3×10^{-4}	0.1789
0.0266	4.4×10^{-4}	0.1352
0.0279	4.5×10^{-4}	0.0896
0.0292	4.6×10^{-4}	0.0263
0.0305	4.7×10^{-4}	0.6425
0.0318	4.8×10^{-4}	0.7392
0.0292	4.6×10^{-4}	0.0265
0.0292	4.6×10^{-4}	0.0265
0.0292	4.6×10^{-4}	0.0265

APPENDIX E

This appendix section serves as an extension to **Chapter 5 sub-section 5.2.1** and **5.2.2**, and **Chapter 6 sub-section 6.2**. Many curves which were not used during discussions were put here for extra viewing. Appendix E.1 (for **sub-section 5.2.1**) contains graphs for the RMBR fouling model for two MLSS level ranges: 3.34 – 4.26 g/L and 6.32 – 7.24 g/L.

Appendix E.1.1 (for **sub-section 5.2.2**) has figures pertaining to the RMBR model calibration verification curves for two MLSS levels: 3.89 g/L at TMP of 45 kPa and 6.82 g/L at TMP of 15 and 45 kPa. Finally, Appendix E.2 (for **sub-section 6.2**) depicts TMP steps curves for the SMBR fouling model for one MLSS level range: 6.32 – 7.24 g/L.

APPENDIX E.1

This sub-section includes the TMP steps (i.e. 15, 30, 45 and 58 kPa) curves for MLSS level range of 3.34 – 4.26 g/L and 6.32 – 7.24 g/L for the RPU-185 RMBR. Note that these curves were not used during discussions in the thesis proper as they produce similar analyses to the ones used.

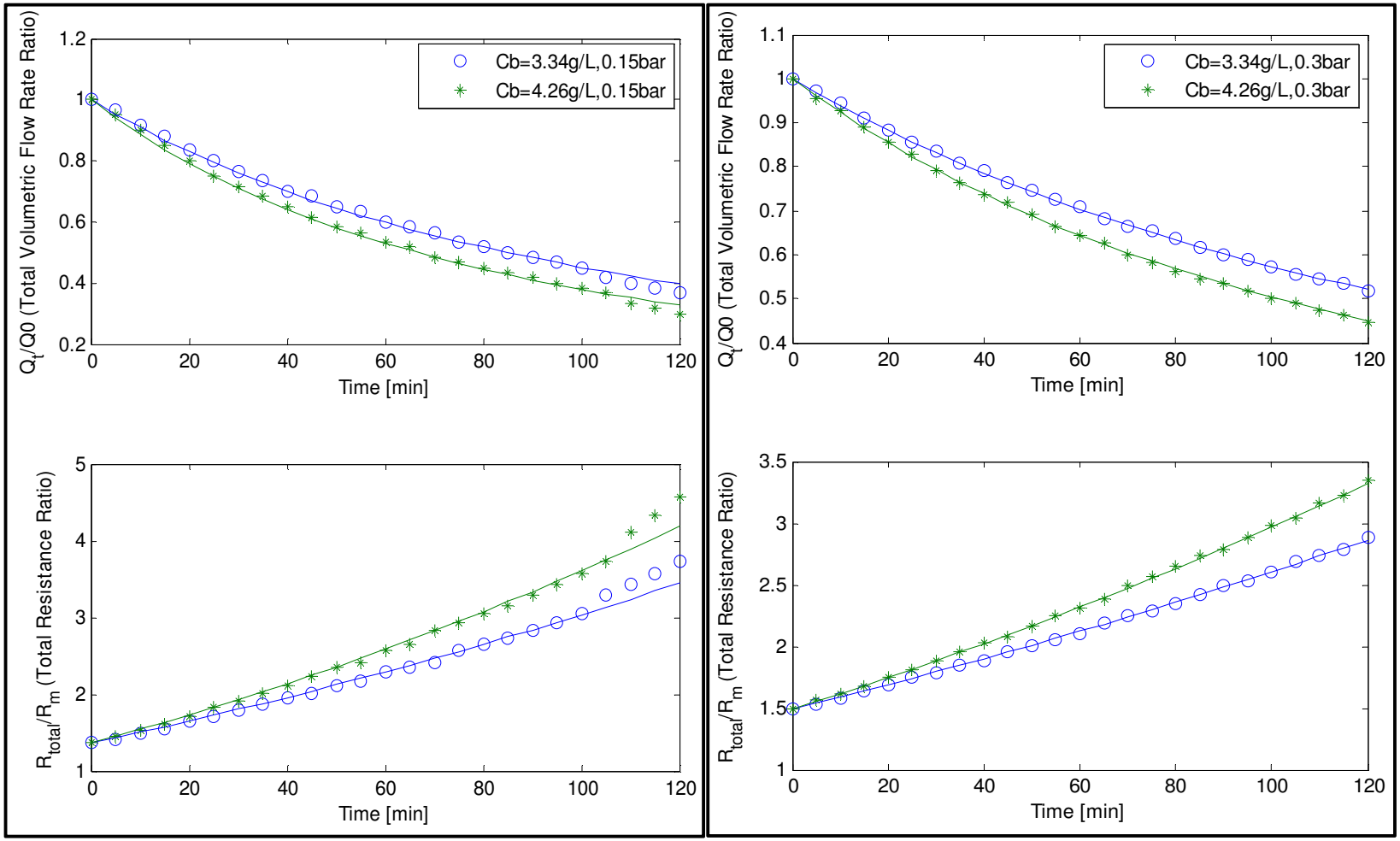

Figure AP.E.1. Left - Flux decline and total resistance for TMP step at 15 kPa for MLSS levels of 3.34 and 4.26 g/L
Figure AP.E.2. Right - Flux decline and total resistance for TMP step at 30 kPa for MLSS levels of 3.34 and 4.26 g/L

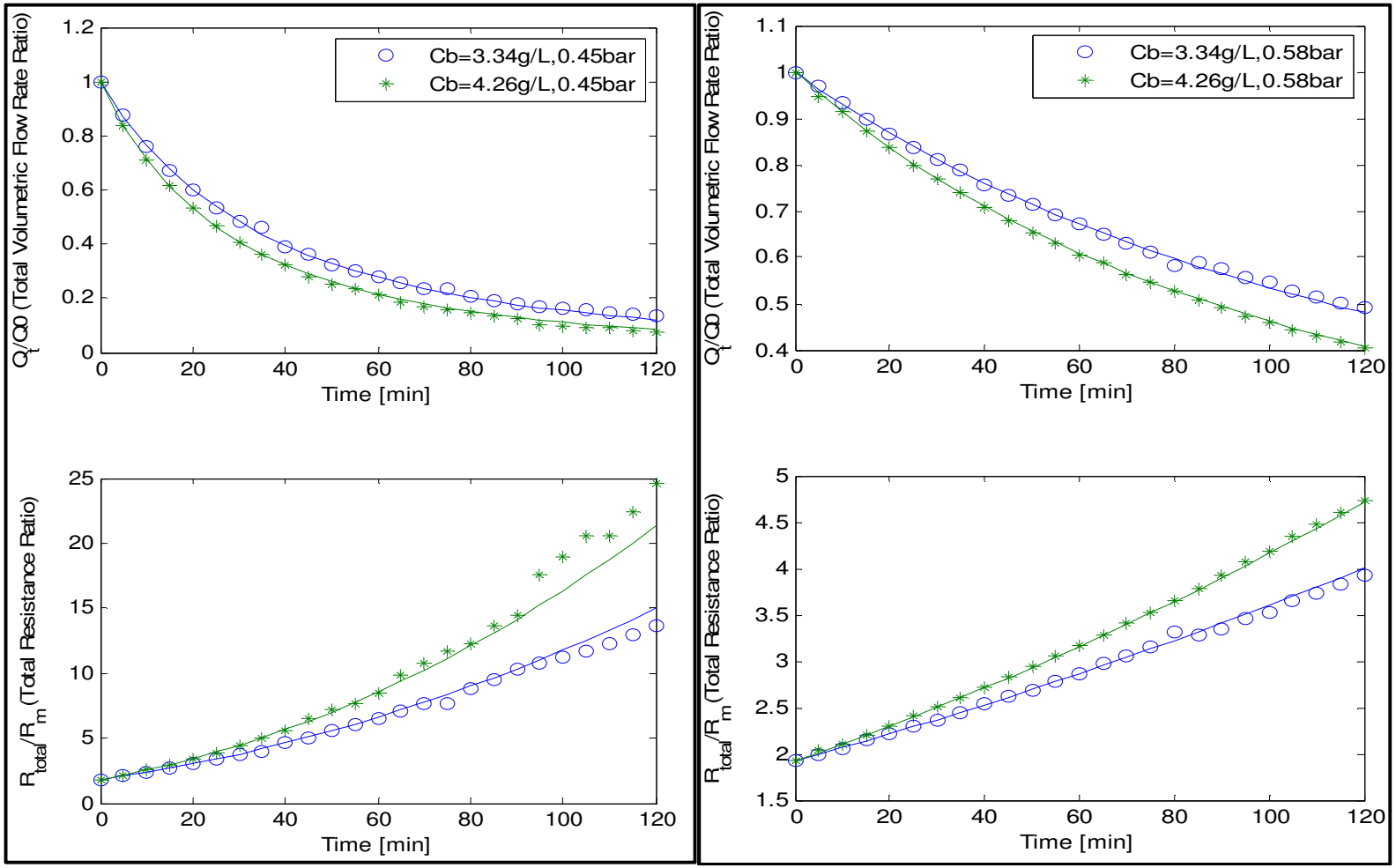

Figure AP.E.3. Left - Flux decline and total resistance for TMP step at 45 kPa for MLSS levels of 3.34 and 4.26 g/L
Figure AP.E.4. Right - Flux decline and total resistance for TMP step at 58 kPa for MLSS levels of 3.34 and 4.26 g/L

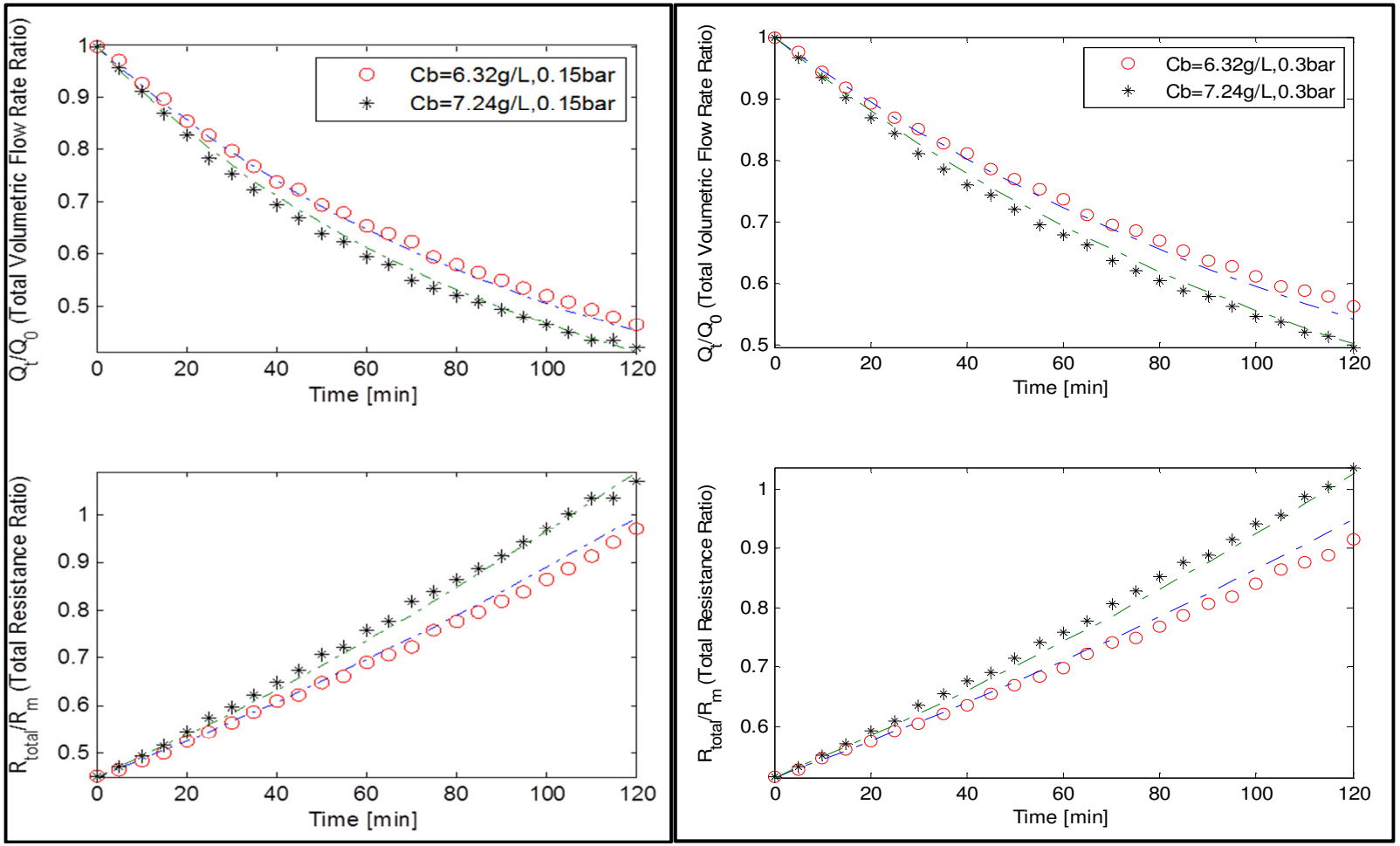

Figure AP.E.5. Left - Flux decline and total resistance for TMP step at 15 kPa for MLSS levels of 6.32 and 7.24 g/L
Figure AP.E.6. Right - Flux decline and total resistance for TMP step at 30 kPa for MLSS levels of 6.32 and 7.24 g/L

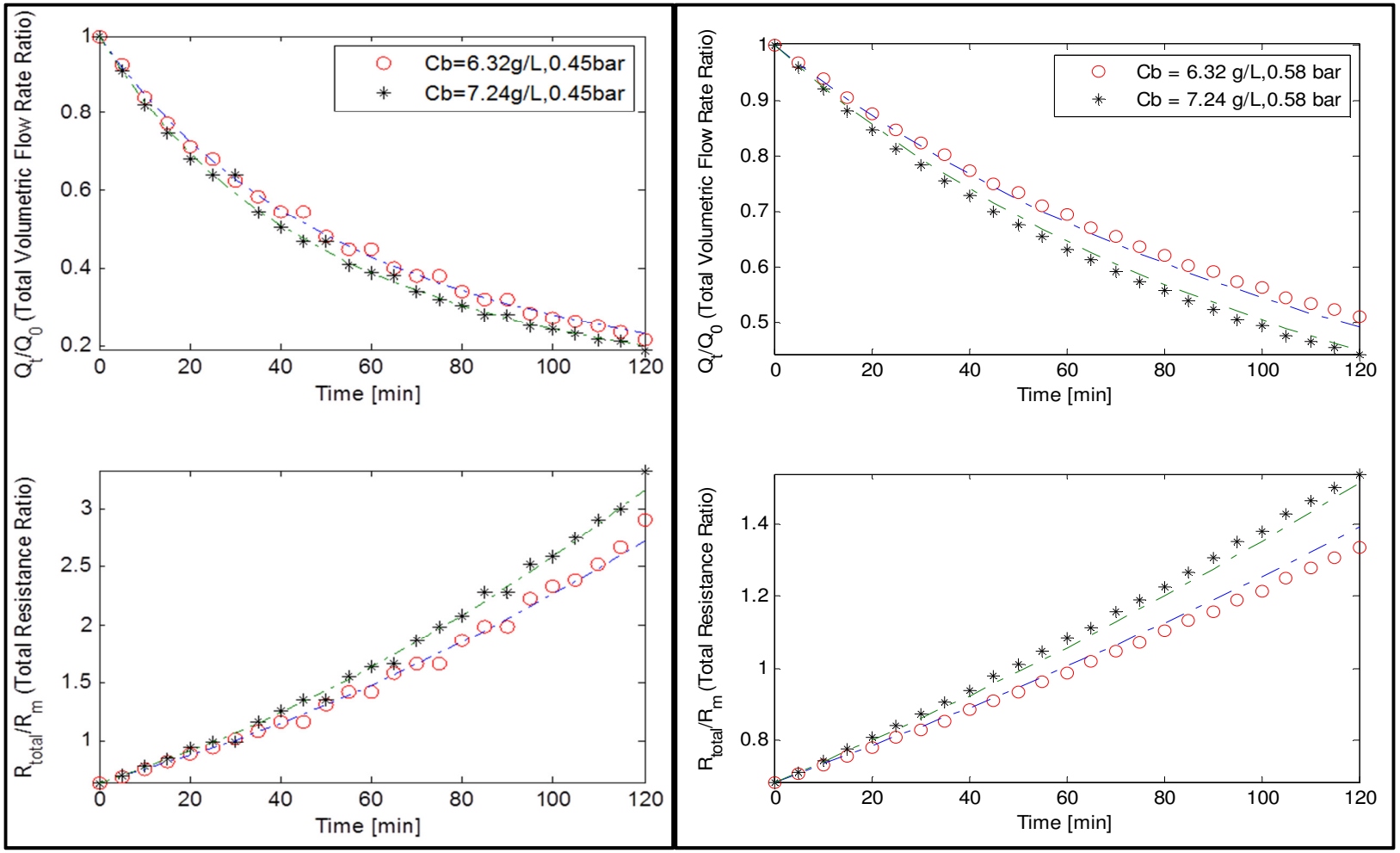

Figure AP.E.7. Left - Flux decline and total resistance for TMP step at 45 kPa for MLSS levels of 6.32 and 7.24 g/L
Figure AP.E.8. Right - Flux decline and total resistance for TMP step at 58 kPa for MLSS levels of 6.32 and 7.24 g/L

APPENDIX E.1.1

This sub-section contains the calibration verification curves that were not used for analyses in the actual thesis as they are similar in discussion to the ones used. They are: 3.89 g/L at TMP of 45 kPa and 6.82 g/L at TMP of 15 and 45 kpa for the RPU-185 RMBR.

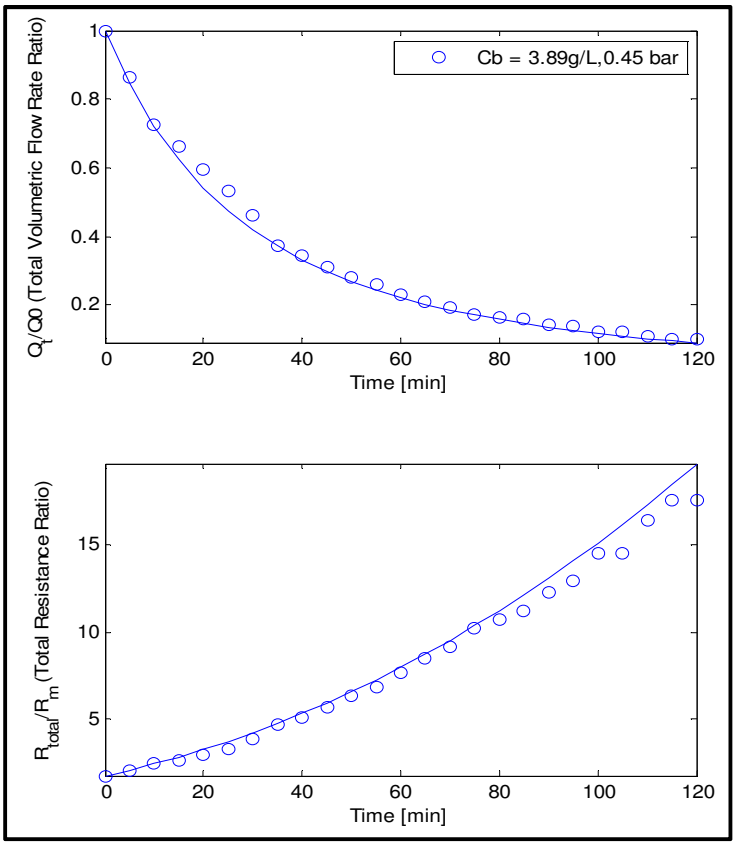

Figure AP.E.9. Model calibration curve verification for TMP step at 45 kPa for MLSS level of 3.89 g/L

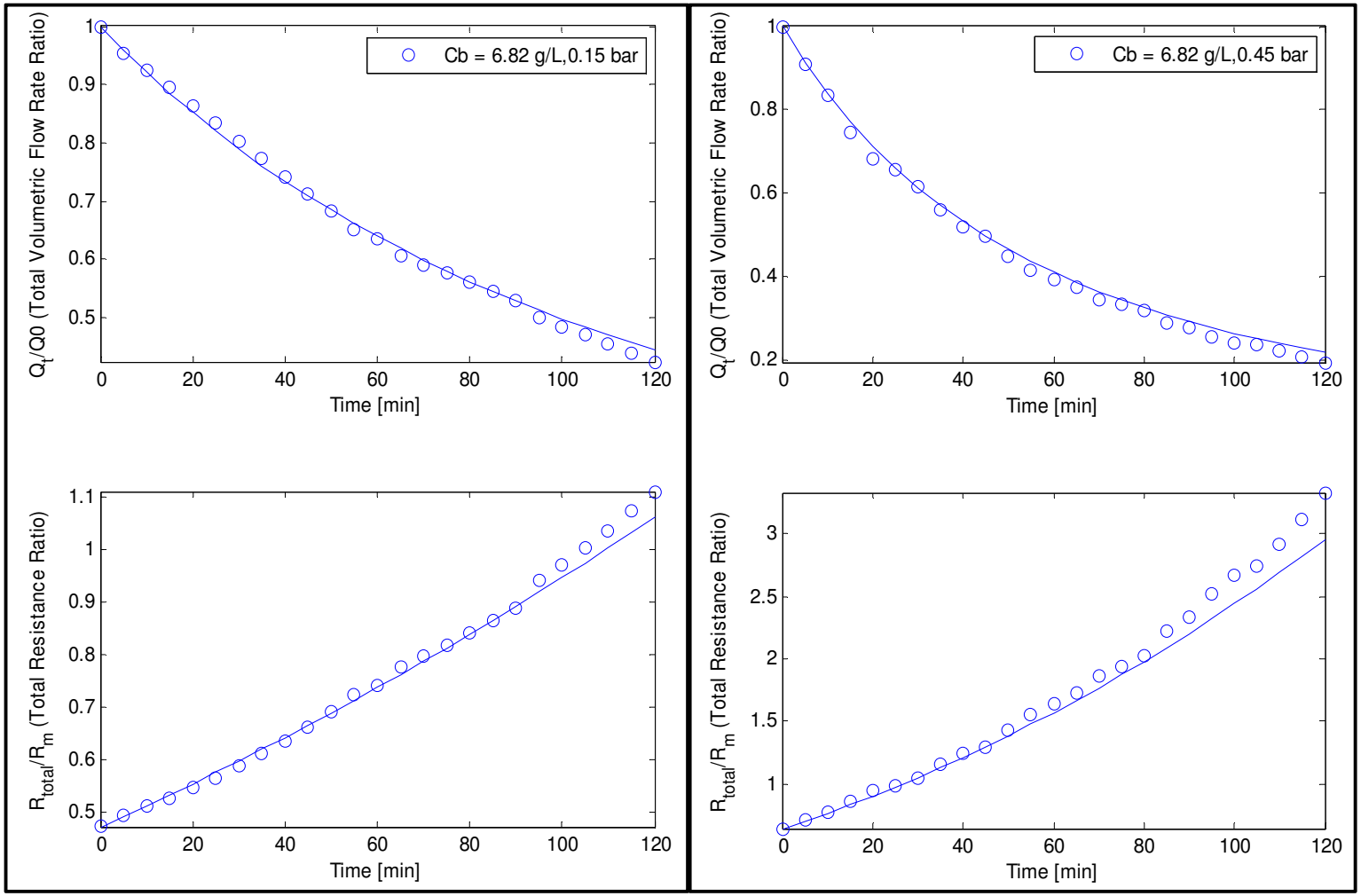

Figure AP.E.10. Left – Model calibration curve verification for TMP step at 15 kPa for MLSS level of 6.82 g/L
Figure AP.E.11. Right – Model calibration curve verification for TMP step at 45 kPa for MLSS level of 6.82 g/L

APPENDIX E.2

This sub-section comprises the TMP steps (15, 30, 45 and 58 kPa) curves for MLSS level range of 6.32 – 7.24 g/L for the constructed SMBR rig. Note that these curves were not used during discussions in the thesis proper as they produce similar analyses to the ones used.

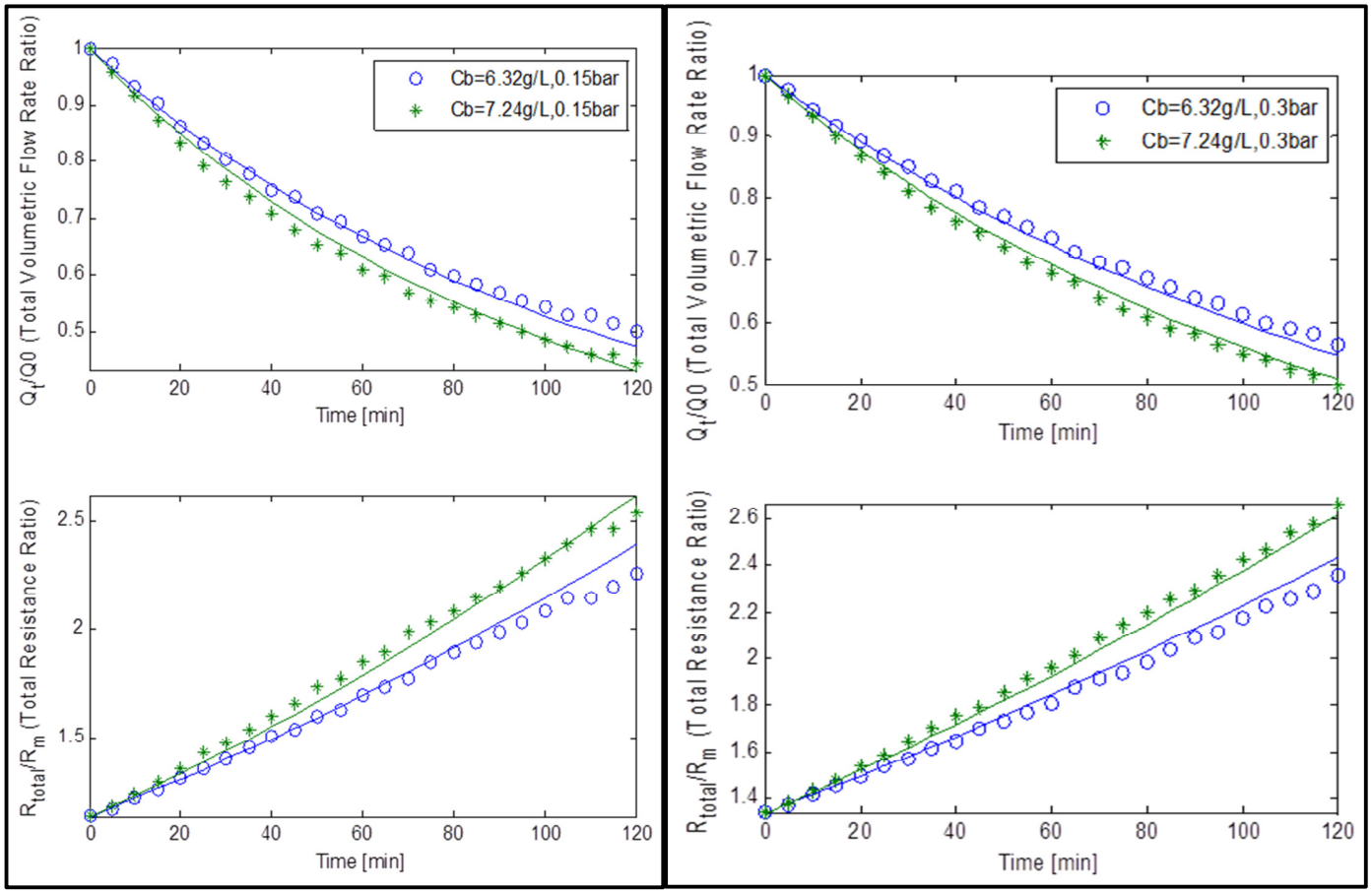

Figure AP.E.12. Left - Flux decline and total resistance for TMP step at 15 kPa for MLSS levels of 6.32 and 7.24 g/L
Figure AP.E.13. Right - Flux decline and total resistance for TMP step at 30 kPa for MLSS levels of 6.32 and 7.24 g/L

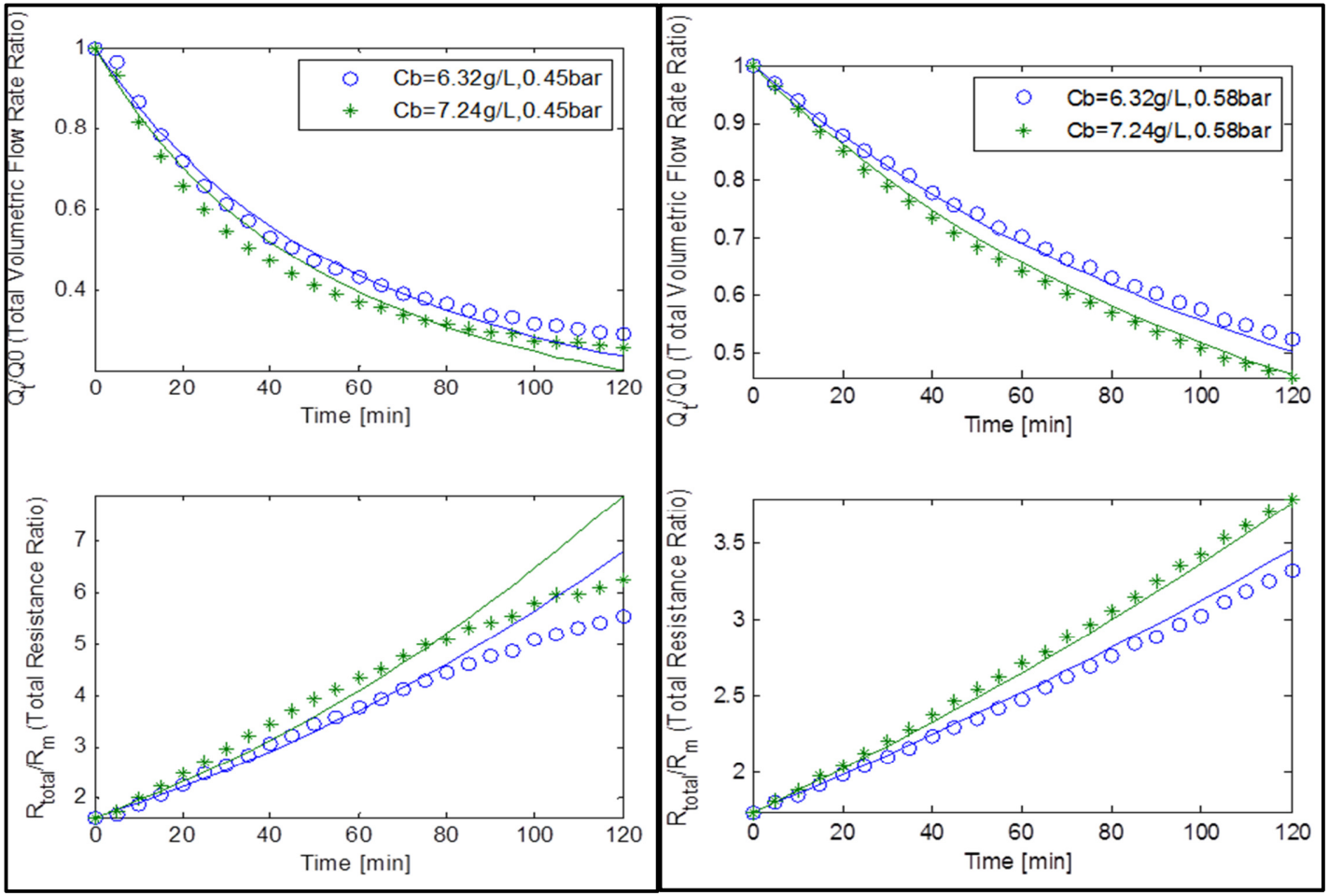

Figure AP.E.14. Left - Flux decline and total resistance for TMP step at 45 kPa for MLSS levels of 6.32 and 7.24 g/L
Figure AP.E.15. Right - Flux decline and total resistance for TMP step at 58 kPa for MLSS levels of 6.32 and 7.24 g/L

APPENDIX F

This appendix section deals with **Chapter 7**. Appendix F.1 (for **sub-section 7.1**) contains pictures associated with cake being formed on both MBRs membranes (for comparative purposes) as well as covers cake compressibility test for the RMBR and some text about membrane autopsy. Appendix F.2 (for **sub-section 7.2**) contains activated sludge flocs pictures taken under 40 and 100 times magnification and general microscopy experimental information.

APPENDIX F.1

- Some pictures concerning caking formed on the membranes of both MBR plants are presented below on Figure AP.F.1,

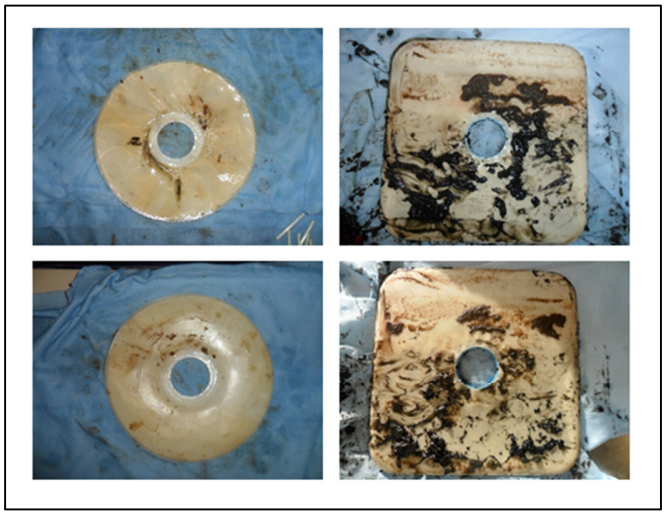

Figure AP.F.1. (Left) – RMBR caking pattern even; (Right) – SMBR caking pattern, uneven

- Cake compressibility test was carried out for the RMBR and is detailed as follows:

The first stage was to find cake resistance and specific cake resistance (by mass). They were determined through experiments that had protocols similar to those of membrane resistance and SMP inclusion tests. The cake resistance was then later computed through model (for verification with carried out experiments). To measure the required cake resistance, the following steps were taken:

i. After a filtration period of two hours, total membrane resistance, R_{total} (m^{-1}) was determined using Darcy's law (see Equation 2.2). It should be noted that after this period, the membrane will be fouled but, more importantly the formation of a cake layer becomes apparent. This cake layer is almost evenly

distributed on the membrane discs of the module (which can be largely attributed to the low rotational speed).

ii. The resistance sum of clean membrane resistance and pore blocking resistance was used to determine the cake resistance. After the cake formed was removed, the batch tank was emptied, and new a filtration process was carried out with distilled water instead of activated sludge for about one hour. The cake resistance, R_{cake} (m^{-1}), was calculated by subtracting the resistance sum of clean membrane and pore blocking resistance from R_{total}.

For the cake compressibility test, UF of permeate was performed through the cake formed for a period of 30 minutes (with flow rate of 1.17×10^{-5} $m^3.s^{-1}$). Experiments were done for four MLSS concentrations: 3.34 g/L, 3.86 g/L, 4.26 g/L and 5.24 g/L. TMPs were recorded for each and ensuing calculations were performed. Average specific cake layer resistance by mass, R'_{cake} ($m.kg^{-1}$), is denoted by Equation AP.F.1 (Holdich 2002, Lee et al. 2003).

$$R'_{cake} = R'_{cake_0}.TMP^{k} \rightarrow \ln(R'_{cake}) = k.\ln(TMP) + \ln\left(R'_{cake_0}\right) \qquad \text{(AP.F.1)}$$

Where, R'_{cake0}, is the specific cake layer resistance by mass at zero pressure;

Thus, by plotting logarithm of specific cake layer resistance by mass against logarithm of TMP, the so-called cake compressibility factor, k (–), was determined. The specific cake layer resistance by mass was obtained using the membrane area, measured cake mass and resistance, which are all linked through Equation AP.F.2 (Holdich 2002, Listiarini et al. 2009) as follows:

$$R'_{cake} = \frac{R_{cake}.Area_{membrane}}{mass_{cake}} \qquad \text{(AP.F.2)}$$

For model verification, the cake resistance was computed using Equation 4.15 and 4.17. Table AP.F.1 highlights the results found.

Table AP.F.1. Cake compressibility factor for RPU-185 RMBR

MLSS [g/L]	**R_m [m^{-1}]**	**R_{cake} [m^{-1}] (Measured)**	**R_{cake} [m^{-1}] (Calculated with model)**	**k (–)**
3.34	6.26×10^{11}	6.52×10^{11}	6.66×10^{11}	0.67
3.86	–	6.85×10^{11}	6.97×10^{11}	
4.26	–	7.35×10^{11}	7.06×10^{11}	
5.24	–	7.66×10^{11}	7.90×10^{11}	

The results in Table AP.F.1 appear to be consistent with that of the model with the largest deviation being observed at 4.26 g/L. The results outputted in form of graph are found on Figure AP.F.2.

On Figure AP.F.2, y represents the values of y-axis (vertical axis), and x represents the values of x-axis (horizontal axis). Experimental data are small crosses whilst simulation best fit is a solid line.

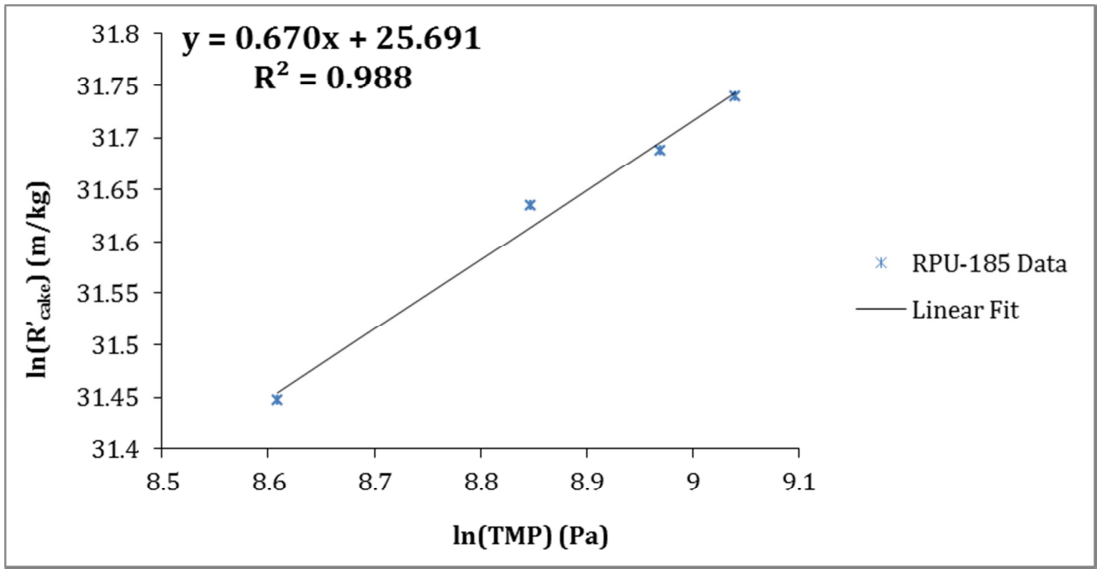

Figure AP.F.2. Graph of log specific cake layer resistance by mass plotted against log TMP. Cake compressibility factor, k, is the gradient of this line (i.e. 0.67) while R'_{cake0}, the specific cake layer resistance by mass at zero pressure, is $e^{25.691}$.

The coefficient of determination, R^2, for the linear fit procedure was found to be 0.988. This indicated a respectable fit for the power law model (Equation AP.F.1) since the sum of the squared residuals were also minimised.

Cake compressibility, defined by the compressibility factor k (Figure AP.F.2), varies from 0 to 1 and the closer it is to 0 the more incompressible the cake formed will be. Thus, when k is 0, the cake layer is regarded as incompressible. The obtained value of k from the experiments suggested that the cake layer formed (during UF for MLSS level range of 3.34 to 5.24 g/L) was compressible (as 0.67 > 0); thus, it is safe to assume that the fouling was mainly reversible.

- The ensuing text briefly talks about membrane autopsy (Dudley and Darton 1996, Nghiem and Schäfer 2006) as follows:

Eventually, throughout their lifespan, all membranes without fail will experience performance deterioration. There are many mechanisms that cause declined membrane performance. They include fouling (of course), membrane surface and structural damage, ineffective pre-treatment, and/or unsuitable cleaning of the membrane surface.

Membrane autopsy can thus be used to find the specific mechanism causing the change in membrane performance (i.e. it is used as a routine operating tool for MBR plant operators to help evaluate the performance of their membranes).

In other words, the objective of membrane autopsy is to identify if there is any damage on membrane surface, to identify foreign compounds on membrane surface, and to assess how these compounds affect the membrane operation. Consequently, the autopsy's results can be used to make an informed decision about how best to:

- Improve pre-treatment for large-scale WWTPs;
- Ameliorate the cleaning regimes used by the MBR plant;
- Regulate MBR rig operating conditions

Several analytical methods can be used to conduct membrane autopsy analysis,

i. **Loss on Ignition***:* This method is usually utilised to quantify the level of organic vs inorganic deposits on the membrane.

ii. **Stereo Microscopy**: A microscope is used to examine the membrane surface. This method is particularly useful for hollow fibre membrane examination.

iii. **NMR Nuclear Magnetic Resonance**: This analytical method can be used to determine specific organic compounds present as foulants deposit on membrane surface.

iv. **Liquid Chromatography Organic Carbon Detection**: This technique can be used to categorise the organic material found on membrane surface based on the molecular weight of the organic compounds.

APPENDIX F.2

General information about activated sludge flocs observation experiments under microscope

- Microscope used: Olympus BX51, magnification 2, 10, 40 and 100;
- Software: QCapturePro;
- Camera: Colour RTV 10-bit;
- Experiments done by Franck Anderson Jones, Parneet Paul, Gerald Edwardson and Kofi Renner;
- Conducted at Brunel University Institute for Environment, Health & Societies

Figure AP.F.3 displays the activated sludge flocs structure (part of it) that were observed under the microscope at respectively 40 and 100 times magnification,

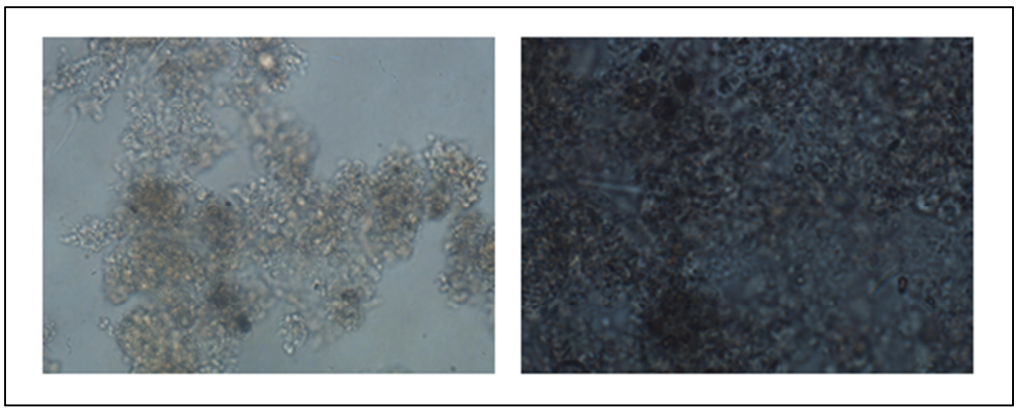

Figure AP.F.3. (Left) – Flocs structure at 40 times magnification.
(Right) – Flocs structure at 100 times magnification